

THE UNIVERSITY OF HULL

SYNTHESIS AND EVALUATION OF SOME NOVEL

FERROELECTRIC LIQUID CRYSTAL MATERIALS

being a Thesis submitted for the Degree of

Doctor of Philosophy

in the University of Hull

by

Daniel James Young, B.Sc.

October 1989

for Cowboy

## Acknowledgements

Many thanks to Professor George Gray and Dr. David Lacey for their guidance and friendship throughout the course of this work; and to Dr. Peter Gemmell, who provided many of the ideas in my first year.

More thanks to David Coates, Mathew Bone and Tony Davey of STL, Harlow, for helping me to understand the phenomenon of ferroelectricity a little better, and for carrying out many of the physical measurements on my materials.

I am indebted to the University of Hull for research facilities, and to STL, Harlow, for financial support.

I will also be eternally grateful to....

Maxine Staples, for managing to interpret my original drawings and turning them into feasible diagrams;

Mr. M. Beattie of Edufund for restoring order to the typing of my thesis;

Aubrey Rendell, for producing the micrographs for this work, and for keeping us all laughing at the same time.

Finally, a very big 'thank you' to everyone involved with the Liquid Crystal Group at Hull between 1983 and 1987, for contributing to such a good time, both in and out of the laboratory.

## 1. INTRODUCTION

1.1	General.	1
1.2	Thermotropic Liquid Crystals.	2
1.2.1	The Nematic (N) and Cholesteric (Ch) Phases.	4
1.2.2	The Smectic A ( $S_A$ ) Phase.	6
1.2.3	The Smectic D ( $S_D$ ) Phase.	7
1.2.4	The Smectic C ( $S_C$ ) Phase.	8
1.2.5	The Hexatic Smectic B ( $S_{B\text{ hex}}$ ), Smectic I ( $S_I$ ) and Smectic F ( $S_F$ ) Phases.	11
1.2.6	The Crystal Smectic B ( $S_{B\text{ cryst}}$ ), Smectic J ( $S_J$ ) and Smectic G ( $S_G$ ) Phases.	12
1.2.7	The Smectic E ( $S_E$ ), Smectic K ( $S_K$ ) and Smectic H ( $S_H$ ) Phases.	13
1.2.8	Assymetric Smectic Phases.	14
1.3	Ferroelectricity.	16
1.3.1	Ferroelectric Crystals.	16
1.3.2	Ferroelectric Liquid Crystals.	19
1.3.3	Symmetry of the $S_C$ Phase.	20
1.3.4	Symmetry of the $S_C^*$ Phase.	21
1.3.5	Spontaneous Polarisation.	21
1.3.6	The Surface Stabilised Structure.	23
1.3.7	Device Application.	26
1.4.	Materials Parameters.	30
1.4.1	Helical Twist Sense.	31
1.4.2	Determination of Pitch-Length.	34
1.4.3	Temperature Variation of Pitch-Length.	34
1.4.4	Increasing the Pitch-Length.	35
1.4.5	Measuring the Tilt Angle.	37
1.4.6	Determining the Magnitude of the Spontaneous Polarisation.	41
1.4.7	Determining the Sign of the Spontaneous Polarisation.	44
1.4.8	Increasing the Spontaneous Polarisation.	46
1.5	Summary and Aims of the Work.	47

## 2. RESULTS AND DISCUSSION.

2.1	Compounds (5a-c) and (8a-d), with Summary.	50
2.2	Compounds (9a-c), with Summary.	54
2.3	Compounds (12a-c), (16a-d) and 17, with Summary.	57
2.4	Compounds (19a-c), (20a,b) and (23a-c), with Summary.	64
2.5.	Compounds (28a-j) and (31a-i), with Summary.	73

2.6	Compounds (38a-r), with Summary.	88
2.7	Compounds (45a,b) and (53a-k), with Summary.	100
2.8	Compounds (57a-d), with Summary.	111

### 3. EXPERIMENTAL.

3.1.	Physical Measurements.	118
3.1.1	Transition Temperatures.	118
3.1.2	Characterisation of Materials.	118
3.1.2.1	Infra-red Spectroscopy (ir).	118
3.1.2.2	Mass Spectrometry (ms).	118
3.1.2.3	Proton Nuclear Magnetic Resonance ( <sup>1</sup> Hnmr).	118
3.1.2.4	Polarimetry ( $[\alpha]_D^{20}$ ).	119
3.1.3	Purity of Materials.	119
3.2	Starting Materials.	120
3.3	Methods.	121
3.3.1	Scheme 1 - Compounds (5a-c).	122
3.3.1.1	4-alkoxybenzaldehydes (1a-c).	122
3.3.1.2	4-nitrobenzoyl chloride (2).	123
3.3.1.3	(S)-(-)-2-methylbutyl-4-nitrobenzoate (3).	123
3.3.1.4	(S)-(-)-2-methylbutyl-4-aminobenzoate (4).	123
3.3.1.5	4-n-alkoxybenzylidene 4'-amino-[(S)-(-)-2-methylbutyl]carboxylates (5a-c).	124
3.3.2	Scheme 2 - Compounds (8a-d).	126
3.3.2.1	4-n-alkoxybenzoyl chloride (6a-d).	126
3.3.2.2	(S)-(-)-2-methylbutyl 4-hydroxybenzoate (7).	126
3.3.2.3	(S)-(-)-2-methylbutyl 4'-(4-n-alkoxyphenyl-1-carboxy) benzoate (8a-d).	127
3.3.3	Scheme 3 - Compounds (9a-c).	129
3.3.3.1	(S)-(-)-4-n-heptyl-, -heptoxy- and - octoxy-phenyl 3-chloro-4-(2-methylbutoxy) benzoates (9a-c).	129
3.3.4	Scheme 4 - Compounds (12a-c).	130
3.3.4.1	4-n-alkoxybiphenyl carboxylic acid (10b-d).	130
3.3.4.2	4-n-alkoxybiphenyl -4'-yl carboxylic acid chloride (11b-d).	130

3.3.4.3	(S-2-methylbutyl) 4'-n- alkoxybiphenyl-4-carboxylate (12a-c).	131
3.3.5	Scheme 5 - Compounds (16a-d).	132
3.3.5.1	S-(-)-propan-2,3-diol (13)	132
3.3.5.2	R-(-)-ethyl-2-chloropropanoate(14).	132
3.3.5.3	R-(-)-2-chloropropanol (15).	133
3.3.5.4	(R-(-)-2-chloropropyl) 4-n- alkoxybiphenyl -4'-carboxylate (16a-c).	133
3.3.5.5	(S-(-)-2-hydroxypropyl) 4-n- octyloxybiphenyl -4'carboxylate (16d).	134
3.3.6	Scheme 6 - Compound (17).	136
3.3.6.1	((-)-isopinocampyl) 4-n- nonyloxybiphenyl -4-carboxylate (17).	136
3.3.7	Scheme 7 - Compounds (19a-c).	137
3.3.7.1	(R-(-)-2-chloropropyl) 4- hydroxybenzoate (18).	137
3.3.7.2	(R-(-)-2-chloropropyl) 4-(4'-n- alkoxybiphenyl-4-yl carboxybenzoate (19a-c).	137
3.3.8	Scheme 8 - Compounds (20a,b).	139
3.3.8.1	(S)-(-)-(2-methylbutylphenyl) and (S)-(-)-4-(3-methylpentylphenyl) 4- n-octyloxybiphenyl-4'-carboxylate (20a,b).	139
3.3.9	Scheme 9 - Compounds (23a-c).	140
3.3.9.1	4-hydroxyphenyl <sup>4'</sup> carboxylic acid (21).	140
3.3.9.2	(S-(-)-2-methylbutyl) 4- hydroxyphenyl -4'-carboxylate (22).	140
3.3.9.3	(S-(-)-2-methylbutyl) 4'- (4-n- alkoxyphenyl-1-carboxy) biphenyl-4- carboxylates (23a-c).	140
3.3.10	Scheme 10 - Compounds (28a-j).	142
3.3.10.1	4-n-alkoxy, 4-n-alkylbiphenyl-4'- carboxylic acid chloride (11a-j).	142
3.3.10.2	4-benzyloxybenzoic acid (24).	142
3.3.10.3	4-benzyloxybenzoic acid chloride (25).	143
3.3.10.4	(S)-(-)-ethyl-2-(4- benzyloxyphenylcarboxy) propanoate (26).	143

3.3.10.5	(S)-(-)-ethyl-2-(4-hydroxyphenylcarboxy) propanoate (27).	144
3.3.10.6	(S)-(-)-ethyl-2-[4-(4-n-alkoxy-, and -alkylbiphenyl-4-yl carboxy) benzyloxy] propanoate (28a-j).	144
3.3.11	Scheme 11 - Compounds (31a-i).	147
3.3.11.1	Compounds (29a-d).	147
3.3.11.2	Compounds (30a-d).	147
3.3.11.3	Compounds (31a-i).	148
3.3.12	Scheme 12 - Compound (32).	150
3.3.12.1	3-cyano-4-hydroxybenzoic acid (32).	150
3.3.13	Scheme 13 - Compound (33).	151
3.3.13.1	3-fluoro-4-hydroxybenzoic acid (33).	151
3.3.14	Scheme 14 - Compounds (38a-r).	152
3.3.14.1	Compounds (34a-f).	152
3.3.14.2	Compounds (35a-f).	153
3.3.14.3	Compounds (36a-f).	153
3.3.14.4	Compounds (37a-f).	154
3.3.14.5	Compounds (38a-r).	154
3.3.15	Scheme 15 - Compounds (45a,b).	157
3.3.15.1	ethyl 2,3-dichloro-4-hydroxybenzoate (39).	157
3.3.15.2	ethyl 4-benzyloxy -2,3-dichlorobenzoate (40).	157
3.3.15.3	4-benzyloxy -2,3-dichlorobenzoic acid (41).	157
3.3.15.4	4-benzyloxy -2,3-dichlorobenzoyl chloride (42).	158
3.3.15.5	(S)-(-)-ethyl 2-(4-benzyloxy -2,3-dichlorophenylcarboxy) propanoate (43).	158
3.3.15.6	(S)-(-)-ethyl 2-(2,3-dichloro-4-hydroxyphenylcarboxy) propanoate (43).	158
3.3.15.7	(S)-(-)-ethyl 2-[4-(4'-nonoxy- and -decyl-biphenyl-4-yl carboxyl) 2,3-dichlorobenzyloxy] propanoate (45a,b).	159
3.3.16	Scheme 16 - Compound (48).	160
3.3.16.1	4-bromo-3-fluorophenol (46).	160
3.3.16.2	2-fluoro-4-hydroxybenzotrile (47).	160
3.3.16.3	2-fluoro-4-hydroxybenzoic acid (48).	161

3.3.17 - Compounds (53a-k).	162
3.3.17.1 Compounds (49a,b).	162
3.3.17.2 Compounds (50a-c).	162
3.3.17.3 Compounds (51a-c).	163
3.3.17.4 Compounds (52a-c).	163
3.3.17.5 Compounds (53a-k).	164
3.3.18 Scheme 18 - Compounds (57a-d).	166
3.3.18.1 4'-benzyloxybiphenyl carboxylic acid chloride (54).	166
3.3.18.2 (S)-(-)-ethyl 2-(4-benzyloxybiphenylcarboxy)propanoate (55).	166
3.3.18.3 (S)-(-)-ethyl 2-(4-hydroxybiphenylcarboxy)propanoate (56).	166
3.3.18.4 Compounds (57a-d).	167

#### 4. APPENDICES.

4.1. Origin of Ferroelectricity in the $S_C^*$ Phase.	168
4.2. The Pseudo-Homeotropic Texture of the $S_C^*$ Phase.	173

5. REFERENCES.	179
----------------	-----

6. CONCLUDING REMARKS.	183
------------------------	-----

1. INTRODUCTION

## 1.1 General.

Over the last twenty five years there has been rapid growth in the development of liquid crystal materials (mesogens) and in their use in optical and electro-optical devices. Much of this work has centred on optimising the properties of the liquid-like nematic phase for use in the twisted nematic cell<sup>1</sup> and its device modifications, which have been widely used over the last ten years. These devices of high contrast ratio and low power consumption have largely replaced the light emitting diode in digital displays e.g., those in wrist watches and calculators, and account for the majority of liquid crystal display devices in use today.

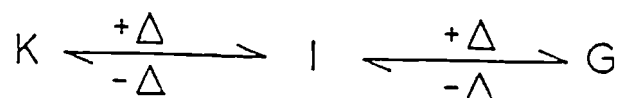
In recent years however, attention has focused on the more ordered (smectic) liquid crystal phases, and in particular on the device potential of tilted smectic phases consisting of optically active molecules. Some of these phases have been shown to exhibit fast (microsecond), bistable, sharp voltage threshold electro-optic effects,<sup>2</sup> which generate the possibility of many novel device applications. Mesogenic materials exhibiting tilted smectic phases with these properties are generally referred to as **ferroelectric liquid crystal materials**, and since their initial prediction and discovery in 1975<sup>3</sup>, much academic and commercial interest in them has arisen.

As a result of this interest, there has been a major drive to synthesise and characterise new ferroelectric liquid crystal materials, in order to ascertain the optimum structural features for use in electro-optical devices.

The most extensively studied and likeliest candidate for practical use in the near future is the chiral smectic C  $(S_C^*)^I$  phase, and it is with this phase that the majority of the following work will be concerned.

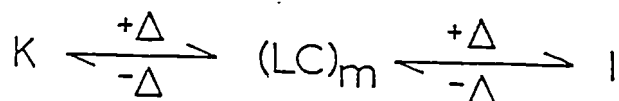
## 1.2 Thermotropic Liquid Crystal Phases.

At any given temperature, a material will usually exist in one of three states - solid, liquid or gas. The relationship between these states with variation in temperature is generally of the form:



where K, I and G denote the crystalline, isotropic liquid and gaseous states respectively.

However, certain structurally anisotropic organic materials will melt on heating to give one or more phases intermediate in molecular organisation between that of the crystalline and the liquid states. These structured phases are called thermotropic liquid crystal phases<sup>II</sup> and the situation can be represented by:



where L.C. denotes a thermotropic liquid crystal phase and  $m$ , a smaller integer, may indicate a number of phases.

- I. When referring to a phase, the symbol \* will be used to indicate that it is composed of chiral molecules and is optically active.
- II. Thermotropic liquid crystals are distinct from lyotropic liquid crystals. Lyotropic mesogens can exhibit a number of phases, depending on both the concentration of amphiphilic mesogen(s) in a polar solvent (usually water) and temperature.

Although thermotropic liquid crystal phases may be formed from disk-like molecules, giving 'discotic' phases, this thesis will be concerned solely with the phases formed by 'rod-like' elongated molecules.

A brief description of the structures of the known liquid crystal phases will now be given. Distinguishing between these phases can usually be accomplished by a combination of optical microscopy and differential scanning calorimetry (D.S.C.), since the phases of highest thermal stability (N, Ch, S<sub>A</sub>, S<sub>D</sub>, S<sub>C</sub> and S<sub>B</sub>) and the S<sub>E</sub> phase have very distinct microscopic textures. Differentiating between phases of lower thermal stability (S<sub>I</sub>, S<sub>F</sub>, S<sub>J</sub>, S<sub>G</sub>, S<sub>K</sub> and S<sub>H</sub>) is generally more difficult and may require x-ray analysis of well aligned samples in order to establish the true structure. <sup>III</sup>

Phase identification can also be facilitated by the use of miscibility experiments. A compound with an unknown phase is mixed with a standard material of known phase characteristics. If the unknown phase and a known phase of the standard material are found to be comiscible in all proportions, then they are assumed to have the same phase structure. Nevertheless, two such phases having the same structure may sometimes prove to be immiscible due to molecular incompatibilities and so this technique can only be used for positive identification of an unknown phase.

-----  
III. For a detailed discussion on the structure, microscopic textures and relative thermal ordering of phases, see: Goodby, J.W., and Gray, G.W., "Smectic Liquid Crystals" (Leonard Hill), 1984.

### 1.2.1 The Nematic (N) and Cholesteric (Ch) Phases.

The nematic phase is the most liquid-like mesophase, having a higher thermal stability than any of the smectic phases; it can only undergo a transition to the isotropic liquid on heating. Within the nematic phase, individual molecules possess free translational and rotational motion. They have no positional ordering, but their long molecular axes are roughly aligned with respect to a preferred local orientation given by the director ( $\bar{n}$ ), (Fig. 1). A measure of this molecular ordering can be expressed by the equation:

$$S = \langle 3\cos^2\theta - 1 \rangle / 2$$

Where  $\theta$  is the angle between  $\bar{n}$  and the long molecular axis at any given point.  $\langle \rangle$  represents an average, and S becomes unity for  $\theta$  equal to zero. Actual values of S can vary on heating from between 0.8 to 0.4 at the nematic to isotropic transition.<sup>4</sup> In a bulk sample of nematic material the director will not be constant, but will fluctuate enormously due to the free-flowing, liquid-like nature of the phase. This variation in  $\bar{n}$  gives rise to arbitrary gradients in the refractive index and light scattering effects throughout the medium which cause the characteristic 'milky' appearance observed.

If a nematic phase is composed of optically active molecules, then its gross structure is modified to give a cholesteric phase. In this structure the same relationship exists between molecular orientation and  $\bar{n}$  as in the nematic phase. However, due to the molecular chirality<sup>5</sup>, the director itself varies uniformly throughout the medium in a

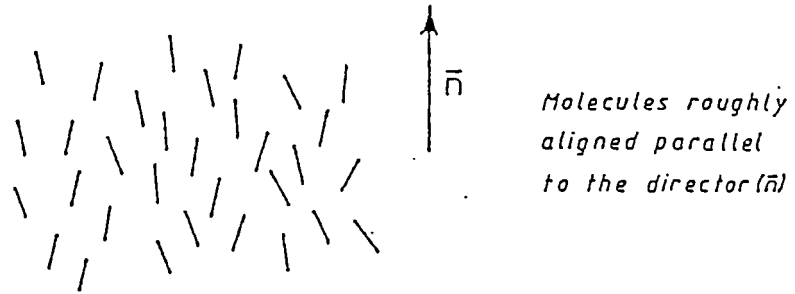


Fig.1. Ordering in the nematic phase.

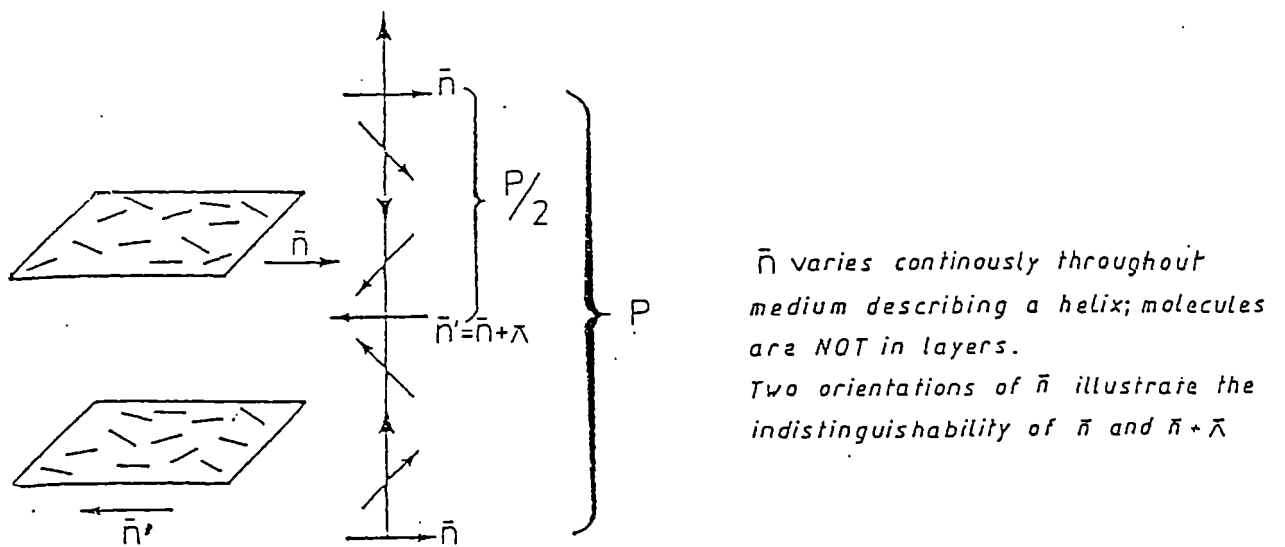


Fig.2. Structure of cholesteric phase.

direction orthogonal to the molecular long axis, describing a helix of half-pitch<sup>IV</sup> length  $P/2$ . (Fig. 2). Two important effects can be observed as a direct result of this helical ordering. Firstly, the helical structure selectively reflects light<sup>6</sup> according to the equation:

$$\lambda = nP \sin \theta$$

where  $\lambda$  is the wavelength of reflected light and  $\theta$  is the angle between the incident light beam and the normal to the helical axis.

As  $P$  usually decreases with increasing temperature and is often in the visible spectral range, a variation in temperature will give rise to a corresponding shift (red-blue) in the observed colour. This phenomenon has already been exploited in the fabrication of cholesteric liquid crystal thermometers and other thermochromic devices.

Secondly, the helix is itself chiral and will rotate plane polarised light to the right (D) or left (L), depending on both the absolute configuration and position of the asymmetric centre within the constituent molecules.<sup>7</sup>

The cholesteric phase may also be induced from a nematic phase by the addition of optically active molecules. The extent of this 'doping' will affect the helical pitch length and thermal stability of the induced cholesteric phase,

---

IV. Two arbitrarily chosen orientations  $\bar{n}$  and  $\bar{n} + \pi$  are indistinguishable (see Fig. 2), and therefore the periodicity observed optically<sup>6</sup> corresponds to  $P/2$  and not  $P$ .

according to the mixing compatibility and mesogenic properties of the 'dopant'. Generally, as dopant concentration increases<sup>V</sup>, helical pitch length and thermal stability decreases.

Finally, it should be apparent that a material cannot exhibit both a nematic and a cholesteric phase, as the existence of one precludes the other, i.e., the cholesteric phase is simply a chiral nematic phase (Ch=N\*).

### 1.2.2 The Smectic A (S<sub>A</sub>) Phase.

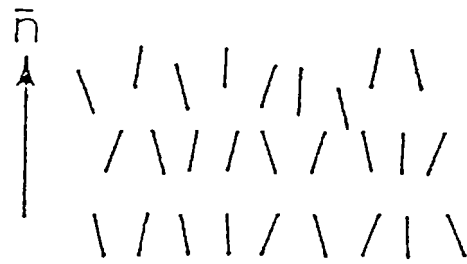
The smectic A (S<sub>A</sub>) phase is the smectic phase of highest thermal stability and can only be preceded by the nematic (or cholesteric) phase on cooling an isotropic liquid.

Within the S<sub>A</sub> phase the molecules are arranged in layers, with their centres of mass randomly distributed and their molecular long axes aligned roughly parallel to the layer normal. (Fig. 3). The molecules are ordered haphazardly, in a head to tail manner and undergo free rotation about their molecular long axes.

The friction between layers is very small, allowing them to slide over one another easily. This may be illustrated simply by placing S<sub>A</sub> material between a glass support and cover slip and observing how easily the cover slip is moved.

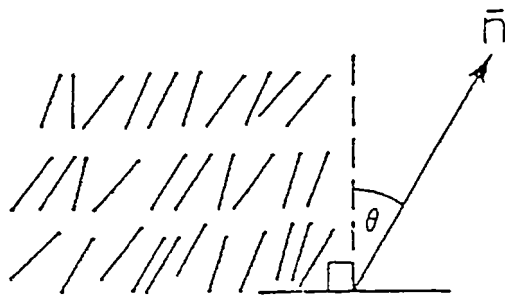
---

V. Even the addition of an infinitesimal amount of a chiral dopant will result in the formation of a cholesteric phase from a nematic phase, although the pitch length in this case would approach infinity.



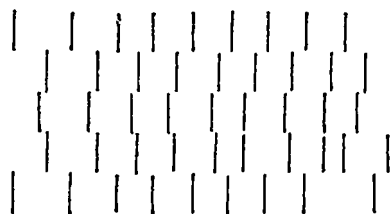
*molecules are in layers  
and aligned roughly parallel  
to the layer normal.*

*Fig.3. Ordering in the  $S_A$  phase.*



*Molecules have their m.l.a.  
roughly aligned parallel to  
the director, which is tilted  
at an angle  $\theta$  with respect  
to the layer normal.*

*Fig.4. Ordering in the  $S_C$  phase.*



*molecules have local positional  
order within each layer, but there  
is little or no positional correlation  
between layers.*

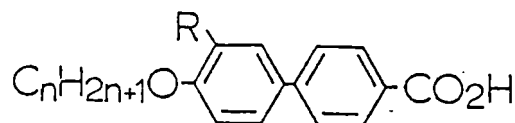
*Fig.5. Ordering in the  $S_B$  hex phase.*

X-ray measurements show that the layer spacing ( $d$ ) in the  $S_A$  phase may sometimes be less than<sup>VI</sup> the extended molecular length ( $l$ ).<sup>8</sup> This observation might seem to be consistent with a tilted structure, which would contradict observations that show the  $S_A$  phase to be optically uniaxial. These apparently conflicting facts can be reconciled if the molecules are slightly tilted with respect to the layer normal, but with totally random tilt directions. Passing through a large enough number of layers, the tilt direction will average to zero, resulting in an optical uniaxis normal to the layers and represented by the director ( $\bar{n}$ ).

Alternatively, since the molecules of many smectogens terminate in long flexible alkyl chains, the situation  $d < l$  can be explained by deviations of the liquid-like alkyl chains from an extended all trans-conformation.

### 1.2.3. The Smectic D ( $S_D$ ) or D Phase.

The smectic D ( $S_D$ )<sup>VII</sup> or D phase is extremely rare and up to the present day has only been observed in four compounds<sup>9,10</sup> having the general formula:



Where  $n = 16, 18$  and  $R = -\text{NO}_2, -\text{CN}$ .

VI. X-ray measurements have also revealed  $S_A$  phases where  $d > l$ . This is explained by the existence of different types of bilayer, usually caused by either dimer formation or anti-parallel correlations of the molecules.

VII. The term 'smectic' implies a stratified or layered arrangement of the molecules. As this is evidently not the case (see text) for this phase, it has been suggested<sup>11</sup> that it should simply be referred to as the D phase.

This phase may be formed either directly on cooling the isotropic liquid or indirectly via the  $S_A$  phase; this depends upon  $\bar{n}$  and  $R$ . In all four cases, the  $S_D$  phase has a higher thermal stability than the smectic C ( $S_C$ ) phase which therefore occurs below it.

The actual structure of the D phase has not been completely elucidated, but x-ray studies by Etherington et al.<sup>11</sup>, have established the existence of a primitive cubic lattice, possibly made up of micelles of uncertain dimensions. The unit cell contains ca 700 molecules. Optical observations show that the D phase is optically isotropic, supporting the x-ray evidence for a cubic structure.

#### 1.2.4. The Smectic C ( $S_C$ ) Phase.

The smectic C ( $S_C$ ) phase can be formed directly upon cooling the isotropic liquid, or indirectly via one or more of the phases outlined above. Its structure is essentially the same as the  $S_A$  phase but with the director tilted at an angle  $\theta$  with respect to the layer normal, (Fig. 4).

The tilt angle ( $\theta$ ) in the  $S_C$  phase can exhibit two distinct kinds of behaviour,<sup>VIII</sup> depending on the nature of the preceding phase.<sup>12</sup> On cooling from the  $S_A$  phase, as the

---

VIII. A claim had been made for a third type of behaviour, in which the layer spacing ( $d$ ) remained constant throughout both the combined ranges of the  $S_A$  and  $S_C$  phases.<sup>8</sup> However, this was later disproved by more precise measurements described in reference<sup>12</sup>.

temperature decreases,  $\Theta$  will initially increase relatively quickly. However, once the temperature has fallen to  $10^{\circ}\text{C}$  or  $15^{\circ}\text{C}$  below the transition temperature ( $T_c$ ), then usually  $\Theta$  will increase only slightly with further decrease in temperature. If the  $S_C$  phase persists over a wide temperature range then  $\Theta$  will normally acquire a value of between  $20^{\circ}$  and  $30^{\circ}$ .

The  $S_C$  phase formed on cooling the nematic (or cholesteric) phase or the isotropic liquid results in a large and essentially temperature independent value of  $\Theta$ , which remains in the range  $35^{\circ}$  to  $45^{\circ}$  throughout the phase range. IX

Although it is generally assumed that it is the molecules which tilt when the  $S_C$  phase is formed, this is not necessarily the case. Studies on liquid crystalline polyacrylates<sup>13</sup> revealed that, in field-orientated samples, at the  $S_A$  to  $S_C$  transition, the polymer side chains remained aligned in the electric field direction. The actual  $S_C$  structure was in fact achieved by the polymer backbones becoming inclined relative to the mesogenic groups which underwent translation, resulting in a more dense packing arrangement.

Many attempts have been made to explain the origin of the tilt in the  $S_C$  phase, though no single theory has been universally accepted. A brief summary of the more widely discussed hypotheses is given below.

---

IX. If the preceding phase is nematic, it may possess cybotactic groups of molecules in an  $S_C$ -like arrangement. The tilt angle in these cybotactic groups can be similar to that found in the  $S_C$  phase.

In 1973 McMillan<sup>14</sup> observed that many of the S<sub>C</sub> materials known at that time consisted of fairly symmetrical molecules, which contained polar groups linking the aromatic core to alkyl chains. He argued that at the S<sub>A</sub> to S<sub>C</sub> phase transition, the molecular rotations were 'frozen' out. These polar functions ('terminal' or 'outboard' dipoles) could then create an electrical torque, causing the molecules to tilt with respect to the layers. However, as molecules in the S<sub>C</sub> phase have subsequently been shown to rotate freely, and not all S<sub>C</sub> materials possess such polar groups, considerable doubt has been thrown on the validity of this theory.

Wulf suggested<sup>15</sup> that as most S<sub>C</sub> materials consisted of roughly symmetrical molecules, having 2 alkyl chains linked to a central aromatic core, their overall shape would be of a zig-zag nature. He proposed that these zig-zag shaped molecules could pack more efficiently when tilted and that this was the root cause of tilting in the S<sub>C</sub> phase.

A variation on this steric model was provided by Goodby<sup>16</sup> who presented an elaborate computer simulation of swept out rotational volumes for certain S<sub>C</sub> molecules. Based on the resulting shapes, he also concluded that most efficient packing could be achieved within a tilted structure. However, the importance of polar groups was also acknowledged by Goodby in relation to the thermal stability of the S<sub>C</sub> phase.

More recently, a new polar model has been proposed for the S<sub>C</sub> phase.<sup>17</sup> According to this theory, the rotating permanent dipole of one molecule induces a dipole in the

polarisable core of a neighbouring molecule. The induced attraction between molecules then causes an overall tilted structure in the phase. This theory, unlike that of McMillan, does not rely on the 'freezing' out of molecular rotation, but again it cannot be applied universally due to the non-polar nature of some  $S_C$  materials. It is clear therefore, that a satisfactory and universal explanation of tilt origin in the  $S_C$  phase must ultimately take into account the steric (zig-zag) features of the individual molecules, but must not depend on the presence of strong permanent dipoles.

#### 1.2.5 The Hexatic Smectic B ( $S_B$ hex), Smectic I ( $S_I$ ) and Smectic F ( $S_F$ ) Phases.

The hexatic smectic B ( $S_B$  hex) phase can be obtained directly on cooling the isotropic liquid or indirectly, via one or more of the preceding phases already described.

Within each layer the molecules have local hexagonal ordering and lie with their long axes parallel to the layer normal. This positional ordering is rarely correlated from layer to layer (although possibly in some cases between two layers); therefore individual layers (or pairs of layers) can slide over one another with relative ease, as in the  $S_A$  and  $S_C$  phases, (Fig. 5). The molecules do not rotate freely about their m.l.a., but in a co-operative manner, due to their mutual proximity. This co-ordinated rotational order is termed '6-fold degenerate' and arises from the hexatic nature of the molecular structure.

The smectic I ( $S_I$ ) and smectic F ( $S_F$ ) phases have essentially the same structure as the  $S_B$  hex phase, except that their molecular long axes are tilted with respect to the layer planes. In the  $S_I$  phase the molecules tilt towards an apex of the pseudo hexagonal net, whereas molecules in the  $S_F$  phase are tilted towards a pseudo hexagonal face,<sup>18</sup> (Fig. 6). Although this difference between the two phases appears superficial, x-ray and miscibility studies have confirmed their separate identities and well defined  $S_F$  to  $S_I$  transitions occur with a distinct enthalpy of transition.

Both the  $S_I$  and  $S_F$  phases can be obtained on cooling one or more of the previously mentioned phases or directly from the isotropic liquid. In cases where both phases are exhibited by a material<sup>19</sup> or mixture, the  $S_I$  phase has been shown to have the higher thermal stability.

#### 1.2.6. The Crystal Smectic B ( $S_B$ cryst), Smectic J ( $S_J$ ) and Smectic G ( $S_G$ ) Phases.

The crystal B ( $S_B$  cryst) phase can be formed immediately on cooling the isotropic liquid, or through one or more of the preceding phases outlined above. Within each layer, the molecules have an extensive hexagonal arrangement with their long axes parallel to the layer normal. In contrast with the  $S_{Bhex}$  phase, this positional order is correlated over many layers, thus giving the  $S_B$  cryst phase a crystal-like structure.<sup>X</sup> (Fig. 7).

---

X. The layers as shown in Fig. 7 are stacked in an ABAB...manner. This is not necessarily the case as they could just as well be stacked AAA...ABC...ABAC... etc. Furthermore, changes in stacking with change in temperature have been observed for  $S_B$  phases.

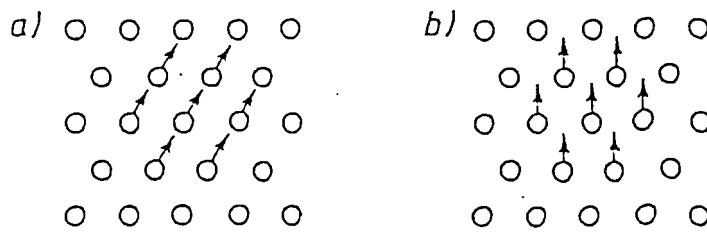


Fig.6. Plan view showing the molecular tilt direction (arrows) in; a), the  $S_I$  phase ~ toward an apex; b), the  $S_F$  phase ~ toward a face of the pseudo-hexagonal net.

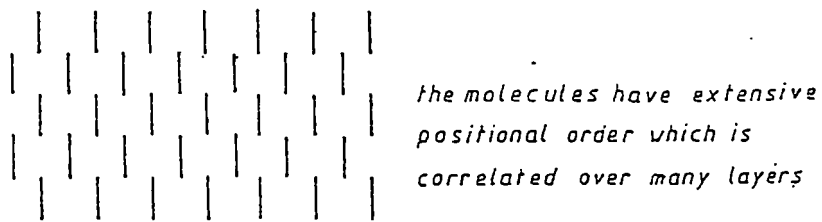


Fig.7. Ordering in the crystal  $S_\beta$  phase.

Although the layers can still undergo shear, the frictional forces opposing this motion are very much greater than those in smectic phases of higher thermal stability. The molecules again do not freely rotate about their long axes, but possess a six-fold degenerate rotational order, as in the  $S_B$  hex phase.

The smectic J ( $S_J$ ) and smectic G ( $S_G$ ) phases<sup>XI</sup> have the same fundamental structures as the  $S_B$  cryst phase, but their constituent molecules are tilted with respect to the layer normal. Molecules in the  $S_J$  phase tilt towards an apex and those in the  $S_G$  phase towards a face of the pseudo hexagonal net. From this description it is clear that they are in fact crystal-like analogues of the  $S_I$  and  $S_F$  phases respectively.

Both the  $S_J$  and  $S_G$  phases may be formed on cooling the isotropic liquid, but are usually obtained via one or more of the previously described phases, including the crystal  $S_B$  phase. Although little is known of their relative thermal stabilities, miscibility studies suggest that the  $S_J$  phase has a higher thermal stability than the  $S_G$  phase.<sup>20</sup>

#### 1.2.7. The Smectic E ( $S_E$ ), Smectic K ( $S_K$ ) and Smectic H ( $S_H$ ) Phases.

The smectic E ( $S_E$ ) phase may be obtained directly on cooling the isotropic liquid or the  $S_C$  or the  $S_A$  phase, although more commonly it is formed on cooling a hexatic or crystal B phase.

---

XI. These phases are also referred to as Crystal J (or G') and Crystal G phases. Similarly, the smectic E, K and H phases may be called Crystal E, K (or H'), and Crystal H phases respectively.

Within each layer, the molecules are tightly packed to give a 'chevron' or 'herring-bone' like arrangement defined by the rectangular cross-sections of the molecules. The molecular long axes lie parallel to the layer normal but the packing arrangement is orthorhombic and the positional order is strongly correlated through many layers. The layers may still undergo shearing, but the frictional forces opposing shear are very much stronger than in the  $S_A$  phase. As a result of the close packing, the molecules cannot rotate fully; instead they oscillate quickly about their long axes amongst six equivalent positions, the oscillations again occur in a co-ordinated fashion.

The smectic K ( $S_K$ ) and smectic H ( $S_H$ ) phases are the two tilted modifications of the  $S_E$  phase. As in the  $S_I$  and  $S_F$  phases they are differentiated by the direction of the tilt of their constituent molecules. However, it is still unclear as to which of the two phases correspond to a given tilt direction.

It is evident from the above that the  $S_E$ ,  $S_K$  and  $S_H$  phases are structurally very ordered and are indeed sometimes referred to as orientationally disordered crystals. Certainly they have more regular ordering than some polymeric materials that are regarded as being crystalline. Nevertheless, on the criterion of miscibility, these phases may still be classified as smectic liquid crystals.

#### 1.2.8. Asymmetric Smectic Phases.

Using optically active molecules, it has been possible

to synthesise mesogenic materials which exhibit any of the smectic phases outlined above, apart from the D phase.

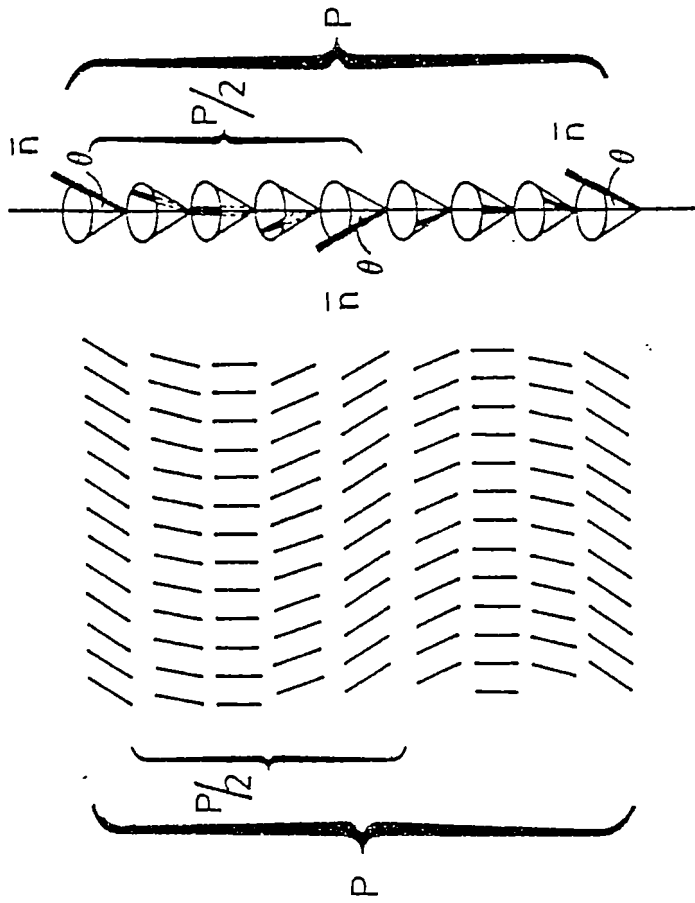
The use of chiral molecules does not in fact affect the gross structure of any of the orthogonal and crystalline smectic phases, but it does have a profound effect on the structures of the uncorrelated tilted smectic phases, ( $S_C$ ,  $S_I$  and  $S_F$ ). The occurrence of chiral centres in materials which exhibit tilted phases is indeed fairly common, as these phases are often associated with branching of alkyl chains.<sup>16.21</sup> That is, branching tends to promote the incidence of tilted phases.

The  $S_C$  phase composed of optically active molecules ( $S_C^*$ ) differs fundamentally from the  $S_C$  phase. The in-layer molecular ordering and rotational freedom are identical, but the interlayer interactions between chiral molecules causes a continuous and smooth change in the orientation of the director. On passing through a succession of layers, the director rotates about the surface of a cone, describing a helix of pitch-length  $P$  (Fig. 8).  $P$  commonly lies within the range of a few micrometers and decreases with falling temperature.

As in the cholesteric phase, this helical ordering means that the  $S_C^*$  phase is itself chiral and therefore, depending on the chiral nature of the material, will rotate plane polarised light to the right (D), or left (L).

Also by analogy to cholesterics, the  $S_C^*$  phase will exhibit the property of selective reflection of incident light. However, in contrast to the cholesteric phase,  $P$  and  $P/2$  are now distinguishable (Fig. 8), so that the  $S_C$  helix

molecular ordering      orientation of director



On passing through many layers, the director can be represented as precessing around the surface of a cone, describing a helix. The director maintains a constant tilt angle ( $\theta$ ) to the helical axis, which is normal to the smectic layers.

Fig.8. Helical ordering of the  $S_C^*$  phase.

shows an additional reflection band (full pitch band) at about twice the wavelength of the 'normal' band.<sup>6</sup>

The chiral smectic I ( $S_I^*$ ) and chiral smectic F ( $S_F^*$ ) phases also have helical structures similar to that of the  $S_C^*$  phase and consequently may exhibit the properties outlined above. They will however, tend to show larger pitch-lengths than in the  $S_C^*$  phase due to their more extensive bond orientational order.<sup>22</sup>

In the more crystalline tilted phases composed of optically active molecules ( $S_J^*$ ,  $S_G^*$ ,  $S_K^*$  and  $S_H^*$ ), the long-range positional ordering of the molecules between layers tends to suppress helix formation.<sup>19</sup> It has however, been reported<sup>23</sup> that the  $S_J^*$  phase of optically active  $8SI^{XII}$  does have a helical structure of pitch-length  $3\mu\text{m}$ .

Despite differences in structure and fluidity, the seven tilted asymmetric phases have one important property in common. They may all exhibit ferroelectric properties.

### 1.3. Ferroelectricity.

#### 1.3.1. Ferroelectric Crystals.

Until 1975, all known ferroelectric compounds were either inorganic crystalline oxides or salts, and their derivatives in the form of ceramics. The first of these compounds to be so recognised was sodium potassium tartrate tetrahydrate, or Rochelle salt. Although originally

---

XII. S-(+)-4-(2-methylbutyl) phenyl 4' -n-octylbiphenyl-4-carboxylate.

synthesised in the 17th. century as a laxative, it was only in 1920 that its ferroelectric properties were discovered and the phenomenon was reported.<sup>24</sup>

The characteristic of a ferroelectric material is that it can exhibit a net (spontaneous) polarisation in the absence of an applied field (E) and that this polarisation can be reoriented by an applied field. This effect can be directly observed on an oscilloscope, when a ferroelectric compound is subjected to a high frequency (ca 50 Hz) A.C. field. A non-ferroelectric substance, under these conditions, will display a linear relationship between polarisation (P) and applied field, whereas for a ferroelectric sample, the effect of this interaction is described by a hysteresis loop.<sup>25</sup> (Fig. 9). The term 'ferroelectricity' has no relationship to iron, but arises by analogy with ferromagnetism, where magnetic induction and magnetic field interactions portray a similar hysteresis loop.

The fundamental origin of spontaneous polarisation ( $P_s$ ), though not fully understood, emanates from an ionic displacement or molecular movement within a crystal lattice. In Rochelle salt, the effect is associated with hydrogen bonds which can rearrange with a reversal of field. In barium titanate, one of the most extensively studied ferroelectric materials, it has been suggested that the polarisation arises from a very small (0.1 Å) displacement of the titanium ion relative to the octahedral distribution of oxygens.<sup>26</sup> What is certain is that spontaneous polarisation is only associated with a crystal lattice having a unit cell

Polarisation ( $P$ ) increases steeply ( $AB$ ) and then linearly ( $BC$ ) as the field ( $E$ ) increases. As field is reduced, the polarisation falls at a slower rate than it rose, so that at  $E=0$  a residual polarisation ( $P_r$ ) exists. A coercive field ( $E_{coerc}$ ) is then needed to lower the polarisation to zero and a higher negative field reverses the  $P$ - $E$  interaction. The value of spontaneous polarisation ( $P_s$ ) is obtained by extrapolating  $CB$  to zero field, but in a homogeneously aligned (or a single domain) sample  $P_s = P_r$  (see later text).

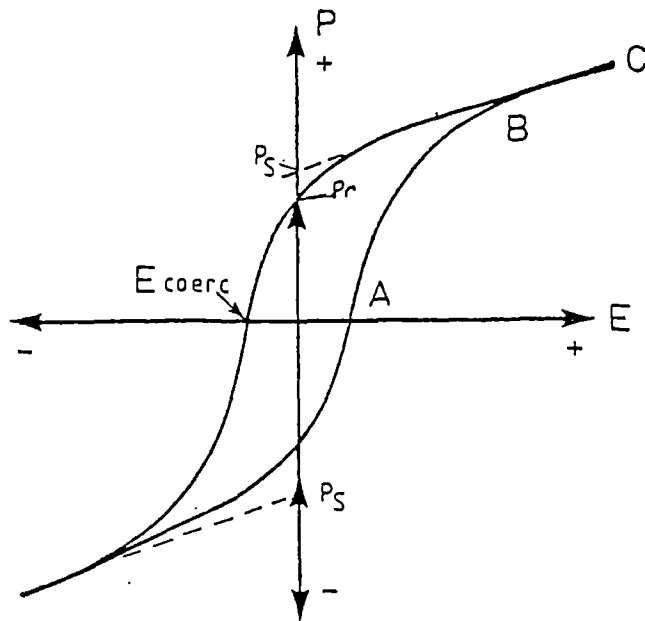


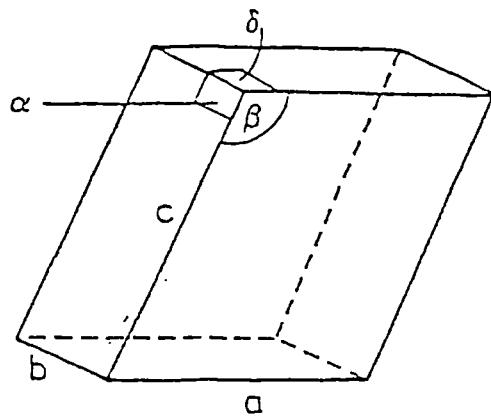
Fig. 9. Hysteresis loop obtained for a ferroelectric sample.

of low symmetry, e.g. monoclinic (Fig. 10), and more importantly, where the resulting structure has no centre of symmetry.

A general feature of ferroelectric materials is that the spontaneous polarisation only exists over a limited temperature range and falls to zero on approaching certain temperature boundaries (Fig. 11). These sudden changes in behaviour stem from crystal-crystal transitions and are accompanied by an increase in lattice symmetry. The temperature at which a change of this nature occurs is commonly referred to as the transition temperature ( $T_c$ ) or Curie point.

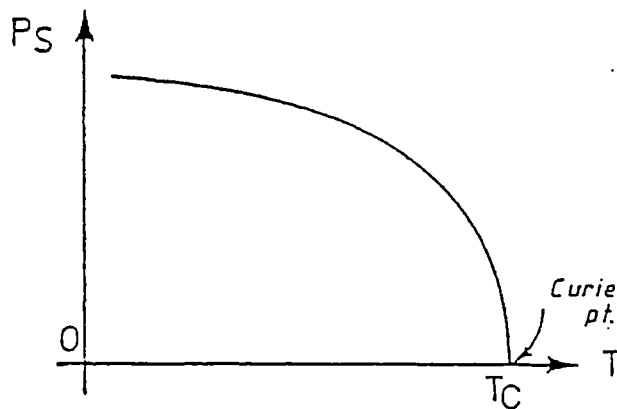
Rochelle salt has a monoclinic crystal structure in its ferroelectric phase which exists between  $-18^\circ\text{C}$  (lower Curie point) and  $24^\circ\text{C}$  (upper Curie point). Outwith these limits the crystal structure is orthorhombic, i.e., of higher symmetry, and no longer ferroelectric. Similar behaviour is observed for barium titanate which has a cubic perovskite structure above  $120^\circ\text{C}$ . On cooling below this Curie point, the material passes through a sequence of three crystal structures of lower symmetry, each of these being ferroelectric.

In figure 9 it was shown that when  $E = 0$ , the remnant polarisation ( $P_r$ ) was less than the spontaneous polarisation ( $P_s$ ) obtained by extrapolation of the linear part of the hysteresis loop. This can be explained by considering that the ferroelectric sample actually consists of many unique regions called domains. The direction of  $P_s$  varies from one



$$a \neq b \neq c, \alpha = \delta = 90^\circ \\ \beta > 90^\circ$$

Fig.10. An example of a low symmetry monoclinic unit cell.



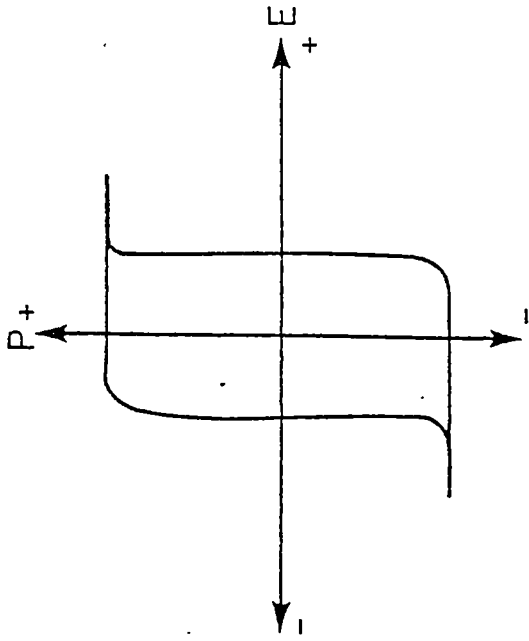
As temperature is increased  $P_S$  begins to decrease, dropping sharply to zero at the transition temperature (Curie point)  $T_C$ .

Fig.11. Spontaneous polarisation vs temperature.

domain to another, so that in a non-aligned sample the overall polarisation is reduced to zero. When a field is applied, the domains reorientate so that their polarisations are aligned with the field. When the field is removed, there will be a tendency for some domains to revert to their original positions and so  $P_r$  will be lower than the true  $P_S$ . However, in a large single domain crystal or homogeneously aligned sample, the domains will be more inclined to remain in their field-orientated positions once the field is removed, and will only be reoriented by a reversal of <sup>the</sup> field. The hysteresis loop stemming from this type of sample will be almost rectangular in shape, giving  $P_r$  equal to  $P_S$  (Fig. 12).

### 1.3.2. Ferroelectric Liquid Crystals.

At present it seems that no all-embracing theory of ferroelectricity has been universally accepted. However, it is apparent that the phenomenon necessitates a structure having a low symmetry environment and no centre of symmetry. Bearing this in mind, Meyer realised that the  $S_C^*$  phase, or any tilted smectic phase composed of optically active molecules, ought to be ferroelectric. By first describing the symmetry operations of molecules in the  $S_C$  phase, he went on to show how the introduction of chirality resulted in a structure capable of displaying ferroelectric properties. Although in his discussion, Meyer assumed a molecule which was symmetrical about its central core, this is not generally the case. Perhaps the arguments can be better illustrated by considering two unsymmetrical molecules in a head to tail arrangement and using these to demonstrate the symmetry



*For a single domain crystal or homogeneously aligned sample, an almost rectangular hysteresis loop is obtained.*

*At  $E = 0$  ;  $P_r = P_s$ .*

*Fig.12. Hysteresis loop obtained for a single domain crystal.*

operations of molecules within a single layer of the  $S_C$  and  $S_C^*$  phases.

The unsymmetrical molecules can be given zig-zag representations (Fig. 13), which illustrate the aromatic core and dissimilar alkyl chains. Analogous models for describing molecules in the  $S_C$  and  $S_C^*$  phases have already been proposed<sup>27,28</sup> and imply a time-averaged, all-trans (anti) conformation of the alkyl chains. Other models also infer that the aromatic core has a different tilt angle from the alkyl chains. Although this is not necessarily always the case, it has been confirmed for some  $S_C$  materials<sup>12</sup> and is also suggested by other evidence which will be discussed later (measurement of  $\theta$ ).

### 1.3.3. Symmetry of the $S_C$ Phase.

In a tilted smectic phase, the plane which contains both the layer normal and the director ( $\bar{n}$ ) is called the tilt plane. Molecules within a layer of the  $S_C$  phase can be said to have a low symmetry, monoclinic environment and to lie approximately in a plane parallel to the tilt plane.<sup>29</sup>

Reference to figure 13 demonstrates the three symmetry elements of molecules within a layer of the  $S_C$  phase, as defined by Meyer. These are:

- a) a centre of symmetry: a line drawn from any point on molecule X (e.g. A) and passing through this centre, encounters an identical point on molecule Y.

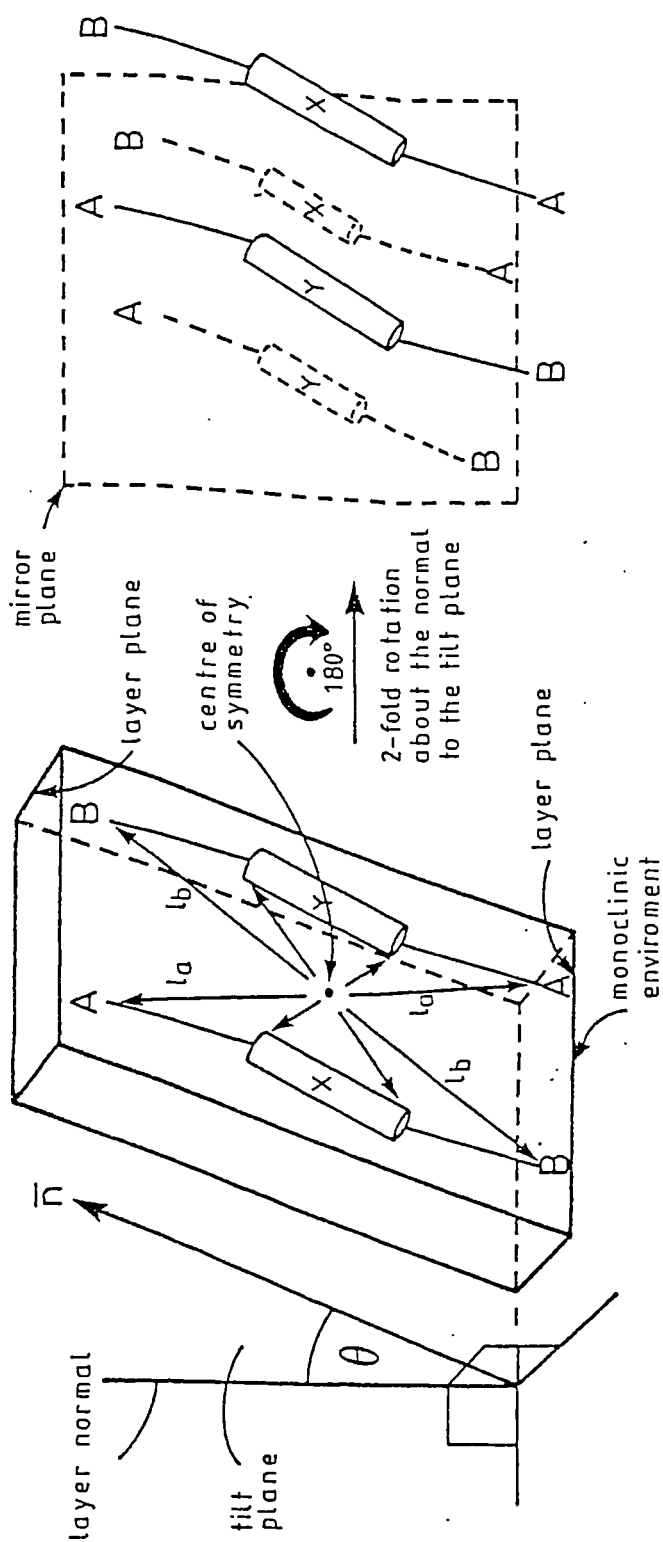
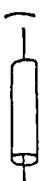


Fig.13. Molecules in a layer of the  $S_C$  phase.

The in layer structure is represented by two unsymmetrical molecules having a head to tail arrangement. The zig-zag model shows the aromatic core (——) and two dissimilar alkyl chains (—A, and —B).

- b) a mirror plane, parallel to the tilt plane:  
molecules have the same random head-to-tail  
arrangement on both sides of such a plane.
- c) a two-fold rotational axis: parallel to the plane  
of the layer and normal to the tilt plane.

An undisturbed bulk sample of the  $S_C$  phase with the director uniformly oriented could also undergo the above symmetry operations, as the structure would be identical throughout.

#### 1.3.4. Symmetry of the $S_C^*$ Phase.

By introducing a chiral centre into the molecules, the symmetry of the in-layer structure is further reduced. The centre of symmetry and mirror plane disappear, leaving only a two-fold axis parallel to the layer plane and perpendicular to the tilt plane, (Fig. 14).

The resulting in-layer structure of the  $S_C^*$  phase is therefore compatible with a structure generally associated with a ferroelectric material, i.e., it has a low symmetry (in this case monoclinic) environment and no centre of symmetry.

#### 1.3.5. Spontaneous Polarisation.

The statistical head-to-tail model can also be used to demonstrate how a spontaneous polarisation may arise in the layers, (Fig. 15). Consider a significant dipole ( $\mu$ ) arbitrarily assigned to the  $C^*—B$  bond;

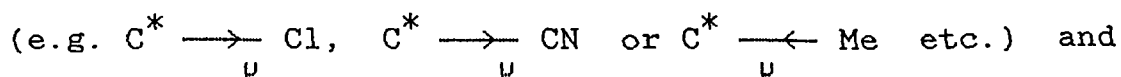
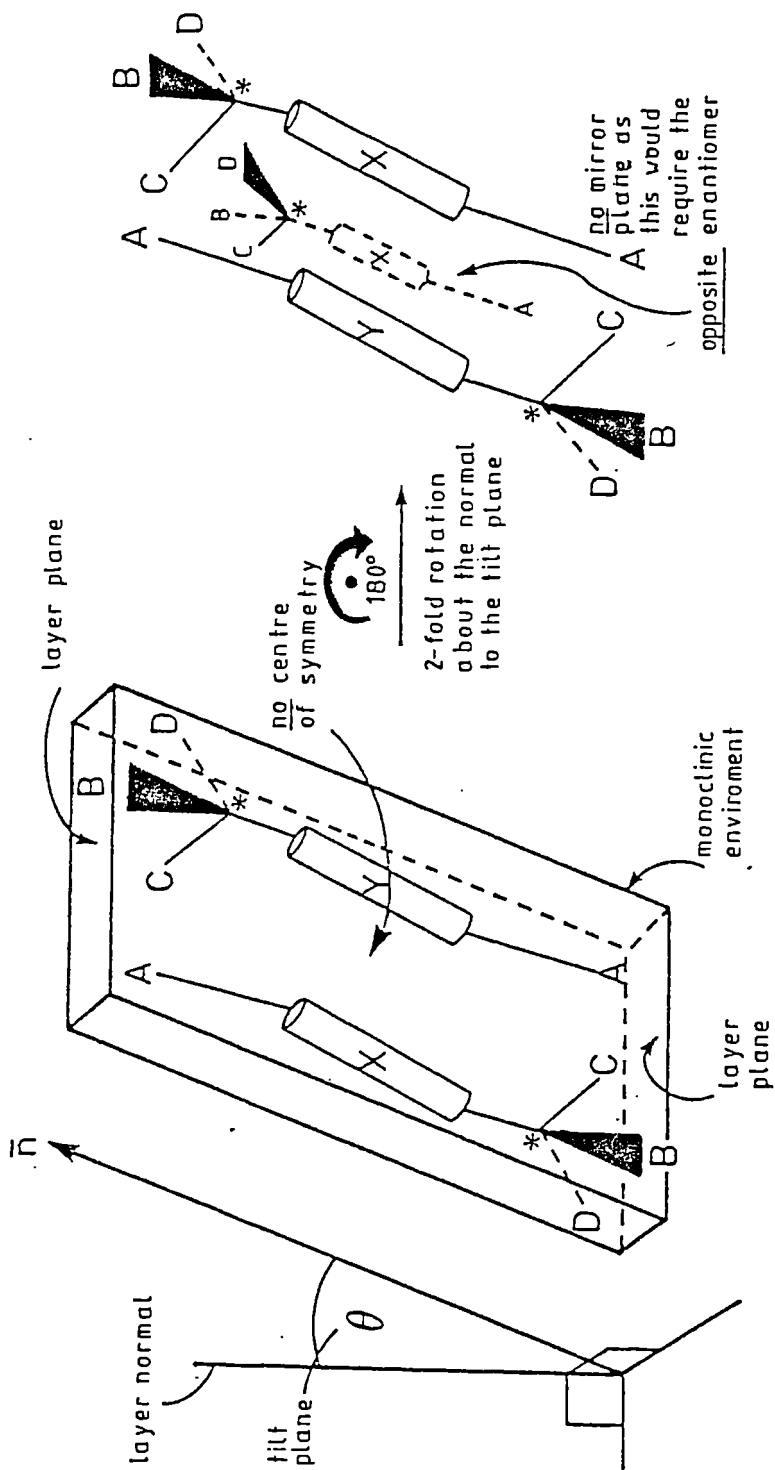
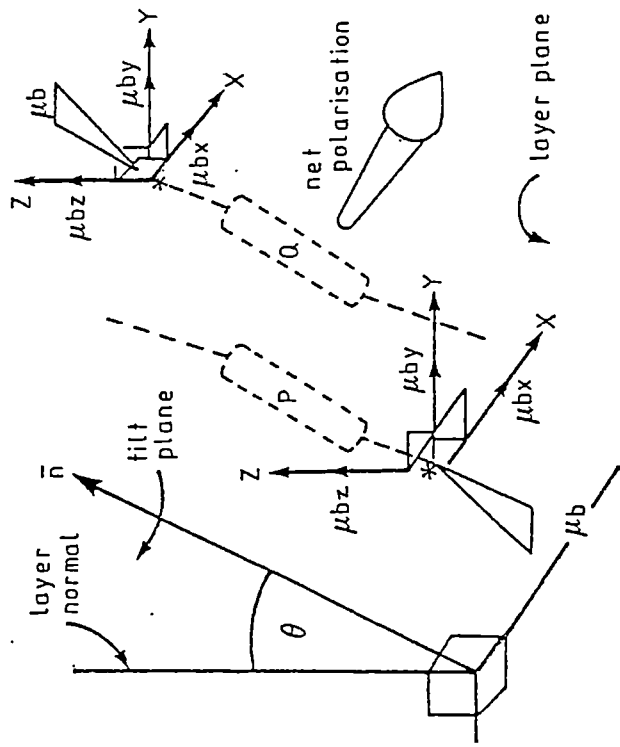


Fig.14. Chiral molecules in a layer of the  $S_C^*$  phase.



$B, C, D$  and core- represents the 4 dissimilar groups attached to a carbon atom which is therefore asymmetric, and show how introduction of chirality results in a structure having low symmetry (monoclinic) environment and no centre of symmetry.



X, Y, and Z directions are mutually perpendicular  
 X normal and Y parallel to tilt plane; Z parallel  
 to layer normal  
 For molecule P, dipole moments in X, Y and Z direction:  
 +  $\mu_{bx}$ , -  $\mu_{by}$ , -  $\mu_{bz}$ .  
 For molecule Q, dipole moments in X, Y and Z direction:  
 +  $\mu_{bx}$ , +  $\mu_{by}$ , +  $\mu_{bz}$ .  
 Therefore the overall polarisation is zero in every  
 direction except the X direction, i.e. parallel to the  
 plane of the layers and normal to the tilt plane.

Fig. 15. Schematic showing direction of polarisation within the layers.

split into three component dipole moments at right angles to each other ( $\mu_{bx}$ ,  $\mu_{by}$  and  $\mu_{bz}$ ). Throughout a whole layer it is evident that any component of this dipole acting in a direction normal to the layers ( $\mu_{bz}$ ), or parallel to the tilt plane ( $\mu_{by}$ ), will be cancelled. Consequently a net polarisation can only exist in the direction of the two-fold rotational axis, i.e. parallel with the plane of the layers and normal to the tilt plane ( $\mu_{bx}$ ).

As mentioned previously, the  $S_C$  phase is characterised by a helical distribution of the director on passing through a succession of layers. Therefore a bulk sample of the  $S_C^*$  phase will also undergo a symmetry operation of two-fold rotation, about an axis perpendicular to the helical axis.<sup>30</sup>

A more important consequence of this helical structure is that as the direction of polarisation in each layer is inextricably linked to the orientation of the director, the overall polarisation of the sample will be averaged to zero. (Fig. 16). Only if the helix can be in some way unwound will a bulk sample of  $S_C^*$  material be capable of exhibiting a macroscopic ferroelectric effect.

The symmetry considerations applied to a single layer of the  $S_C^*$  phase, can also be used to account for the appearance of a spontaneous polarisation in other tilted, asymmetric smectic phases. However, as in the  $S_C^*$  phase, bulk samples of these phases have their overall polarisation reduced to zero. In the  $S_I^*$  and  $S_F^*$  phases this is again due to helix formation. In the  $S_J^*$ ,  $S_G^*$ ,  $S_K^*$  and  $S_H^*$  phases, the helix may be largely, or totally unwound by interlayer 'crystal

$\oplus$  and  $\ominus$  represent positive and negative charge respectively protruding from the plane of the paper.

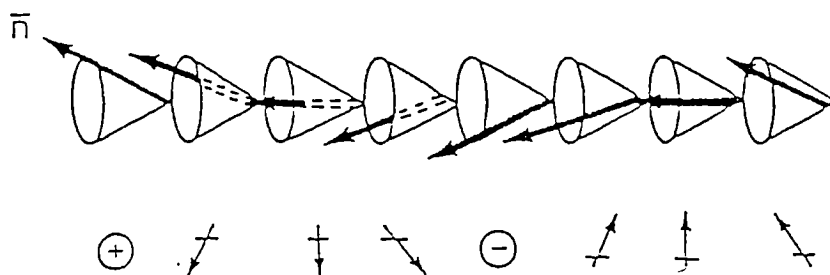
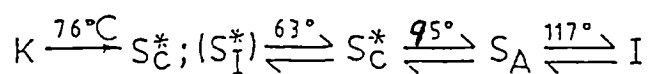
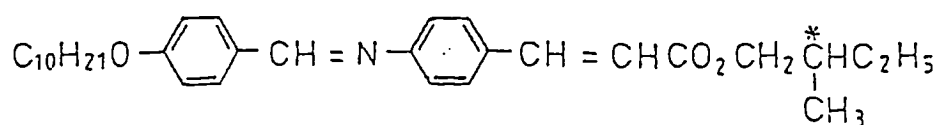


Fig.16. Helical distribution of the director reduces polarisation to zero.



Where brackets ( ) indicate a monotropic phase (see later).

Fig.17. Structure of DOBAMBC.

forces'. Any ferroelectric behaviour then arises from the effect over many layers in single unwound domains. Over the entire sample, the domains are likely to adopt all possible orientations, and the polarisation is again averaged to zero. Only if most domains could be aligned, would a macroscopic ferroelectric effect be possible.

As a result of his hypothesis, Meyer et al. went on to synthesise a  $S_C^*$  material, 'DOBAMBC'.<sup>XIII</sup> They were able to confirm the existence of a spontaneous polarisation, thereby providing the first evidence for ferroelectric liquid crystals, (Fig. 17).

#### 1.3.6. The Surface Stabilised Structure.

Clearly, for the  $S_C^*$  phase to exhibit a bulk spontaneous polarisation, the helical distribution of the director must be unwound. This is usually achieved by one of the three methods outlined below:

- a) Application of a shear in a direction parallel to the layers induces a spontaneous polarisation at right angles to the shear direction.<sup>31</sup> This technique was first used to corroborate the existence of spontaneous polarisation in DOBAMBC.<sup>32</sup>
- b) Application of a d.c. or low frequency a.c. field normal to the helical axis (i.e. parallel to the

---

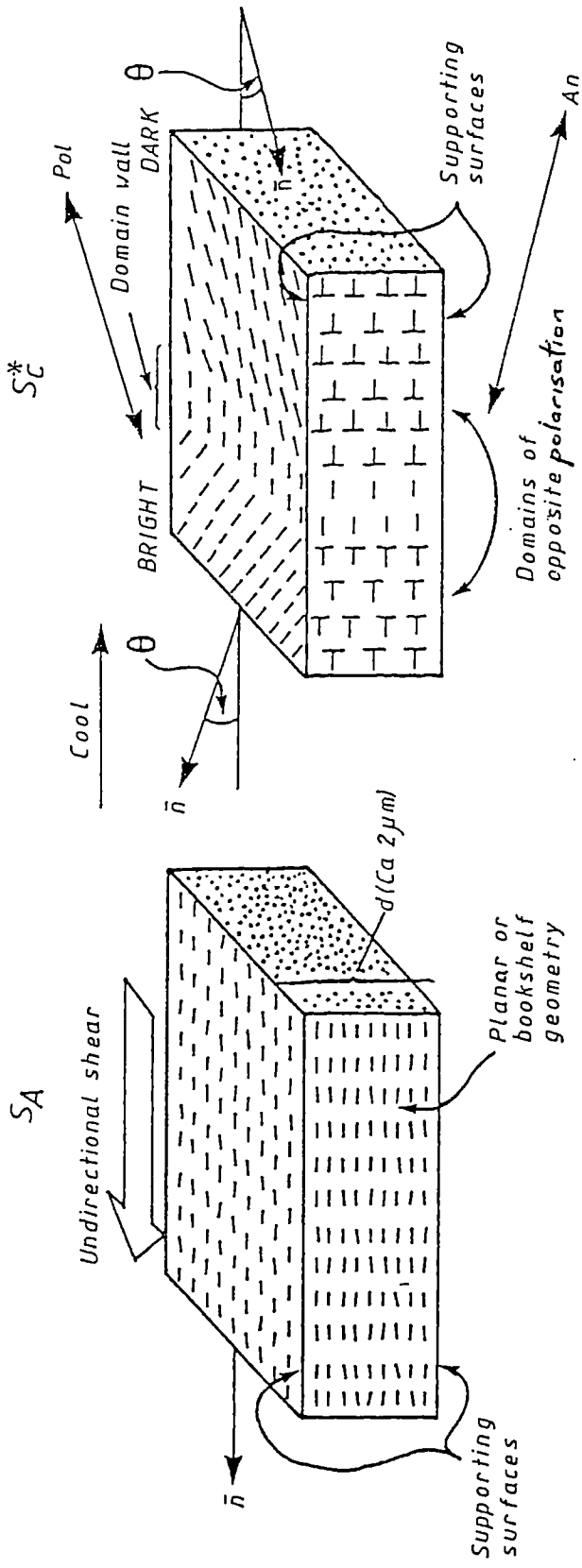
XIII. p-decyloxybenzylidene-p'-amino  
2-methylbutylcinnamate<sup>3</sup> or more correctly named  
S-2-methylbutyl 4-(4'-n-decyloxybenzylidene)  
aminocinnamate.

smectic layers) couples with the polarisation in the layers.<sup>33</sup> As the field increases, the pitch-length increases, until at a crucial field ( $E_c$ ) the helix is unwound.

- c) **Surface interactions in very thin samples** (ca  $2\mu\text{m}$ ) may be used to unwind the helix elastically and so give a surface stabilised ferroelectric liquid crystal structure (SSFLC structure). This structure was first described by Clark and Lagerwall<sup>2,34</sup> and has subsequently become the model on which the majority of molecular and device considerations are based.

There are two important requirements which must be met in order to achieve this structure. Firstly, the material in question must have a  $S_A$  phase above the  $S_C^*$  phase for ease of alignment. Secondly, the supporting surfaces must be prepared so that the individual molecules will lie with their molecular long axes in the plane of the surfaces, but with no strong tendency to align in any particular direction.

The sample is usually cooled from the isotropic liquid into the  $S_A$  phase and given a gentle unidirectional shear in order to promote a uniform orientation of the director. This, in combination with an appropriate surface preparation, forces the smectic layers to stand perpendicular to the supporting surfaces and adopt a 'planar' or 'book-shelf' geometry, normal to the shear direction, (Fig. 18). Further cooling into the  $S_C^*$  phase causes the molecules to tilt with respect to the normal to the layers. If the sample thickness



On cooling into  $S_C^*$  phase, molecules tilt into one of two orientations. By aligning the polariser (pol) with orientation of the director in one domain, this domain appears dark, while an adjacent domain will appear bright. Each domain shown is ferroelectric but of opposite polarisation.

Fig.18. Planar geometry of SSFLC structure in SA and  $S_C^*$  phase.

(d) is sufficiently small (ca  $2\mu\text{m}$ ) and is less than the pitch-length ( $p$ ) of the material, then the surface interactions will tend to quench the helical structure and constrain the molecules to lie in one of two stable, equal energy states of opposite alignment. Areas adopting each state are ferroelectric and are called 'domains', by analogy with the structures occurring in crystalline ferroelectrics. These domains can be directly observed using a polarising microscope. Aligning the polariser with the director in one domain will make all domains having that orientation dark, while domains having the alternative orientation will appear bright,<sup>35</sup> (Fig. 18). Moving the polariser so that the appearance of adjacent domains is reversed requires a rotation of  $2\theta$ .

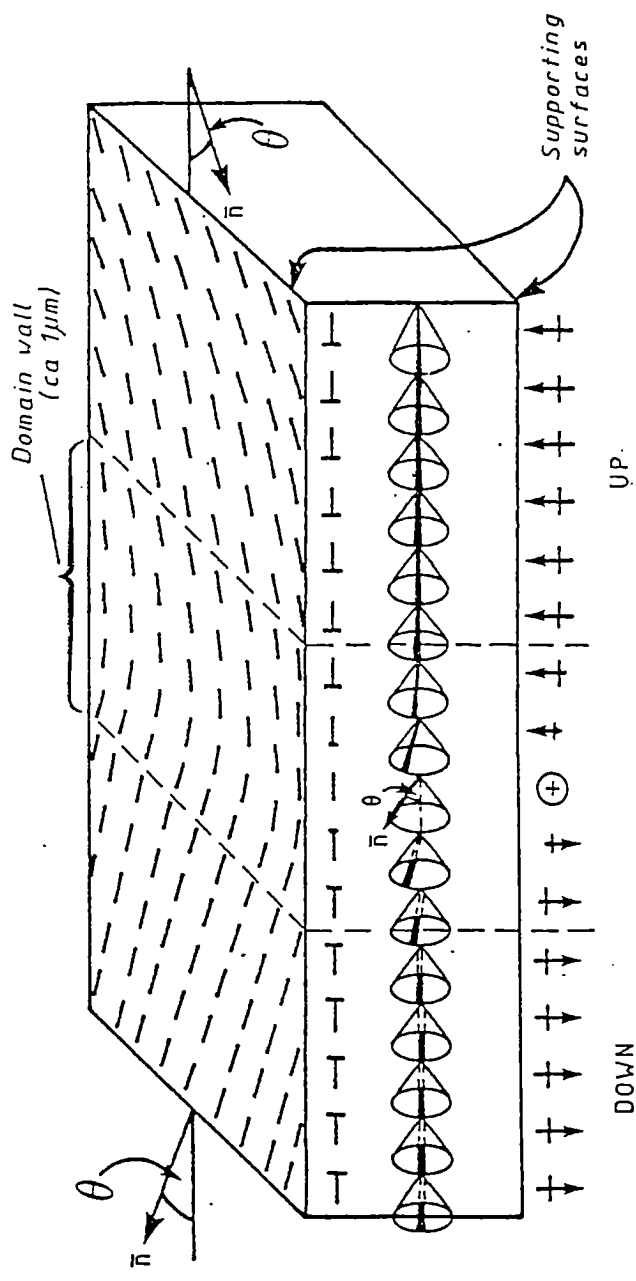
However, if the polariser is placed so that neither orientation contrasts with the other, adjacent domains can still be distinguished by dark boundaries called 'domain walls'. These walls are approximately  $1\mu\text{m}$  across and are in fact areas of continuous degeneracy connecting domains of one preferred alignment to the other, (Fig. 19).

As indicated in figure 19, each domain is itself a ferroelectric volume and is associated with a polarisation facing UP or DOWN according to the orientation of the local director. Over a large sample area many domains may be present, resulting in a net polarisation averaged to zero.

Nevertheless, by applying an electrical field across the sample, domains with their polarisation in the direction of the field will grow through domain wall motion, until the



Molecules precess about the surface of a cone on passing through a domain wall, connecting one preferred alignment to another.



(—|) Indicates molecule with its right end closer to the observer.

(↑ and ↓) Indicates magnitude and direction of polarisation associated with each layer.

Fig.19. Schematic of a domain wall.

whole sample becomes a monodomain. This monodomain structure can also be achieved by slowly cooling the  $S_A$  phase in the presence of a magnetic or electric field, thus preferentially ordering the molecules in the  $S_C^*$  phase. When the field is removed, there remains a monodomain structure having a net polarisation in the UP or DOWN state and possessing electro-optical and switching characteristics ideal for device application.

### 1.3.7. Device Application.

The major device application of liquid crystals so far has been based on the liquid-like nematic phase and its use in the twisted nematic cell. Although this has been a very successful electro-optic device, it does have three important drawbacks which restrict its use.:

- a) the response time ( $\tau$ ) is limited to the millisecond range.
- b) the field must be maintained continuously in order to preserve the on state.
- c) multiplex driving becomes more complicated as the number of pixels increase, thereby limiting the size and definition of the display and compounding the inherent viewing angle problem.

A novel electro-optical device using  $S_C^*$  materials in the SSFLC geometry is suggested<sup>35</sup> as a means of overcoming some of the above restrictions. The mode of operation is as follows: The glass-supporting surfaces are coated with a transparent conducting material such as indium-tin oxide (ITO), which may be etched to obtain a desired electrode

pattern. A uniform sample thickness (2-3  $\mu\text{m}$ ) is maintained by evaporating strips of silicon oxide ( $\text{SiO}$ ) on to the inner surfaces of the supports.<sup>XIV</sup> The  $\text{S}_\text{C}^*$  material is aligned as described earlier and an electric field is applied across the cell. The spontaneous polarisation of the sample couples with the field, forcing the molecules to adopt a particular orientation, which they retain once the field is removed. Aligning the polariser with the director gives a position of extinction and makes the cell appear DARK. Reversing the field polarity re-orientates the molecular director so that it is aligned with neither the polariser nor the analyser; this gives a BRIGHT state, (Fig. 20). If the field is again removed, the cell will remain bright and a resultant spontaneous polarisation will persist in the same direction. This property is referred to as bistability and illustrates the true ferroelectric behaviour of the device. Initial studies indicated that the resulting electro-optical effects were characterised by:

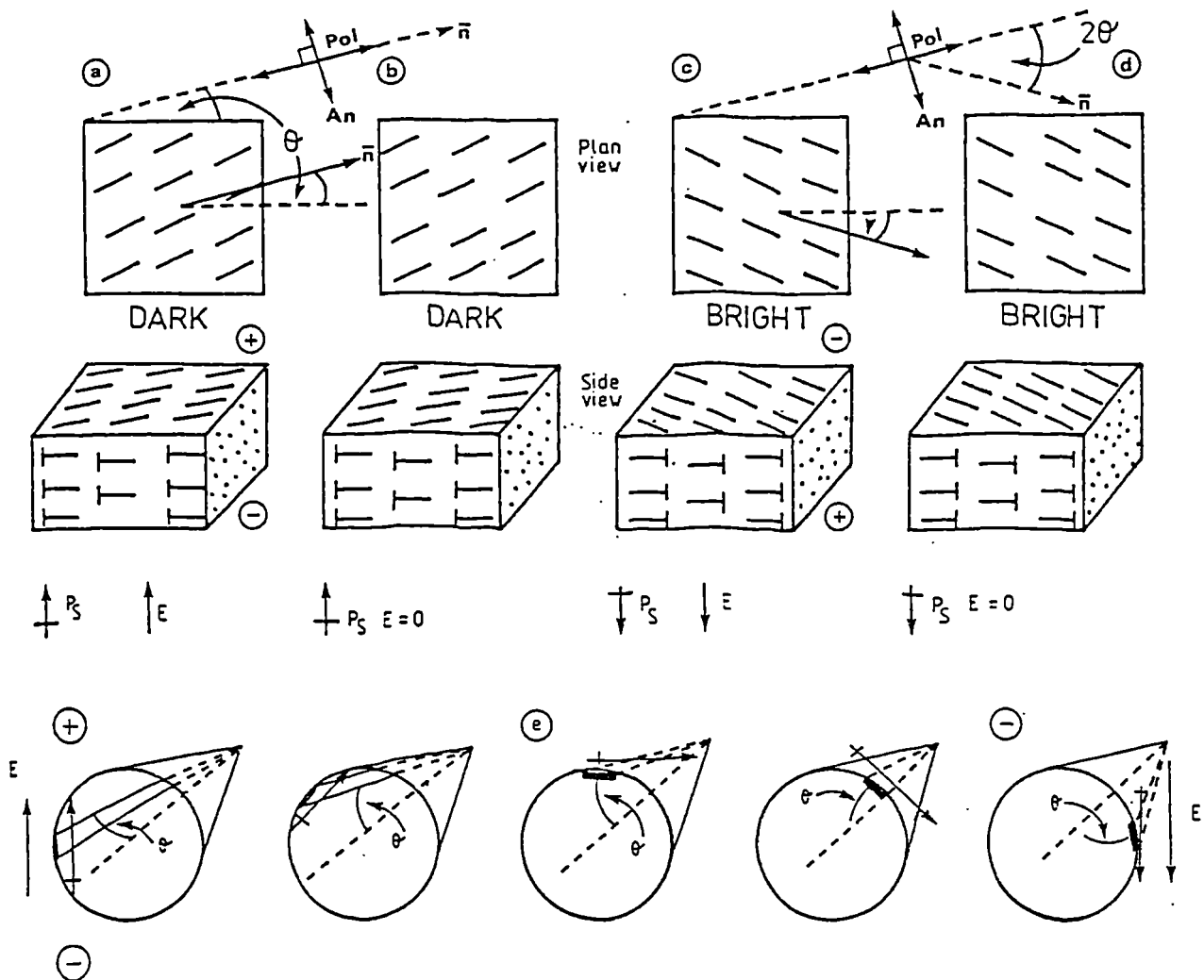
- a) fast responses in the microsecond range;
- b) bistability;
- c) a sharp threshold voltage.

The combination of b) and c) in principle gives greater ease of multiplexing the device, enabling fabrication of larger and better defined displays.

---

XIV. More recently, small plastic spheres of known diameter have been used to obtain a uniform sample thickness by intimately mixing them with the  $\text{S}_\text{C}^*$  material before this is put into the cell.

Fig. 20. Possible mode of operation for a ferroelectric cell.



- (a)  $P_S$  aligned with field ( $E$ ), polariser (Pol) and analyser (An) mutually perpendicular and set for maximum extinction, i.e. polariser parallel to director ( $\bar{n}$ ); cell appears DARK.
- (b) + (d) These illustrate the bistability. Surface anchoring or 'latching' enables molecules to retain their orientation with the field removed.
- (c) A reverse field results in a change in the molecular orientation. The director ( $\bar{n}$ ) now makes an angle  $2\theta$  with polariser and so the cell appears BRIGHT.
- (e) When the field is reversed the molecules rotate about the surface of a cone from one orientation to the other as in (b)  $\rightarrow$  (c).

The advantage in the response times of  $S_C^*$  materials over nematic materials arises for two reasons. Firstly, although both systems have similar viscosities in relation to switching, the coupling of the spontaneous polarisation of a  $S_C^*$  material with the applied field is several orders of magnitude greater than the dielectric coupling of nematics with comparable fields. Secondly, switching from both DARK to BRIGHT and BRIGHT to DARK states is controlled by the field polarity in the  $S_C^*$  device. In the twisted nematic cell however, only formation of the ON state is controlled by the field and the response time for attaining the OFF state depends on the relaxation frequency of the molecules; this is commonly in the millisecond range.

From figure 20 it is apparent that for maximum contrast between the DARK and BRIGHT states, the optimum value of  $2\theta$  is  $45^\circ$ , therefore requiring that the director in the  $S_C^*$  phase makes an angle of  $22.5^\circ$  with the layer normal. As previously mentioned, on cooling from an  $S_A$  phase, the tilt angle of a  $S_C/S_C^*$  phase often acquires a value close to this figure, with only a weak temperature dependence of the tilt at more than  $10^\circ - 15^\circ$  from the  $S_C - S_A$  transition temperature. If the above condition is met, then the contrast between the two states is found to be comparable with that of a nematic device.

In the twisted nematic cell, it is necessary for the molecules to have a positive dielectric anisotropy ( $\Delta\epsilon > 0$ ) in order to align their long axes parallel to the field in the ON state. However, in the SSFLC device, the molecules are required to lie with their long axes in a plane normal to the

field direction and parallel to the supporting surfaces in both states. A positive dielectric anisotropy would tend to 'pull' the molecules out of the surface when a field is applied across the cell, thus hindering the switching response and destroying the bistability. Therefore,  $S_C^*$  materials used in these devices should desirably have a negative dielectric anisotropy ( $\Delta\epsilon < 0$ ).

Other important material considerations relating to this device are the pitch-length of the  $S_C^*$  helix and the magnitude and sign of the spontaneous polarisation; these factors will be discussed under the appropriate sections.

Variations on the SSFLC device have also been suggested by Lagerwall et al.<sup>36</sup> One incorporating  $S_C^*$  materials with a tilt angle approximating to  $45^\circ$ . Presumably this  $S_C^*$  phase would be obtained directly by cooling a Ch phase or the isotropic liquid, as discussed earlier. Using just one or no polariser, these devices would take advantage of the inherent birefringent properties of the material or the presence of dichroic dyes to obtain an optical effect.

Although all seven asymmetric tilted smectic phases are potentially ferroelectric, the device applications given above relate specifically to ferroelectric properties of the  $S_C^*$  phase. This is largely due to the lower order and viscosity within a  $S_C^*$  layer (resulting in faster switching responses) in addition to availability of suitable materials. Nonetheless, Bone et al.<sup>22</sup> have constructed an electro-optical device similar to the one already described, using the hexatic, tilted, asymmetric  $S_I^*$  and  $S_F^*$  phases. Switching

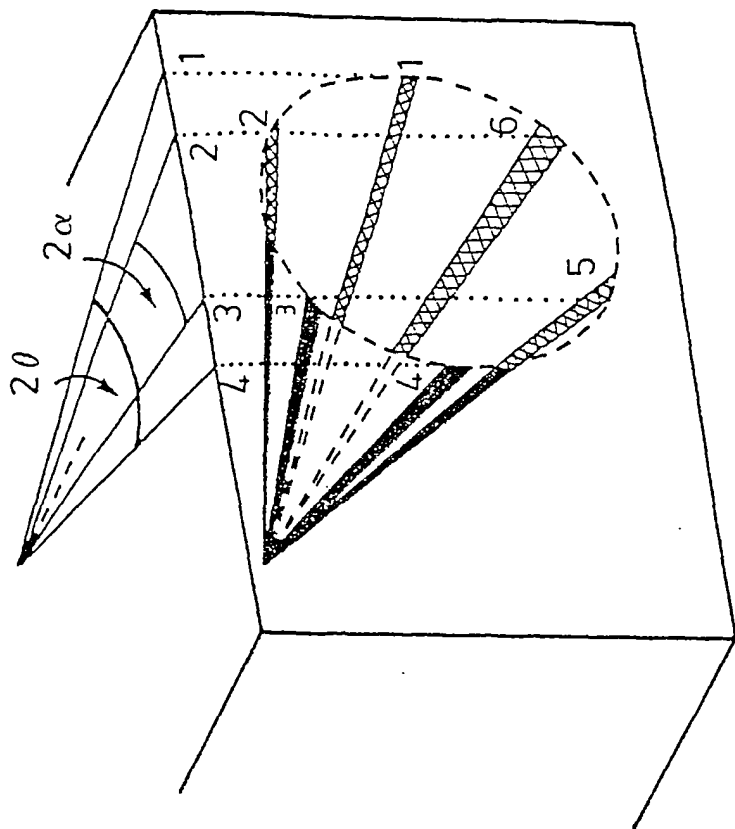
times for these phases are slower than for the  $S_C^*$  phase with comparable fields, but they do tend to show greater bistability, allowing thicker cells (6 - 10  $\mu\text{m}$ ) to be used.

The hexatic nature of the  $S_I^*$  and  $S_F^*$  phases also raises the possibility of switching between more than two optical states, as each of these phases has six possible tilt orientations of equal energy, (Fig. 6). However, when arranged for display purposes, only four of these positions remain optically distinguishable, as two of the orientations for the inner 'states' coincide, (Fig. 21). By varying the pulse width of an applied field across the cell, Bone *et al* have observed switching between the two outer states (1  $\longleftrightarrow$  4) and the two inner states (2  $\longleftrightarrow$  3). A faster response time is reported for switching between states 2 and 3 and despite the smaller optical angle ( $2\alpha$ ), good contrast is maintained between the DARK and BRIGHT states.

Commercial realisation of any or all of these devices will depend on the development of (i) materials with optimised properties and (ii) compatible cell technology. The most important material parameters will now be outlined in greater detail. These properties relate specifically to the  $S_C^*$  phase, but, apart from the helical pitch-length, which applies only to the  $S_C^*$ ,  $S_I^*$  and  $S_F^*$  phases, they are generally relevant to all tilted asymmetric phases.

#### 1.4. Materials Parameters.

It is generally acknowledged that no single compound will meet all the required molecular parameters, and that the desired optimal properties will ultimately be achieved by the



$$\tan \alpha = (\tan \theta) / 2$$

six possible tilt orientations exist, only four of which are optically distinguishable.

Fig. 21. Switching states from the  $S_I^*$  and  $S_F^*$  phases.

mixing of compounds. An important element of such a mixture will be the resulting helical pitch-length. This influences bistability and therefore determines to a large extent the cell thickness which can be used.

This is a critical consideration, as bistability in the SSFLC structure described earlier was not exhibited in electro-optic cells more than 2 - 3 $\mu$ m thick, and commercial problems in constructing cells with a uniform 2 $\mu$ m thickness could prove to be a major obstacle. It was assumed that this limiting factor was due to the short pitch-lengths of the materials used (ca3 $\mu$ m) and that if the pitch-lengths were increased, then bistability would persist in thicker cells.

The pitch-length (P) can be increased by applying a magnetic or electric field normal to the helical axis, but the most practical method is by mixing materials having helices of opposite handedness. It is therefore necessary to know the helical twist sense of a compound (D or L) in order to assess its effect on P when it is mixed with other materials.

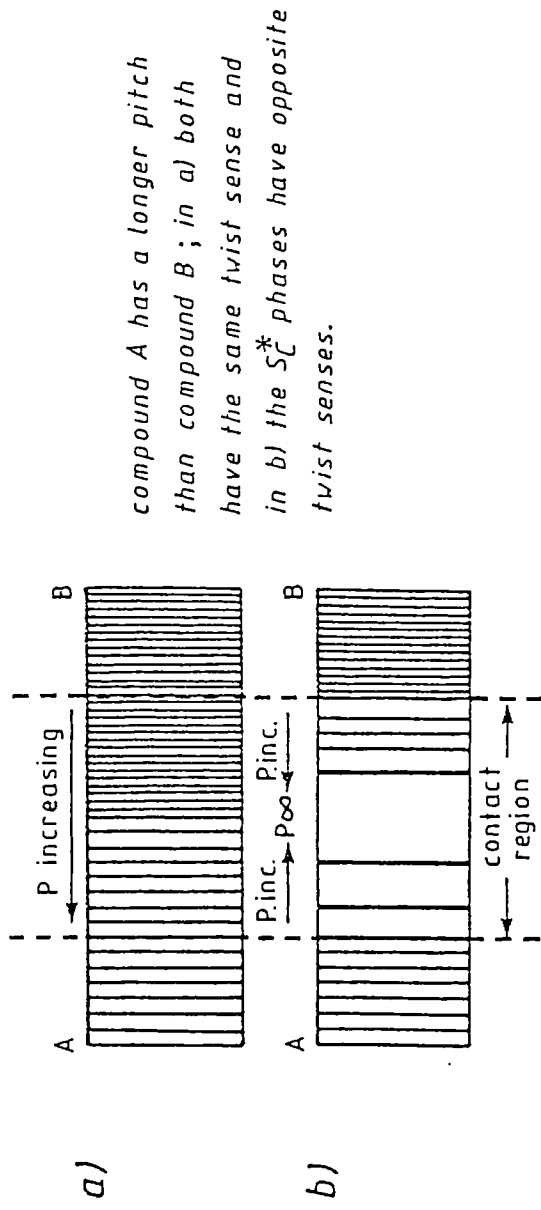
#### 1.4.1. Helical Twist Sense

A direct method of determining the twist sense is by observing the rotational effect of the helix on plane polarised light.<sup>27</sup> When looking towards the source of the beam, polarised light directed along the helical axis and rotated to the right is denoted D (dextro), whereas a rotation to the left is denoted L (Laevo).

A simpler technique can be employed once the twist senses have been established. This is based on the contact method outlined by Gray and McDonnell<sup>7</sup> for the determination of twist senses of cholesteric helices. In thick cells ( $d \gg P$ ), a planar aligned sample of the  $S_C^*$  phase will show characteristic 'pitch lines' having a regular space, when viewed between crossed polarisers. These lines occur when the director orientation ( $\bar{n}$ ) coincides with the normal to the vibration direction of the polariser or analyser. When this planar alignment is obtained for a 'contact' preparation of a standard material and a test material (both in their  $S_C^*$  phases), then, if the materials have the same twist sense, the pitch lines will progress continuously across the contact region. (Fig. 22). However, if the materials are of opposite twist sense, the pitch lines in each half of the cell will become more widely spaced as they approach the contact region, finally disappearing at the composition corresponding to mutual compensation ( $P \rightarrow \infty$ ).

By adapting the above technique, a more convenient method was used to determine the helical twist sense of  $S_C^*$  compounds in this thesis. The  $S_C^*$  compound is dissolved in material having a wide temperature range nematic phase. The helical twist sense of the resulting cholesteric phase (and therefore the  $S_C^*$  phase) can then be identified by comparison with a cholesteric material of known helical twist sense, via the contact method.

A general guide to the cholesteric twist sense of a compound can be obtained by simply considering its molecular structure<sup>7</sup>. Rules relating the twist sense of the  $S_C^*$  helix to

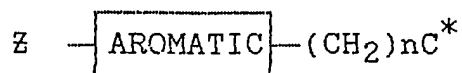


compound A has a longer pitch than compound B ; in a) both have the same twist sense and in b) the  $S_C^*$  phases have opposite twist senses.

Fig. 22. Representation of pitch lines in a contact cell. (plan view)

the absolute configuration and position of the chiral centre within a molecule have been suggested by Goodby et al.<sup>27</sup>

These rules are derived from the rules relating to cholesteric helices given in reference 7, but have been modified to account for the influence of polar groups on the asymmetric centre<sup>†</sup>. Electron donating groups (e.g. CH<sub>3</sub> -->--C\*) are denoted as +I, while electron withdrawing groups (e.g. Cl --<--C\*) are denoted as -I. Goodby's results confirmed that specifically for the structure.



where Z represents an alkyl or alkloxy chain and n is a small integer, if the absolute configuration of the chiral group is constant, then incremental increases in n produce an alteration in the twist sense of the S<sub>C</sub>\* helix. Furthermore, determination of the twist sense for many other S<sub>C</sub>\* materials provided evidence to support the following relationships:

+I ≡ R o D, R e L, S o L, S e D.

-I ≡ R o L, R e D, S o D, S e L.

Here R and S represent the absolute configuration of the asymmetric centre, e and o denote whether the centre of asymmetry is at an even or odd number of atoms respectively from the aromatic core, and D and L refer to the twist sense of the helix.

---

† It should be mentioned that since this introduction was written, evidence has come to light that in some mixtures, the handedness of the cholesteric phase is opposite to that of the S<sub>C</sub>\* phase.

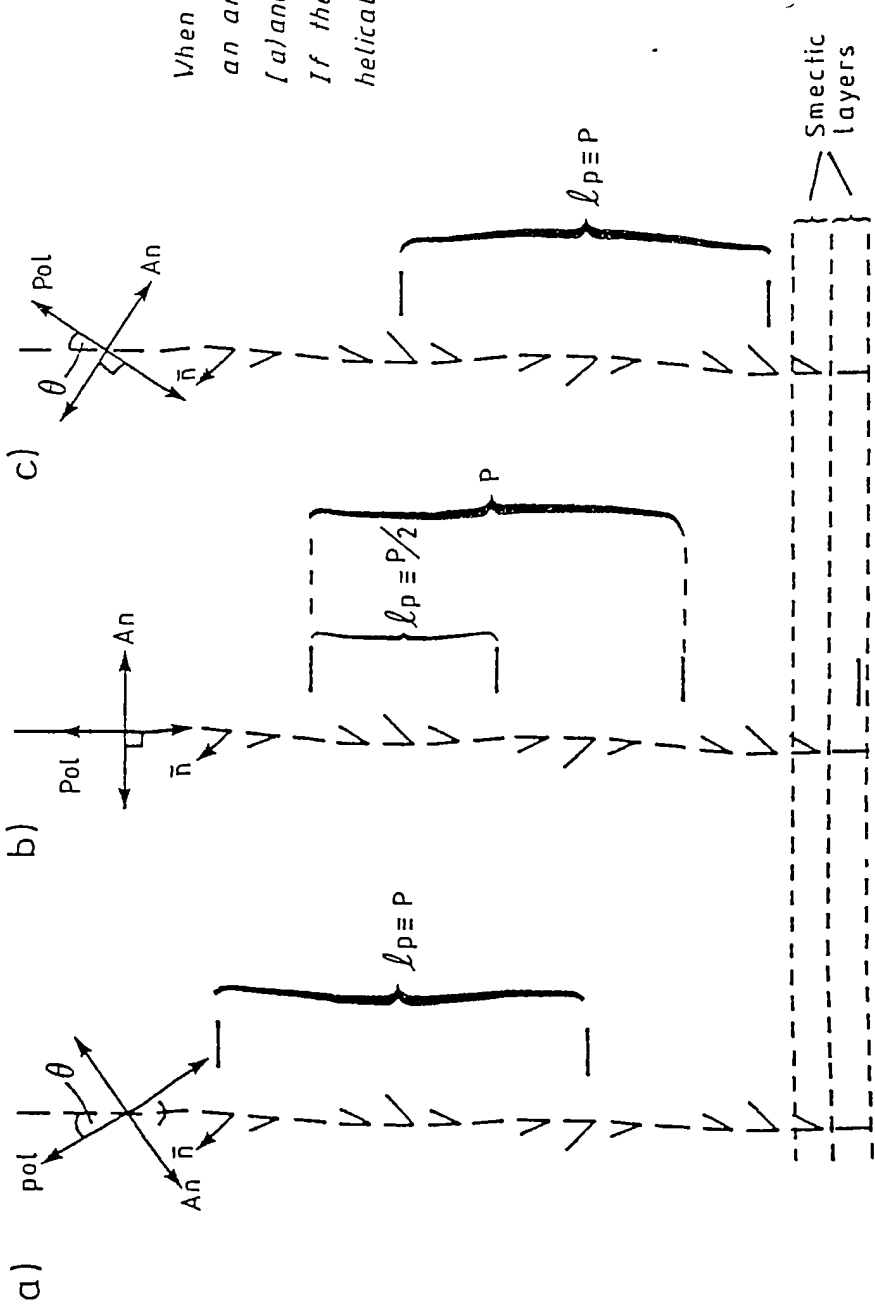
#### 1.4.2. Determination of Pitch-Length

A convenient method of determining the helical pitch-length of a material is provided by measuring the distance between the pitch lines exhibited by a uniform planar sample. This can be done using optical microscopy, employing a calibrated graticule for counting the number of lines within a given distance.<sup>33</sup> Although there has been debate as to whether or not the line spacing is equal to  $P$  or  $P/2$ , it has now been shown that this depends on the relative orientation of the  $90^\circ$  crossed polarisers with respect to the helical axis.<sup>37</sup> If the polarisers make an angle  $\theta$  with the helical axis, the line spacing  $l_p$  will be equal to  $P$ , whereas, if the polarisers are parallel and perpendicular to this axis, then the spacing corresponds to  $P/2$ , (Fig. 23).

In an alternative method for pitch determination, a Helium-Neon laser is directed perpendicular to the helical axis and the resultant diffraction pattern is observed.<sup>38</sup> Both methods become less accurate when the pitch-length becomes very small. Values of  $P$  less than ca.  $2\mu\text{M}$  must be estimated from the wavelength of the light that is selectively reflected by the phase, or calculated from the critical field ( $E_c$ ) necessary to unwind the helix completely.<sup>39</sup>

#### 1.4.3. Temperature Variation of the Pitch-Length

A general feature of the  $S_C^*$  pitch-length is that its value is greatest close to the upper transition temperature ( $T_c$ ) and decreases with the decreasing temperature and increasing  $\theta$ , attaining a relatively constant value further



When the polarisers (pol) makes an angle  $\theta$  with the helical axis (a) and c), the line spacing  $l_p \equiv P$ . If the polariser is parallel to the helical axis, (b)  $l_p \equiv P/2$ .

Fig. 23. Pitch lines observed for a planar aligned sample in the  $S_C^*$  phase (plan view).

from  $T_c^{40}$  (Fig. 24). Some materials have been reported as having a constant value of  $P$  throughout the temperature range of the  $S_C^*$  phase<sup>38</sup>, but this is possibly due to surface interactions 'holding' the pitch. These interactions can be overcome by applying a D.C. field across the cell to unwind the helix completely. Switching the field off allows the helix to rewind and enables the pitch to reach an 'equilibrium' value for a particular temperature<sup>30</sup>.

It has also been reported that the pitch-lengths of a number of  $S_C^*$  compounds decrease sharply within 2° C of  $T_c$ ,<sup>30,38</sup> approaching very small values at the actual transition. Although the root cause of this phenomenon is not clear, a complicated mathematical explanation has been suggested, based on a flexoelectric effect arising from steric interactions between chiral, banana shaped molecules.<sup>41</sup>

#### 1.4.4. Increasing the Pitch-Length

It was mentioned before that it is highly desirable to obtain materials having a long pitch-length, and that this can be achieved by mixing compounds with helices of opposite twist sense. Ideally, this will result in a pitch-length approaching infinity which persists over a wide temperature range. An effective method of accomplishing this may be used if the  $S_C^*$  materials have a cholesteric phase above the  $S_A$  phase. Compensation of the pitch in the cholesteric phase can extend into the  $S_C^*$  phase where  $P$  remains large and fairly temperature independent.

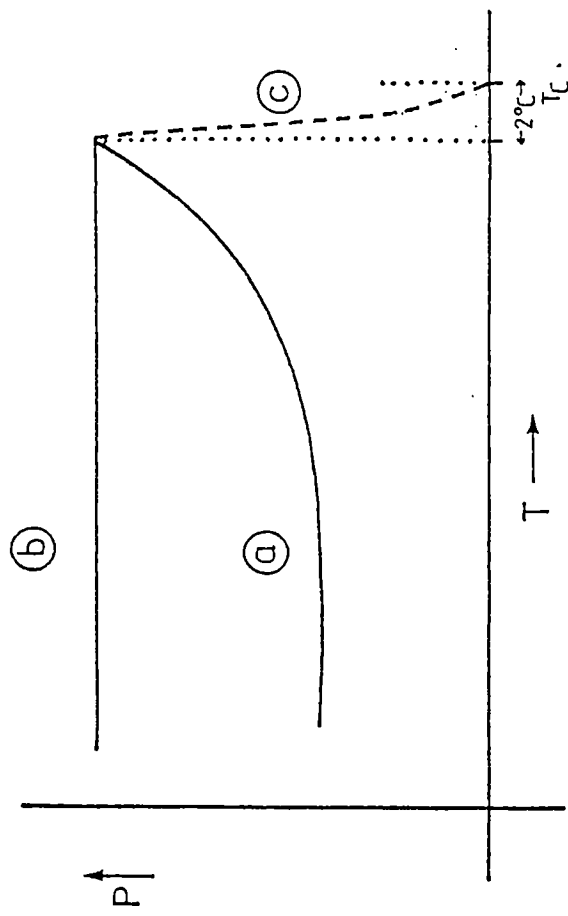


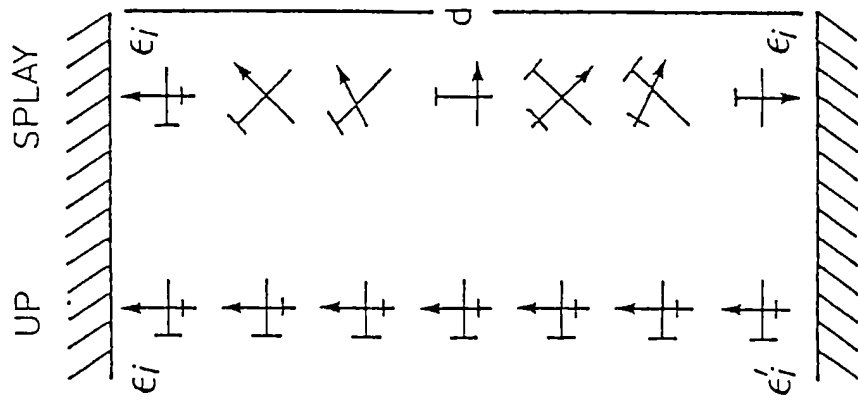
Fig. 24. Temperature dependence of pitch for  $SC^*$  phase.

- (a) usual curve for  $P$  vs.  $T$ .
- (b) 'constant'  $P$ .
- (c) some materials exhibit sharp decrease in  $P$  close to  $T_c$ .

On a molecular scale, the pitch-length tends to increase in a homologous series as the chiral centre is moved progressively away from the aromatic core. This does not however, provide a practical solution, as this structural change has a detrimental effect on the magnitude of the spontaneous polarisation.

Probably the simplest method of producing  $S_C^*$  phases of long pitch-length is by doping a non-chiral  $S_C$  phase with a small amount of optically active material; this does not require a knowledge of the helical twist sense. Working in this way, Pavel et al.<sup>42</sup> found an approximately inversely proportional relationship between molar concentration of dopant and  $P$  over the region 3-25 $\mu$ M.

It has been assumed that increasing the pitch-lengths of materials would lead to a corresponding increase in the persistence of bistability for thicker cells. However, recent evidence has indicated that this is not necessarily the case. Cladis et al.<sup>43</sup> obtained long pitch-length (10-100 $\mu$ M)  $S_C^*$  materials by mixing non-chiral  $S_C$  compounds with small amounts of cholesteric 'dopants', but for 10 $\mu$ M cells bistability was not observed, even with high fields. This loss of bistability was accounted for by a tendency of the molecules to adopt a splay state.<sup>36</sup> If the UP state of an SSFLC structure is considered, it is apparent that the molecular interactions with each surface may have different energies (Fig. 25). If this is the case, then the surface interaction of lower energy will be preferred, and in thicker cells this will lead to the formation of a splay state. The most obvious way to counter this tendency is to prepare



Interaction energy between molecules and the upper surface ( $\epsilon_i$ ) will differ from that between molecules and the lower surface ( $\epsilon'_i$ ) for the UP (or DOWN) state. In thicker cells if  $\epsilon_i < \epsilon'_i$  then a splay state may arise, even if  $P > d$ .

Fig. 25. Occurrence of splay in thick cells.

surfaces which will minimise these energy differences and so stabilise both the UP and DOWN states with respect to the splay configuration.

Despite this problem, bistability has been observed in thicker cells<sup>36</sup> and although this has been of a more transient nature, it may still prove useful for device application. Bearing this in mind the importance of a long pitch-length is still significant, as the problems of the splay state may be overcome by developing new alignment techniques.

#### 1.4.5. Measuring the Tilt Angle

The tilt angle ( $\theta$ ) of a  $S_C^*$  material is a very important parameter, as this largely determines the optical brightness and contrast of a device. Values of  $\theta$  depend to some extent on the method of measurement and on the orientation of the sample under examination, and this may sometimes lead to large discrepancies in the results obtained. The principal methods of evaluating  $\theta$  are based on either a simple calculation from results of x-ray studies on, or optical measurements made in conjunction with, an applied field.

X-ray studies of unoriented samples require the material to exhibit a  $S_A$  phase above its  $S_C^*$  phase in order to determine  $\theta$ , (Fig. 26). The layer spacing ( $d_{S_A}$ ) remains fairly constant throughout the  $S_A$  phase and is therefore regarded as the effective molecular length;<sup>XV</sup> this is then

---

XV. As mentioned previously, molecules in the  $S_A$  phase do not necessarily stand normal to the layer plane, but may adopt random tilt orientations so that  $d_{S_A} \neq$  molecular length.

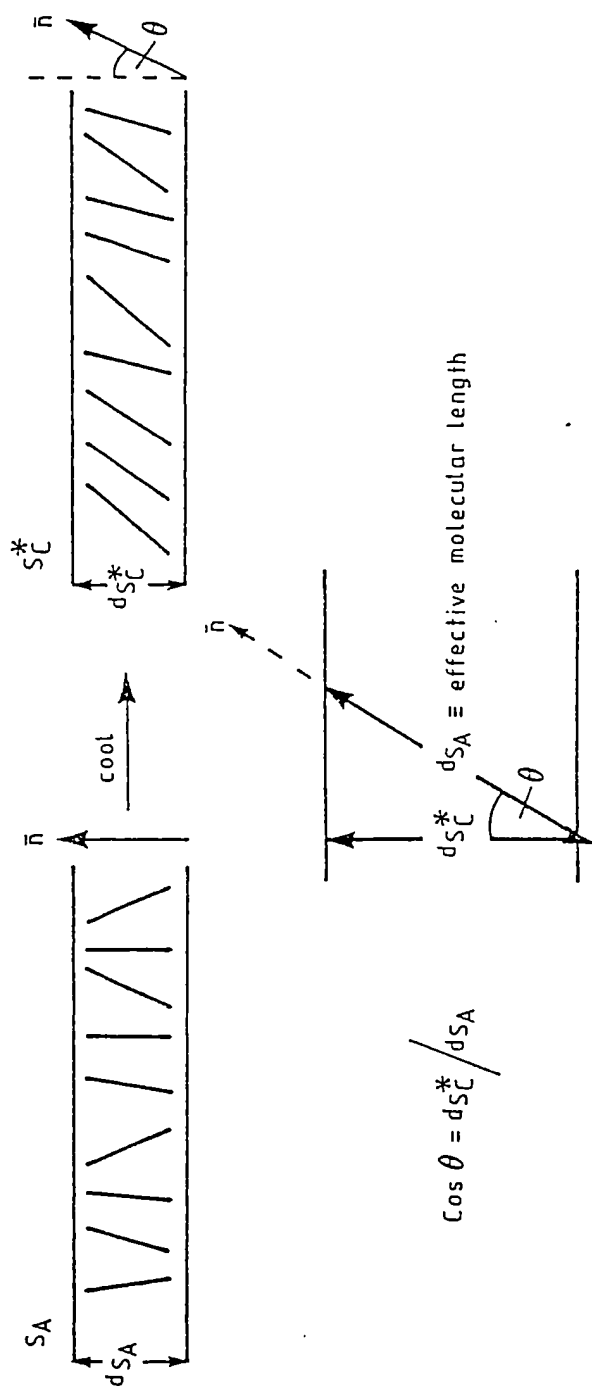


Fig.26. Determination of  $\theta$  from the layer spacings in the SA and SC\* phases.

assumed to remain constant in the  $S_C^*$  phase. On cooling into the  $S_C^*$  phase, the observed layer spacing ( $dS_C^*$ ) decreases in accordance with an increase in the tilt angle; the relationship is given by the equation:

$$\cos \theta = \frac{dS_C^*}{dS_A} \quad 12$$

For aligned samples,  $\theta$  may be obtained by direct observation of x-ray diffraction patterns,<sup>44</sup> but this is a less accurate measurement and may therefore only be used as a rough guide.

The simplest and most common method of determining  $\theta$  optically, is by examining a planar sample between  $90^\circ$  crossed polarisers and using an electrical field ( $E \gg E_c$ ) large enough to unwind the helical structure, (Fig. 27). The director then exhibits a uniform orientation over a large area of the sample and the polarisers can be positioned so that maximum extinction is obtained. The polarity of the field is then reversed and the polarisers are turned through the smallest possible angle required to regain extinction. The angle of rotation is equal to  $2\theta$ ;  $\theta$  is obtained simply by halving this value.<sup>37</sup>

A similar method can be used whereby the polarisers are aligned with the rubbing direction of a planar sample in the  $S_A$  phase, resulting in maximum extinction. On cooling into the  $S_C^*$  phase, an electrical field is again applied across the cell to unwind the helix; the smallest angle through which the polarisers must be turned to regain extinction is now equal to  $\theta$ .<sup>27</sup>

In the homeotropic geometry, the planes of smectic A layers align parallel with the supporting surfaces so that

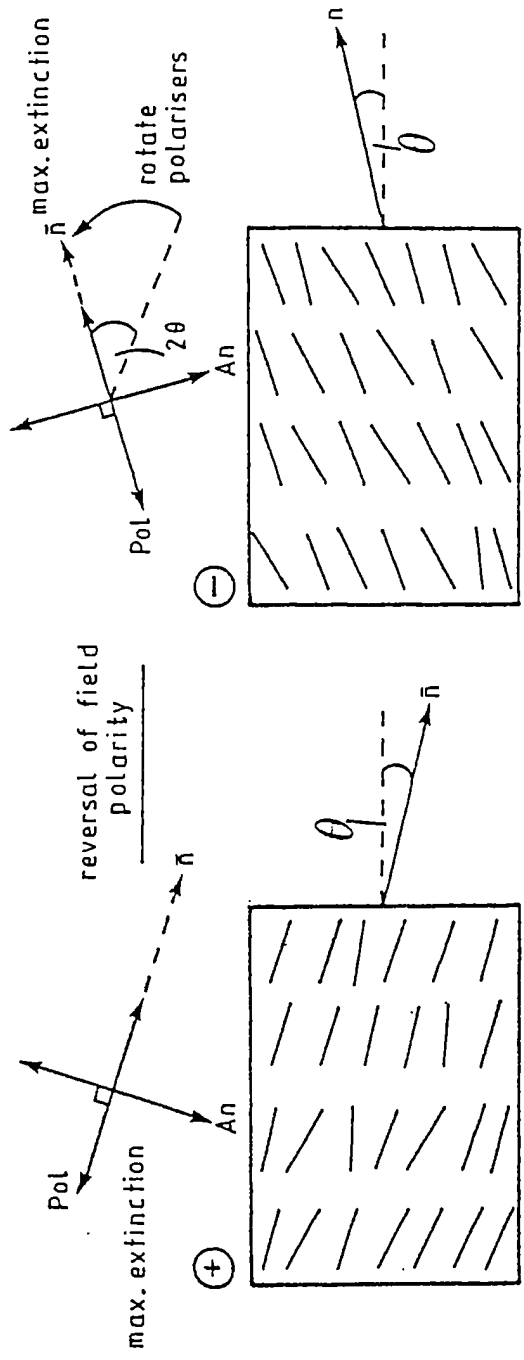


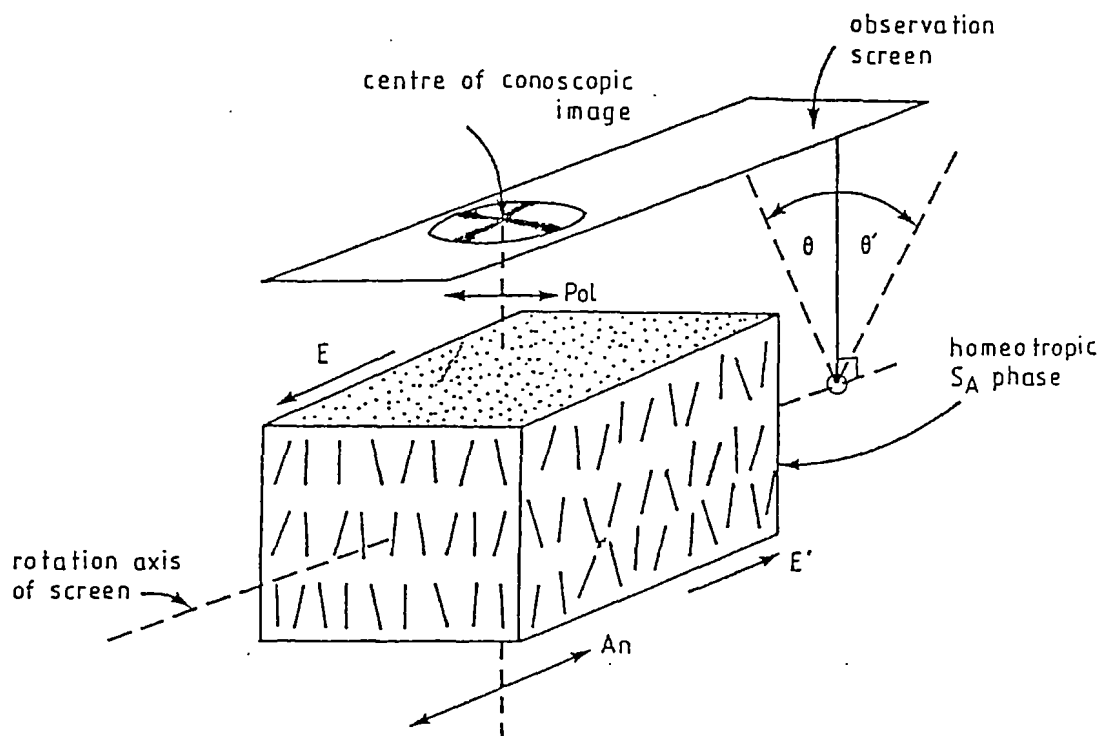
Fig.27. Determination of  $\theta$  by reversing field polarity on a sample with planar geometry (plan view).

the molecules stand approximately perpendicular to these surfaces. Convergent polarised light focused inside such a sample and passing through a second polariser at right angles to the first, results in the formation of a 'conoscopic' image, similar to that normally obtained for aligned uniaxial crystals.<sup>45</sup> Matinot-Lagarde et al.<sup>30</sup> observed that on cooling such a S<sub>A</sub> geometry into the S<sub>C</sub>\* phase, while applying an electrical field ( $E \gg E_c$ ) parallel to the layers, the centre of the conoscopic image moves in a direction perpendicular to the field in accordance with the molecular tilt. Reversing the field polarity moves the centre of the image in the opposite direction, but by the same amount. By measuring this movement on a screen which rotated about an axis passing through the sample (Fig. 28), values of  $\theta$  were obtained; these were comparable to, but slightly larger than, those determined in experiments using the planar geometry.

The lower values of  $\theta$  observed for planar samples have been explained in terms of a 'junction layer', whereby molecules very close to the supporting surfaces may have a tendency to remain aligned in the rubbing direction, leading to an apparently lower overall tilt angle.

A feature of the optical measurements using both the planar and homeotropic alignments is that increasing the applied field above  $E_c$  does not result in a larger observed tilt angle; this indicates that  $\theta$  is the same in both the wound and unwound states.

Fig. 28. Determination of  $\theta$  from a precursor  $S_A$  phase with Homeotropic Geometry.



The conoscopic image is observed for the  $S_A$  phase. Cooling into the  $S_C^*$  phase and applying a field  $E$  or  $E'$  parallel to the layers results in a molecular tilt. This is determined by rotating the screen through  $\theta$  or  $\theta'$  in order to recentre the image.

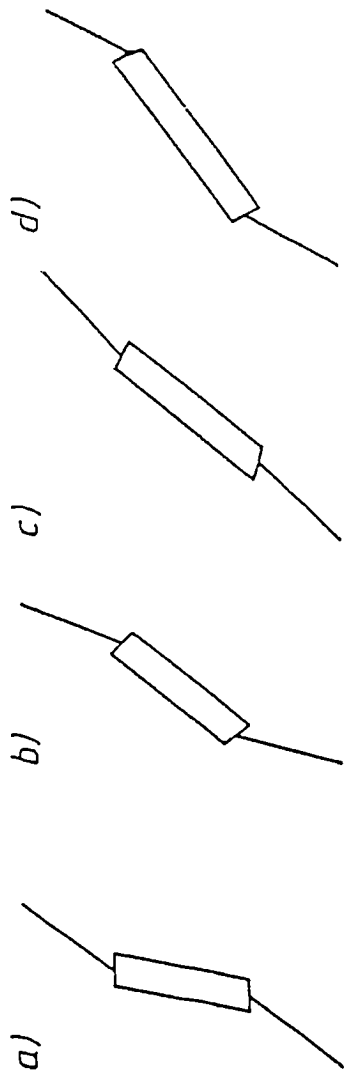
When discussing molecular models for the  $S_C/S_C^*$  phase, it was suggested that the axis of the aromatic core of a molecule may attain a different tilt angle to that of the axis of a terminal alkyl chain. Evidence for this emanates from the fact that the tilt angles measured by optical and x-ray studies often differ, the value that is greater depending upon the particular material under examination. This is because the two methods are actually measuring two different properties. Optical measurements disclose the tilt angle of the overall optical dielectric tensor, which is approximately the long axis of the aromatic core, whereas, x-ray studies reveal the overall tilt angle of the molecule. By comparing the results and assuming an all trans (anti) conformation of the molecules, it follows that if the optical tilt angle ( $\theta^\circ$ ) is greater than the tilt angle obtained by x-ray methods ( $\theta^x$ ), then the aromatic cores are tilted more than the aliphatic chains, and vice versa.<sup>46</sup> XVI

Taking such factors into account, and considering that  $\theta$  commonly attains a value of around  $25^\circ$  or  $45^\circ$ , depending on the preceding phase, four different tilt orientations become possible, (Fig. 29) for the  $S_C/S_C^*$  phase, and according to Goodby et al.<sup>46</sup> may account for the occurrence of injected orthogonal phases in mixtures of different  $S_C$

-----

XVI. A most startling example of this type of orientational behaviour had already been found by Bryan et al.<sup>12</sup>, who were examining the relationship between alkyl chain length and the smectic layer spacing for a homologous series of 4-n-alkyloxycinnamic acids, which form dimers in their crystal and smectic phases. From x-ray studies alone, they concluded that in the  $S_C$  phase, the aromatic cores were almost parallel to the layer planes and that the aliphatic chains made an angle of ca  $30^\circ$  with the layer normal.

Fig. 29. Four possible tilt orientations in  $S_C/S_C^*$  phases.



a) and b) are low tilt orientations (ca 25°) with the aromatic core less, or more tilted respectively than the aliphatic chains;  
c) and d) are high tilt orientations (ca 45°) also with the aromatic core less, or more tilted respectively than the aliphatic chains.

materials. XVII

Although no single technique gives a 'correct' value of  $\theta$ , each method does reveal the same relationship between  $\theta$  and temperature described earlier. However, the most relevant method of determining  $\theta$  is probably that using the optical technique and a planar aligned sample, as this measures the optical effect which also operates in the SSFLC device.

#### 1.4.6. Determining the Magnitude of the Spontaneous Polarisation

The essential property of ferroelectric liquid crystals is the spontaneous polarisation, as this enables both extremely fast responses to electrical fields and the existence of multi-orientational states. The magnitude of  $P_s$  and its temperature variation ultimately determine the threshold voltage required to switch between orientational states, and are therefore important considerations for commercial devices.

Early experiments confirmed the existence of spontaneous polarisation in asymmetric tilted smectic phases, but were only able to estimate its value roughly.<sup>32</sup> A direct quantitative means of measurement, now called the 'field reversal' method, was not developed until 1977.<sup>47</sup> The principle behind this technique is that a planar sample of

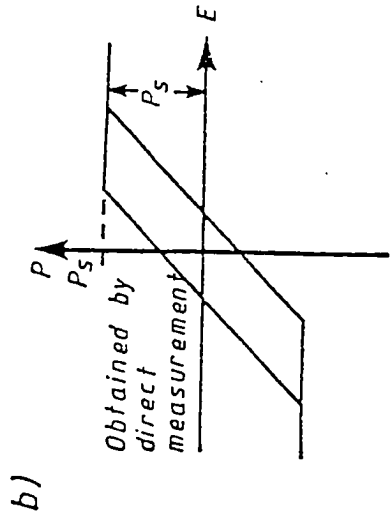
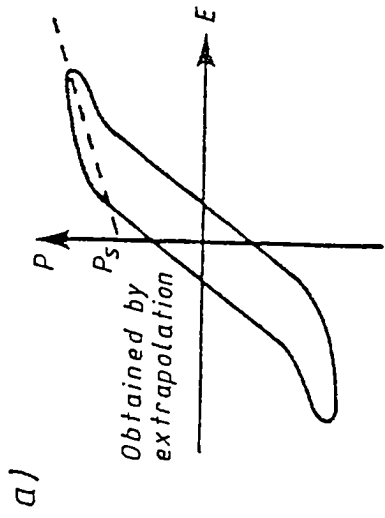
---

XVII. Although Goodby *et al.*<sup>46</sup> describe only four tilt orientations for molecules in a layer of the  $S_C/S_C^*$  phase, the possibility exists that the aliphatic chains acquire the same tilt angle as the aromatic core, whereon  $\theta^o \equiv \theta^x$ , and  $d_{SA} \equiv$  molecular length of the all trans conformation of the molecule.

low conducting ferroelectric material is oriented in a particular direction by a D,C, field ( $E > E_C$ ) which is then rapidly reversed. The current flowing through the sample is monitored on an oscilloscope screen and recorded.

The experiment is then repeated at different field strengths and temperatures. Ionic contributions to this current are eradicated by comparing data for the preceding non-ferroelectric  $S_A$  phase, and the  $P_s$  is thus obtained as the voltage independent part of the charge.

As described earlier, a hysteresis loop arises from the interaction between the spontaneous polarisation and a low frequency A.C. field, and is peculiar to ferroelectric materials. A method for determining  $P_s$  for planar oriented ferroelectric liquid crystals has been developed whereby the behaviour of the hysteresis loop is modified using a Diamant bridge.<sup>48,49</sup> By off-setting residual capacitance and resistance within the circuitry, a 'compensated' hysteresis loop is produced, (Fig. 30) thereby avoiding the need for extrapolation and enabling a direct measurement of  $P_s$  to be made. This technique has the added advantage of giving accurate results for relatively highly conducting samples, as the conductivity can be cancelled out by adjusting internal capacitors and resistors. Yoshino et al.<sup>50</sup> noted that the magnitude of  $P_s$  measured in this way varied with the frequency of the A.C. field. They showed that this was due to the material relaxing back into its helical structure at low frequencies, whereas, at higher frequencies, this could not occur. The highest and most



Conducting samples usually give rise to a hysteresis loop with rounded ends (a), whereas the diamond bridge technique produces a 'compensated' loop enabling  $P_s$  to be determined by direct measurement (b).

Fig. 30. Determination of  $P_s$  using the 'compensated' hysteresis loop.

correct values of  $P_s$  were therefore attained when the measuring frequency of the field was comparable to the relaxation frequency of the material.

An easier but less accurate way of determining  $P_s$  is by calculation. Although numerous equations have been derived,<sup>29.30.33.38.51.</sup> they are usually based on a simple measurement of the applied field ( $E_c$ ) necessary to unwind the helical structure, and on an estimate of the twist elastic constant ( $K$ ). Values of  $P_s$  acquired by this method often differ from those obtained by direct measurements, but they are useful as a rough guide and may also help to elucidate the phenomenon of ferroelectricity in liquid crystals.

By using one of the methods outlined above, values of  $P_s$  may also be obtained for chiral materials having no inherent ferroelectric, or even liquid crystalline properties. As discussed previously, mixing chiral compounds with non-chiral  $S_C$  materials can result in the formation of the  $S_C^*$  phase. The measured  $P_s$  of such a mixture is proportional to the amount of chiral dopant present,<sup>52</sup> therefore allowing a direct estimate of the 'virtual'  $P_s$  for the pure chiral substance to be made.

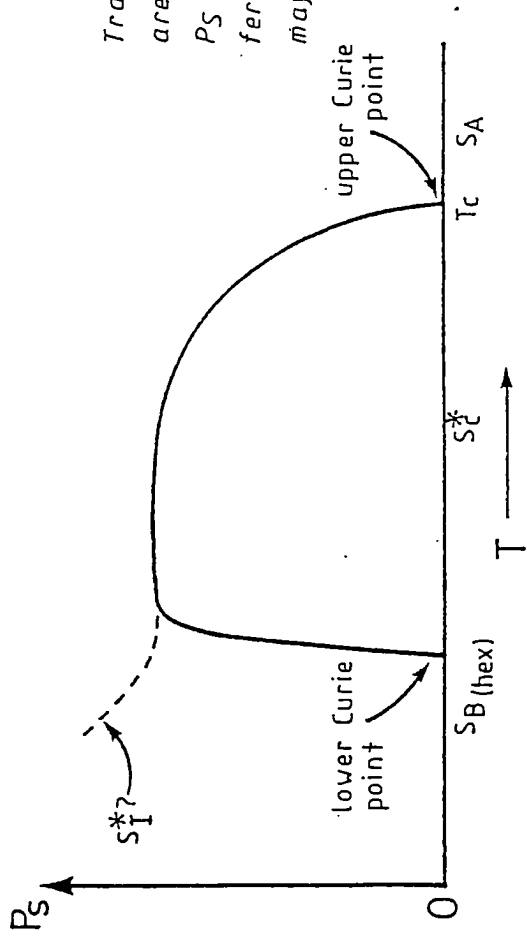
By comparison with crystalline ferroelectrics, the magnitude of  $P_s$  for ferroelectric liquid crystals is very small, even though the molecular dipoles involved are similar. This is primarily due to rotational and conformational motions of the molecules which do not occur in crystalline solids and which reduce the effective dipole in liquid crystal phases to only a few percent of its

potential. That Ps exists at all has been explained by a tendency of the molecules to adopt lowest energy conformations associated with a particular dipole direction and tilt orientation.<sup>28.46.</sup>

Variation of Ps with temperature in ferroelectric liquid crystals follows a similar curve to that exhibited by crystalline ferroelectrics. On cooling from the  $S_A$  phase to the  $S_C^*$  phase, a Ps suddenly appears at the transition temperature ( $T_c$ ) which can therefore be regarded as a Curie point. Further cooling of the  $S_C^*$  phase may produce an orthogonal phase (e.g.  $S_{hex}$ ), at which stage the Ps will rapidly fall back to zero, giving a second (or lower) Curie point, (Fig. 31). If instead, the  $S_C^*$  phase is followed by another ferroelectric phase (e.g.  $S_I^*$ ), then the value of Ps has been shown to increase.<sup>39</sup> However, this is not necessarily the case for all  $S_C^* \rightarrow S_I^*$  transitions<sup>22</sup> and further study in this area is needed.

#### 1.4.7. Determining the Sign of the Spontaneous Polarisation

Another important aspect of the Ps is its sign, i.e. its direction with respect to the tilt orientation. This can be determined simply by using the technique already described for obtaining  $\theta$  in planar samples, and cooling from the  $S_A$  to the  $S_C^*$  phases in the presence of an electrical field. Depending on the sign of Ps, the molecules in the  $S_C^*$  phase will tilt to the left [Ps  $< 0$  or (-)] or to the right [Ps  $> 0$  or (+)] when the upper plate is positively charged, (Fig. 32). This movement is then easily followed by an appropriate rotation of the crossed



Transitions to orthogonal phases are in fact Curie points at which the  $P_S$  falls to zero. Transitions to other ferroelectric phases (broken curve) may result in an increase in  $P_S$ .

Fig. 31. Schematic representation of  $P_S$  vs. temperature.

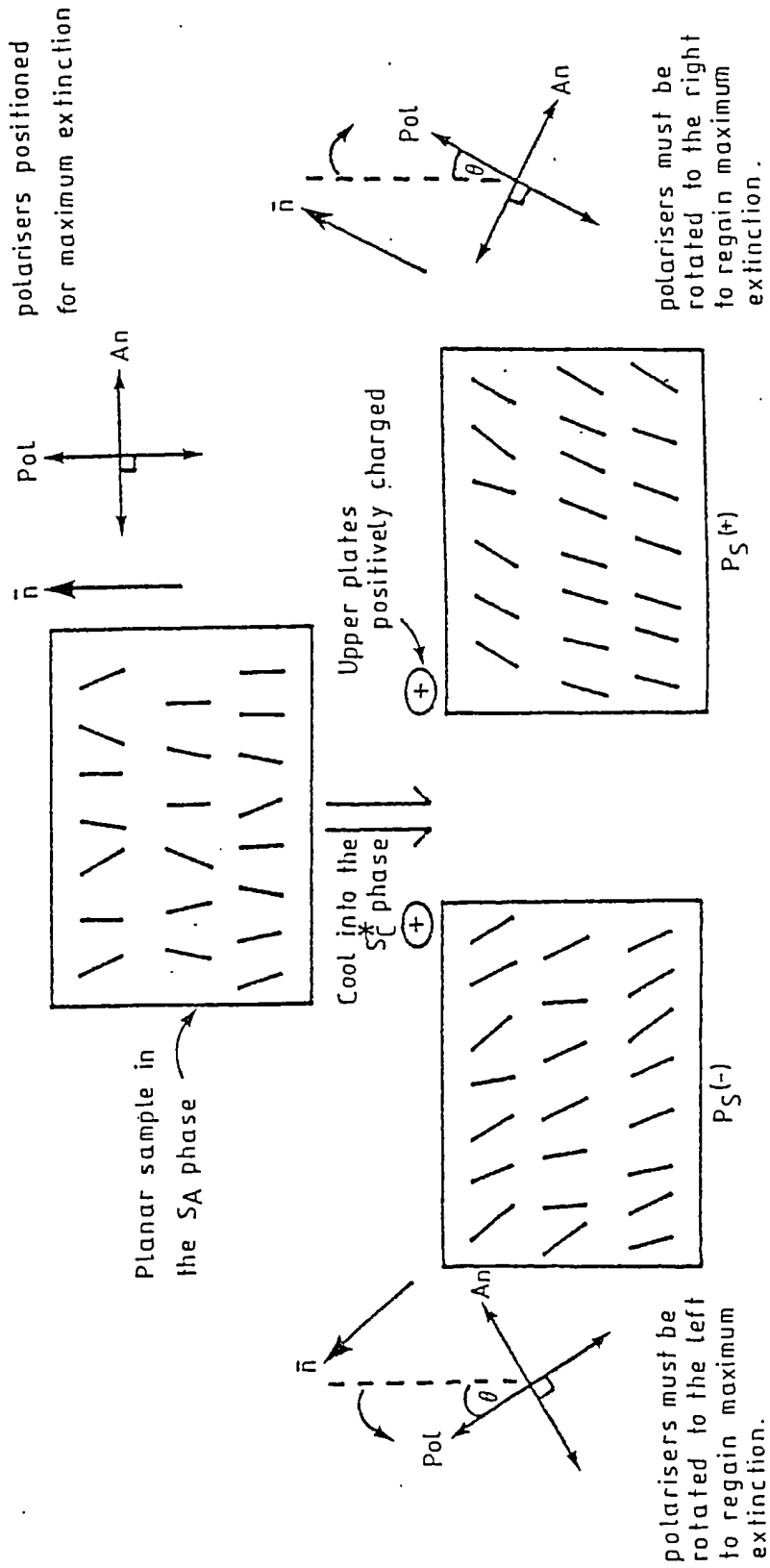
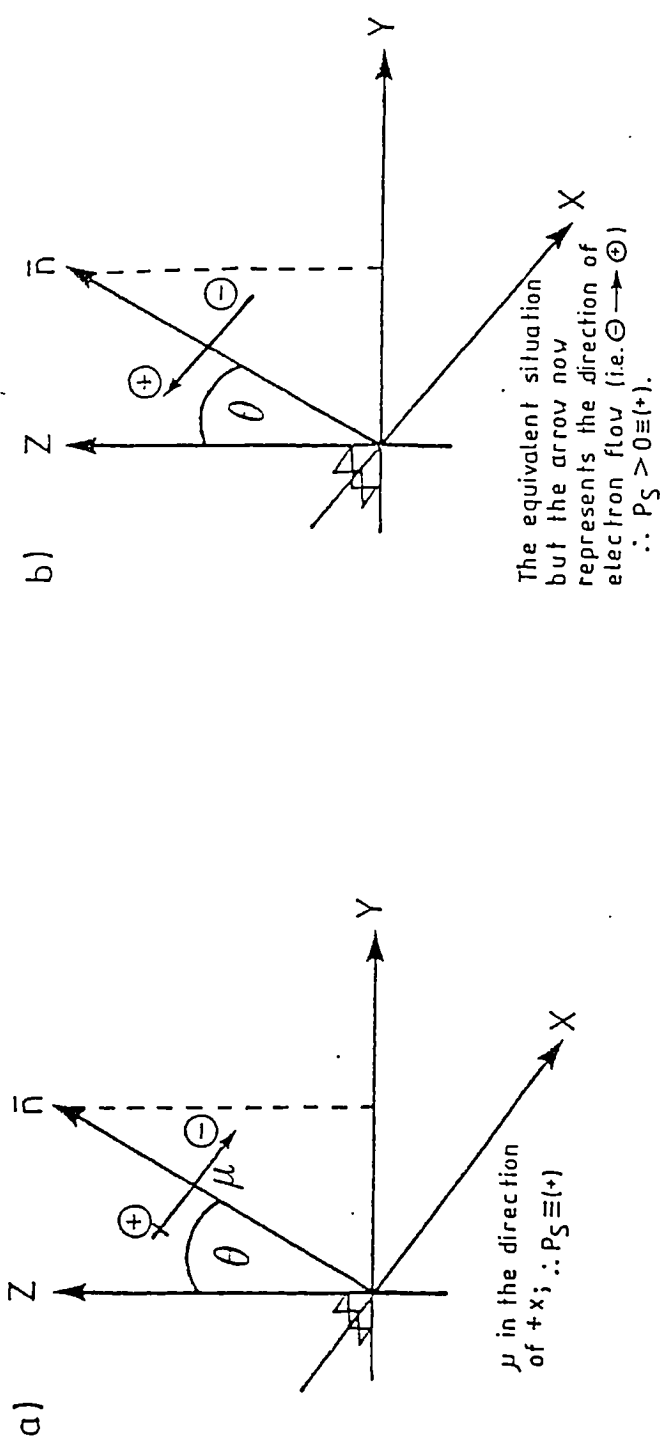


Fig. 32. Determination of the sign of  $P_S$ . Plan view of planar sample.

polarisers to regain maximum extinction.<sup>27</sup> Until recently, there has been confusion over the actual definition of the sign of  $P_s$ , with chemists regarding it as the direction of the overall lateral dipole moment ( $\mu$ ),<sup>22</sup> and physicists associating it with the overall lateral direction of the electron flow (i.e. - ----> +).<sup>40.53</sup> In this thesis, the sign will relate to the former definition, although it should be pointed out that both definitions result in the same relationship between sign of  $P_s$  and tilt orientation, (Fig. 33).

As in the case of the twist sense of the helix, the actual sign of  $P_s$  becomes a very important factor when considering mixtures of materials. Mixing of compounds of opposite  $P_s$  sign, clearly lowers the overall magnitude of  $P_s$ , whereas, mixing compounds of the same  $P_s$  sign results in values of  $P_s$  intermediate between those of the individual components, depending on their relative proportions. Both signs of  $P_s$  can be associated with either a D or L helix and therefore a material may exhibit one of four possible combinations of the two parameters; D(+), D(-), L(+), or L(-). To obtain mixtures of long pitch-length whilst maintaining the value of  $P_s$ , compounds of opposite helical twist sense, but the same sign of  $P_s$  must be mixed, i.e. D(+) with L(+) or D(-) with L(-).

For a homologous series, where the absolute configuration remains constant, there is an alteration<sup>n</sup> in the sign of  $P_s$  as incremental increases occur in the distance of the asymmetric centre from the aromatic core.<sup>18</sup> This has



*X, Y and Z mutually perpendicular and arbitrarily chosen so that  $\bar{n}$  projects onto the Y axis.*

*Fig. 33. Definition of  $P_S (+)$  ( $P_S > 0$ ).*

been accounted for by orientational changes which occur in an all trans conformation on passing from one carbon atom to the next. An attempt has also been made<sup>46</sup> to relate this alteration to changes in the twist sense of the helix and to the inductive nature of substituents at the chiral centre. Although this is plausible for a particular homologous series and has even been extended in its application to a few other systems, the proposed rules do not apply generally. For a specific series of compounds, the sign of Ps must be determined experimentally.

#### 1.4.8. Increasing the Spontaneous Polarisation

Although the magnitude of Ps in ferroelectric liquid crystals is much lower than that in crystalline ferroelectrics, certain molecular features may still influence its relative value considerably. The two factors which probably have the greatest effect on Ps are the strength of the lateral dipole and the extent of its coupling with the chiral centre. In DOBAMBC, the chiral centre carries only a weakly polar methyl substituent and is separated from the large carbonyl dipole. Therefore very little coupling occurs between the two, resulting in a small value of Ps. However, replacement of the methyl group by a more highly polar substituent [e.g. chlorine<sup>30</sup>], or simply putting the chiral centre in closer proximity to the carbonyl dipole<sup>49</sup> leads to a marked increase in Ps.

It has also been shown that extending the alkyl chain length beyond the chiral centre may enlarge the magnitude of Ps,<sup>50,54</sup> but this effect is only significant for materials which already fulfil one or both of the above requirements.

Finally, the simplest method of increasing the value of  $P_s$  of a ferroelectric material is by admixing with a chiral dopant having a large actual or 'virtual'  $P_s$  of the same sign.<sup>46.52.55</sup> However, until recently, many such dopants have had little or no affinity for  $S_C^*$  phase formation. Even additions of small amounts of dopants have led to sharp decreases in the thermal stability of the  $S_C^*$  phases of the mixtures, compared with that of the  $S_C^*$  phase of the host material.

### 1.5. Summary and Aims of the Work

The lack of a molecular centre of symmetry combined with a low symmetry monoclinic environment enables tilted asymmetric smectic phases to exhibit ferroelectric properties. The  $S_C^*$  phase has been the most widely studied of the seven potentially ferroelectric smectic liquid crystalline phases, because of availability of suitable materials. At present, it offers the greatest potential for device applications because of the short response times of the phase. Novel electro-optical devices exploiting the ferroelectric properties of the  $S_C^*$  phase have major advantages over currently used liquid crystal displays in terms of much faster switching, bistability and ease of multiplexing; at the same time, they maintain the advantages of low threshold voltages, good optical contrast and low power consumption.

Although the most significant molecular parameters - spontaneous polarisation ( $P_s$ ), pitch-length ( $P$ ), and tilt angle ( $\theta$ ) affecting mainly switching times, bistability and

optical contrast respectively - have been described in detail, other factors such as dielectric anisotropy ( $\Delta \epsilon$ ) and alignment are also known to be important factors.<sup>XVIII</sup> The effect of viscosity ( $\eta$ ) on switching speed has not been discussed in detail, as this is very difficult to define or determine accurately.

Values of  $\eta$  are often obtained from measurements of the switching or 'response' time ( $\tau$ ) which not only varies with temperature and field strength, but is also complicated by the effects of  $P_s$ ,  $\Theta$  and  $\Delta \epsilon$ .

At the time of commencing this work, many of the available ferroelectric liquid crystal materials exhibited only short temperature range  $S_C^*$  phases and low values of  $P_s$ . The aim of this research was to synthesise new materials which would allow a more accurate assessment of the device potential of the  $S_C^*$  phase to be made and hopefully provide useful materials for future device applications. Bearing these points in mind, a range of novel materials was required in order to provide:

- a) wide temperature range  $S_C^*$  phases, occurring around room temperature.
- b) large values of  $P_s$ , enabling faster switching and lower threshold voltages to be used in devices.
- c) large values of  $P$ , facilitating helix 'quenching' and encouraging bistability.

---

XVIII. More recently, the importance of birefringence ( $\Delta n$ ) has been realised in terms of optical contrast and brightness of the SSFLC device<sup>36.56</sup> The intensity of light transmitted through the device depends critically on the cell thickness and the birefringence of the material.

- d) combinations of both signs of  $P_s$  and  $P$ , allowing long pitch-lengths and high values of  $P_s$  to be maintained in mixtures.
- e) a  $S_A$  phase above the  $S_C^*$  phase, providing a value for  $\theta \approx 22.5^\circ$  and enabling well-aligned planar samples to be attained.
- f) a  $Ch$  phase above the  $S_A$  phase, facilitating achievement of helical twist sense compensation and a planar alignment.
- g) a low value of  $\eta$ , enabling faster switching times.
- h) a negative value of  $\Delta \epsilon$ , thus facilitating the switching operation.

This thesis describes the synthesis of a range of such experimental materials and studies of those properties relevant to applications in ferroelectric devices.

## 2. Results and Discussion

## Results and Discussion

### 2.1 Compounds (5a-c) and (8a-d).

The first priority of this work was to obtain materials having a wide, room temperature  $S_C^*$  phase and relatively large values of spontaneous polarisation ( $P_S$ ). As a starting point, initial investigation focused on known  $S_C^*$  materials and on the physical effects of removing or replacing certain structural features. DOBAMBC, the original  $S_C^*$  compound studied by Meyer et al is unsuitable for device application due to its fairly high melting point (76°C), high temperature  $S_C^*$  range (63°C - 95°C) and low  $P_S$  (ca.5 nCcm<sup>-2</sup>). By removing the cinnamate linkage of DOBAMBC it was thought that the value of  $P_S$  may increase due to the greater proximity of the chiral centre to the polarisable aromatic core. Compounds [5a-c (Table I)] were therefore synthesised in order to verify this assumption and also to ascertain the effect on melting point and thermal stability of the  $S_C^*$  phase with respect to DOBAMBC.

A direct comparison between compounds (5a-c) and DOBAMBC cannot be made as  $n = 10$  was not prepared. However, the data for the hexyl, heptyl and octyl homologues, indicate that the thermal stabilities of both the  $S_C^*$  and  $S_A$  phases would be lowered by ca 55°C and that, despite a general tendency for the thermal stabilities of both phases to increase slightly with  $n$ , the overall depression in thermal stability is so great that the underlying monotropic  $S_I^*$  phase of DOBAMBC

The conjugated core in compounds (5a-c) is shorter than that in DOBAMBC, but the chiral centre is still adjacent to polarisable conjugated  $\pi$  electrons.

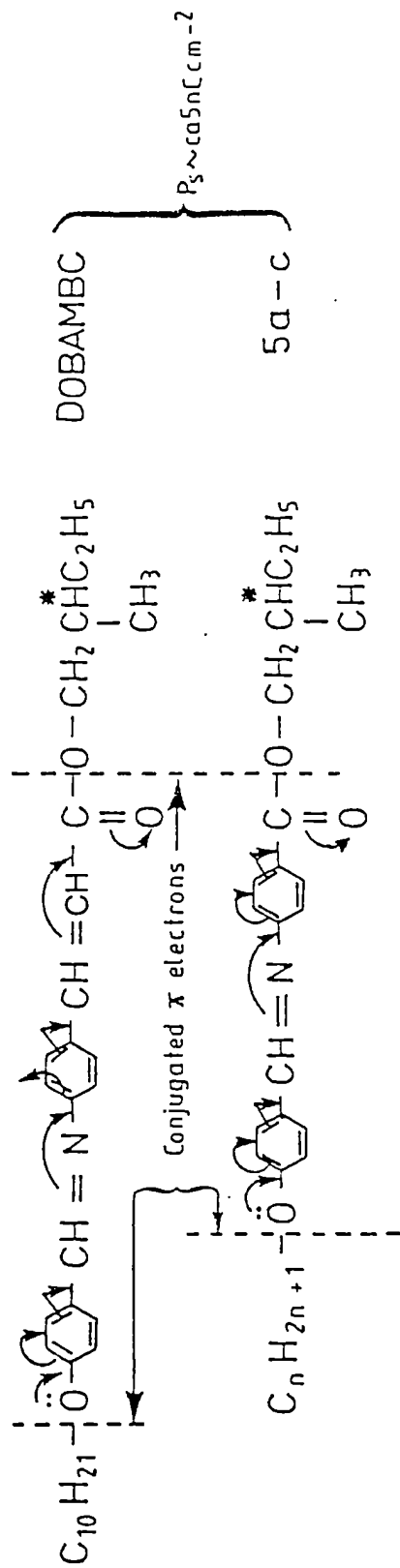
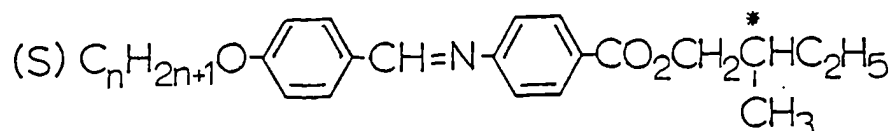


Fig. 34. Effect of removing cinnamate linkage on  $P_s$ .

Table I; Compounds 5a-c



n	mp (°C)	S <sub>C</sub> <sup>†</sup> -S <sub>A</sub> (°C)	S <sub>A</sub> -I (°C)	P <sub>G</sub> (nC cm <sup>-2</sup> )	sign of P <sub>G</sub> (+/-)	Helical twist sense <sup>†</sup> (D/L)
5a.. 6	46.8	(20.0) <sup>-10</sup>	61.1			
5b.. 7	46.9	(35.5)	61.1	ca5	-	D
5c.. 8	41.5	(38.5)	65.5			

† In this thesis, the helical twist sense was determined via the adapted 'contact' method, discussed in Section 1.4.1.

Figures in round brackets indicate a monotropic phase transition, i.e. one which occurs below the melting point and is only observed on supercooling the material.

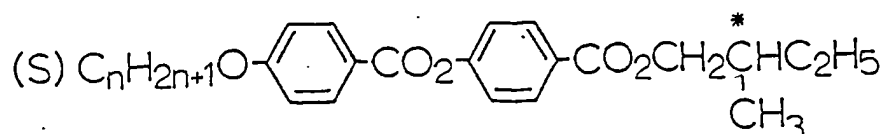
The convention XY is used to denote a transition temperature (X) that was determined from D.S.C. measurements at a heating rate of Y °C min<sup>-1</sup>.

would be lost altogether. The ranges of the S<sub>C</sub><sup>\*</sup> phases of compounds (5a-c) have been lowered to around room temperature, but as the corresponding melting points are lowered by only ca 30°C, the S<sub>C</sub><sup>\*</sup> phases become monotropic.

A disappointing result for compounds (5a-c) is that the value of P<sub>G</sub> has not increased with respect to DOBAMBC. This may be surprising at first, but can be explained by considering that the cinnamate linkage of DOBAMBC forms an extended conjugation of the π electrons of the aromatic core. Although removing this cinnamate linkage brings the chiral centre closer to the aromatic core in compounds (5a-c); the chiral centre still remains adjacent to polarisable π-electrons as in DOBAMBC, and therefore a similar value of P<sub>G</sub> is retained, (Fig. 34).

A further drawback with DOBAMBC in terms of device suitability is the chemical and u.v. instability of the Schiff's base linkage. Electro-optical experiments using Schiff's base materials often show a marked drop in transition temperatures, even after only a few hours exposure to light and electric fields.<sup>57</sup>

Table II; Compounds 8a-d



n	mp (°C)	S <sub>C</sub> <sup>*</sup> -S <sub>A</sub> (°C)	S <sub>A</sub> -I (°C)	P <sub>S</sub> (nCc <sub>m</sub> -2)	sign of P <sub>S</sub> (+/-)	Helical twist sense <sup>+</sup> (D/L)
8a.. 6	41.0					
8b.. 7	42.0	(23.7)	53.0	ca5	-	D
8c.. 8	34.5	(30.6)	58.1			
8d.. 9	55.7	(37.6)	57.8			

<sup>+</sup> see footnote to Table I

For this reason, compounds (8a-d) were synthesised in order to eliminate the unstable schiff's base linkage of compounds (5a-c) and replace it by the more stable ester group (Table II).

The thermal stabilities of both the S<sub>C</sub><sup>\*</sup> and S<sub>A</sub> phases of compounds (8b,c) are lowered by ca 8°C compared with compounds (5b,c). This is accompanied by only a slight depression in the melting points of these materials (between 5~7°C), and so the S<sub>C</sub><sup>\*</sup> phases remain monotropic. Compounds (8a-d) demonstrate again how the thermal stability of the S<sub>C</sub><sup>\*</sup> phase increases steadily with n, although this is not the

case for the  $S_A$  phase which appears to have reached a maximum thermal stability at  $n=8$ ; allowance must be made however for possible alternation in  $S_A$ -I temperature.

As expected, the values of  $P_g$  for compounds (8a-d) are similar to those for compounds (5a-c), since the local molecular environment of the chiral centre remains unchanged.

### Summary of Section 1

In summary, it can be seen that removing the cinnamate function of DOBAMBC and replacing the Schiff's base linkage with an ester group, has led to some desirable effects on molecular properties - lowering the melting points (e.g.; 8c...; mp=34.5 °C), depressing the range of the  $S_C^*$  phase to room temperature (e.g.; 8d...;  $S_C^* - S_A = 37.6^\circ\text{C}$ ) and ejecting the underlying  $S_I^*$  phase.

However, removing the cinnamate linkage has not resulted in an increase in  $P_g$  and the resulting  $S_C^*$  phases of compounds (5a-c) and (8a-d) are all monotropic.

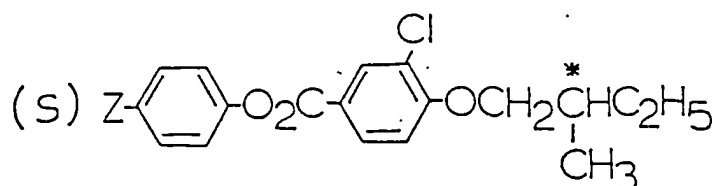
Finally, it is worth noting that the sign of  $P_g$  for all these materials is negative (as defined earlier), and that the twist sense of the helices follow the rules given by Goodby for an overall positively inducting substituent at the chiral centre, i.e.; S e D; (+I).

## 2.2 Compounds (9a-c).

Compounds (9a-c) were synthesised in an effort to obtain materials with higher values of  $P_S$  (Table III). The chiral centre was brought closer to the aromatic core by replacing the adjacent ester function with an ether linkage. Also, a lateral chlorine atom was introduced into the adjoining phenyl ring, with its dipole directed towards the asymmetric carbon atom. It was hoped that these two changes would result in a more hindered rotation of the chiral centre with respect to the aromatic core, leading to larger values of  $P_S$ .

Both alkyl and alkyloxy homologues were made in order to determine the relative effects on melting points and mesogenic behaviour.

Table III; Compounds (9a-c).



	Z	mp (°C)	<sup>+</sup> K-K/ (°C)	<sup>++</sup> P <sub>S</sub> (n <sub>D</sub> 20 <sup>-2</sup> )	Sign of P <sub>S</sub> (+/-)	helical <sup>+++</sup> twist sense (D/L)
9a...	C <sub>7</sub> H <sub>15</sub> <sup>-</sup>	-14.0 <sup>10</sup>	(-25.0) <sup>10</sup>			
9b...	C <sub>7</sub> H <sub>15</sub> <sup>0-</sup>	56.0	-	ca 2.5	(-)	L
9c...	C <sub>8</sub> H <sub>17</sub> <sup>-</sup>	16.5 <sup>10</sup>	(-29.0) <sup>-10</sup>			

+ K-K/ indicates a crystal-crystal transition, observed by D.S.C.

++ Determined by calculation from results on an 8 wt% mixture of compound 9b in optically active CEB, 10°C below the S<sub>A</sub> to S<sub>C</sub><sup>\*</sup> transition of the mixture [this calculation was complicated by the fact that CEB has an opposite sign of P<sub>S</sub> to compounds (9a-c)].

+++ See footnote to Table I.

Although a lateral chlorine atom has been introduced and the orientation of the ester function in compounds (9a-c) has been reversed with respect to compounds (8a-d), their core structures are still reasonably comparable in terms of shape and size. The end groups are also very similar.

Nevertheless, compounds (9a-c) do not exhibit any liquid crystalline behaviour, even on supercooling.

Another significant point is that the melting points of compounds 9a and 9c are lower than the melting point of compound 9b by 40° C and 70° C respectively. This is generally true for materials having an alkyl end chain rather than the corresponding alkyloxy group.

The magnitude of  $P_g$  for these materials is disappointingly small and indicates that, despite bringing the asymmetric carbon atom closer to the phenyl ring, the lateral chlorine atom is having little or no effect in restricting rotation about the chiral centre.

### Summary of Section 2

As compounds (9a-c) have no mesogenic properties and the calculated  $P_g$  value of only  $2.5 \text{ nCcm}^{-2}$  is still low, their suitability for device application is obviously limited. However they do illustrate how fairly small differences in molecular structure can dramatically influence both liquid crystalline behaviour and melting points.

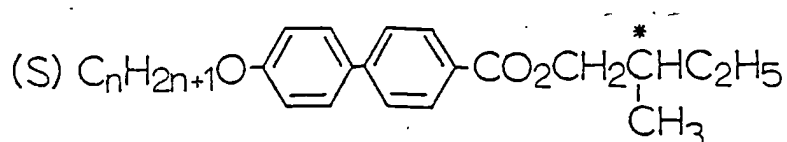
Compounds (9a-c) have a negative value for the sign of  $P_g$  and again demonstrate the applicability of the rules governing helical twist sense, absolute configuration and

distance of the chiral centre from the ring system. The asymmetric carbon atom is now an odd number of atoms from the aromatic core and so the helical twist sense has altered with respect to compounds (5a-c) and (8a-d) to give; S o L; (+I).

### 2.3 Compounds (12a-c), 16a-d) and (17).

In a continuation of the work on compounds (5a-c) and (8a-d), compounds [12a-c (Table IV)] were synthesised in order to establish the relative effect on liquid crystalline behaviour of removing the linking group between the phenyl rings altogether. A negligible effect on  $P_S$  was expected as the local environment of the asymmetric centre would remain unchanged.

Table IV; Compounds (12a-c).



n	mp (°C)	$S_C^*-S_A$ (°C)	$S_A-I$ (°C)	$P_S$ ( $nC_{cm}-2$ )	Sign of $P_S$ (+/-)	helical <sup>++</sup> twist sense (D/L)
P6a. <sup>+6</sup>	47.0	-	65.2			
P6b. <sup>+7</sup>	43.0	(42.0)	62.5			
12a..8	48.5	(43.1)	64.4			
12b..9	60.1	(42.6)	63.8	3*4	-	D
12c..10	48.5	(42.7)	65.9			

<sup>+</sup> synthesised by Dr. Peter Gemmill

<sup>++</sup> see footnote to table I

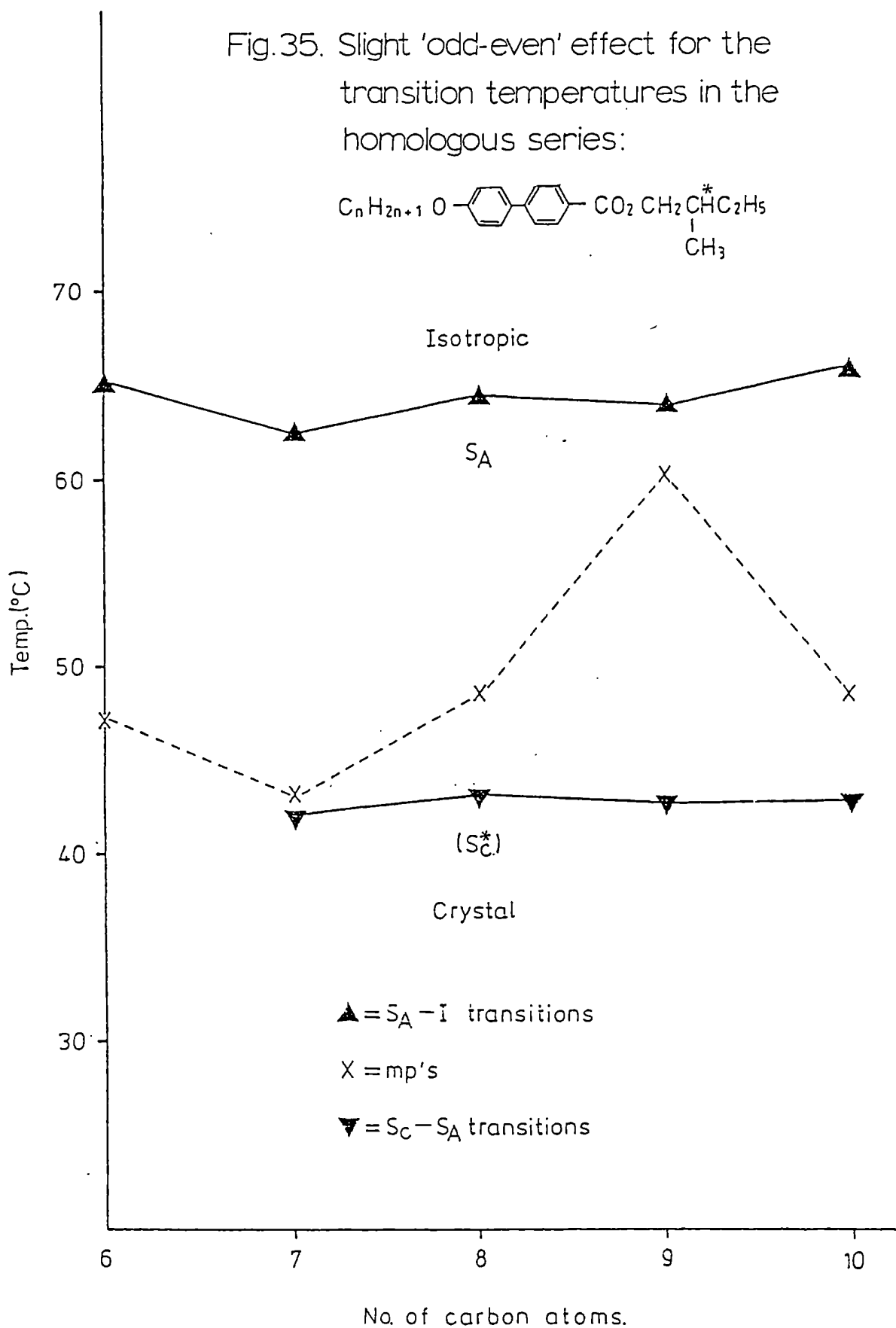
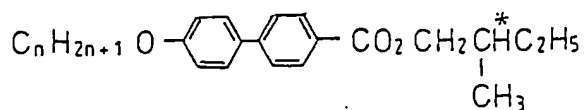
The most notable feature of the homologous series shown in Table IV is the disappearance of the  $S_C^*$  phase at  $n = 6$ . This type of behaviour, whereby a phase appears or disappears at a given chain length is not uncommon and seems to occur frequently with  $S_C/S_C^*$  phases.

For the heptyl, octyl and nonyl homologues in Table IV, the thermal stability of the  $S_C^*$  phase has been increased by between 6-18°C in relation to compounds (8b-d), but as the corresponding melting points have also increased by between 1-14°C, the  $S_C^*$  phases are still monotropic. However, in the case of the heptyl homologue, the  $S_C^*$  to  $S_A$  phase transition occurs just 1°C below the melting point and the  $S_C^*$  phase is very easily obtained by supercooling the preceding  $S_A$  phase. The thermal stability of the  $S_A$  phase has also been increased in comparison with compounds (8b-d), but by between 6-9°C.

Unlike compounds (5a-c) and (8a-d), the homologous series in Table IV does not show any real increase in thermal stability of the  $S_C^*$  and  $S_A$  phases with increase in alkoxy chain length. A small 'odd-even' effect is exhibited whereby, in this case, 'even' members of the series (ie.  $n = 6, 8$  and  $10$ ) have slightly higher thermal stabilities of both the  $S_C^*$  and  $S_A$  phases than the corresponding 'odd' members of the series (Fig 35). Again, this type of behaviour is not unusual and can be particularly noticeable when, starting with short chains, a large number of odd and even homologues is under consideration.

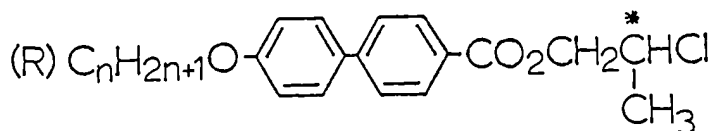
A surprising result arising from compounds (12a-c) is the drop in  $P_g$  from ca  $5n\text{Ccm}^{-2}$  to around  $3-4n\text{Ccm}^{-2}$  in relation to compounds (5a-c) and (8a-d). One explanation for this may be that although the local environment of the chiral centre has remained the same, removing the ester/Schiff's base linkage from between the phenyl rings has slightly reduced the number of polarisable  $\pi$ -electrons available and thereby slightly lowered the resulting value of  $P_g$ .

Fig.35. Slight 'odd-even' effect for the transition temperatures in the homologous series:



It had already been demonstrated by Meyer et al.<sup>29</sup> that replacing the  $\text{C-ethyl}$  unit of a DOBAMBC type molecule<sup>xix</sup> with a  $\text{C-Cl}$  unit dramatically increased the value of  $P_S$ . Therefore in order to obtain larger values of  $P_S$ , compounds (16 a-c) were prepared with the 2-methylbutyl end group of compounds (12 a-c) replaced by a 2-chloropropyl group (Table V).

Table V; Compounds (16a-c).



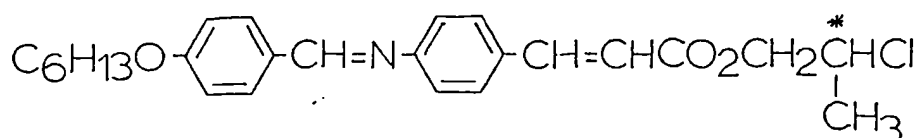
n	mp (°C)	S <sub>A</sub> -I (°C)	P <sub>S</sub> (nCcm <sup>-2</sup> )	Sign of P <sub>S</sub> (+/-)	helical <sup>+++</sup> twist sense (D/L)
FGc. <sup>+6</sup>	73.0	86.4			
FGd. <sup>+7</sup>	79.0	86.7			
16a. 8	77.5	86.2			
16b. 9	84.0	86.7	ca18 <sup>++</sup>	-	D
16c. 10	82.8	87.0			
FGe. <sup>+12</sup>	85.5	86.1			

+ Synthesised by Dr. Peter Gemmell.

++ Calculated by extrapolating from the P<sub>S</sub> value of a 10% mixture of compound 16b in a S<sub>C</sub> host having a negligible P<sub>S</sub>.

+++ See footnote to table I

XIX p-Hexyloxybenzylidene-~~p~~-amino-2-chloropropylcinnamate (HOBACPC) or more correctly 2-chloropropyl 4-(4-n-hexyloxybenzylidene) aminocinnamate.



mp. 60.0°C

S<sub>I</sub><sup>\*</sup> 64.0° ↔ S<sub>C</sub><sup>\*</sup> 78.0° ↔ S<sub>A</sub> 135.0°C | P<sub>S</sub> ~10-20nCcm<sup>-2</sup>

Comparing compounds (16a-c) with the structurally similar compounds (12a-c) reiterates the point that fairly small molecular differences can lead to quite drastic changes in mesogenic behaviour. Substituting the ethyl group for a chlorine atom at the chiral centre has increased the thermal stability of the resulting  $S_A$  phases by ca22°C and has caused the disappearance of the previously underlying, monotropic  $S_C^*$  phases. The homologous series in Table V also contrasts with earlier series in that the thermal stability of the  $S_A$  phase varies by less than 1°C overall and therefore appears to be independent of alkoxy chain length for  $n = 6-12$ .

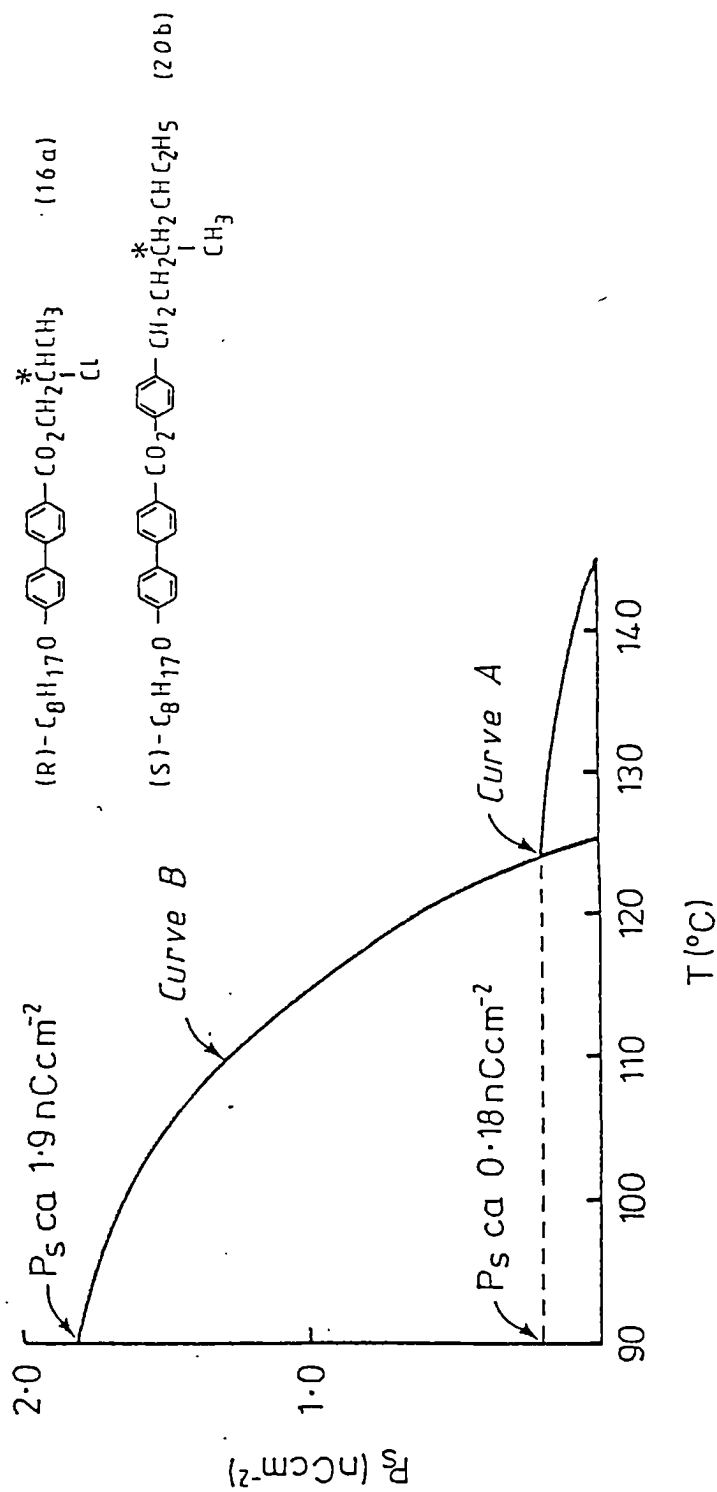
The melting points of compounds (16a-c) have increased by between 24°-34° C with respect to corresponding compounds (12a-c), so that in terms of liquid crystalline properties, replacing the 2-methylbutyl end group with a 2-chloropropyl end group is an undesirable structural modification.

More importantly though, this substitution has led to an approximately five fold increase in  $P_S$  for compounds (16a-c), and this can be directly attributed to the increased polarity of the  $C^*-Cl$  bond over that of the  $C^*-CH_3$  bond.

As these materials have no inherent tilted chiral phases,  $P_S$  values cannot be obtained directly and so must be determined by the extrapolation procedure described earlier. In this particular case, a small amount of the dopant was mixed with a  $S_C^*$  host having a negligible  $P_S$  (Fig. 36).

In order to make a direct comparison between chloro and hydroxy groups as polar substituents at the chiral centre, compound [16d (Table VI)] was prepared. Although replacing

Fig.36: Determination of  $P_S$  by extrapolation for compound (16a)



Curve A shows the low  $P_S$  values recorded for compound (20b).

Curve B indicates how just 10% of compound (16a) in compound (20b) increases the  $P_S$  value of the resultant  $S_C^*$  phase. Extrapolating this value for 100% compound (16a) leads to the value of  $P_S$  shown in table IV.

(Note also how only 10% of compound (16a) has decreased the thermal stability of the resulting  $S_C^*$  mixture by ca 20°C v.r.t. pure compound (20b)).



Replacing the 2 - methylbutyl end group of compound (12b) with the isopinocampheyl group has led to a drop in thermal stability of the  $S_A$  phase by  $15^\circ\text{C}$  and to an increase in the melting point by  $7^\circ\text{C}$ , resulting in a monotropic  $S_A$  phase and the loss of the monotropic  $S_C^*$  phase. This modification has nevertheless introduced in compound (17) a monotropic cholesteric phase above the  $S_A$  phase, and this may be useful in aiding sample alignment in electro-optic cells.

The most important breakthrough though was the enormous increase in  $P_g$ , from  $3\sim 4 \text{ nCcm}^{-2}$  for compound (12b) to an extrapolated value of  $58.5 \text{ nCcm}^{-2}$  for compound (17). As the substituents at the chiral centre are equally polar in both materials, the approximately fifteen fold increase in  $P_g$  must be attributed to a combination of steric hindrance and proximity of the asymmetric centre to the polarisable conjugated  $\pi$ -electrons of the aromatic core, (Fig. 37).

### Summary of Section 3

In this section it has been shown that removing the linkage between the phenyl rings of compounds (5a-c) and (8a-d) generally leads to a fairly small increase in melting points and thermal stabilities of both the  $S_C^*$  and  $S_A$  phases. A slight drop in the value of  $P_g$  and the appearance of an 'odd-even' effect also arise from this modification.

Replacing the ethyl substituent at the chiral centre of compounds (12a-c) with a chlorine atom or hydroxy group has an adverse effect on mesogenic properties, particularly in the case of the hydroxy compound. Nonetheless these substituent changes give rise to a five fold increase in  $P_g$  for compounds (16a-d).

A more dramatic result emanates from replacing the 2-methylbutyl end group in compound (12b) by the isopinocampheyl group. This results in the loss of the  $S_C^*$  phase and a depression in the thermal stability of the  $S_A$  phase. However the introduction of a monotropic cholesteric phase and a fifteen fold increase in  $P_g$  may make such a material useful in terms of device potential and future research.

Although it was not possible to determine the sign of  $P_g$  and helical twist sense for compound (16d) due to lack of material, all other compounds in this section exhibited a negative  $P_g$  and followed the rules given earlier relating helical twist sense and absolute configuration etc., ie:

Compounds (12a-c)	S e D, (+I);
Compounds (16a-c)	R e D, (-I);
and Compound (17)	R o D, (+I).xx

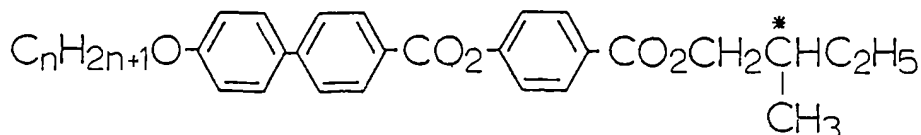
---

XX. Compound (17) has 4 chiral centres (1R, 2R, 3R, 5S), but it is the asymmetric carbon atom adjacent to the carbonyl function which should have the greatest effect in determining helical twist sense.

## 2.4. Compounds (19a-c), (20a,b) and (23a-c).

Now that high  $P_S$  materials had been prepared, it was necessary to concentrate on obtaining new compounds having wide temperature range, enantiotropic  $S_C^*$  phases. Fortunately, at this point Dr. Peter Gemmell succeeded in synthesising two such materials, again using 2-methylbutyl as the end group. The melting points, transition temperatures and  $P_S$  values of these compounds are given in Table VII.

Table VII: Wide temperature range  $S_C^*$  materials synthesised by P. Gemmell.



	n	mp (°C)	<sup>+</sup> $S_C^*-S_C^*$ (°C)	$S_C^*-S_A$ (°C)	$S_A-I$ (°C)	$P_S$ (n°C <sup>-2</sup> )
PGf...	8	67.0	(61.5)	139.0	187.0	ca 8.
PGg...	9	52.5	57.0	143.5	184.5	

<sup>+</sup>  $S_C^*$  phase not yet confirmed by miscibility or X-ray studies.

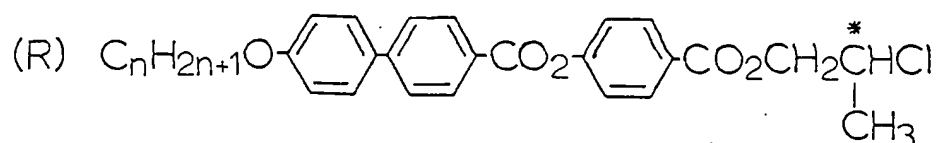
Although the  $S_C^*$  phases of these materials occur well above room temperature ( $S_C^* - S_C^* = 57.0^\circ\text{C}$  for  $n=9$ ), their very wide temperature ranges ( $86.5^\circ\text{C}$  for  $n=9$ ) implied that this general structure would induce  $S_C^*$  phases even when using different end group.

Of the three high  $P_S$  end groups employed in the previous section, 2-chloropropyl had had the least detrimental effect on liquid crystalline properties. It was therefore decided to use the  $S_C^*$  promoting core structure given above with 2-chloropropyl as the ester function, hoping that

compounds (19a-c) would exhibit wide temperature range  $S_C^*$  phases having large values of  $P_S$ .

For the two compounds in Table VII, as  $n$  increases, the melting point decreases and the temperature range of the  $S_C^*$  phase increases. Therefore the decyl and undecyl homologues were prepared in addition to the octyl and nonyl homologues; the results are given in Table VIII.

Table VIII; Compounds (19a-c).



	$n$	mp (°C)	$S_C^*-S_A$ (°C)	$S_A-I$ (°C)	$P_S$ (nCcm-2)	Sign of $P_S$ (+/-)	helical <sup>++</sup> twist sense (D/L)
19a...	8	95.0	(93.0)	194.0			
19b...	9	88.0	106.5	191.6	ca5	-	D
PGh...	<sup>+</sup> 10	90.0	113.0	193.0			
19c...	11	92.0	99.5	189.0			

<sup>+</sup> Prepared by Dr. P Gemmill.

<sup>++</sup> see footnote to Table I.

Replacing the 2-methylbutyl end-group of compounds (PGf,g) with 2-chloropropyl has effected a rise in the thermal stabilities of the corresponding  $S_A$  phases of compounds (19a,b) by 7°C. It has also led to big increases in the melting points of compounds (19a,b) by 28° and 35°C, and to large decreases in the thermal stabilities of the  $S_C^*$  phases by 46° and 37°C respectively, thereby considerably reducing the  $S_C^*$  phase temperature ranges.

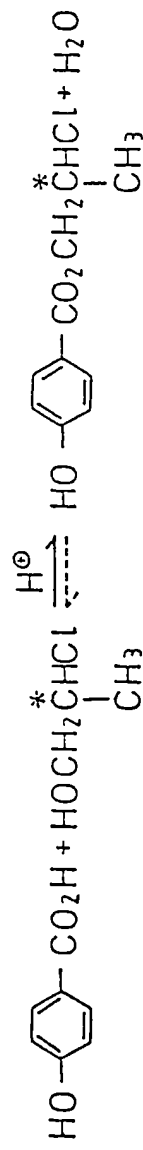
Considering all the compounds in Table VIII, the thermal stability of the  $S_A$  phase again exhibits an 'odd-even' effect, with the 'even' members of the series tending to exhibit slightly higher thermal stabilities. As anticipated, the thermal stability of the  $S_C^*$  phase does indeed rise with increasing alkoxy chain length, but this peaks at  $n=10$  and begins to fall again as  $n$  increases further. Overall then, substituting the 2-methylbutyl end group with 2-chloropropyl has had an adverse effect on the required liquid crystalline properties, as in section 3. On the other hand, the underlying  $S_F^*$  phases of the two 2-methylbutyl compounds have been eliminated, and the nonyl, decyl and undecyl homologues have all retained enantiotropic  $S_C^*$  phases.

A more disappointing and surprising result is that the  $P_g$  values of these compounds are even smaller than those of the corresponding 2-methylbutyl compounds. However, a reasonable explanation for this may be provided by the fact that the specific rotations of compounds (19a-c) are very small in comparison with those of compounds (16a-c), implying that some racemisation may have taken place during synthesis. It is most likely that this occurs in step 7.1, where (R) 2-chloropropanol and 4-hydroxybenzoic acid interact under acid catalysis at elevated temperatures, to give (R-(-)-2-chloropropyl) 4-hydroxybenzoate.

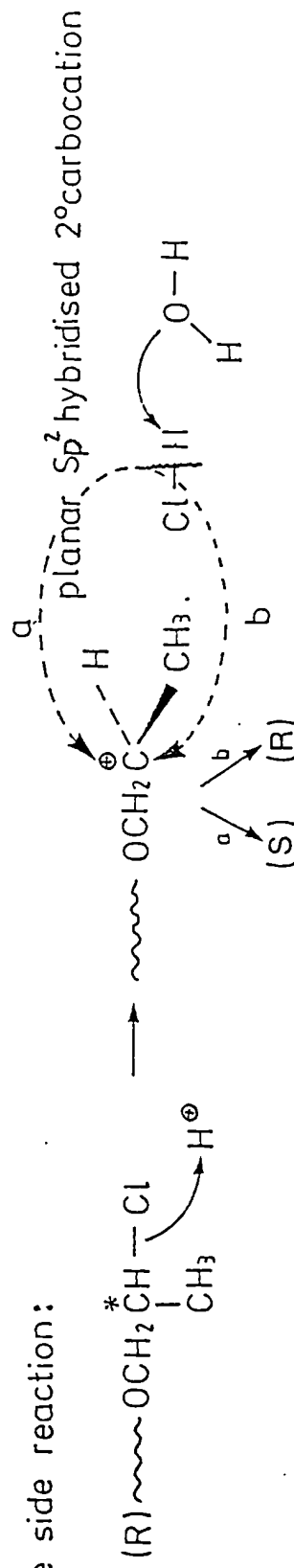
The possibility arises that under these conditions, as well as the main esterification reaction, a reversible elimination/addition reaction involving the chlorine atom at the chiral centre may take place, via a  $sp^2$  hybridised carbocation (Fig. 38). An addition to this carbocation can

Fig.38: Racemisation of (R)-2-chloropropyl 4-hydroxybenzoate.

Main reaction:



Possible side reaction:

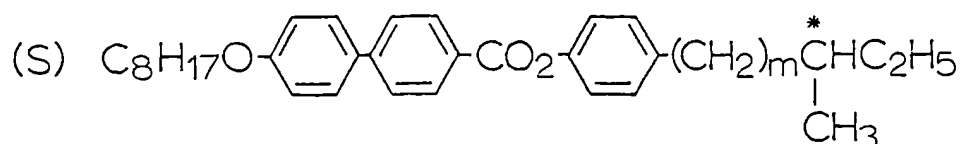


Chlorine ion may attack from above or below  $2^\circ$  carbocation, leading to racemisation of the asymmetric carbon atom.

obviously take place either above or below the molecular plane, thereby lowering the optical purity and ultimately the  $P_S$  of the final product.

As compounds (19a-c) were being prepared, work was also under way on other materials which might exhibit wide temperature range  $S_C^*$  phases. The first of these, compounds [20a,b (Table IX)], used the same basic  $S_C^*$  - promoting core structure as compound (PG f), but with the aryl-alkyl ester function removed and variations in the distance of the chiral centre from the phenyl ring.

Table IX. Compounds (20a,b).



	n	mp (°C)	$^+S - S_C^*$ (°C)	$^{++}S_C^* - S_C^*$ (°C)	$S_C^* - S_A$ (°C)	$S_A - \text{Ch/I}$ (°C)	Ch - I (°C)	$P_S$ ( $n_D^{20} \text{ cm}^{-2}$ )	Sign of $P_S$ (+/-)	helical <sup>+++</sup> (D/L)
20a	1	81.0	(75.5)	(80.0)	131.4	169.9	174.2	2.2	+	D
20b	2	83.5	—	96.5	144.6	180.3 <sup>10</sup>	—	0.2	-	L

+ unidentified smectic phase

++ not confirmed by miscibility or X-ray studies

+++ see footnote to table I

Removing the aryl-alkyl ester function from compound (PG f) has introduced a cholesteric phase and an unidentified monotropic smectic phase into compound (20a), and converted the monotropic  $S_C^*$  phase of the former compound into a monotropic  $S_C^*$  phase. The melting point has been increased by 14°C for compound (20a), and the thermal stabilities of the

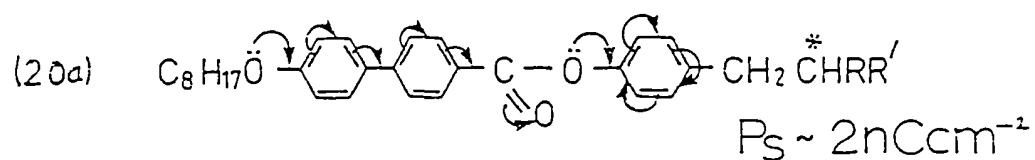
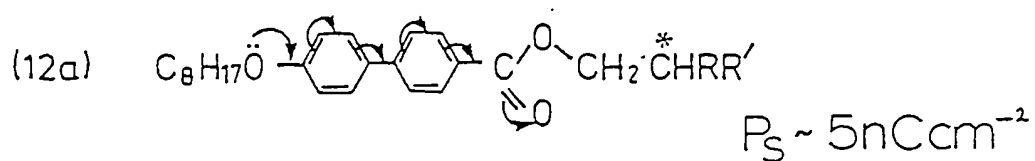
$S_C^*$  and  $S_A$  phases have been lowered by  $8^\circ$  and  $17^\circ$  C respectively. Moving the chiral centre one carbon atom further away from the phenyl ring in compound (20b) further increases the melting point by  $2.5^\circ$  C and in addition causes the cholesteric phase and the unidentified smectic phase of compound (20a) to disappear. This displacement of the asymmetric centre also leads to an enhancement of the thermal stability of the  $S_C^*$  phase by  $13^\circ$  C and of the  $S_A$  phase by  $10^\circ$  C.

Although the mesogenic character of compounds (20a,b) is not as suitable for device purposes as that of compounds (PG f,g), removing the aryl-alkyl ester linkage of the latter materials has maintained an  $S_C^*$  temperature range of approximately  $50^\circ$  C and led to the useful introduction of a cholesteric phase in compound (20a).

Despite the fact that the chiral centre in compound (20a) is closer to the phenyl ring than in compound (17), the value of  $P_g$  is even lower than that in compounds (12a-d). This situation is akin to that in compounds (9a-c), and again highlights the importance of coupling between the asymmetric centre and the polarisable  $\pi$  electron conjugation of the aromatic core, which in this case breaks down at the adjacent methylene group. Comparing the  $P_g$  values of compounds (12a) and (20a) also implies that the carbonyl function is important not only as an extension for this conjugation, but additionally because of its large dipole moment, (Fig. 39).

Moving the chiral centre just one carbon atom further away from the phenyl ring as in compound (20b), has reduced the value of  $P_g$  to one tenth of its value in compound (20a).

Fig. 39: Importance of carbonyl function to  $P_S$ .

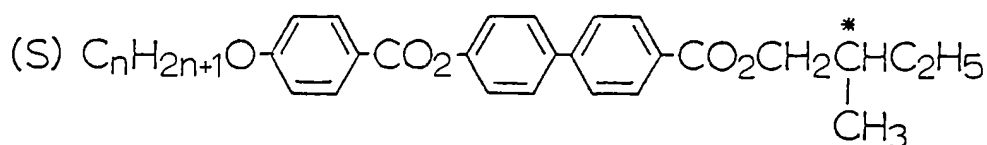


The carbonyl function not only extends  $\pi$  electron conjugation, but also acts as a large dipole in its own right. This results in a greater value of  $P_S$  for compound (12a), even though the chiral centre of compound (20a) is closer to the  $\pi$  electrons of the core.

This confirms the importance of situating the asymmetric carbon atom as closely as possible to the polar part of the molecule, in order to obtain maximum coupling between the two.

Like compounds (20a,b), compounds [23a-c (Table X)] were synthesised in an effort to obtain new materials having wide temperature range  $S_C^*$  phases. They were also prepared in order to investigate the effects on liquid crystalline properties of reversing the positions of the phenyl and biphenyl rings in compounds (PGf,g).

Table X; Compounds (23a-c).



	n	mp (°c)	$S_C^*-S_A$ (°c)	$S_A-Ch$ (°c)	Ch-I (°c)	$P_S$ (at $T_C-T=10^\circ C$ ) ( $nCc m^{-2}$ )	sign of $P_S$ (+/-)	helical twist sense <sup>+</sup> (D/L)
23a...	7	67.5	120.9	164.2	172.6			
23b...	8	84.0	123.4	166.0	171.8	ca3	-	D
23c...	9	83.5	126.7	165.1	168.0			

<sup>+</sup> see footnote to table I.

Comparing compounds (23b,c) directly with those in Table VII shows that the initial effects of reversing the positions of the phenyl and biphenyl rings have been to lower the thermal stabilities of the  $S_A$  phases by ca 20°C and of the  $S_C^*$  phases by ca 16°C. Conversely, the melting points of compounds (23b,c) are higher by 17 and 31°C respectively, so that the enantiotropic temperature ranges of the corresponding  $S_C^*$  phases have been reduced to about 40°C.

However, the melting point of compound (23a) is approximately 16° C lower than the melting point of compounds (23b,c), thereby extending the temperature range of its enantiotropic  $S_C^*$  phase to ca53° C.

Despite the overall reduction in  $S_C^*$  tendencies brought about by reversing the position of the phenyl and biphenyl rings, this modification has given rise to two useful changes - the introduction of a cholesteric phase and the ejection of the  $S_F^*$  phases present in compounds (PGf,g).

Although at first glance the  $P_g$  values of compounds (23a-c) are lower than those of comparable materials, in actual fact they are quite similar. This difference in the apparent value of  $P_g$  arises from a change at STC technology in the conditions under which its magnitude is assessed. Previously quoted values were usually taken, at the lower end of the  $S_C^*$  temperature range, where the magnitude of  $P_g$  is greatest and undergoes least temperature variation. As most of the materials discussed in this thesis so far have reasonably short temperature range  $S_C^*$  phases, differences in the magnitude of  $P_g$  emanating from temperature effects are largely insignificant. However, the advent of new, wider temperature range  $S_C^*$  phase materials necessitated that a standard procedure be adopted to allow more meaningful comparisons of  $P_g$  values made; this is achieved by measuring all  $P_g$  values at 10° C below the  $S_C^*$  to  $S_A$  transition.

#### Summary of Section 4

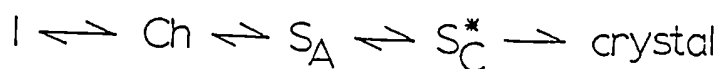
The work in this section has been concerned with increasing the  $P_g$  and modifying the mesogenic properties of

two, wide temperature range  $S_C^*$  materials (PGf,g) originally synthesised by Dr. Peter Gemmell.

Replacing the 2-methylbutyl end group of these materials with 2-chloropropyl leads to a large increase in melting points and a massive reduction in the temperature ranges of the  $S_C^*$  phases. Even more disappointing are the low values of  $P_g$  associated with compounds (19a-c), although this is probably due to some racemisation during synthesis.

Removing the aryl-alkyl ester function of compound (PGf) has brought about a reduction in the temperature range of the  $S_C^*$  phase to ca 50° C, although it has also introduced a cholesteric phase into the system. The relatively low  $P_g$  of compound (20b) dramatically illustrates the importance of positioning the chiral centre as closely as <sup>is</sup> possible to the polar region of the molecule.

Reversing the positions of the phenyl and biphenyl rings of compounds (PGf,g) also results in a large increase in melting point and a narrowing of the enantiotropic  $S_C^*$  temperature range to approximately 40° C. However, the corresponding heptyl homologue, compound (23a), does have a relatively low melting point and consequently a wider enantiotropic  $S_C^*$  temperature range of 53° C. The positive effects of this modification have been the introduction of a cholesteric phase and the ejection of the underlying  $S_F^*$  phase, thereby giving the desired phase sequence:



The sign of  $P_S$  for compound (20a) is positive, whereas for all the other materials in this particular section it is negative. The helical twist senses of these materials again adhere to the rules described earlier, ie,

Compounds (19a-c), R e D (-I);

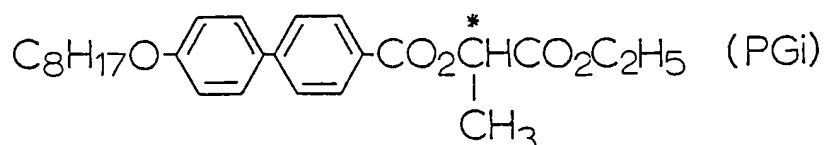
Compounds (23a-c), S e D (+I);

Moreover, compounds (20a,b) demonstrate the alternating effect on helical twist sense of an incremental increase in the distance of the chiral centre from the aromatic core, ie., S e D (+I); S o L (+I)

## 2.5 Compounds (28a-j) and (31a-i).

Although attempts made in section 4 to combine a wide temperature range  $S_C^*$  core structure with high  $P_S$  end groups had failed to produce the required results, comparison of the various materials confirmed that compounds (PGf,g) had by far the greatest  $S_C^*$  tendencies.

Additionally, the results for compounds (17) and (20a,b) highlighted the importance of the ester function and the position of the chiral centre with respect to the ring system, with regard to the magnitude of  $P_S$ . These observations were supported further by the very high  $P_S$  value (ca  $60nCc m^{-2}$  at  $T_C - T = 10$ ) associated with the compound (PGi) shown below, which was synthesised by Dr. Peter Gemmell.



Here the isopinocampyl end group of compound (17) has been replaced by the group derived from (S)-ethyl lactate. However, the asymmetric centre retains its position, adjacent to the aryl-alkyl ester function.

Bearing the above observation in mind, efforts were again made to combine high  $P_S$  properties with the  $S_C^*$  - promoting structure of compounds (PGf,g) using (S)-ethyl lactate, (R) isopinocampheol and various other chiral alcohols, to make esters in which the chiral centre would be directly adjacent to the aryl-alkyl ester function.

However, before this could be achieved, an alternative method of synthesising the various 4-hydroxybenzoate esters

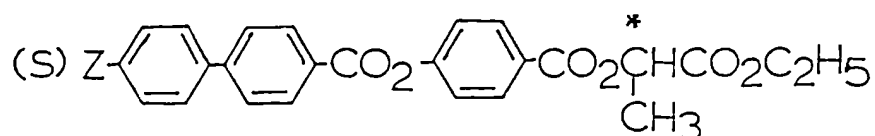
had to be found. The procedure must avoid the use of strongly acidic or basic conditions that might lead to significant racemisation.

Initially, 4-methoxybenzoyl chloride was used in a direct esterification with (S)-ethyl lactate, but the subsequent demethylation of the ester with phosphorous tribromide at  $-78^{\circ}\text{C}$ , caused saponification of the alkyl-alkyl ester function.

A second method involved preparation of 4-benzyloxybenzoic acid (step 10.2) and direct esterification of its acid chloride with (S)-ethyl lactate (step 10.4). Hydrogenolysis of this material (step 10.5) gave the required 4-hydroxybenzoate ester in good yield. More importantly, detailed inspection of the  $\text{H}^1\text{nmr}$ . spectra of this compound, obtained using differing amounts of an added chiral shift reagent, showed no splitting of the  $\text{CH}-\overset{*}{\text{C}}\text{H}_3$  peak, implying a high enantiomeric purity.

The 4-hydroxybenzoate ester with S-ethyl lactate was then used to prepare compounds (28 a-j); series of both alkyl and alkyloxy homologues were made, in order to establish the relative effects on melting points and liquid crystalline behaviour (Table XI).

Table XI Compounds (28a-j)



Z	mp (°C)	<sup>†</sup> S <sub>I</sub> <sup>*</sup> /S <sub>F</sub> <sup>*</sup> -S <sub>C</sub> <sup>*</sup> (°C)	S <sub>C</sub> <sup>*</sup> -S <sub>A</sub> (°C)	S <sub>A</sub> -I (°C)	P <sub>S</sub> (T <sub>C</sub> -T=10°C) (n <sub>D</sub> cm <sup>-2</sup> )	θ(T <sub>C</sub> -T=10°C) (°C)	sign of P <sub>S</sub> (+/-)	helical twist <sup>††</sup> sense D/L
28a..C <sub>7</sub> H <sub>15</sub> 0-	90.0	(67.0) <sup>-10</sup>	108.5	166.7	63.1	18.0		
28b..C <sub>8</sub> H <sub>17</sub> 0-	75.0	(62.6) <sup>-10</sup>	117.5	163.3	50.9	19.5		
28c..C <sub>9</sub> H <sub>19</sub> 0-	60.0	(46.0) <sup>10</sup>	122.4	157.8	55.4	20.5	+	L
28d..C <sub>10</sub> H <sub>21</sub> 0-	60.5	(36.9) <sup>-20</sup>	123.2	154.8	53.4	21.0		
28e..C <sub>11</sub> H <sub>23</sub> 0-	65.0	(38.0) <sup>-10</sup>	122.0	151.1	48.1	23.0		
-	-	S <sub>B</sub> <sup>-</sup> S <sub>C</sub> <sup>*</sup> /S <sub>A</sub> (°C)	-	-	-	-	-	-
28f..C <sub>8</sub> H <sub>17</sub> -	49.0	(48.5)	-	130.5	†††53.5	†††19.0		
28g..C <sub>9</sub> H <sub>19</sub> -	48.5	(43.5)	-	128.5	†††39.0	†††17.0		
28h..C <sub>10</sub> H <sub>21</sub>	57.0	(38.4) <sup>20</sup>	72.5	124.0	35.4	15.4	+	L
28i..C <sub>11</sub> H <sub>23</sub>	53.0	(42.3) <sup>10</sup>	71.0	122.3	38.7	17.0		
28j..C <sub>12</sub> H <sub>25</sub>	44.0	(35.0) <sup>-10</sup>	70.5	120.1	38.8	17.0		

† phase appears to be S<sub>I</sub><sup>\*</sup> or S<sub>F</sub><sup>\*</sup> by microscopy but this has not been confirmed by miscibility or X-ray studies.

†† See footnote to Table I.

††† Compounds (28f,g) have no chiral tilted phase; therefore P<sub>S</sub> values were determined by extrapolation of results for a 20 wt % solution in racemic CEB.

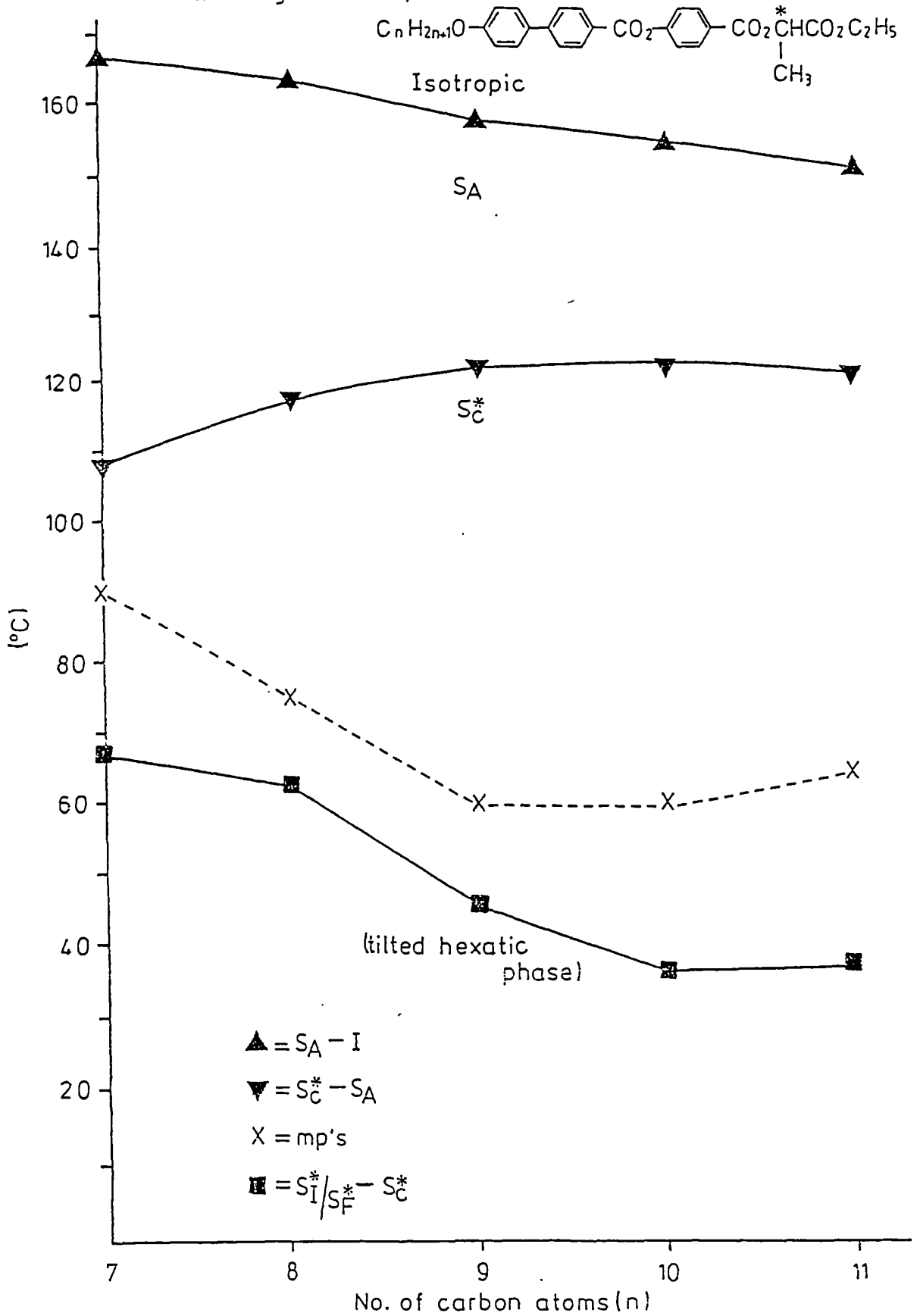
†††† Tilt angle for the S<sub>C</sub><sup>\*</sup> phase of a 20 wt % mixture of compound (28f) or (28g) in racemic CEB.

Furthermore, the setting up of new apparatus at STC Technology enabled accurate values of the tilt angle ( $\theta$ ) for  $S_C$  phases to be measured for the first time, providing further useful information from these two homologous series. As in the case of  $P_S$  values, to allow more meaningful comparisons between materials, values of  $\theta$  are all quoted at  $10^\circ\text{C}$  below the  $S_C^*$  to  $S_A$  transition.

A direct comparison between compounds (PGf,g) and (28b,c) shows that esterification with ethyl lactate has led to decreases in the thermal stabilities of the  $S_C^*$  phases by ca  $21^\circ\text{C}$  and of the  $S_A$  phases by ca  $25^\circ\text{C}$ . This modification has also led to a small rise in melting points by about  $8^\circ\text{C}$ , and to an unusual effect on the thermal stabilities of the underlying, monotropic hexatic phases. For the octyloxy homologue the thermal stability of this phase has risen by  $1^\circ\text{C}$ , whereas for the nonyloxy homologue it has fallen by  $11^\circ\text{C}$ , relative to compounds (PGf,g) respectively. However, looking at the homologous series of compounds (28e,f) as a whole (Fig. 40), these results fit a general pattern, in that the thermal stability of the tilted hexatic phase falls as the alkyloxy chain length increases.

Examination of figure 40 also reveals that as the alkyloxy chain length increases: the thermal stability of the  $S_A$  phase decreases fairly regularly; the thermal stability of the  $S_C^*$  phase rises quickly at first and then begins to level off after the nonyloxy homologue; the melting point falls rapidly before it also levels off at the nonyloxy homologue.

Fig. 40: Transition temperatures vs. no. of carbon atoms (n) for the homologous series;

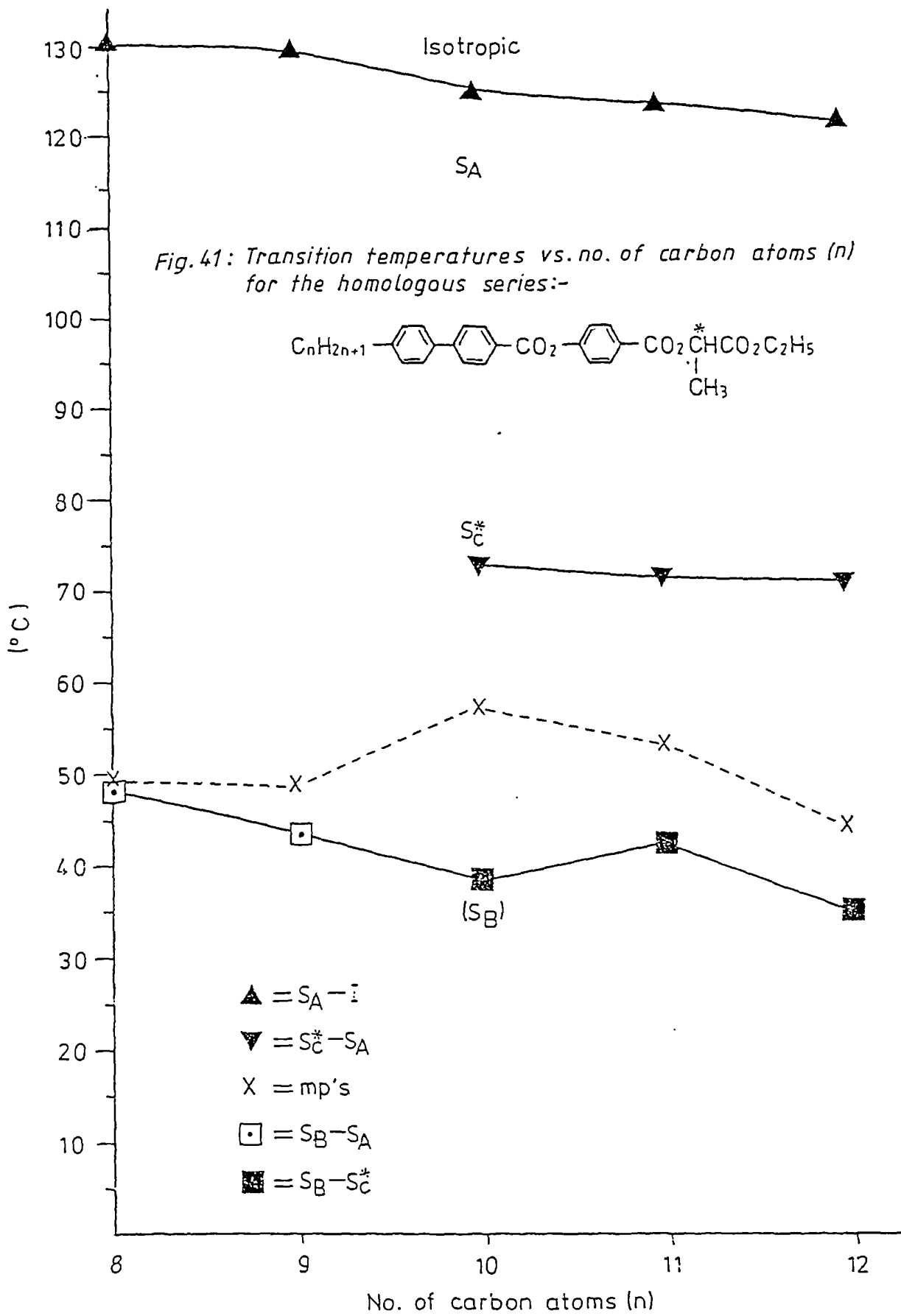


Overall therefore, derivation of the end groups in compounds (28a-e) from ethyl lactate has had a slightly adverse effect on the required mesogenic properties. Nevertheless, fairly similar melting points have been retained along with an approximately 60° C  $S_C^*$  temperature range for the compounds (28a-e).

In relation to the n-alkyloxy homologues (28a-e), the analogous n-alkyl homologues (28 f-j) will have very similar molecular shapes and chain lengths, differing significantly only in polarity. Nonetheless, this small structural change always effects substantial alterations to liquid crystalline properties; here it reduces the thermal stabilities of the  $S_A$  phases by between 31°-36° C and those of the remaining  $S_C^*$  phases by ca. 50° c. The monotropic tilted hexatic phases of compounds (28a-e) have also been replaced by monotropic  $S_B$  phases in compounds (28f-j); this structural modification has a variable effect in reducing melting points (by between 3-41° C).

This great variation in the depression of the melting points stems mainly from the large range of melting points exhibited by the alkyloxy materials (60°-90° C) and not from major variation in the melting points of the compounds (28f-j); these are much less diverse (44°-57° C).

Figure 41 illustrates the changes in mesogenic behaviour with increasing alkyl chain length for compounds (28f-j). The fairly uniform decrease in thermal stability of the  $S_A$  phase, the general decrease in thermal stability of the monotropic  $S_B$  phase, and most notably, the sudden injection of an  $S_C^*$  phase at the decyl homologue. This demonstrates

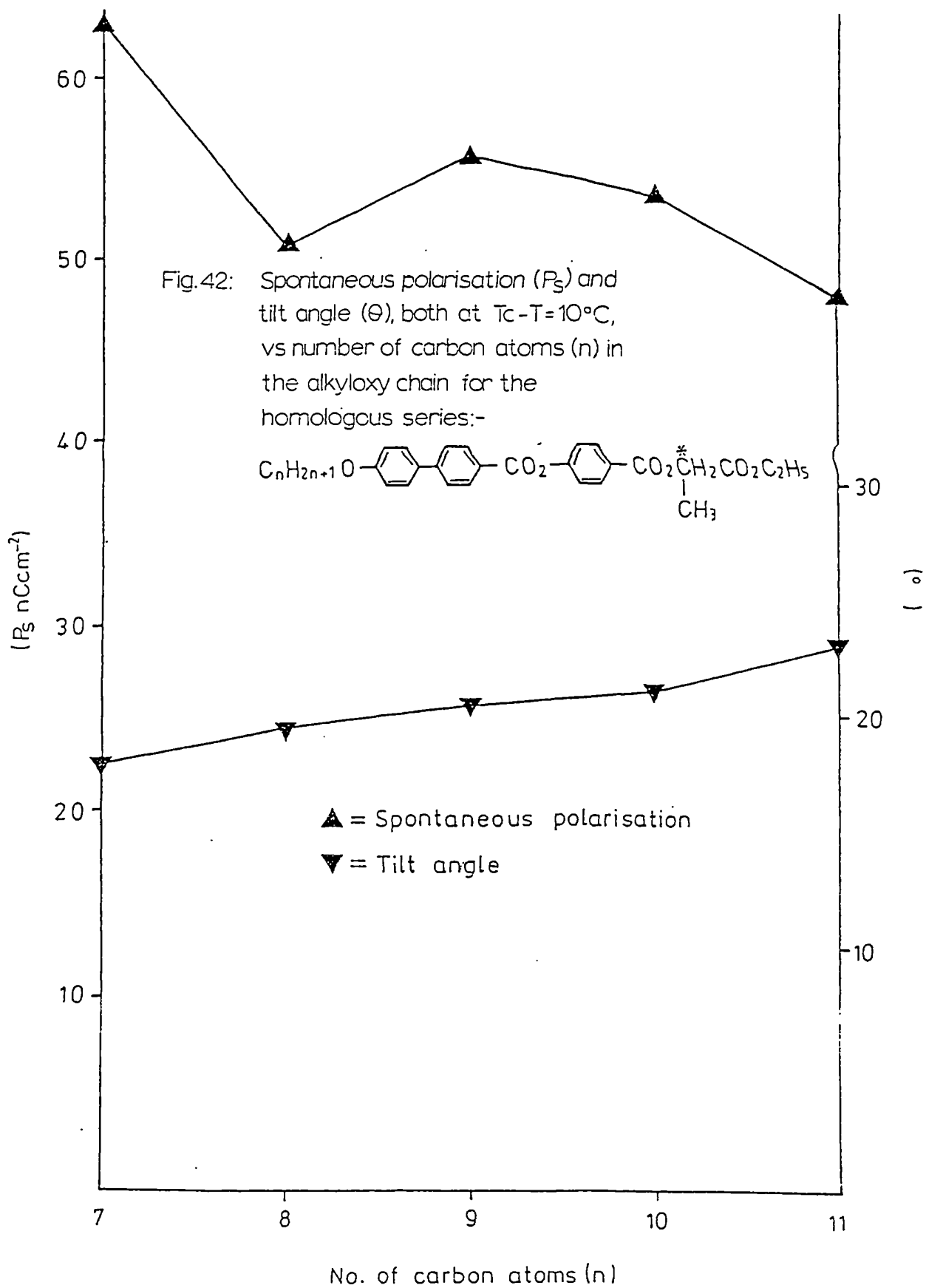


once more the particular vulnerability of the  $S_C^*$  phase to small structural changes, which in this case amount only to slight incremental changes in the number of carbon atoms in a long alkyl chain.

The most exciting results from compounds (28a-j) are the high  $P_S$  values recorded at  $10^\circ\text{C}$  below the  $S_C^*$  to  $S_A$  transition. For the alkyloxy homologues, these  $P_S$  values are roughly equivalent to those of compounds (17) and (PGi) and are approximately an order of magnitude greater than those for compounds (PGf,g).

The values of  $P_S$  associated with the alkyloxy compounds are about 30% higher than those for the similar alkyl materials, and this corresponds to similar differences in their respective tilt angles. Although this observation seems to lend some support to Meyer's original hypothesis that  $P_S$  is a function of tilt angle, a more detailed study of the results infers otherwise (Fig. 42).

From Figure 42, it is quite apparent that as the alkyloxy chain length of compounds (28a-e) increases, the tilt angle changes accordingly in a roughly linear fashion, probably due to the regular increase in molecular length. However, despite this increase in  $\theta$ , the corresponding values of  $P_S$  exhibit a definite decrease with increasing alkyloxy chain length, even though each homologue has exactly the same environment about the chiral centre. This therefore implies that  $P_S$  is not entirely dependent on  $\theta$ . Furthermore, the higher  $P_S$  values of compounds (28a-e) in relation to compounds (28f-j) are more likely to be explained by the greater polarity of the former materials due to the presence of the oxygen atom of the ether linkage.



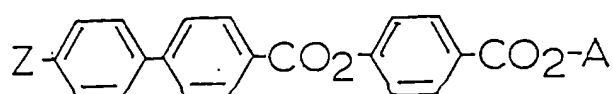
As the data for compounds (28f,g) were obtained from mixtures in racemic CE8, the results for  $P_S$  and  $\theta$  for the alkyl series cannot be evaluated in the same way. Although the effect of the host on the magnitude of  $P_S$  may not be significant, the values of  $\theta$  are much more likely to be influenced by the host material than the dopant.

Whilst compounds (28a-j) were being prepared, further work was being done on other potentially wide temperature range  $S_C^*$  materials with high  $P_S$  values. Again, the  $S_C^*$  - promoting structure of compounds (PGf,g) was used, but with a variety of different end groups which all retain the chiral centre in a position adjacent to the aryl-alkyl ester function. Compounds [31a-i (Table XII)] involve alkyl as well as alkyloxy materials, in order to obtain lower melting points and to confirm more fully the relative effects on the thermal stabilities of the phases.

In comparing compound (31a-e) with compound (28b,c), the most striking result occurs when the (S)-ethyl lactate end group of compound (28c) is replaced with the (R)-menthyl end group of compound (31a). As a consequence of this alteration, there has been a complete loss of all liquid crystalline properties. This is probably due to the bulky lateral isopropyl group projecting from the 2-position of the alicyclic ring and reducing the overall rod-like shape of the molecule. However, a second factor contributing to the loss of mesomorphic behaviour may be the high melting point, which in common with the melting points of the other two alkyloxy substituted terpenoid esters (31b,c), is about 48°C

greater than that of the corresponding ester derived from (S) ethyl lactate. The results shown above from compounds (31b,c) also demonstrate how substituting (R)-isopinocampheol for (S)-ethyl lactate as the esterifying end group of compounds (28b,c) has been followed by the introduction of a cholesteric phase and a rise in the thermal stabilities of both the  $S_C^*$  and  $S_A$  phases by roughly 17°C.

Table XII: Compounds (31a-i)



Z	A	mp (°C)	$S_C^*/S_B-S_C^*$ (°C)	$S_C^* - S_A$ (°C)	$S_A-CH/I$ (°C)	Ch / I (°C)	$P_S(T_C-T=10^\circ C)$ (nCcm <sup>-2</sup> )	$\theta(T_C-T=10^\circ C)$ (°)	Sgn of $P_S$ (+/-)	helical <sup>++</sup> twist sense (D/L)
31a..	C <sub>9</sub> H <sub>19</sub> O-	108.0	-	-	-	-	+++ 60.0	-		L
31b..	C <sub>8</sub> H <sub>17</sub> O-	122.0	-	135.3	178.6	186.6	28.0	18.0		D
31c..	C <sub>9</sub> H <sub>19</sub> O-	108.0	-	140.0	176.4	182.8	-	-		D
31d..	C <sub>9</sub> H <sub>19</sub> O-CHC <sub>6</sub> H <sub>13</sub> CH <sub>3</sub>	71.0	(52.2) <sup>-10</sup>	122.0	142.8	-	77.7	25.0		D
31e..	C <sub>9</sub> H <sub>19</sub> O-CHC <sub>2</sub> H <sub>5</sub> CH <sub>3</sub>	71.0	+(63.0) <sup>-10</sup>	136.2	174.6	-	12.5	18.5	-- (-)	D
31f..	C <sub>10</sub> H <sub>21</sub> -	91.5	-	-	-	-	-	-		L
31g..	C <sub>8</sub> H <sub>17</sub> -	124.0	-	(97.7) <sup>-10</sup>	145.0	156.2	-	-		D
31h..	C <sub>10</sub> H <sub>21</sub> -	89.0	-	102.5	142.5	148.8	-	-		D
31i..	C <sub>10</sub> H <sub>21</sub> -CHC <sub>6</sub> H <sub>13</sub> CH <sub>3</sub>	61.0	-	81.5	102.8	-	61.0	19.8		D

+ unidentified ferroelectric smectic phase.

++ see footnote to Table I.

+++ determined using a 10 wt% mixture in racemic CEB.

In comparison with compound (28c), the melting points of compounds (31d,e) have both risen by 11°C, though the effects

of the respective structural modifications on liquid crystalline behaviour are not so similar. Replacing the (S)-ethyl lactate with the (R)-1-methylheptyl end group of compound (31d) has introduced a  $S_B$  phase in place of the hexatic, tilted, chiral phase of compound (28c), and reduced the thermal stability of the resulting  $S_A$  phase by 15° C. Nevertheless, despite these differences, the  $S_C^*$  to  $S_A$  transition temperature has remained unchanged.

The corresponding structural alteration with (R)-1-methylpropyl has given rise to a more uniform effect on the mesogenic properties of compound (31e). The thermal stability of the  $S_C^*$  phase has risen by 14° C, whereas the thermal stabilities of the underlying ferroelectric phase and of the  $S_A$  phase have both increased by ca. 17° C. Although the monotropic phase of compound (31e) is difficult to identify by optical microscopy, its ferroelectric nature has been ascertained by the increase in  $P_g$  which occurs on cooling from the preceding  $S_C^*$  phase. This is illustrated in Figure 43, which also demonstrates the importance of adopting a standard form when quoting the value of  $P_g$ , as its magnitude varies considerably with temperature.

In order to clarify the relative effects of the various end groups used with respect to that derived from (S)-ethyl lactate, Figure 44a has been constructed to highlight the differences in melting point and  $S_C^*/S_A$  thermal stability for compounds (31a,c-e) relative to compound (28c).

Fig. 4.3: Spontaneous polarisation vs. temperature for compound (31e).

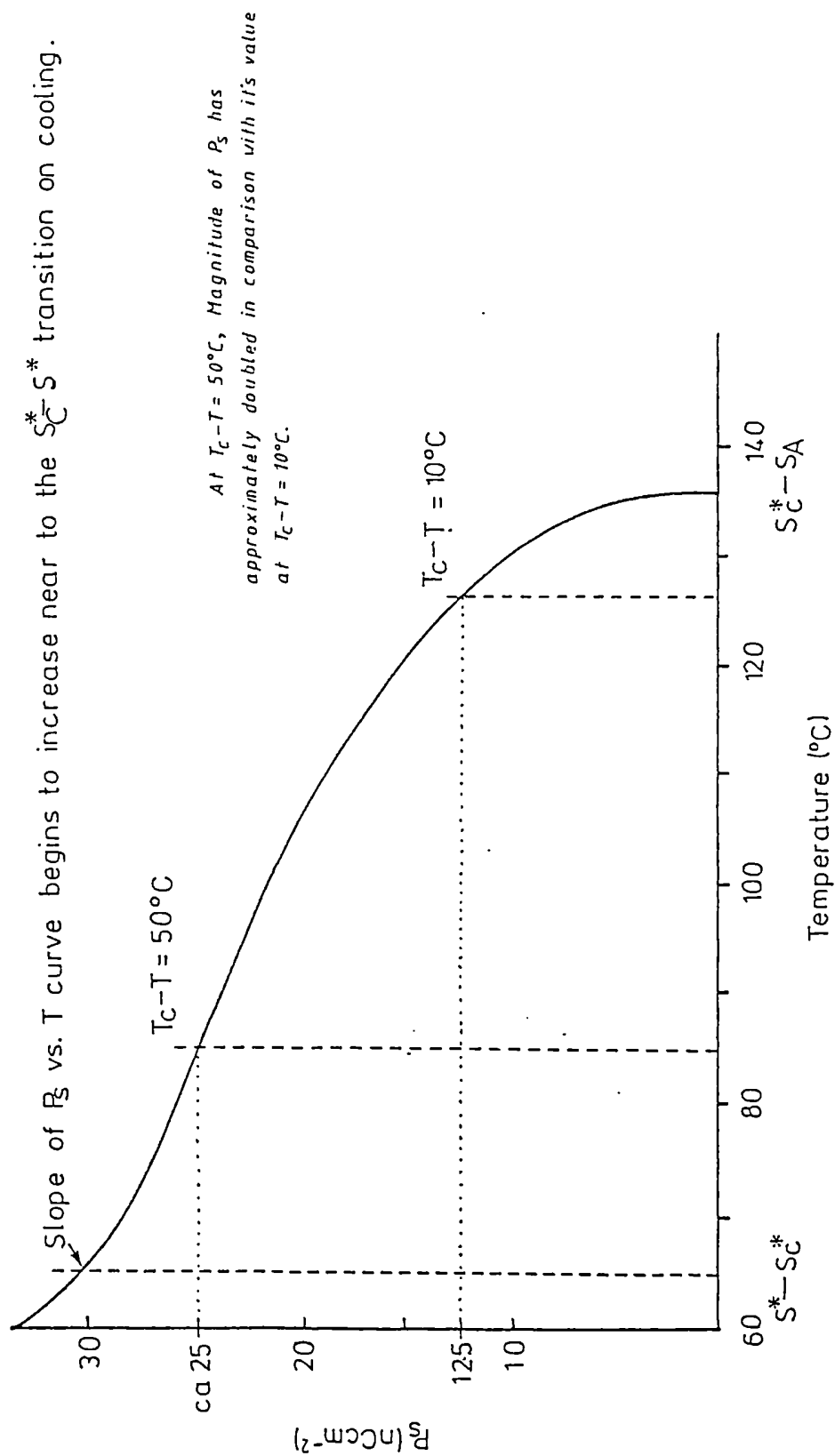
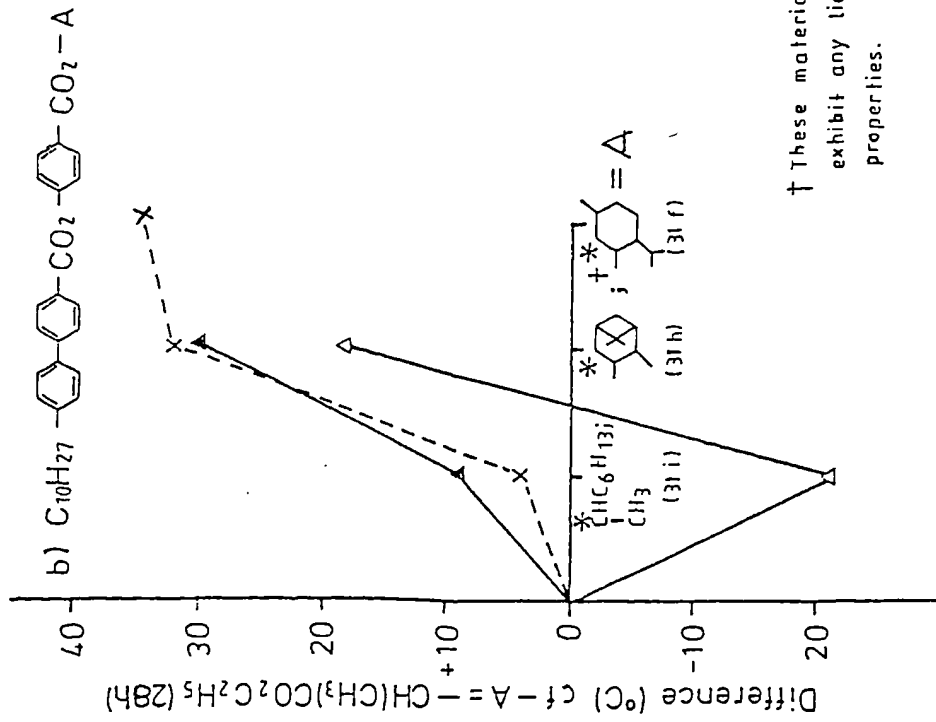
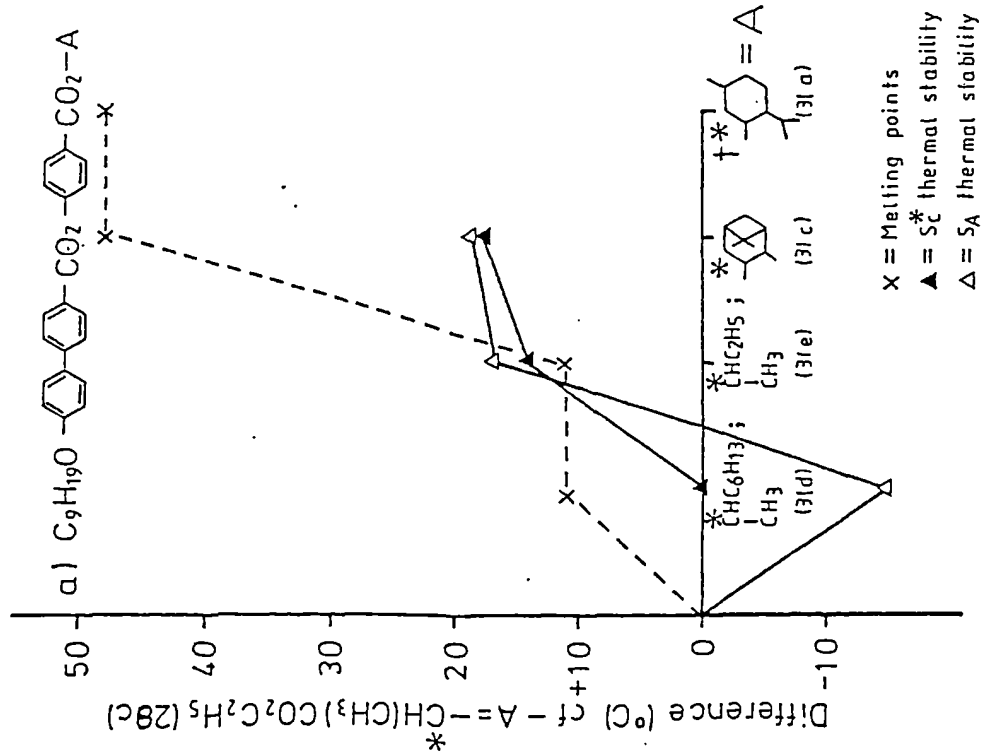


Fig. 44: Relative melting points and  $S_C^*$ / $S_A$  thermal stabilities compared with  $-A = -\overset{*}{\text{C}}\text{HCO}_2\text{C}_2\text{H}_5$   
 $\text{CH}_3$   
 for compounds of structures:



† These materials did not exhibit any liquid crystalline properties.

Similarly, for the analogous alkyl substituted materials, figure 44b illustrates the variations in melting points and  $S_C^*/S_A$  thermal stability for compounds (31f,h,i) relative to compound (28h).

As in the case of the alkyloxy materials, figure 44b shows that the different end groups used to replace that derived from (S)-ethyl lactate, result in higher melting points and higher smectic thermal stabilities, with only the  $S_A$  thermal stability of the (R)-1-methylheptyl ester being reduced. In addition to these differences, the use of the (R)-isopinocampheyl end group in compounds (31g,h) has again introduced a cholesteric phase into the liquid crystalline sequence as well as a monotropic  $S_C^*$  phase into the octyl homologue, compound (31g). Again the most striking effect is that replacement by the (R)-menthyl group, leads to the loss of all mesogenic behaviour for compound (31f).

Comparing compounds (31f-i) with their alkyloxy counterparts tends to reinforce the observations made earlier with respect to melting point depression and lowering of phase thermal stability. Apart from compound (31g), which has an unusually high melting point, the remaining alkyl materials have melting points which are between  $10^\circ$  and  $19^\circ\text{C}$  lower than the analogous alkyloxy materials. Likewise for compounds (31g-i), there is a decrease in the thermal stability of the  $S_C^*$  phases by about  $40^\circ\text{C}$  and of the  $S_A$  phases by between  $33^\circ$  and  $40^\circ\text{C}$ , in relation to the analogous alkyloxy compounds. Finally the cholesteric phase thermal stability of compound (31g,h) is lowered by between  $30^\circ$  and  $34^\circ\text{C}$  compared with the corresponding alkyloxy materials.

The data on  $P_S$  for compound (31a-i) provides some interesting information, which may help to reveal a little more of the true nature of  $P_S$ . In compound (31a), the bulky 2-isopropyl group can interact sterically with the nearby carbonyl function of the ester, presenting a major hindrance to rotation about the bond to the chiral centre. Consequently this material exhibits a very large value of  $P_S$ , which is slightly higher than that of the analogous material, compound (28c), derived using (S)-ethyl lactate.

At first glance the relatively low  $P_S$  value for compound (31b) may be a little surprising, as this is only about half the value given for compound (17), which employs the same end group. However, the latter value is more likely to be a maximum  $P_S$  value for compound (17) and indeed, the magnitude of  $P_S$  at  $T_C - T = 40^\circ\text{C}$  for compound (31b) acquires a similarly high value. The lateral methyl substituent in the (R)-isopinocampheyl end group of compound (31b) is obviously smaller than the lateral isopropyl group of compound (31a). There will therefore be an appropriate reduction in the extent of steric interaction with the neighbouring carbonyl function and a corresponding decrease in the magnitude of  $P_S$ .

The most exceptional result from these materials is that for compound (31d), which exhibits the greatest value of  $P_S$  recorded so far. This is approximately 40% higher than that determined for compound (28c). As this material does not contain a bulky alicyclic group to retard intramolecular rotations about the bond to the chiral centre, an alternative explanation is offered.<sup>54</sup> It is suggested that the

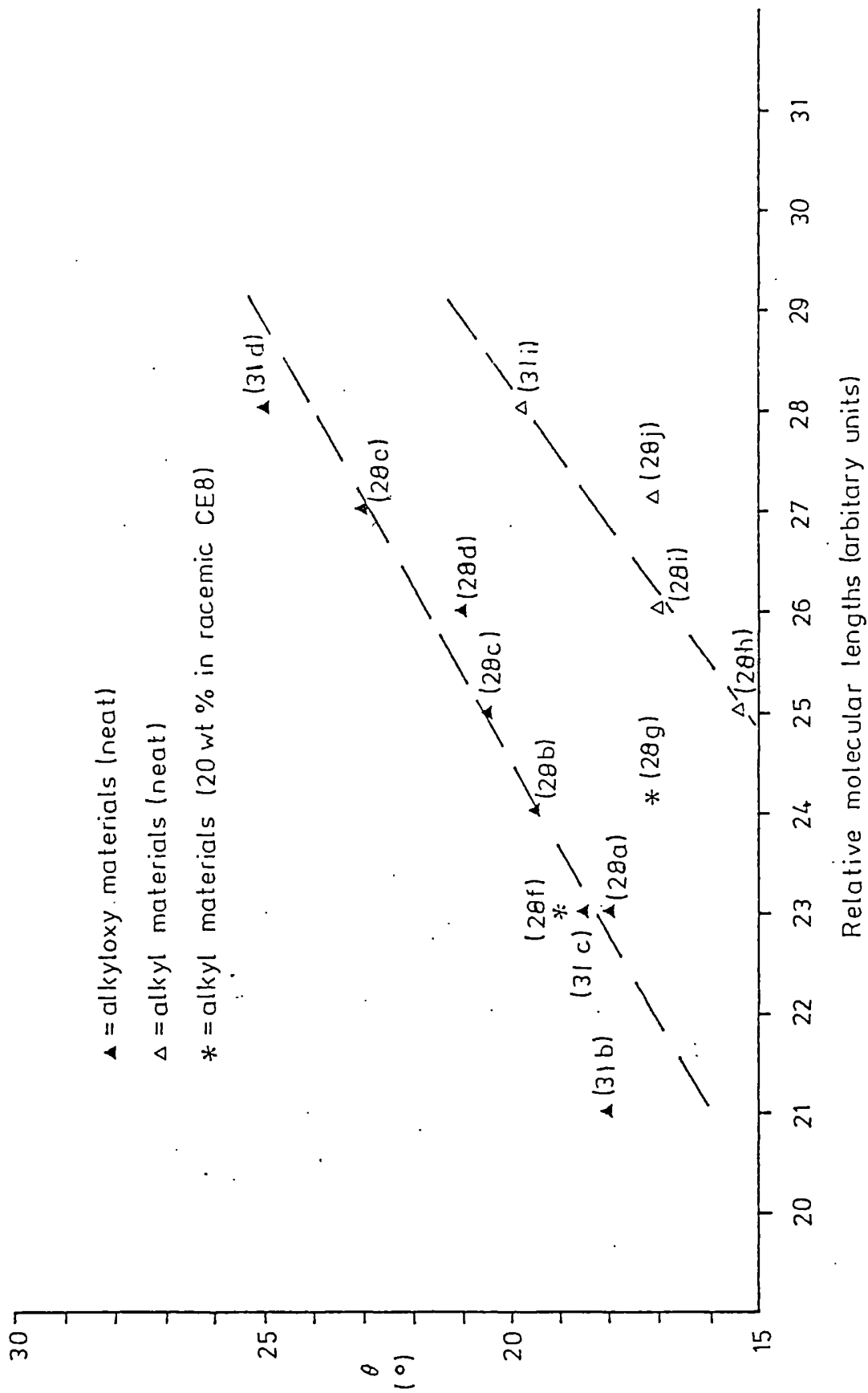
long alkyl tail of the (R)-1-methylheptyl end group can adopt various gauche conformations which, when the proximity of the ester function is taken into account, result in a large degree of steric hindrance to rotation about the bond with the asymmetric carbon atom. The effect of this hindrance, as in compounds (31a,b), would again be a large value of  $P_g$  for compound (31d).

Supporting this hypothesis to some extent is the unexpectedly low value of  $P_g$  associated with compound (31e). This material has very similar polar properties at the chiral centre to compounds (31a,b,d) and indeed differs from compound (31d) only in the length of its alkyl chain. Therefore this large drop in  $P_g$  must be a consequence of reduced steric factors, which in the case of compound (31d) must derive from the long alkyl chain.

Comparing the results for compounds (31d) and (31i) indicates that, as in compounds (28a-j), the alkyloxy material has significantly greater values of both  $P_g$  and  $\theta$  than the analogous alkyl material.

The values of  $\theta$  recorded for compounds (31a-i) tend to fall largely into the range of tilt angles determined for compounds (28a-j), the only exception being compound (31d) which exhibits a notably large tilt angle of  $25.0^\circ$ . However, this is accounted for by the general tendency for  $\theta$  to increase with molecular length, as demonstrated in Figure 45. The values of relative molecular length have been determined by arbitrarily assigning one unit of length for each carbon or oxygen atom in the linear part of the molecule and two

Fig. 45: Relative molecular lengths vs. tilt angle for compounds (28a-j) and (31 b,d,e,i) at  $T_c - T = 10^\circ\text{C}$ .



units of length to each phenyl or alicyclic ring. Although accurate comparisons cannot be made using this technique, it does give a good indication of the approximately linear relationship between tilt angle and molecular length exhibited by both the alkyloxy and alkyl materials.

### Summary of Section 5

As in the previous section, the aim in section 5 has concentrated largely on obtaining high  $P_g$  materials with wide temperature range  $S_C^*$  phases. Attempts to realise this have again centred on replacing the 2-methylbutyl end group of compounds (PGf,g), but this time with a number of potentially high  $P_g$  end groups having a chiral centre adjacent to the ester function.

Substituting (S)-2-methylbutyl with the end group derived from (S)-ethyl lactate in compounds (28b,c) has led to a small increase in melting point, and to a significant decrease in thermal stability of the corresponding  $S_C^*$  phases. Despite these changes, an  $S_C^*$  phase temperature range of ca. 60°C has been maintained. More importantly though, the high values of  $P_g$  associated with these compounds are roughly equivalent to that of compound (17), and therefore the major breakthrough of preparing high  $P_g$ , wide temperature range  $S_C^*$  materials has been achieved.

Extension of this work, in order to obtain both alkyloxy- and alkyl-substituted homologous series [compounds (28a-j)], has provided more evidence of how small molecular changes can have a large effect on mesogenic properties. The most notable case is provided by the sudden appearance of an

$S_C^*$  phase when the alkyl chain length is increased from 9 to 10 carbon atoms. Values of  $P_g$  and  $\theta$ , which are on average 30% higher for the alkyloxy compounds, shed new light on the assumed relationship between the two quantities and imply that  $P_g$  might not be dependent on  $\theta$ .

Replacing the (S)-ethyl lactate derived end group of compounds (28c) with a number of alternative end groups has invariably resulted in higher melting points for compounds (31a-e) and has usually been accompanied by an increase in  $S_C^*$  thermal stability.

Substituting the end group derived from (S)-ethyl lactate by (R)-menthyl led to a complete loss of all liquid crystalline behaviour, whereas a similar structural modification involving the (R)-isopinocampheyl group introduced a cholesteric phase. However the magnitude of  $P_g$  associated with this end group is roughly half that of the lactate analogue. Even smaller still is the value of  $P_g$  arising from the corresponding (R)-1-methylpropyl ester, although this does exhibit a wider range, enantiotropic  $S_C^*$  phase. The (R)-1-methylheptyl ester appears to be the most reasonable alternative to the lactate esters, as it gives a similar enantiotropic temperature range for the  $S_C^*$  phase, yet has a 40% higher value of  $P_g$ .

Comparison of all the compounds in this section reveals an approximately linear relationship between the magnitude of  $\theta$  and the relative molecular length for both alkyloxy and alkyl materials, thereby accounting for the fairly wide spread of tilt angles at  $T_C - T = 10^\circ \text{C}$ .

The sign of  $P_g$  for compounds (28a-j) is positive, whereas for compounds (31a-i) it is negative. Apart from compounds (31a,f), the helical twist senses of all the materials in this section follow the rules relating twist sense to absolute configuration and position of the chiral centre with respect to the aromatic core, i.e.,

compounds (28a-j), S o L, (+I);

compounds (31b-e,g-i), R o D, (+I).

Compounds (31a,f) give the anomolous result:- R o L, (+I)

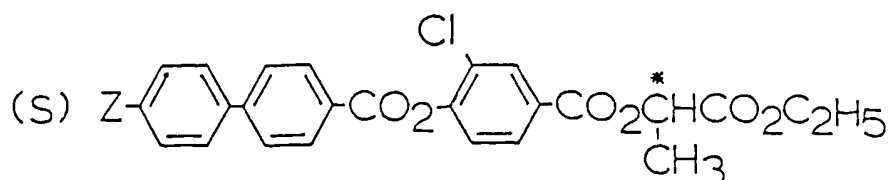
## 2.6 Compounds (38a-r).

The two most promising materials from section 5 were those derived from (S)-ethyl lactate and (R)-octan-2-ol, compounds (28c) and (31d) respectively. While both materials exhibit wide temperature range  $S_C^*$  phases and large  $P_G$  values, compound (28c) gives the lower  $P_G$  and compound (31d) the poorer mesogenic properties. However, more importantly perhaps is the relative expense of the two chiral alcohols involved, (R)-octan-2-ol costing a few pounds per ml., whereas (S)-ethyl lactate costs only a few pounds per litre. Because of this additional factor, the following work has concentrated largely on modifying the properties of compounds (28a-j).

In an attempt to lower the melting points and  $S_C^*$  thermal stabilities of these materials, whilst maintaining the wide temperature range nature of the  $S_C^*$  phases, it was decided to introduce a chlorine atom into the 3-position of the phenyl ring carrying the aryl-alkyl ester function. Also, in order to compare alkyloxy and alkyl materials directly, and assess the importance of variations in alkyloxy/alkyl chain lengths, the two short homologous series of compounds [38a-d, k-m) Table XIII] were prepared.

As expected, the presence of a lateral chlorine atom in these materials has a dramatic influence on the liquid crystalline properties for both homologous series. Comparison of compounds (38a-d) with their non-chlorinated counterparts, compounds (28b-e) reveals a massive reduction in the thermal stabilities of the  $S_C^*$  phases by between 67° and 78° C, and of the  $S_A$  phases by roughly 55° C.

Table XIII Compounds (38a-d, j-m).



Z	mp (°C)	S <sub>C</sub> <sup>*</sup> - S <sub>A</sub> (°C)	S <sub>A</sub> - Ch (°C)	Ch - I (°C)	P <sub>S</sub> (T <sub>C</sub> -T=10°C) (nCm <sup>-2</sup> )	θ(T <sub>C</sub> -T=10°C) (°C)	sign of P <sub>S</sub> (+/-)	helical twist <sup>+</sup> sense
38a..C <sub>8</sub> H <sub>17</sub> O-	60.0	(39.6)10	105.5	(109.0)10	52.0	14.0		
38b..C <sub>9</sub> H <sub>19</sub> O-	47.5	48.0	101.8	(106.0)10	47.8	24.2		
38c..C <sub>10</sub> H <sub>21</sub> O-	74.0	(54.9)10	101.0	(106.0)10	++ca50	-		
38d..C <sub>11</sub> H <sub>23</sub> O-	79.0	(54.8)-10	98.5	(100.0)-10	++ca44	-	-- (+)	-- L
38j..C <sub>9</sub> H <sub>19</sub> -	43.0	-	65.8	67.00	-	-		
38k..C <sub>10</sub> H <sub>21</sub> -	41.5	-	64.0	(69.2)10	+++ 35.0	17.2		
38l..C <sub>11</sub> H <sub>23</sub> -	28.5	-	65.7	(69.3)-10	-	-		
38m..C <sub>12</sub> H <sub>25</sub> -	37.5	-	64.0	(68.5)10	-	-		

+ See footnote to Table I.

++ Poor sample alignment enabled only approximate values of P<sub>S</sub> to be determined and prevented any measurement of θ.

+++ Extrapolated value of P<sub>S</sub>, determined from a 20 wt % mixture in racemic CEB.

The melting points of the corresponding octyloxy and nonyloxy materials have fallen by 15° and 12°C respectively, whereas those of the decyloxy and undecyloxy compounds have both risen by 14°C. As a consequence of these changes, only the low melting nonyloxy homologue (38b) has retained an enantiotropic S<sub>C</sub><sup>\*</sup> phase and this has a temperature range of <1°C! However the S<sub>C</sub><sup>\*</sup> phase of this compound does supercool to below room temperature for long periods without recrystallising, and as a result, this material has already been synthesised on a larger scale by B.D.H. Ltd as a potentially useful host material.

This structural modification has also led to the ejection of the underlying tilted hexatic phases of compounds (28a-e), and furthermore, has introduced a cholesteric phase into the mesogenic phase sequence. It should be noted however, that these cholesteric phases could not be observed by microscopy, and were in fact only detected by D.S.C.

As the alkyloxy chain length of compounds (38a-d) increases, the thermal stabilities of both the cholesteric and  $S_A$  phases tend to decrease, whereas the thermal stabilities of the  $S_C^*$  phases increase, before levelling off at the decyl homologue.

The effect of introducing a lateral chlorine atom into the alkyl substituted series of compounds (38j-m) has been even more drastic. This has resulted in a complete loss of both the  $S_B$  and  $S_C^*$  phases present in compounds (28 g-j), as well as a depression of the thermal stabilities of the corresponding  $S_A$  phases by between  $55^\circ$  and  $62^\circ$  C. This structural alteration has also introduced a cholesteric phase into compounds (38j-m); this phase is generally detectable only by D.S.C., although in the case of the nonyl homologue it can also be observed by optical microscopy. The melting points of compounds (38j-m) are all lower than those of their non-chlorinated counter-parts by between  $5^\circ$  and  $25^\circ$  C; the undecyl homologue, compound (38e) exhibiting a particularly low melting point of  $28.5^\circ$  C.

Relating this homologous series to the analogous alkyloxy series reveals similar depressions in phase thermal stability to those noted in earlier comparisons of alkyl and alkyloxy series; the thermal stabilities of both the

cholesteric and  $S_A$  phases of compounds (38j-m) are reduced by between 31° and 42° C, in comparison with compounds (39a-d). In contrast to the alkyloxy series, as the alkyl chain length increases for compounds (38j-m), the thermal stabilities of the cholesteric and  $S_A$  phases do not rise or fall uniformly, but the thermal stabilities of the  $S_A$  phases do exhibit a definite odd-even effect.

Finally, although the melting points of compounds (38j-m) are all lower than those of the corresponding alkyloxy materials, the extent of the melting point depression varies from 6° C, between the octyloxy and nonyl homologues, to 45.5° C between the decyloxy and undecyl compounds. This large fluctuation is due mainly to the big differences in melting points of the individual alkyloxy materials [e.g. compound (38b)-mp, = 47.5° C; compound (89d)-mp, = 79.0° C] and not to significant differences in the melting points of the different alkyl materials [e.g. compound (38e)-mp = 28.5° C; compound (38j)mp = 43.0].

The  $P_g$  values recorded for compounds (38a-d,k) are slightly smaller than, but still comparable with those of compounds (28a-j). The nonyloxy material exhibits an approximately 36% higher value of  $P_g$  than the equivalent decyl compound, although this latter value could be determined only by the extrapolation procedure.

As the decyloxy and undecyloxy materials do not align well, their  $P_g$  values are not particularly accurate. Nevertheless, compounds (38a-d) do seem to show an odd-even effect in the magnitude of  $P_g$  as the alkyloxy chain length increases.

The tilt angles of compounds (38b,k) are slightly larger than those of the corresponding non-chlorinated materials for compounds (28c,h) by 18% and 11% respectively. Conversely for the equivalent octyl homologues, the chlorinated material exhibits a notably small tilt angle of only  $14.0^\circ$ , which is about 30% lower than that of the non-chlorinated compound. However, this relatively small value of  $\theta$  may be a consequence of the poor aligning qualities of compounds (38a-j); in the case of the decyloxy and undecyloxy homologues, this prevented any values of  $\theta$  from being determined.

In addition to the materials discussed above, compounds [(38e-i, n-r), Table XIV] were prepared in order to compare the effects of introducing other substituents into the 3-position of the phenyl ring. It was decided to make just one alkyloxy and one alkyl homologue for each new type of material, in order to economise in both time and effort. The nonyloxy homologue was chosen, because this alkyloxy group gave the lowest melting point in both the earlier series of lactate esters. Consequently the decyl homologue was also chosen, so that differences between members of the pairs could be attributed to change in polarity and not to variation in molecular length.

Fig. 46: Melting points and Transition temperatures for compounds of structure :-

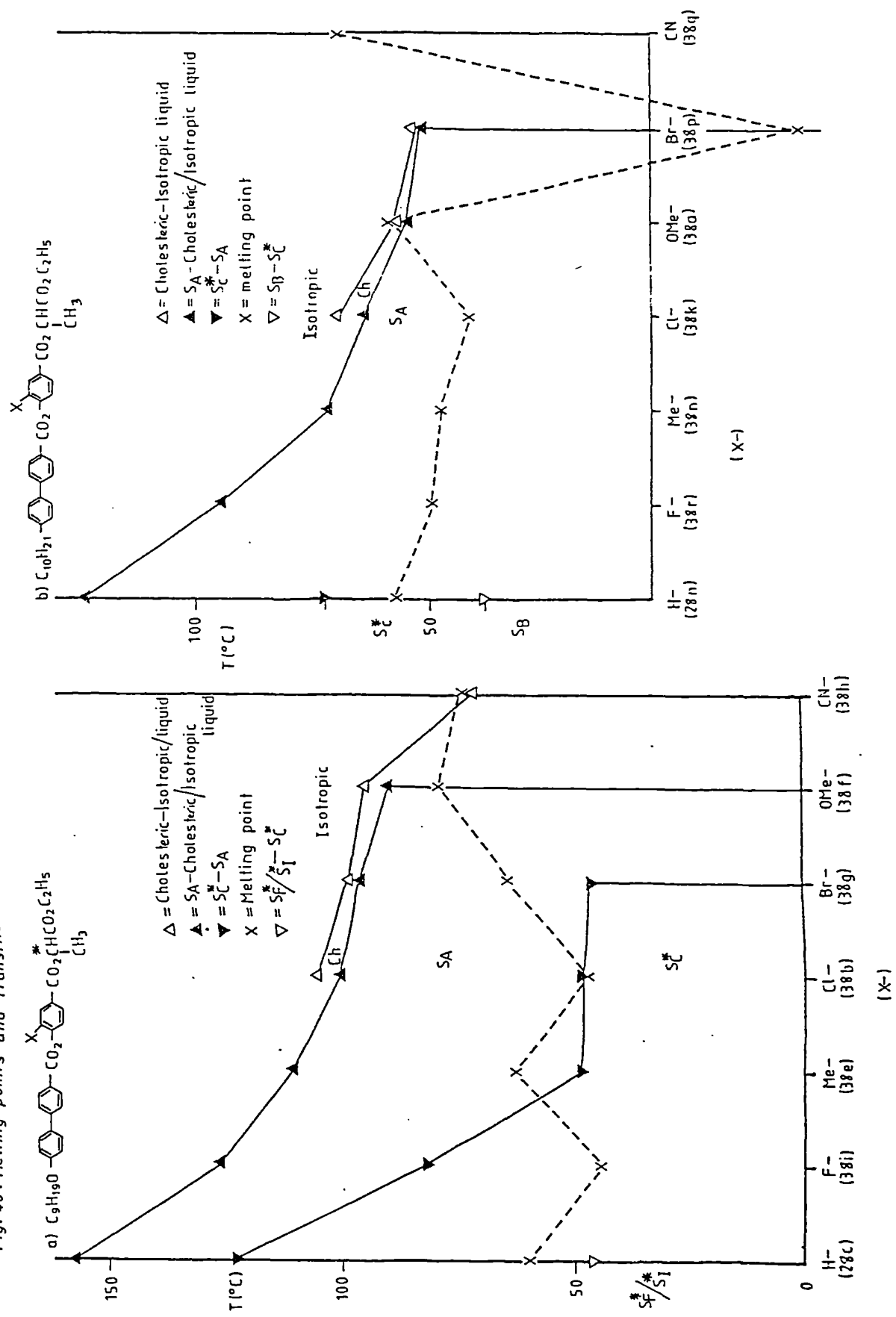
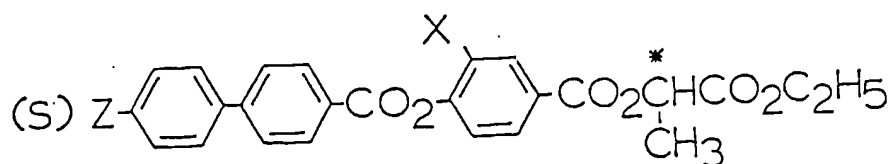


Table XIV Compounds (38 e - i, n - r).



Z	X	mp (°C)	S <sub>C</sub> <sup>*</sup> -S <sub>A</sub> (°C)	S <sub>A</sub> -Ch/I (°C)	Ch - I (°C)	P <sub>S</sub> (T <sub>C</sub> -T=10°C) (n <sub>C</sub> cm <sup>-2</sup> )	θ(T <sub>C</sub> -T=10°C) (°C)	sign of P <sub>S</sub> (+/-)	helical twist <sup>+</sup> sense
38e..C <sub>9</sub> H <sub>19</sub> O-	Me	63.0	(48.2) <sup>10</sup>	110.5	-	42.4	15.4		
38f..C <sub>9</sub> H <sub>19</sub> O-	MeO	78.0	-	89.3	94.0 <sup>10</sup>	++ 31.0	24.2		
38g..C <sub>9</sub> H <sub>19</sub> O-	Br	63.0	(45.5) <sup>-10</sup>	95.2	(97.7) <sup>-10</sup>	+++ 12.3	16.3		
38h..C <sub>9</sub> H <sub>19</sub> O-	CN	73.0	-	-	(70.7)	++ 37.1	18.5	-- (+)	-- L
38i..C <sub>9</sub> H <sub>19</sub> O-	F	44.0	82.0 <sup>10</sup>	126.5	-	35.4	14.5		
38n..C <sub>10</sub> H <sub>21</sub> -	Me	47.5	-	72.0	-	-	-		
38o..C <sub>10</sub> H <sub>21</sub> -	MeO	58.0	-	(55.0)	(57.3) <sup>-10</sup>	-	-		
38p..C <sub>10</sub> H <sub>21</sub> -	Br	-30.0	-	(52.5)	(53.5)	++23.7	20.5		
38q..C <sub>10</sub> H <sub>21</sub> -	CN	70.0	-	-	-	37.0	16.2		
38r..C <sub>10</sub> H <sub>21</sub> -	F	49.5	-	94.8	-	++30.3	-		

+ See footnote to Table I.

++ Derived from a 20% mixture in racemic CEB

+++ Data for the neat material; a 20 wt % mixture in racemic CEB gave P<sub>S</sub> = 36.1 n<sub>C</sub>cm<sup>-2</sup> at T<sub>C</sub> - T = 10°C

The relative effects of introducing substituents at the 3-position of the phenyl ring in compounds (38b,e-i,k,n-r) are illustrated more clearly in figure 46. For the alkyloxy materials (Fig.46a), replacing -x = hydrogen with the different substituents shown, invariably results in the loss of the monotropic tilted hexatic phase and a reduction in the thermal stability of the S<sub>A</sub> phase [by approximately 31°, 47°, 56°, 63° and 68°C for -x = fluoro, methyl, chloro, bromo and methoxy respectively]. Furthermore, the S<sub>A</sub> phase is lost altogether for compound (38h), where -x = cyano. Similarly the thermal stability of the S<sub>C</sub><sup>\*</sup> phase is lowered by

approximately 40°, 74°, 74° and 76° C for -x= fluoro , methyl, chloro and bromo respectively. No  $S_C^*$  phase is exhibited for compounds (38f,h), where -x= methoxy and cyano respectively. A short temperature range cholesteric phase of between 2.5° and 5° C has been introduced for the chloro, bromo and methoxy materials, but in the case of the cyano compound only a monotropic cholesteric phase is found. Of all these cholesteric phases, only that of the cyano compound is observed by microscopy; the remainder were detected by D.S.C.

The effects of the different substituents on melting point are quite variable. While the methyl and bromo compounds melt at very similar temperatures to the unsubstituted material, the melting points of the methoxy and cyano materials have increased significantly, by 18° and 13° C respectively. Conversely, the fluoro material has a 16° C lower melting point than the equivalent unfluorinated compound and along with the corresponding chloro compound discussed earlier, exhibits an enantiotropic  $S_C^*$  phase. However, unlike the chloro compound, the enantiotropic  $S_C^*$  phase of the fluoro material persists over a reasonably wide temperature range of 38° C.

Considering now the analogous alkyl materials, placing any of the above substituents in the 3-position of the phenyl ring leads directly to the loss of the  $S_B$  and  $S_C^*$  phases present in the unsubstituted material, compound (28h). The relative effects on the thermal stability of the  $S_A$  phase are very similar to those for the corresponding alkyloxy compounds, with the fluoro, methyl, chloro, methoxy and bromo substituents causing a depression of roughly 29° ,

52°, 60°, 69° and 71° C respectively. The cyano material again shows no S<sub>A</sub> phase and indeed exhibits no mesomorphic properties whatsoever.

A short temperature range cholesteric phase of between 1° and 5° C is introduced by the chloro, methoxy and bromo substituents. Although this can be observed directly only for the bromo compound, the other two phases were detected by D.S.C. The relative thermal stabilities of the cholesteric and the underlying S<sub>A</sub> phase are reversed for the methoxy and bromo materials, with respect to the equivalent alkyloxy compounds.

The effects of the different substituents on melting point are extremely variable. The methoxy material melts at a very similar temperature to the unsubstituted compound, whereas the cyano substituent has increased the melting point by 13° C. The remaining fluoro, methyl, chloro and bromo substituents cause a depression in melting point of approximately 8°, 10°, 16° and 87° C respectively<sup>XXI</sup>.

Comparison of the alkyloxy and alkyl materials highlights the effects of polarity changes discussed previously. The thermal stability of cholesteric phases is reduced for the alkyl compounds by between 36° and 45° C and that of the S<sub>A</sub> phase by between 31° and 43° C. The relative differences in melting point are less uniform, with the

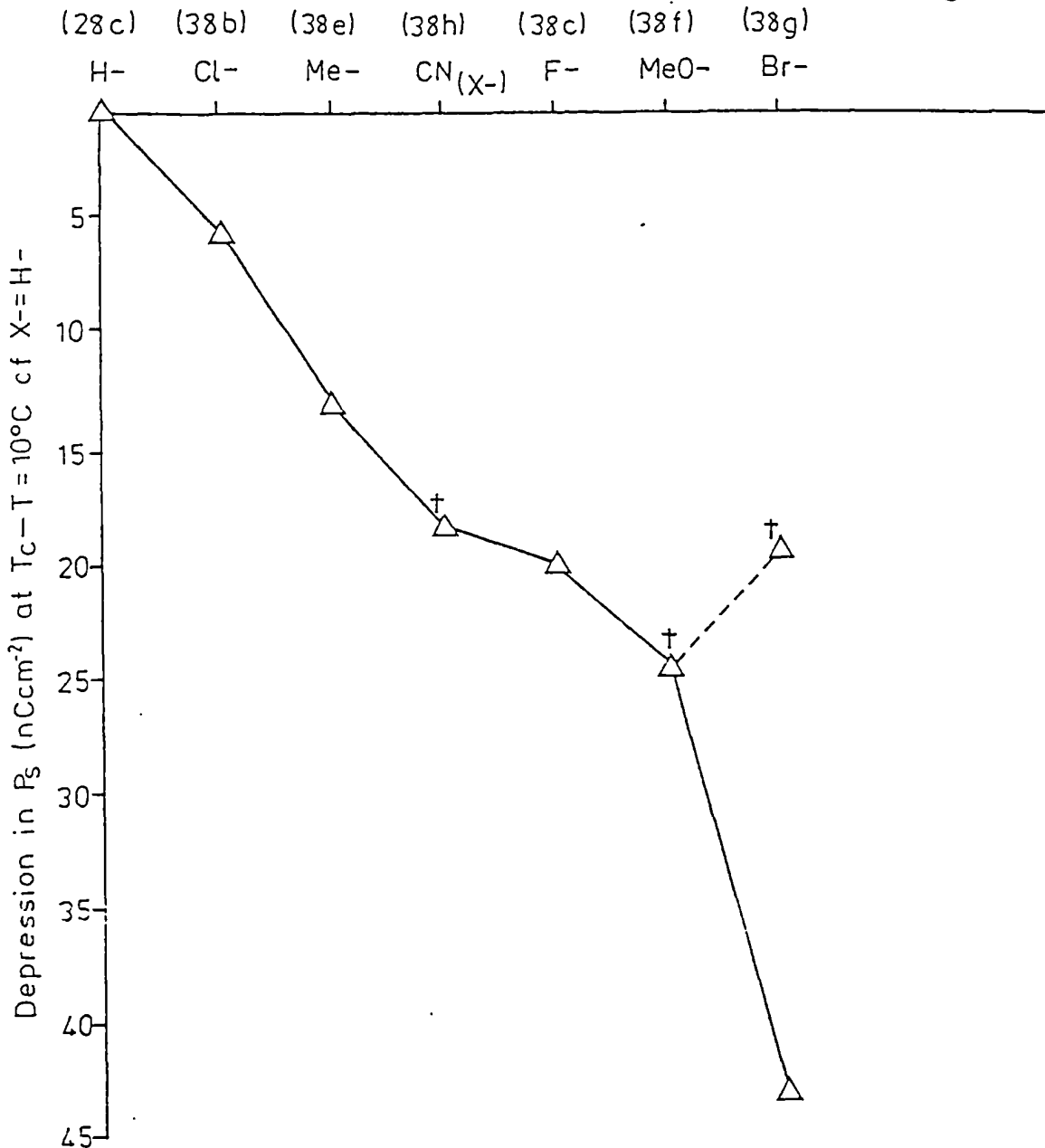
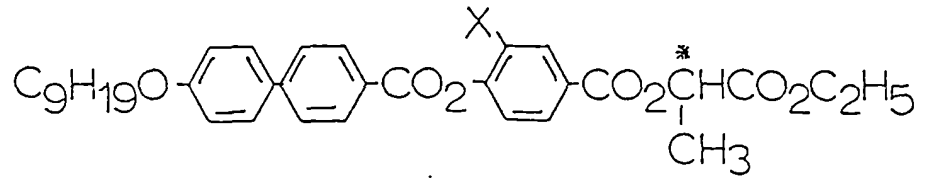
-----

XXI. The ultra-low melting point of the bromo compound could not be determined by the standard capillary method and was in fact obtained by D.S.C., through cooling the sample to -50° C and then slowly heating it at a rate of 10° C min<sup>-1</sup>. However, it is possible that this technique may cause the material to form a glass instead of crystalline solid, and so the melting point given may actually be a glass transition temperature.

chloro, cyano and unsubstituted alkyl materials melting at similar but slightly lower temperatures than their alkyloxy counterparts; on the other hand, the fluoro alkyl compound melts at a slightly higher temperature than the corresponding alkyloxy compound. More significant depressions in melting point occur for the methyl and methoxy substituted alkyl materials, with the equivalent bromo material exhibiting an enormous fall in melting point of 93° C in relation to the analogous alkyloxy compound.

The  $P_g$  values associate with compounds (38e-i) are all significantly lower than those of the corresponding unsubstituted nonyloxy materials (Fig.47); only the methyl substituted material, compound (38e) attains a  $P_g$  value of over  $40 \text{ nCcm}^{-2}$  at  $T_C - T = 10^\circ \text{ C}$ . The equivalent cyano, fluoro and methoxy substituted compounds have progressively smaller, but still reasonably high values of  $P_g$ , whereas the magnitude of  $P_g$  recorded for the neat bromo substituted material, compound (38g), is extremely small at only  $12 \text{ nCcm}^{-2}$ . This value is just half that for the analogous decyl compound, although the latter  $P_g$  value was determined by extrapolation. Carrying out a similar extrapolation procedure for compound (38g) leads to a higher value of  $P_g$  which is comparable with that found for the other 3-substituted nonyloxy materials. This large difference between values of  $P_g$  determined for neat materials and by extrapolation demonstrates that, whereas extrapolation may be a useful means of obtaining a rough guide to  $P_g$ , molecular interactions with the host material can have a great influence on the actual magnitude of  $P_g$ . Nonetheless, the extrapolated  $P_g$  values determined for some of the analogous decyl materials are again lower than those for the corresponding nonyloxy materials.

Fig. 47: Relative effect on  $P_S$  of placing substituents in the X-position, of compounds having the structure:



<sup>†</sup>  $P_S$  determined by extrapolation from 20wt% mixture in racemic CEB

In contrast to the chloro substituent in compound (38b), the introduction of methyl, cyano and fluoro substituents lead to a decrease in the tilt angle compared with the unsubstituted material; the fluoro compound exhibits a notably small tilt angle of only 14.5°.

Finally, bearing in mind what has been stated before, the remaining values of  $\Theta$ , obtained for the materials dissolved in hosts, have little significance and will not be commented on further.

### Summary of Section 6

Due partly to economic considerations, the work in this section has focused on modifying the potentially useful properties of the lactate esters (28a-j), discussed in the previous section.

Introduction of a 3-chloro substituent adjacent to the aryl-alkyl ester function results in massive reductions in  $S_A$  and  $S_C^*$  thermal stabilities for compounds (38a-d,j-m). Furthermore, as this structural modification has a much smaller and more variable effect on melting points, only the nonyloxy homologue compound (38b) has retained a very short enantiotropic  $S_C^*$  phase. A more fortunate consequence of introducing the chloro substituent was the appearance of a very short cholesteric phase in compounds (38a-d,j-m). The values of  $P_g$  exhibited by compounds (38a-d,j-m) are slightly smaller, but comparable with those of the equivalent unsubstituted materials. This may however be a consequence of poor sample alignment, which has been cited as a probable cause of the large differences in tilt angles recorded for these materials.

Following this work, several other substituents have been introduced into the 3-position of the phenyl ring, and by comparing the nonyloxy and decyl compounds, their relative influences have been assessed.

In addition to ejecting the monotropic tilted hexatic phases of compound (28c), 3-substituents in the nonyloxy compounds lead to a decrease in  $S_A$  thermal stability in the order:- H;F;Me;Ce;Br;Ome;CN; the last substituent causes the  $S_A$  phase to disappear completely. Depressions in  $S_C^*$  thermal stability follow the same sequence, but in this case the introduction of both methoxy and cyano substituents result in the  $S_C^*$  phase being eliminated. Furthermore, as a consequence of considerable differences in the melting points of the 3-substituted materials, only the fluoro compound exhibits a significantly wide enantiotropic  $S_C^*$  phase. Lastly, the final four substituents in the above sequence induce short cholesteric phases in compounds (38d,f-h).

Introducing these 3-substituents into the decyl compounds has invariably led to the disappearance of both the  $S_C^*$  and  $S_B$  phases of compound (28c). It has also had similar effects with regard to reducing  $S_A$  phase thermal stability and inducing cholesteric phases, to those for the analogous nonyloxy compounds. Of particular note is the extremely low melting point of the bromo compound and the fact that no mesophases are exhibited by the cyano material, compound (38q).

Chloro substitution at the 3-position has given slightly lower, but comparable values of  $P_S$  to those for the related

unsubstituted materials, and although the corresponding tilt angles are also generally comparable, two notable exceptions do occur. The chloro substituted nonyloxy material exhibits a significantly higher value of  $\theta$  than the equivalent unsubstituted material, whereas the chloro substituted octyl compound has a much smaller tilt angle than the analogous unsubstituted compound. While no explanation is offered for the former result, the exceptionally small tilt angle measured for the latter material may be due to poor alignment.

Other 3-substituents have invariably led to a significant lowering in  $P_S$ , with the bromo substituent causing a particularly large depression. However, a mixture of this compound in racemic CE8 gave a much higher extrapolated value of  $P_S$ , thereby highlighting the limitations of using this extrapolation procedure.

The tilt angles associated with these materials are again lower than that of compound (28c), and a particularly small value is recorded for the 3-fluoro material.

Finally, none of the above substituents have altered the sign of  $P_S$  or helical twist sense compared with the unsubstituted lactate esters; all remain positive and follow the relationship:-

$$S \circ L (+ I)$$

between absolute configuration, helical twist sense and distance of the chiral centre from the aromatic core.

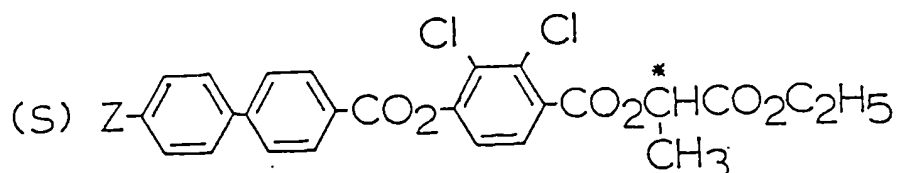
## 2.7 Compounds (45a,b) and (53a-k).

Following the previous work, the next step was to determine the effect of adding a second substituent to the phenyl ring of compounds (28c,h), in this case facing toward the chiral end-group.

Of all the substituted lactate esters in section 6, the chloro compounds give the highest  $P_g$  values and some of the lowest melting points. In addition, the alkyloxy homologues of these chloro compounds all exhibit the desirable phase sequence: - I  $\rightarrow$  Ch  $\rightarrow$   $S_A$   $\rightarrow$   $S_C^*$ .

Bearing these facts in mind, compounds (45a,b) Table XVI were prepared with chloro substituents in both the 2- and 3-positions of the phenyl ring next to the aryl-alkyl ester function.

Table XV Compounds (45a,b)



Z	mp (°C)	$S_C^* - S_A$ (°C)	$S_A - Ch$ (°C)	Ch - I (°C)	$P_g(T_C - T = 10^\circ C)$ (nD <sub>20</sub> <sup>-2</sup> )	$\theta(T_C - T = 10^\circ C)$ (°)	sign of $P_g$ (+/-)	helical twist sense <sup>+</sup> (D/L)
45a..C <sub>9</sub> H <sub>19</sub> O-	50.0	73.3	116.2	117.0-10	68.0	26.0	-- (+)	L
45b..C <sub>10</sub> H <sub>21</sub>	35.0	-	79.3	79.5-10	++ 24.8	17.0		

<sup>+</sup> See footnote to Table I.

<sup>++</sup> Determined by extrapolation of 10 wt % mixture in racemic CEB.

For the dichloro-substituted nonyloxy material, compound (45a), the  $S_A$  and  $S_C^*$  thermal stabilities are lowered by

roughly 42° and 49° C respectively, in comparison with the equivalent unsubstituted material (28c). Disubstitution has also resulted in a 10° C depression in melting point and in the loss of the monotropic tilted hexatic phase present in compound (28c). More importantly, this structural modification has caused the appearance of a useful but very short range cholesteric phase, although as for compound (31b), this can only be detected by D.S.C.

Comparison of the corresponding decyl materials reveals a fall in the thermal stability of the S<sub>A</sub> phase by almost 45° C and a drop in the melting point by 22° C for the dichloro compound. As a consequence of this change in structure, both the S<sub>B</sub> and S<sub>C</sub>\* phases present in the unsubstituted material have been lost. However, a very short cholesteric phase has been introduced for compound (45b), although this is again detected only by D.S.C.

A contrasting situation arises when considering the effect of this disubstitution on the magnitude of P<sub>g</sub>. For the nonyloxy compound, this has led to a significant increase in the value of P<sub>g</sub> by about 22%, whereas for the analogous decyl materials, the unsubstituted material has the higher P<sub>g</sub> value by about 42%. Nevertheless, the values of tilt angle obtained for both the nonyloxy and decyl compounds have increased by 27% and 10% respectively, compared with the corresponding unsubstituted materials.

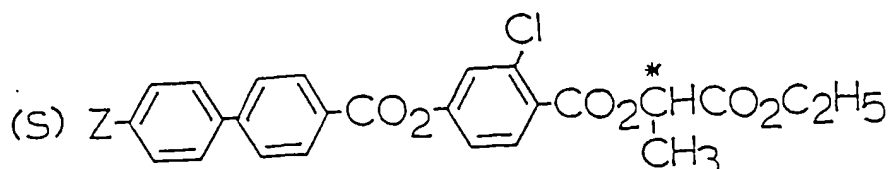
In considering these apparently conflicting results, it must be remembered that the data for the disubstituted decyl material was obtained using a 10 wt % mixture in racemic

CEB. The relevance of the results, particularly for  $\theta$ , are therefore open to question.

The overall effect of this disubstitution has therefore been quite advantageous, particularly in the case of the nonyloxy compound (45a). Although the  $S_C^*$  thermal stability decreased quite markedly, The melting point was also lowered and a 23°C enantiotropic  $S_C^*$  temperature range was therefore maintained. Furthermore, a short cholesteric phase was introduced, and the magnitude of  $P_g$  increased significantly.

To determine the relative influence of the individual chloro substituents on the various properties discussed above, compounds [(53a-c,f-i) Table XVI] were prepared. These materials contain a single chloro substituent facing towards the chiral end-group, i.e. in the 2-position of the phenyl ring adjacent to the aryl-alkyl ester function.

Table XVI Compounds (53a-c,f-i).



Z	mp (°C)	$S_C^*$ - SA (°C)	SA - I (°C)	$P_g(T_C - T = 10^\circ C)$ (nCcm <sup>-2</sup> )	$\theta(T_C - T = 10^\circ C)$ (°C)	sign of $P_g$ (+/-)	helical twist <sup>+</sup> sense
53a..C <sub>9</sub> H <sub>17</sub> O-	44.0	80.9	121.7	-	-		
53b..C <sub>9</sub> H <sub>19</sub> O-	19.0	83.4	117.7	56.5	20.0		
53c..C <sub>10</sub> H <sub>21</sub> O	33.0	83.0	117.6	-	-		
53f..C <sub>9</sub> H <sub>19</sub> O	-33.0	31.0 <sup>20</sup>	85.0	-	-	(+)	L
53g..C <sub>10</sub> H <sub>21</sub> -	- 2.0	32.00	83.7	29.2	15.1		
53h..C <sub>11</sub> H <sub>23</sub> -	28.5	33.0 <sup>-20</sup>	83.2	-	-		
53i..C <sub>12</sub> H <sub>25</sub> -	30.0	34.5 <sup>-20</sup>	81.0	-	-		

+ See footnote to Table I.

A most notable result from Table XVI is that all the chloro compounds prepared have enantiotropic  $S_C^*$  phases. In addition, the presence of a chloro substituent in the nonyl compound has led directly to the introduction of a  $S_C^*$  phase.

Perhaps less obvious, but equally striking is the uniform effect of this chloro substituent on  $S_A$  and  $S_C^*$  thermal stability. This has been depressed by between  $36^\circ$  and  $44^\circ$  C for both the alkyloxy and alky compounds, with respect to the corresponding unsubstituted materials.

Consideration of the relevant alkyloxy materials reveals that the monotropic tilted hexatic phase present in compounds (28b-d) has been ejected and that the melting points are lower for compounds (53a-c) by between  $27^\circ$  and  $41^\circ$  C. Consequently, the most outstanding of these new materials is the nonyloxy homologue which, because of its very low melting point, exhibits a wide range room temperature, enantiotropic  $S_C^*$  phase of almost  $65^\circ$  C.

As this chloro substituted alkyloxy series consists of only three homologues, it is difficult to infer distinct trends in liquid crystalline behaviour. Nonetheless, it does appear that as the alkyloxy chain length increases, the thermal stability of the  $S_A$  phases decreases, whereas that of the  $S_C^*$  phase seems to peak at the nonyloxy homologue.

Comparison of the analogous alkyl materials (53f-i) with compounds (28g-j) shows that introducing the chloro substituent has resulted in elimination of the monotropic  $S_B$  phases of the latter materials and in a lowering of the melting points by between  $14^\circ$  and  $81^\circ$  C. This large variation

in melting point depression stems mainly from the extremely low melting point of  $-33.0^{\circ}\text{C}$  associated with the nonyl homologue (53f). Furthermore, as the corresponding decyl compound has a melting point of  $-2.0^{\circ}\text{C}$ , two room temperature  $S_C^*$  materials have now been prepared, both of which melt below  $0^{\circ}\text{C}$ .

Examining the homologous series (53f-i) indicates that as the alkyl chain length increases, the thermal stability of the  $S_A$  phase decreases irregularly; in contrast, the  $S_C^*$  thermal stability tends to increase uniformly on passing from the nonyl to the dodecyl homologue.

With reference to the equivalent alkyloxy materials, the thermal stabilities of the  $S_C^*$  and  $S_A$  phases of compounds (53f-i) are lowered by approximately  $50^{\circ}$  and  $35^{\circ}\text{C}$  respectively. This is accompanied by a large variation in the decrease in melting point for these materials, although this is mainly due to the extremely low melting points of the nonyl and decyl homologues discussed earlier.

Except for a reduction in the value of  $P_g$  for the decyl compound, the values of  $P_g$  and  $\theta$  for compounds (53b,g) are similar to those for the corresponding unsubstituted materials. Also,  $P_g$  and  $\theta$  are again significantly higher for the nonyloxy material than for the analogous decyl compound.

The relative effects on melting points and  $S_A/S_C^*$  thermal stabilities, of placing chloro substituents at the 2-, 2,3- and 3- positions of the phenyl ring next to the aryl-alkyl ester function, are illustrated in figure 48. For the

nonyloxy compounds (Fig. 48a), a chloro substituent in the 2-position depresses the melting point and the  $S_A/S_C^*$  thermal stabilities by about  $40^\circ\text{C}$  compared with the unsubstituted material, compound (28c). 2,3-Dichloro substitution reduces the  $S_A$  phase thermal stability by another  $1^\circ\text{C}$  and the thermal stability of the  $S_C^*$  phase by a further  $10^\circ\text{C}$ , but in relation to compound (53b) the melting point has now increased by ca.  $40^\circ\text{C}$ . 3-Chlorination results in an additional lowering of the  $S_A$  and  $S_C^*$  thermal stabilities by  $14^\circ$  and  $25^\circ\text{C}$  respectively, although compared with the dichloro compound, the melting point has only been decreased by  $2.5^\circ\text{C}$ .

Varying the number and position of the chloro substituents in the analogous decyl compounds (Fig. 48b) has a virtually identical effect on the  $S_A$  thermal stability to that for the nonyloxy compounds. Substitution in the 2-position has provided the most advantageous mesomorphic changes, with the  $S_C^*$  thermal stability again being lowered by ca.  $40^\circ\text{C}$  and the melting point by the large depression of  $59^\circ\text{C}$ , with respect to the unsubstituted material. However, 2,3-dichloro and 3-chloro substitution have caused the disappearance of the  $S_C^*$  phase and led to increases in melting point of  $37^\circ$  and  $43.5^\circ\text{C}$  respectively, compared with compound (53g).

The relative effects of varying the number and the position of the chloro substituents on the magnitudes of  $P_g$  and  $\theta$ , at  $10^\circ\text{C}$  below the  $S_A-S_C^*$  transition, are shown in figure 49. For the nonyloxy compounds (Fig 49a), substitution in the 2-position has had little influence on either value, whereas 2,3- Disubstitution has caused a large

Fig. 48: Relative effects on melting point and  $S_A/S_C$  phase thermal stability of placing chloro substituents at the 2-, 3-, 3-, and 3-position of the phenyl ring in compounds of structure :-

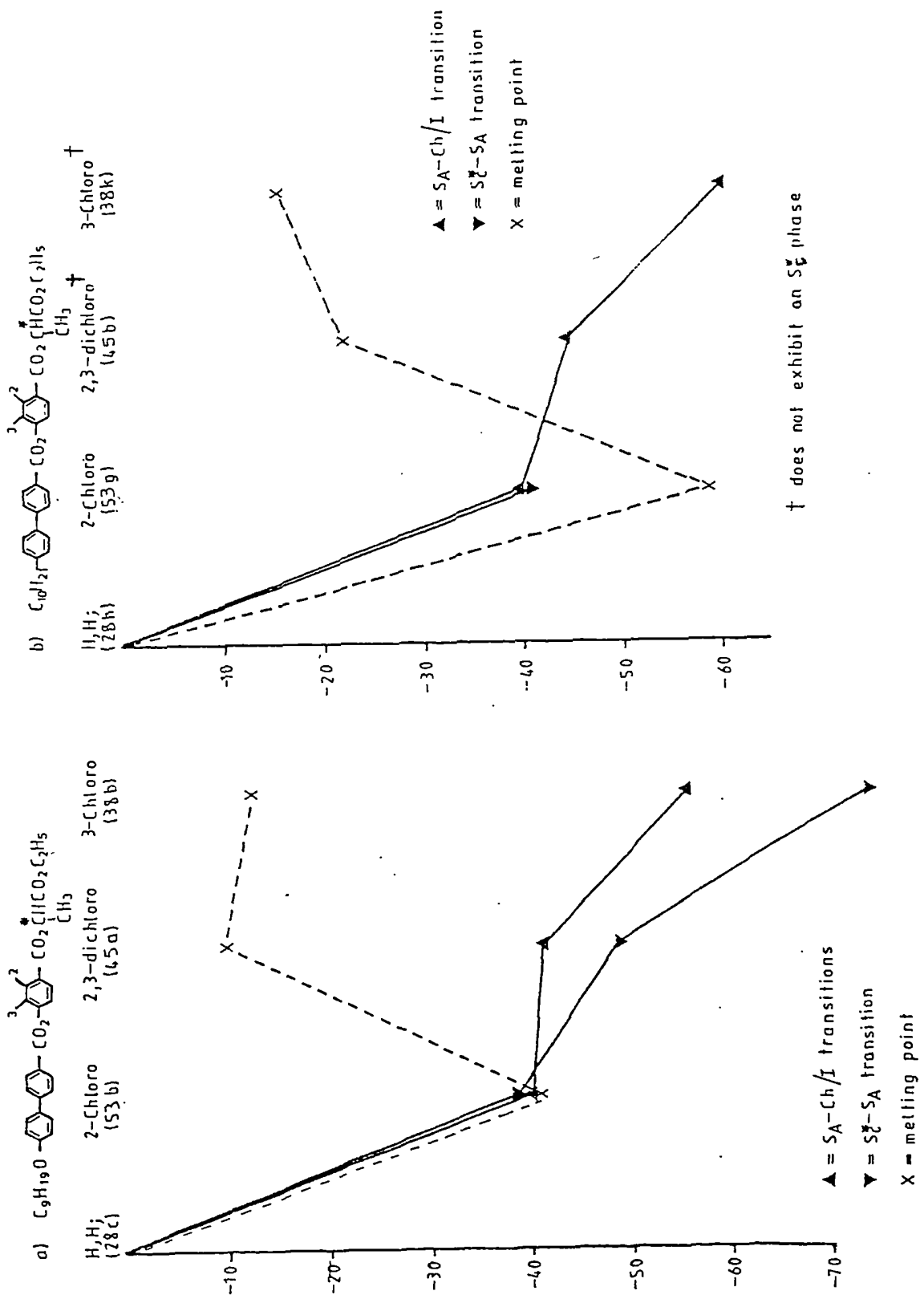
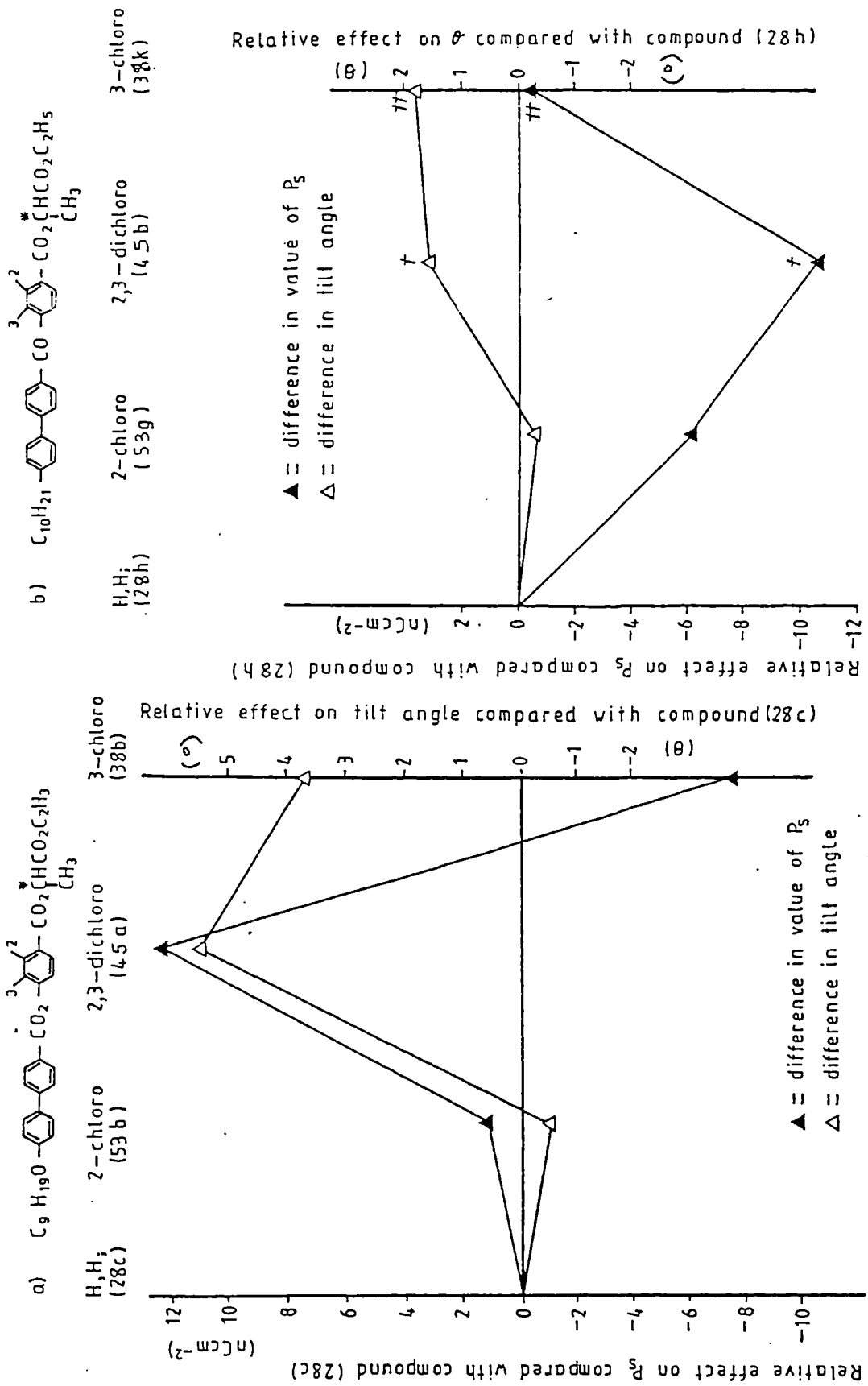


Fig.49: Relative effects on  $P_S$  and  $\theta$ , at  $T_C - T = 10^\circ C$ , of placing chloro substituents at the 2,3- and 3-positions of the phenyl ring, in compounds of structure :-



$t, \#$ : results obtained from 10 wt% and 20 wt% mixtures respectively in racemic CEB.

increase in the values of both  $P_g$  and  $\theta$ . However, a less uniform result arises from monosubstitution in the 3-position, with the magnitude of  $P_g$  being significantly reduced and the tilt angle significantly increased with respect to the unsubstituted compound (28c).

Comparing the similar alkyl materials reveals that a chloro substituent in the 2-position barely lowers the tilt angle, and that the 2,3-dichloro and 3-monochloro substituents cause only ca 10% increase in  $\theta$ . However, it should be remembered that the latter two values are obtained from mixtures with racemic CE8 and are therefore likely to be influenced as much by molecular interactions with the host material as by differences in the substitution. Likewise, the values of  $P_g$  determined for compounds (45b) and (38k) can only be used as a rough guide. Nonetheless, the general tendency is for  $P_g$  values to be lowered by chloro substitution of these alkyl materials, as supported by the significant depression in  $P_g$  for the 2-chloro substituted material compared with that for compound (28h).

Overall then figures 48 and 49 show that a single 2-chloro substituent has by far the most beneficial effect on mesomorphic properties, at the same time maintaining desirable values of  $P_g$  and  $\theta$ . As a consequence of this, compounds [53d,e,j,k (Table XVII)] were prepared with methyl and fluoro substituents replacing the chlorine atom at the 2-position of compounds (53b,g). Methyl and fluoro substituents were chosen, as these gave rise to a combination of similar mesomorphic effects, and  $P_g$  values fairly close to those of the 3-chlorinated compounds [38 a-r (Fig 46)].

Fig. 50 : Melting points and transition temperatures for compounds of structure :-

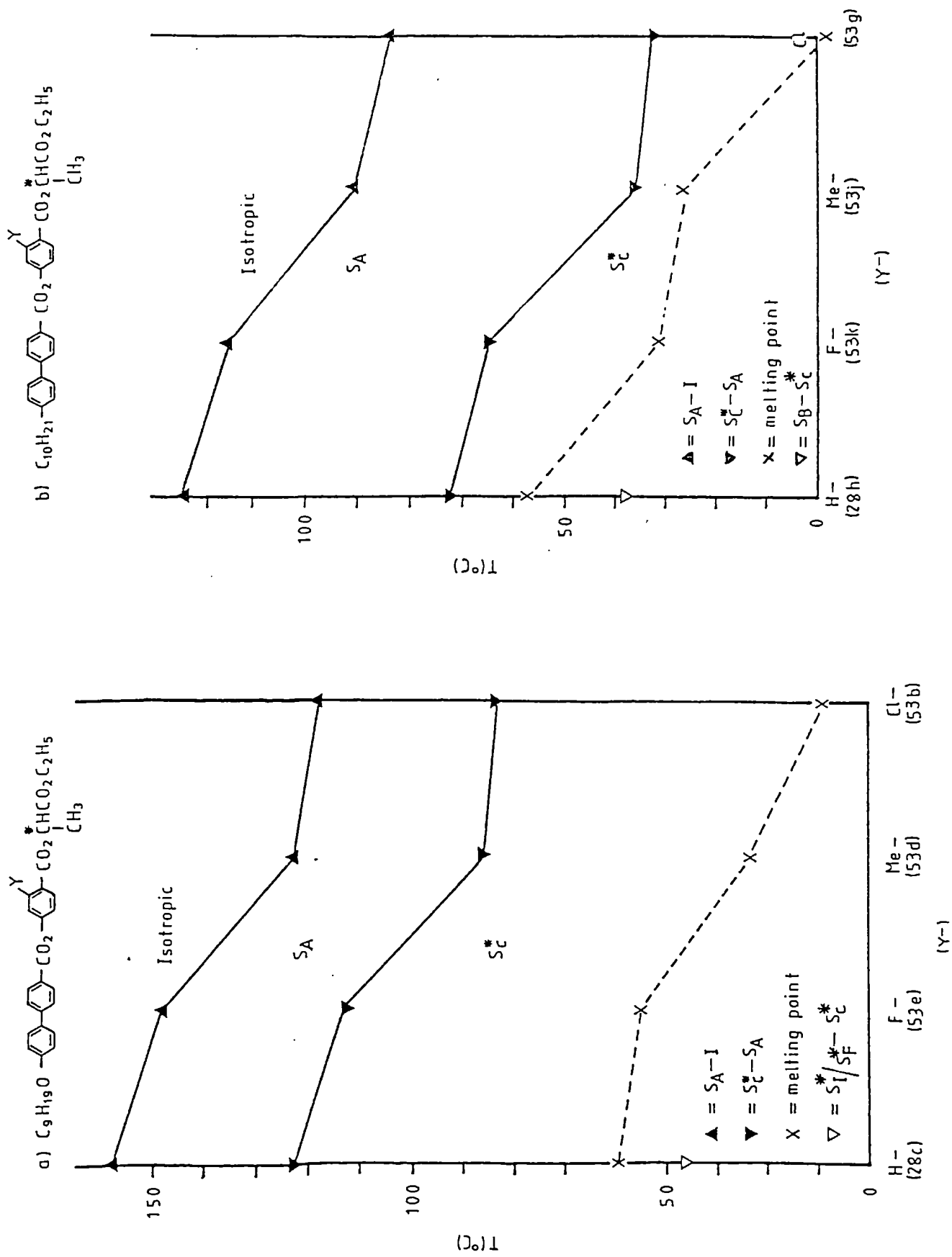
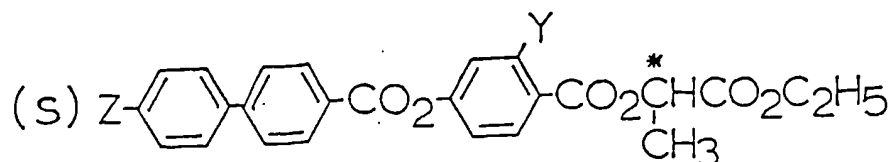


Table XVII Compounds (53d,e,j,k).



Z	mp (°C)	S <sub>C</sub> <sup>*</sup> - S <sub>A</sub> (°C)	S <sub>A</sub> - I (°C)	P <sub>S</sub> (T <sub>C</sub> -T=10°C) (nD <sub>C</sub> ° <sup>-2</sup> )	θ(T <sub>C</sub> -T=10°C) (°C)	sign of P <sub>S</sub> (+/-)	helical twist <sup>†</sup>
53d..C <sub>9</sub> H <sub>19</sub> O- Me	33.0	86.0	122.5	52.3	24.1		
53e..C <sub>9</sub> H <sub>19</sub> O- F	55.0	113.0	148.2	42.0	20.7	(+)	L
53j..C <sub>10</sub> H <sub>21</sub> - Me	26.0	36.0 <sup>-20</sup>	90.2	-	-		
53k..C <sub>10</sub> H <sub>21</sub> O-F	31.5	65.0	115.0	32.9	18.0		

<sup>†</sup> See footnote to Table I.

As in compounds (53 a-c,f-i), the presence of a 2-substituent in compounds (53d,e,j,k) has provided materials with low melting points; room temperature, enantiotropic S<sub>C</sub><sup>\*</sup> phases; and to the ejection of the underlying monotropic phases present in compounds (28c,h). In comparison with the unsubstituted materials, a methyl substituent at the 2-position has depressed the S<sub>A</sub> and S<sub>C</sub><sup>\*</sup> thermal stabilities by approximately 35°C, for both the nonyloxy and decyl compounds, and has also lowered the respective melting points by 27°C and 31°C. Similarly, a fluoro substituent in this position results in a reduction in the thermal stabilities of the S<sub>A</sub> and S<sub>C</sub><sup>\*</sup> phases by roughly 9°C compared with compounds (28c,h), in addition to lowering the melting points by 5° and 25°C respectively, for the nonyloxy and decyl compounds.

Figure 50 illustrates how the melting points and transition temperatures for compounds (53d,e,j,k) fit neatly between those of the unsubstituted and the 2-chloro

substituted materials. The most startling observations from these diagrams are:

(i) the extremely uniform effect that each substituent has in depressing the  $S_A$  and  $S_C^*$  thermal stabilities;

(ii) the most uncommon reflection of these tendencies in melting point behaviour.

It is also worth pointing out that the order of decreasing  $S_A$  and  $S_C^*$  thermal stability caused by substituents in the 2-position, is the same as that for the equivalent 3-substituted materials (Fig. 46), i.e., H; F; Me; Cl.

Following the general trends already outlined for compounds (53a-c,f-i), the thermal stabilities of the  $S_A$  phases are lowered by about  $34^\circ\text{C}$ , and those of the  $S_C^*$  phases by roughly  $50^\circ\text{C}$ , for the decyl homologues in relation to the corresponding nonyloxy compounds (53d,e). Furthermore, the melting points of the methyl and fluoro substituted decyl materials are depressed by  $7^\circ$  and  $23^\circ\text{C}$  respectively compared with the equivalent nonyloxy compounds.

Reasonably high  $P_g$  values are retained by methyl and fluoro substituted nonyloxy materials, although they are lowered by 6% and 25% respectively compared with the corresponding unsubstituted compound (28c).

The tilt angle of the nonyloxy fluoro material remains about the same as that of compound (28c), whereas the tilt angle of the equivalent methyl material has been relatively increased, by approximately 18%, at  $10^\circ\text{C}$  below the  $S_A$  to  $S_C^*$  phase transition.

Finally, the values of  $P_g$  and  $\Theta$  for the nonyloxy fluoro material, compound (53c), are significantly greater than those of the analogous alkyl compound, in accordance with previously obtained results.

### Summary of Section 7

The initial object of the work in this section has been to determine the effect of varying the number and position of chloro substituents on the phenyl ring, adjacent to the chiral end group of compounds (28a-j).

2,3-dichloro substitution has resulted in a large depression of  $S_A$  and  $S_C^*$  thermal stabilities, although it has also lowered melting points and led to the introduction of short cholesteric phases for compounds (45a,b). Disubstitution has also caused a significant increase in  $P_g$  and  $\Theta$  for the nonyloxy material, compound (45a), and has therefore proved to be an advantageous structural modification overall.

Monochloro substitution in the 2-position of the phenyl ring has caused a fairly large and uniform depression in the  $S_A$  and  $S_C^*$  phase thermal stabilities of compounds (53a-c,f-i), compared with the equivalent unsubstituted materials, in addition to reducing their respective melting points considerably. As a result of this, all these compounds exhibit an enantiotropic  $S_C^*$  phase, that for the nonyl homologue being introduced as a result of the substitution. The extremely low melting points exhibited by this compound and by the corresponding decyl homologue have also provided two room temperature  $S_C^*$  materials which melt below  $0^\circ\text{C}$ .

Comparison of the effects of 2,3-dichloro, 2-chloro and 3-chloro substitution shows that despite the non-inducement of cholesteric phases, 2-substitution leads to the best combination of mesomorphic properties and desirable values of  $P_g$  and  $\theta$ . Consequently, both methyl and fluoro substituents were used to replace the chloro substituent in the 2-position. The relative effects of the three 2-substituents highlight a remarkably regular depression in the  $S_A$  and  $S_C^*$  thermal stabilities, which is mirrored to a large extent in the melting points. The order of decreasing thermal stability caused by each substituent follows that for the 3-substituted materials, i.e. H; F; Me; Cl.

Although 2-substitution of the phenyl ring has not led to the introduction of cholesteric phases, it has given rise to many wide range room temperature, enantiotropic  $S_C^*$  materials with desirable values of  $P_g$  and  $\theta$ . The most useful are probably those containing a 2-chloro substituent, as these exhibit the lowest melting points and highest  $P_g$  values. The results in this section again show that the thermal stability of any particular phase, as well as the values of  $P_g$  and  $\theta$ , tend to be significantly higher for the alkyloxy materials than for the equivalent alkyl compounds. Furthermore, all the compounds prepared in section 7 have a positive sign of  $P_g$  and fit the rules described earlier, with regard to helical twist sense, absolute configuration and distance of the asymmetric carbon atom from the aromatic core, i.e.: - S o L (+I).

## 2.8 Compounds (57 a-d).

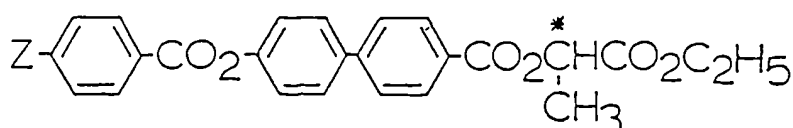
Although the work had by now succeeded in providing many low melting materials with wide range  $S_C^*$  phases and high  $P_S$  values, there was still a lack of such materials having reasonably wide temperature range cholesteric phases. As mentioned earlier, the cholesteric phase is important for aiding alignment of the underlying  $S_A$  and  $S_C^*$  phases in devices and it is therefore a desirable addition to the liquid crystalline phase sequence.

Despite the fact that compounds (45a,b) and many of compounds (38a-r) exhibit cholesteric phases, none of these extends beyond a 5° C temperature range and only three can be actually observed by microscopy. Wider temperature range cholesteric phases are observed for compounds (31b,c,g,h) in section 5, but these materials have very high melting points, as well as high cholesteric phase thermal stabilities, which would make filling of display devices difficult.

It was thought that the best method of obtaining slightly wider temperature range cholesteric phases, while retaining the  $S_C^*$  phase, a high  $P_S$  and reasonably low melting point characteristics, would be to reverse the positions of the phenyl and biphenyl rings of compounds (28c,h). A similar structural modification had already been shown to induce cholesteric phases in compounds (23a-c) compared with compounds (PGf,g), and although this also increased melting points significantly and maintained a fairly high cholesteric phase thermal stability, this did not occur to the same extent as in compounds (31b,c,g,h).

Apart from the nonyloxy and decyl homologues, the heptyloxy and octyl homologues were also prepared, as the results of compounds (23a-c) indicated that lower homologues might provide wider range cholesteric phases and possibly lower melting points. Compounds [(57a-d) Table XVIII] were therefore prepared in order to investigate these possibilities.

Table XVIII. Compounds (57a-d).



Z	mp (°C)	S <sub>C</sub> <sup>*</sup> /S <sub>B</sub> -S <sub>A</sub> (°C)	S <sub>A</sub> -Ch (°C)	Ch - I (°C)	P <sub>S</sub> (T <sub>C</sub> -T=10°C) (n <sub>C</sub> c <sub>m</sub> <sup>-2</sup> )	θ(T <sub>C</sub> -T=10°C) (°)	sign of P <sub>S</sub> (+/-)	helical twist <sup>++</sup> (D/L)
57a..C <sub>7</sub> H <sub>15</sub> O-	82.0	+ 93.3	135.0	137.2	102.0	25.0		
57b..C <sub>9</sub> H <sub>21</sub> O-	72.0	+106.0-10	135.9	137.8	68.5	22.0	+	L
57c..C <sub>8</sub> H <sub>17</sub> -	41.0	(33.9)10	106.2	107.1	++ 63.7	-		
57d..C <sub>10</sub> H <sub>21</sub>	53.0	(46.0)	111.0	(113.5)-20	++ 54.5	-		

+ S<sub>C</sub><sup>\*</sup> - S<sub>A</sub> transition

++ See footnote to Table I.

+++ Determined by extrapolation from results for a 10 wt % mixture in racemic CEB.

For compounds (57a,b), reversing the phenyl and biphenyl rings of compounds (28a,c) has lowered the thermal stabilities of the S<sub>C</sub><sup>\*</sup> phases by roughly 16°C and those of the S<sub>A</sub> phases by 32° and 22°C respectively for the heptyloxy and nonyloxy homologues. The underlying tilted hexatic phases of compounds (28a,c) have been eliminated, and more importantly, a short temperature range cholesteric phase of about 2°C has been introduced for compounds (57a,b). This structural modification has also led to an 8°C decrease in the melting

point of the heptyloxy material, but to an increase of 12°C in that of the nonyloxy material, in relation to compounds (28a,c).

Reversing the ring positions of the corresponding alkyl materials has also led to the introduction of a cholesteric phase, but for the octyl homologue this extends over less than 1°C, and for the decyl homologue the phase can only be detected by D.S.C. The  $S_A$  thermal stabilities of these two homologues are depressed by roughly 24° and 13°C compared with compounds (28f,h), and their respective melting points are lowered by 8° and 4°C.

Comparing the octyl compounds shows that ring reversal has caused a depression in the  $S_B$  thermal stability of compound (57c) by about 15°C. It has also resulted in the  $S_C^*$  phase present in compound (28h) being eliminated from the mesogenic phase sequence of compound (57d), and consequently, the  $S_B$  thermal stability of this latter material has risen by about 8°C.

In relation to the alkyloxy materials, compounds (57a,b), the cholesteric and  $S_A$  thermal stabilities of the analogous alkyl compounds are both depressed by between 24° and 30°C. Furthermore, the melting points of the octyl and decyl homologues are 41° and 19°C lower than those of the respective alkyloxy homologues.

Probably the most unexpected result from these materials is the large increase in the magnitude of  $P_S$  compared with compounds (28a,c,f,h). Compound (57a) has a particularly high  $P_S$  value of  $102n\text{Ccm}^{-2}$  at 10°C below the  $S_A$  to  $S_C^*$  transition; this is over 60% greater than that of the corresponding heptyloxy material, compound (28a).

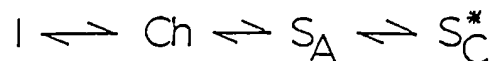
One possible explanation for this might be that the biphenyl ring system causes greater hindrance to intramolecular rotations and provides more polarisable electrons in the vicinity of the asymmetric centre, Nevertheless, it seems unlikely that this would possibly account for such a large increase in  $P_g$ , and in any case, no remotely similar effect was observed for the same structural modification between compounds (Pgf,g) and (23b,c).

A second explanation could lie in the fact that the tilt angle of the  $S_C^*$  phase in compound (57a) is about 40% greater than that for compound (28a), thus lending support to the Meyer hypothesis discussed earlier. However the large increase in  $P_g$  associated with the corresponding nonyloxy compounds is accompanied by only a small increase in tilt angle, thereby throwing some doubt on this argument too.

It should again be noted that the magnitudes of  $P_g$  for the alkyloxy compounds are significantly higher than those of the corresponding alkyl compounds, and that this is probably due to the greater polarity of the former materials.

Of the four materials prepared in this section, compound (57b) is probably the most suitable for device application as it exhibits the widest range enantiotropic  $S_C^*$  phase and the lower melting point of the two alkyloxy compounds, while maintaining a very high  $P_g$  value. In addition to these properties, it has a directly observable cholesteric phase with a fairly low thermal stability. In order to assess compound (57b) more fully, it may be compared with some of the other potentially useful cholesteric materials discussed earlier in this work.

Compound (17) has a cholesteric phase of 7° C range, with a low thermal stability and a fairly high extrapolated value of P<sub>g</sub>. Although it also has a slightly lower melting point than compound (57b), it does not exhibit a S<sub>C</sub><sup>\*</sup> phase, and therefore does not have the required phase sequence:



Compound (20a) has this phase sequence; it also displays an enantiotropic S<sub>C</sub><sup>\*</sup> phase of 50° C range and a cholesteric phase of 5° C range. It does however possess a higher melting point and a higher cholesteric thermal stability greater than that of compound (57b); the P<sub>g</sub> value is also very small.

Compound (23a) has a similarly small P<sub>g</sub>, although it too exhibits the desired phase sequence, with an enantiotropic S<sub>C</sub><sup>\*</sup> phase range of 53° C and a cholesteric phase extending over 8° C. It also has a slightly lower melting point than compound (57b), but again suffers from a very high cholesteric thermal stability.

Compound (31h) exhibits the correct order of phases with a wide cholesteric phase of 11° C and relatively short-range, enantiotropic S<sub>C</sub><sup>\*</sup> phase of 13° C. In addition to this, it possesses a reasonably high P<sub>g</sub> value and reduced cholesteric phase thermal stability, compared with compound (23a). However, compound (57b) has a significantly lower melting point and cholesteric phase thermal stability than compound (31h), and it also has a higher value of P<sub>g</sub> and a wider range S<sub>C</sub><sup>\*</sup> phase.

Compound (38b) has the lowest melting point of the potentially useful cholesteric materials discussed here. It also exhibits the phase sequence required and a high  $P_S$  value. Nonetheless, compound (57b) displays an even higher  $P_S$  and also wider range  $S_C^*$  and cholesteric phases. Furthermore, although compound (38b) possesses a very low cholesteric phase thermal stability, this can only be detected by D.S.C.

Compound (45a) has a lower melting point, a lower cholesteric thermal stability and a wider range enantiotropic  $S_C^*$  phase than compound (57b). In addition to this it exhibits an equivalent value of  $P_S$  as well as the desired phase sequence. However, like compound (38b), its cholesteric phase cannot be detected by optical microscopy and may only be determined by D.S.C.

#### Summary of Section 8

The work in this section has focused on the preparation of materials having a suitable cholesteric phase, as well as  $S_A$  and  $S_C^*$  phases, in order to aid sample alignment in fabricating ferroelectric display devices. From the results of earlier work, the attempt to induce this desired phase sequence involved reversing the positions of the phenyl and biphenyl rings in compounds (28a,c,f,h,).

For the alkyloxy compounds, this ring reversal has led to the loss of the underlying tilted hexatic phase, to a decrease in the thermal stabilities of the  $S_A$  and  $S_C^*$  phases and to the introduction of a short cholesteric phase. The effect of this structural modification on the corresponding

alkyl materials has been to reduce the thermal stability of the  $S_A$  phase and to introduce a very short cholesteric phase into the phase sequence. However, it has also led to the ejection of the underlying  $S_C^*$  phase.

A surprising consequence of reversing the phenyl and biphenyl rings has been the large upsurge in the magnitude of  $P_S$ , with the heptyloxy compound attaining a  $P_S$  value in excess of  $100 \text{ nCcm}^{-2}$  at  $10^\circ \text{C}$  below the  $S_A$  to  $S_C^*$  transition. No satisfactory explanation of the phenomenon has been obtained.

The most suitable material for device application found in this section [compound (57b)] is compared with some of the other potentially useful cholesteric materials previously discussed in this work. Although compound (57b) has only a short cholesteric phase range and its melting point is a little too high, it displays overall significant advantages over all other comparable materials; only compound (45a) provides a possible alternative.

As for all the other lactate esters, compounds (57a-d) possess a positive sign of  $P_S$  and follow the relationship:

$$S \circ L (+I)$$

between absolute configuration; distance of chiral centre from the ring system and helical twist sense.

### 3. EXPERIMENTAL

### 3.1 Physical Measurements.

#### 3.1.1 Transition Temperatures.

Transition temperatures were initially measured by optical microscopy using an Olympus Polarising Microscope Model BHSP, in conjunction with a Mettler FP5 hot-stage and temperature control unit. Confirmation of phase transitions was obtained by differential scanning calorimetry using a Perkin-Elmer DSC-2C with Data Station.

#### 3.1.2 Characterisation of Materials.

Confirmation of all final structures, and when necessary the structures of intermediate compounds, was ascertained by a combination of the following techniques:-

##### 3.1.2.1 Infra-red Spectroscopy (ir).

The ir. spectra of the compounds were recorded on Perkin-Elmer 457 and 580B grating ir spectrophotometers. Solid samples were prepared as KCl discs and liquid samples were prepared as neat films between KBr plates.

##### 3.1.2.2 Mass Spectrometry (ms).

Mass spectroscopic data was obtained using either an A.E.I.M.S. 902 and / or a Finnigan Mat 1020 Automated GC / MS mass spectrometer.

##### 3.1.2.3 Proton Nuclear Magnetic Resonance (<sup>1</sup>Hnmr).

The <sup>1</sup>Hnmr data was obtained using a Jeol J.N.M.-P.M. x 60 spectrometer. Samples were dissolved in deuterated

chloroform ( $\text{CDCl}_3$ ) or when necessary, a mixture of  $\text{CDCl}_3$  and deuterated dimethyl sulphoxide (D.M.S.O. -  $\text{D}_6$ ).

#### 3.1.2.4 Polarimetry ( $[\alpha]_D^{20}$ )

Specific rotations were determined using a Bendix - NPL Automatic Polarimeter 143A on samples dissolved in chloroform, at  $20^\circ\text{C}$ .

Optical microscopy (see sub-section entitled 'Transition Temperatures') was used to identify the phase or phases exhibited by the compounds prepared for this thesis. When necessary, confirmation of phase type was obtained by miscibility or X-ray diffraction studies.

#### 3.1.3 Purity of Materials.

The purity of all final products was checked by high pressure liquid chromatography (hplc) on a Partisil 10 ODS II reverse phase column, using the following solvents;

I: Methanol.

II: Methanol: Water (95:5).

III: Methanol: Water (90:10).

The purity of all intermediates was checked routinely by silica gel thin layer chromatography (t.l.c.) using Merck Kieselgel 60F<sup>254</sup> precoated t.l.c. plates.

The stationary phase for flash column chromatography was Merck Kieselgel 60 [(230 - 400)] using the following solvent mixtures as eluants;

- A. Chloroform: Petroleum fraction (60° - 80° C), 2 : 1.
- B. Chloroform: Petroleum fraction (60° - 80° C), 1 : 1.
- C. Chloroform: Petroleum fraction (60° - 80° C), 1 : 2.

### 3.2 Starting Materials.

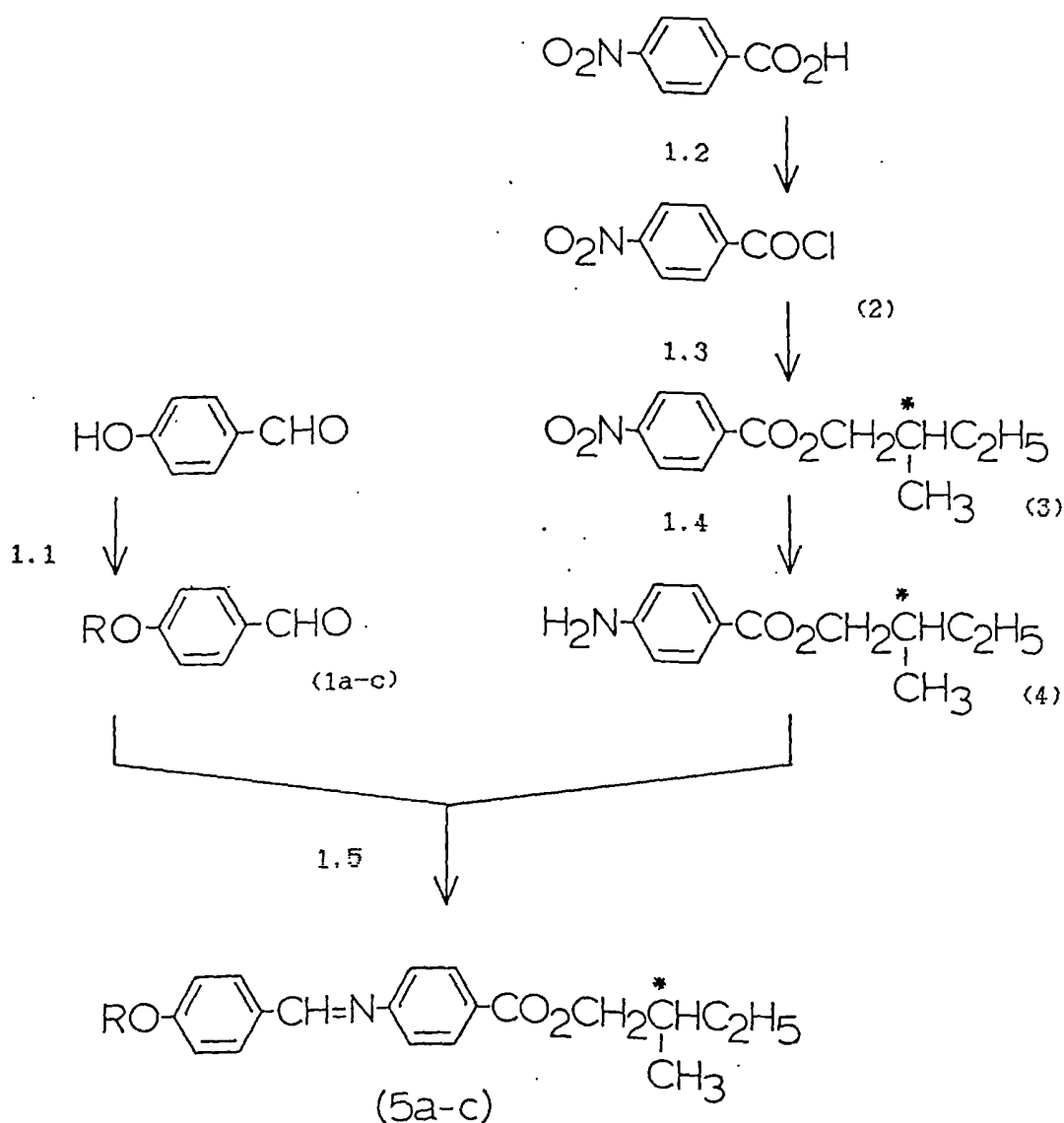
The optically active alcohols used in the following experimental section were (R)-(-)-2-butanol, (S)-(-)-ethyl lactate, (1R, 2R, 3R, 5S)-(-)-Isopinocampheol, (1R, 2S, 5R)-(-)-menthol (supplied by Aldrich) and S(-)-2-methyl-1-butanol, R(-)-2-octanol (supplied by Fluka).

Under the JOERS ALVEY Display research programme (GR/D/598892 MMI/131) in collaboration with Standard Telecommunication Laboratories (STL) (Harlow), BDH. Ltd. (Poole), RSRE. (Malvern) and Thorn - EMI (Hayes), the following compounds were supplied by :

1. B.D.H.: 4-cyano-4'-hydroxybiphenyl and a number of 4-cyano-4'-alkoxy and -alkylbiphenyls.
2. S.T.C. Technology: 3 chloro-4-benzyloxybenzoic acid.

### 3.3 METHODS

SCHEME 1



1a,5a...R=C<sub>6</sub>H<sub>13</sub>-; 1b,5b...R=C<sub>7</sub>H<sub>15</sub>-; 1c,5c...R=C<sub>8</sub>H<sub>17</sub>-.

11: n-RBr, K<sub>2</sub>CO<sub>3</sub>, .

12: SOCl<sub>2</sub>.

13: HOCH<sub>2</sub>CH(CH<sub>3</sub>)C<sub>2</sub>H<sub>5</sub>, (C<sub>2</sub>H<sub>5</sub>)<sub>3</sub>N, CH<sub>2</sub>Cl<sub>2</sub>.

14: (i) Fe, CH<sub>3</sub>CO<sub>2</sub>H; (ii) NaCO<sub>3</sub>.

15: CH<sub>3</sub>CO<sub>2</sub>H, C<sub>2</sub>H<sub>5</sub>OH.

### 3.3.1: Scheme 1 - Compounds (5a-c).

#### 3.3.1.1: 4-alkoxybenzaldehydes (1a - c).

The appropriate 4-n-alkyl bromide (0.25 mol) was added dropwise to a stirred suspension of 4-hydroxybenzaldehyde (0.175 mol) and potassium carbonate (0.7 mol) in cyclohexanone (150ml). The reaction mixture was then heated under reflux for 3h. The potassium carbonate was filtered off and the filter cake washed with acetone until the washings ran clear. The cyclohexanone and acetone were removed by distillation under reduced pressure and the resulting product was then purified by distillation under reduced pressure to afford the 4-alkoxybenzaldehydes (1a-c) as colourless liquids.

The yields, M/Z values and bps for compounds (1a - c) are given below. The ir and <sup>1</sup>Hnmr data for these compounds is exemplified by the data given below for the hexyloxy homologue (1a).

1a: The yield was 11.5g (32%); bp 118° C / 0.01 mm Hg; M/Z 206 (M<sup>+</sup>); ir (neat), 2830, 2720, 1695, 1260, 835 cm<sup>-1</sup>; <sup>1</sup>Hnmr. δ 0.84 - 2.06 (11H,M), 4.00(2H,T), 6.82 - 7.81 (8H,M), 9.80 (1H,S).

1b: The yield was 17.7g (46%); bp 120° C / 0.01 mm Hg; M/Z 220 (M<sup>+</sup>).

1c: The yield was 19.6g (48%); bp 127° C / 0.01 mm Hg; M/Z 234 (M<sup>+</sup>).

### 3.3.1.2: 4-nitrobenzoyl chloride (2).

4-Nitrobenzoic acid (50g, 0.3mol) was dissolved in Thionyl chloride (250ml) and gently heated under reflux with the exclusion of moisture, for 3h. The reaction mixture was allowed to cool and then the unreacted thionyl chloride was removed by addition of a small amount of dry toluene to the residue and then removing the toluene / thionyl chloride by distillation under reduced pressure. The crude product was used immediately in step 1.3 without further purification.

### 3.3.1.3: (S)-(-)-2-methylbutyl-4-nitrobenzoate (3).

A solution of compound (2) (0.3 mol) in dry dichloromethane (50 ml) was added dropwise to a stirring solution of (S)-(-)-2-methylbutanol (29.0g, 0.33 mol) and dry triethylamine (35 ml) in dry dichloromethane (200 ml) at room temperature. The reaction mixture was then stirred for 16h. The reaction mixture was poured into dilute hydrochloric acid (100 ml), and the crude product extracted into chloroform (200 ml). The organic layer was separated, washed with saturated brine (2 x 100 ml) and then dried (MgSO<sub>4</sub>). The product was purified by distillation under reduced pressure to yield compound (3) as a yellow oil, 60g (84%); bp 120° C / 0.01 mm Hg; M/Z 237 (M<sup>+</sup>).

### 3.3.1.4: (S)-(-)-2-methylbutyl-4-aminobenzoate (4).

A stirring suspension of compound (3) (30.0g, 0.126 mol), iron pin dust (60.0g, 1.08g atom), 20% v/v aqueous acetic acid (180 ml) and ethanol (500 ml) was heated under reflux for 4h. Anhydrous sodium carbonate (48.0g, 0.45 mol)

was added slowly to the reaction mixture, which was then refluxed for a further 30 min. The hot reaction mixture was filtered, using 'hyflo - supercell' filter aid, to remove inorganic mixed oxides and salts. The filter cake was then washed several times with hot ethanol.

The ethanol was removed from the filtrate by distillation under reduced pressure, and the resulting residue was treated with chloroform, (200 ml). The chloroform layer was then washed with saturated aqueous sodium carbonate (2 x 100 ml) and dried (MgSO<sub>4</sub>).

Recrystallisation from a 2 = 1 mixture of toluene / petroleum fraction (bp 60° - 80° C) afforded compound (4) as a white crystalline solid, 9.2g (35%); mp 46.0° C; M/Z 207 (M<sup>+</sup>); [α]<sub>D</sub><sup>20</sup> + 6.2; ir 3420, 3340, 1785, 1275, 775 cm<sup>-1</sup>; <sup>1</sup>Hnmr. δ 0.79 - 1.90 (9H, M), 3.90 (2H, brS), 4.08 (1H, D), 6.48 - 7.92 (4H, M).

### 3.3.1.5: 4-n-alkoxybenzylidene 4'-amino- (S)-(-)-2-methylbutyl) carboxylates (5a - c).

Compounds (1a - c) (0.008 mol) and glacial acetic acid (1 drop) were added to a stirred solution of compound (4) (0.007 mol) in hot ethanol (3 ml), and the reaction mixture gently heated under reflux for 20 min. After cooling slowly, (refrigeration to 5° C was usually required to induce crystallisation of the crude product), the solidified product was dried (CaCl<sub>2</sub>) under reduced pressure.

The dried crystals were then recrystallised alternately from petroleum fraction (bp 40° - 60° C) and ethanol until constant transition temperatures were obtained.

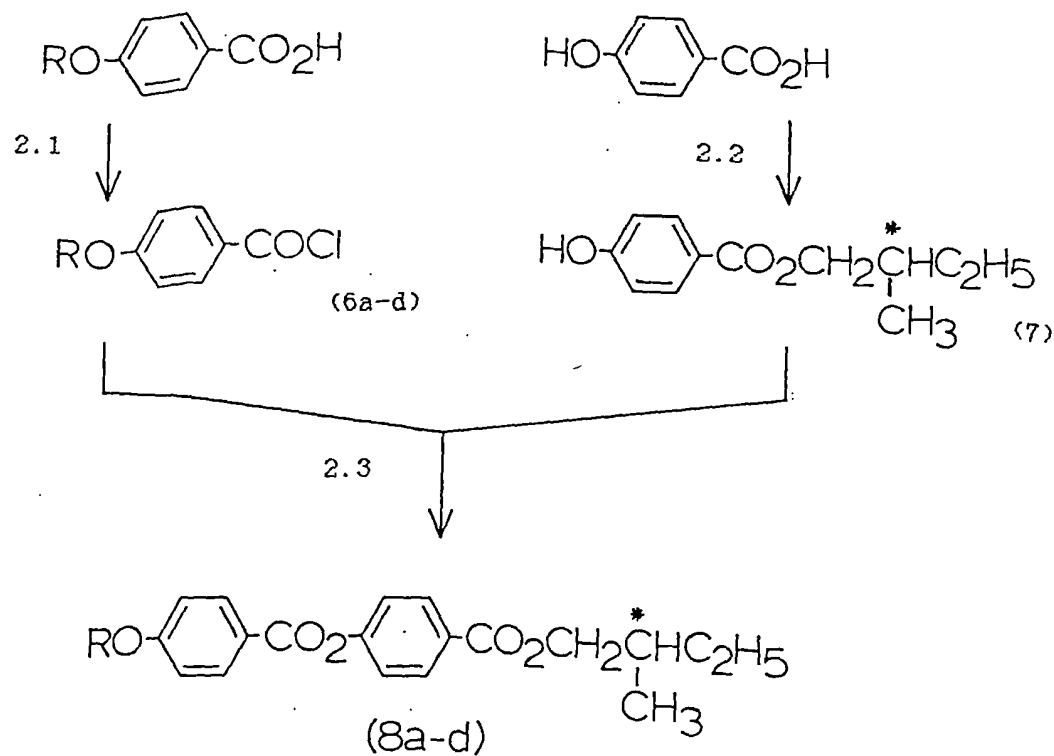
The ir. and  $^1\text{Hnmr.}$  data for compounds (5a - c) is exemplified by the data given below for the hexyloxy homologue (5a). The transition temperatures for compounds (5a - c) are given in Table I, page 51.

5a: The yield was 1.13g (41%) ; mp.  $47.0^\circ\text{C}$ ; M/Z 395 ( $\text{M}^+$ ) ;  $[\alpha]_{\text{D}}^{20} + 4.2^\circ$ ; purity (hplc) > 99.9% (solvent 1); ir. 1710, 1255, 1105,  $840\text{ cm}^{-1}$ ;  $^1\text{Hnmr.}$   $\delta$  0.94 - 2.25 (20H, M), 4.03 (2H,T), 4.20 (2H,D), 6.88 - 8.38 (9H, M).

5b: The yield was 1.31g (46%) ; mp.  $47.0^\circ\text{C}$  ; M/Z 409 ( $\text{M}^+$ );  $[\alpha]_{\text{D}}^{20} + 4.5^\circ$  purity (hplc) > 99.9% (solvent 1).

5c: The yield was 1.94g (66%); mp.  $41.5^\circ\text{C}$ ; M/Z 423 ( $\text{M}^+$ ) ;  $[\alpha]_{\text{D}}^{20} + 2.9^\circ$ ; purity (hplc) > 99.9% (solvent 1).

SCHEME 2



6a,8a...R=C<sub>6</sub>H<sub>13</sub>-; 6b,8b...R=C<sub>7</sub>H<sub>15</sub>-; 6c,8c...R=C<sub>8</sub>H<sub>17</sub>-;

6d,8d...R=C<sub>9</sub>H<sub>19</sub>-.

2.1: SOCl<sub>2</sub>.

2.2: HOCH<sub>2</sub>CH<sup>\*</sup>(CH<sub>3</sub>)C<sub>2</sub>H<sub>5</sub>, H<sub>2</sub>SO<sub>4</sub>.

2.3: (C<sub>2</sub>H<sub>5</sub>)<sub>3</sub>N, CH<sub>2</sub>Cl<sub>2</sub>.

### 3.3.2: Scheme 2 - Compounds (8a-d).

#### 3.3.2.1: 4-n-alkoxybenzoyl chloride (6a-d).

The preparation of compounds (6a-d) was achieved by a procedure similar to that described in step 1.2: using 4-n-alkoxybenzoic acid (0.037 mol) as the starting material. The crude products were purified by distillation under reduced pressure to give compounds (6a-d) as colourless liquids. The ir. and  $^1\text{Hnmr.}$  data for compounds (6a-d) is exemplified by the data given below for the hexyloxy homologue (6a).

6a: The yield was 8.3g (93%); bp. 115° C / 0.01 mmHg; M/Z 268 ( $\text{M}^+$ ); ir. 1775, 1605, 1510, 1270, 850  $\text{cm}^{-1}$   
 $^1\text{Hnmr.}$   $\delta$  0.64 - 2.02 (11H,M), 3.98 (2H,T), 6.71 - 8.12 (4H, M).

6b: The yield was 8.1g (86%); bp. 130° C / 0.01 mm Hg; M/Z 254 ( $\text{M}^+$ ).

6c: The yield was 7.6g (76%), bp. 130° C / 0.01 mm Hg; M/Z 268 ( $\text{M}^+$ ).

6d: 10.2g (97%); bp. 144° C / 0.01 mm Hg; M/Z 282 ( $\text{M}^+$ ).

#### 3.3.2.2: (S)-(-)-2-methylbutyl 4-hydroxybenzoate (7).

A stirred suspension of 4-hydroxybenzoic acid (40.0g, 0.29 mol) in a large excess of (S)-(-)-2-methylbutanol (100 ml) was heated until the acid had dissolved. The solution was cooled to room temperature before concentrated sulphuric acid (0.5 ml) was added, and the stirred reaction mixture was then heated under reflux for 16h. The reaction mixture was

allowed to cool and the product extracted into chloroform (200 ml). The organic layer was washed with saturated aqueous sodium hydrogen carbonate (100 ml), water (100 ml) and finally dried (MgSO<sub>4</sub>). The chloroform and unreacted (S)-(-)-2-methylbutanol were removed by distillation under reduced pressure, and the product was purified by distillation under reduced pressure to afford compound (7) as a colourless viscous liquid, 54g (90%); bp 172°C; M/Z 208 (M<sup>+</sup>); [α]<sub>D</sub><sup>20</sup> + 1.7°; ir. 3320 (broad), 1680, 1310, 1165, 850 cm<sup>-1</sup>; <sup>1</sup>Hnmr. δ 0.68 - 2.32 (9H, M), 4.18 (2H, D), 6.76 - 8.12 (5H, M).

3.3.2.3: (S)-(-)-2-methylbutyl 4'-(4-n-alkoxyphenyl-1-carboxy) benzoate (8a-d).

Compounds (6a - d) (0.0079 mol) were dissolved in dry dichloromethane (10 ml) and added dropwise to a stirring solution of compound (7) (0.0083 mol) and dry triethylamine (3 ml) in dry dichloromethane (10 ml) at reflux. The stirred reaction mixture was heated under reflux for a further 3h then allowed to cool to room temperature. The product was extracted into chloroform (200 ml), washed with dilute hydrochloric acid (100 ml), saturated brine (2 x 100 ml) and finally dried (MgSO<sub>4</sub>).

The crude product was dissolved in a minimum amount of chloroform and purified by column chromatography on silica gel (60 - 120 μm, 200g), using chloroform as eluant. Recrystallisation from petroleum fraction (bp 80° - 100° C) and then ethanol afforded compounds (8a - d) as white crystalline solids. The ir and <sup>1</sup>Hnmr data for compounds

(8a - d) is exemplified by the data given below for the hexoxy homologue (8a). The transition temperatures for these compounds are given in Table II, page 52.

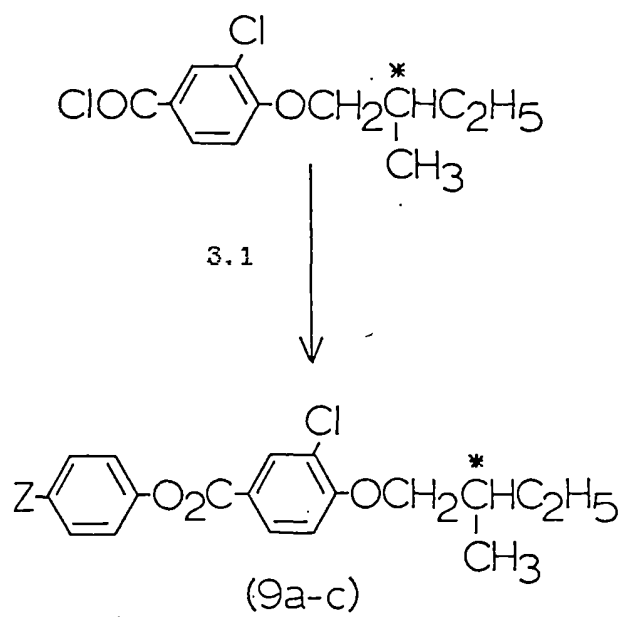
8a: The yield was 0.87g (27%); mp. 41.0° C; M/Z 412 (M<sup>+</sup>);  $[\alpha]_D^{20} + 2.1^\circ$ ; purity (hplc) 99.5% (solvent I); ir. 1735, 1715, 1260, 1060, 850 cm<sup>-1</sup>; <sup>1</sup>Hnmr,  $\delta$  0.79 - 2.00 (20H, M), 4.00 (2H, T), 4.15 (2H, D), 6.82 - 8.18 (8H, M).

8b: The yield was 2.3g (68%); mp. 42.0° C; M/Z 426 (M<sup>+</sup>);  $[\alpha]_D^{20} + 2.6^\circ$ ; purity (hplc) > 99.5% (solvent II).

8c: The yield was 2.5g (72%); mp. 34.5° C; M/Z 440 (M<sup>+</sup>);  $[\alpha]_D^{20} + 3.4^\circ$ ; purity (hplc) 99% (solvent II).

8d: The yield was 2.3g (65%); mp. 55.5° C; M/Z 454 (M<sup>+</sup>);  $[\alpha]_D^{20} + 2.7^\circ$ ; purity (hplc) 99% (solvent II).

SCHEME 3



9a...Z=C<sub>7</sub>H<sub>15</sub><sup>-</sup>; 9b...Z=C<sub>7</sub>H<sub>15</sub>O<sup>-</sup>; 9c...Z=C<sub>8</sub>H<sub>17</sub><sup>-</sup>.

31: Z--OH, (C<sub>2</sub>H<sub>5</sub>)<sub>3</sub>N, CH<sub>2</sub>Cl<sub>2</sub>.

### 3.3.3: Scheme 3 - Compounds (9a-c).

#### 3.3.3.1: (S)-(-)-4-n-heptyl-, -heptoxy- and -octoxy-phenyl 3-chloro-4-(2-methylbutoxy) benzoates (9a-c).

The preparation of compounds (9a-c) was achieved by an esterification procedure similar to that described in step 2.3, using the acid chloride of 3-chloro-4-[(S)-(-)-2-methylbutyloxy] benzoic acid and either 4-heptyl-, 4-heptoxy-, or 4-octyl-phenol as starting materials. Purification was also carried out as outlined in step 2.3. Compounds (9a, c) were obtained as viscous colourless liquids and would not crystallise even when cooled for long periods of time at 0°C. The melting points given below for compounds (9a, c) were determined by D.S.C. Recrystallisation from ethanol afforded compound (9b) as a crystalline solid.

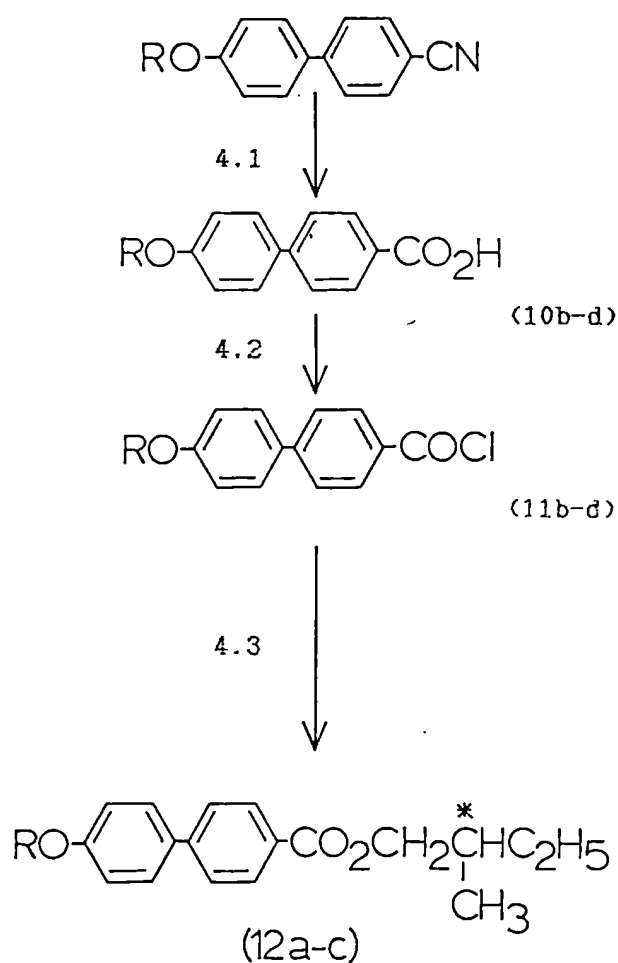
The ir and <sup>1</sup>Hnmr data for compounds (9a-c) is exemplified by the data given below for the heptyl homologue (9a). None of the above compounds exhibited liquid crystal behaviour. More physical data for compounds (9a-c) are presented in Table III, page 54.

9a: The yield was 2.2g (55%); mp. -14°C ; M/Z 416 (M<sup>+</sup>) ; purity (hplc) >99.9% (Solvent II); ir. 1735, 1270, 1235, 1080, 890, 855 cm<sup>-1</sup>; <sup>1</sup>Hnmr.  $\delta$  0.78 - 2.01 (22H, M); 2.65 (2H, T), 3.95 (2H, D) 6.86 - 8.25 (7H, M).

9b: The yield was 2.6g (64%); mp. 56.0°C; M/Z 432 (M<sup>+</sup>) ; purity (hplc) >99.9% (solvent II); ir. 1735, 1270, 1235, 1080, 890, 855 cm<sup>-1</sup>; <sup>1</sup>Hnmr.  $\delta$  0.69 - 2.20 (22H M), 3.88 (2H, D), 3.92 (2H, T), 6.72 - 8.18 (7H, M).

9c: The yield was 3.4g (82%); mp. 16.5°C M/Z 430 (M<sup>+</sup>); purity (hplc) 99.5% (solvent II).

SCHEME 4



10b,11b,12a...R=C<sub>8</sub>H<sub>17</sub>-; 10c,11c,12b...R=C<sub>9</sub>H<sub>19</sub>-; 10d,11d,12c...R=C<sub>10</sub>H<sub>21</sub>-.

41: CH<sub>3</sub>CO<sub>2</sub>H, H<sub>2</sub>SO<sub>4</sub>, H<sub>2</sub>O.

42: SOCl<sub>2</sub>.

43: HOCH<sub>2</sub>CH<sup>\*</sup>(CH<sub>3</sub>)C<sub>2</sub>H<sub>5</sub>, (C<sub>2</sub>H<sub>5</sub>)<sub>3</sub>N, CH<sub>2</sub>Cl<sub>2</sub>.

For compounds (10a) and (11a), see scheme 10.

### 3.3.4: Scheme 4 - Compounds (12a-c).

#### 3.3.4.1: 4-n-alkoxybiphenyl carboxylic acid (10b-d).

A solution of concentrated sulphuric acid (250g) in water (250 ml) was added to a stirred suspension of the 4-n-alkoxy 4'-cyanobiphenyl (0.13 mol) in glacial acetic acid (500 ml). The resulting solution was heated under reflux for 48h. The reaction mixture was then allowed to cool before the product was filtered off. Recrystallisation from glacial acetic acid afforded compounds (10b-d) as white crystalline solids.

The ir. and  $^1\text{Hnmr}$ , data for compounds (10b-d), prepared by this method are exemplified by the following data for the n-octyloxy homologue (10b) shown below.

10b: The yield was 38.7g (91%); mp.  $182^\circ\text{C}$  (lit.  $183^\circ\text{C}$ ); M/Z 326 ( $\text{M}^+$ ); ir. 3000 (broad), 1685, 1255, 940, (broad,  $850\text{ cm}^{-1}$ );  $^1\text{Hnmr}$ .  $\delta$  0.88 - 2.00 (15H, M), 12.30 (1H, br.S).

10c: The yield was 41.4g (94%); mp.  $176.0^\circ\text{C}$ , (lit.  $176^\circ\text{C}$ ); M/Z 340 ( $\text{M}^+$ ).

10d: The yield was 27.2g (59%); mp.  $170.0^\circ\text{C}$ ; M/Z 354 ( $\text{M}^+$ ).

#### 3.3.4.2: 4-n-alkoxybiphenyl-4'-ylcarboxylic acid chloride (11b-d).

The preparation of compounds (11b - d) was carried out using a similar procedure to that outlined in step 1.2, using compounds (10b - d) (0.0147 mol) as the starting material.

Compounds (11b - d) were then used immediately, without further purification in step 4.3.

3.3.4.3: (S-2-methylbutyl) 4'-n-alkoxybiphenyl-4-carboxylate (12a-c).

The preparation of compounds (12a-c) was achieved by an esterification procedure similar to that outlined in step 2.3, using compounds (11b-d) (0.0147 mol) and S-2-methylbutanol (0.016 mol) as starting materials.

Recrystallisation twice from ethanol afforded compounds (12a-c) as white crystalline solids.

The ir. and  $^1\text{Hnmr}$ , data for these compounds are exemplified by the data given below for the n-octyloxy homologue (12a).

Transition temperatures for compounds (12a-c) are given in Table IV, page 57.

12a: The yield was 3.2g (56%); mp. 48.5°C; M/Z 396 ( $\text{M}^+$ );  $[\alpha]_{\text{D}}^{20} - 2.7^\circ$ ; purity (hplc) 99.5% (solvent II); ir. 1720, 1255, 1110, 835  $\text{cm}^{-1}$ ;  $^1\text{Hnmr}$ .  $\delta$  0.74 - 2.08 (26H, M), 3.95 (2H, T), 4.14 (2H, D), 6.80 - 8.14 (8H, M).

12b: The yield was 0.9g (13%); mp. 60.1°C; M/Z 410 ( $\text{M}^+$ );  $[\alpha]_{\text{D}}^{20} + 3.6^\circ$ ; purity (hplc) 99.5% (solvent II).

12c: The yield was 1.7g (28%); mp. 48.5°C; M/Z 424 ( $\text{M}^+$ );  $[\alpha]_{\text{D}}^{20} - 2.3^\circ$ ; purity (hplc) 99% (solvent II).



### 3.3.5: Scheme 5 - Compounds (16a-d).

#### 3.3.5.1: S-(-)-propan-2,3-diol (13).

A solution of S-(-)-ethyl lactate (93.7g, 0.8 mol) in dry ether (30 ml) was added dropwise to a stirred mixture of lithium aluminium hydride (0.66 mol) in sodium dried ether (1000 ml). The reaction mixture was then gently heated under reflux for 24h. The unreacted lithium aluminium hydride was decomposed by the cautious addition of ethyl acetate (20 ml) and the diol released from the corresponding lithium aluminium salt by the addition of 10% w/v aqueous sodium hydroxide (200 ml). The ether layer was separated and any remaining product in the aqueous phase extracted by continuous ether extraction for 24h. The organic layers were combined, washed with water and dried (MgSO<sub>4</sub>). The crude product was purified by distillation to afford the S-propan-2,3-diol as a colourless liquid, 14.7g (25%); bp. 87° - 90° C; M/Z 76 (M<sup>+</sup>); [ $\alpha$ ]<sub>D</sub><sup>20</sup> + 25.5°; ir. 3350 (v. broad), 2970, 1075, 1045 cm<sup>-1</sup>; <sup>1</sup>Hnmr.  $\delta$  (3H, D), 3.45 (2H, D), 3.55 - 4.00 (1H, M), 4.33 (2H, S).

#### 3.3.5.2: R-(-)-ethyl-2-chloropropanoate (14).

Thionyl chloride (125g, 1.05 mol) and ethyl lactate (118g, 1.0 mol) were gently heated under reflux for 6h, all moisture being excluded. After removing the excess thionyl chloride, the product was then distilled from the reaction mixture to give compound (14) as a colourless liquid, 97g (71%); bp. 144° - 146° C; M/Z 136 (M<sup>+</sup>); [ $\alpha$ ]<sub>D</sub><sup>20</sup> + 19.3°; ir. 2990, 1745 cm<sup>-1</sup>; <sup>1</sup>Hnmr. 1.30 (3H, T), 1.68 (3H, D), 4.18 (2H, Q), 4.25 (1H, Q).

### 3.3.5.3: R(-)-2-chloropropanol (15).

A solution of compound (14) (40g, 0.29 mol) in sodium dried ether (20 ml) was added dropwise to a stirred mixture of lithium aluminium hydride (5.9g, 0.155 mol) in sodium dried ether (400 ml) at 0°C. The reaction mixture was stirred at this temperature for 2h, before water was added cautiously, to decompose any unreacted lithium aluminium hydride. Separation of the ether layer from the resulting emulsion was obtained by the addition of dilute sulphuric acid (50 ml). Any remaining product in the aqueous phase was extracted by continuous ether extraction for 24h. The organic layers were then combined, washed with water and dried (MgSO<sub>4</sub>). The crude product was purified by distillation to afford the S(-)-2-chloropropanol as a colourless liquid, 15.2g (55%); bp. 130°C (lit. 133 - 134°C); M/Z 94 (M<sup>+</sup>); [α]<sub>D</sub><sup>20</sup> - 16.2°; ir. 3450, (broad), 2980, 1280, 1035 cm<sup>-1</sup>; <sup>1</sup>Hnmr. δ 1.32 (3H, D), 2.82 (1H, S), 3.70 (2H, D), 3.80 - 4.44 (1H, M).

### 3.3.5.4: (R(-)-2-chloropropyl) 4-n-alkoxybiphenyl-4'-carboxylates (16a-c).

Compounds (16a - c) were prepared using a similar procedure to that outlined in Step 2.3, using compounds (11b - d) (0.009 mol) as starting materials.

The ir. and <sup>1</sup>Hnmr. data for compounds (16a - c) are exemplified by the respective data given below for the octyloxy homologue. Transition temperatures for these compounds appear in Table V, page 59.

16a: 2.3g (64%), mp. 77.5°C, M/Z 402 ( $M^+$ ),  $[\alpha]_D^{20}$  - 8.8°, purity (hplc) 99.5% (solvent II); ir. 1725, 1605, 1255, 835  $\text{cm}^{-1}$ ,  $^1\text{Hnmr}$ .  $\delta$  0.12 - 1.96 (18H, M), 3.94 (2H, T), 4.22 - 4.52 (3H, M), 6.80 - 8.16 (8H, M), 3.94 (2H, T), 4.22 - 4.52 (3H, M), 6.80 - 8.16 (8H, M).

16b: 2.2g (59%), mp. 84.0°C M/Z 416 ( $M^+$ ),  $[\alpha]_D^{20}$  - 8.6°, purity (hplc) 99.5% (solvent II).

16c: 1.6g (41%), mp. 82.5°C, M/Z 430 ( $M^+$ ),  $[\alpha]_D^{20}$  - 12.6°C, purity (hplc) 99.5% (solvent II).

3.3.5.5: (S-(-)-2-hydroxypropyl) 4-n-octyloxybiphenyl-4'-carboxylate (16d).

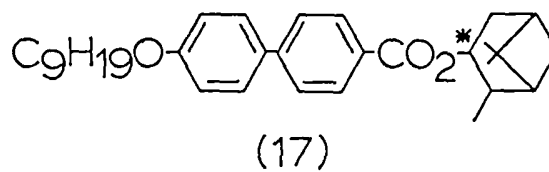
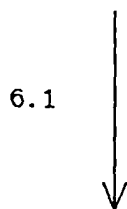
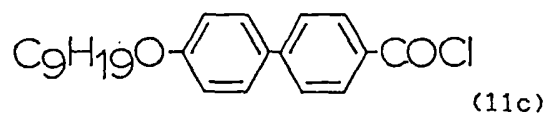
A solution of compound (11b) (3g, 0.009 mol) in dry tetrahydrofuran (20 ml) was added dropwise to a stirred solution of compound (13) (7g, 0.09 mol) in dry triethylamine (5 ml) and dry tetrahydrofuran (25 ml) at - 78°C. The reaction mixture was allowed to warm to room temperature and stirred for 48h. The solution was poured onto ice-cold water (200 ml) and the precipitated ester was filtered off and dried under reduced pressure. The crude product was purified by column chromatography (60 - 120  $\mu\text{m}$ , 200g) using chloroform as eluant.

Recrystallisation from 1 : 1 mixtures of ethanol : methanol and ethanol : petroleum fraction (bp. 60° - 80° C) gave compound (16d) as a white crystalline solid, 0.7g (20%); mp. 119.5°C; M/Z 384 ( $M^+$ );  $[\alpha]_D^{20}$  + 9.4°; purity (hplc) 99.5% (solvent II); ir. 3520 (broad, 1700, 1255, 1060, 835  $\text{cm}^{-1}$ ;

<sup>1</sup>Hnmr. δ 0.70 - 2.25 (18H, M), 2.45 (1H S), 1.66 (2H. T),  
3.33 - 3.68 (3H, M), 7.24 - 8.58 (8H, M).

The transition temperatures for compound (16d) are given  
in Table VI, page 61.

SCHEME 6



6:1: HO\*, (C<sub>2</sub>H<sub>5</sub>)<sub>3</sub>N, CH<sub>2</sub>Cl<sub>2</sub>.

3.3.6: Scheme 6 - Compound (17).

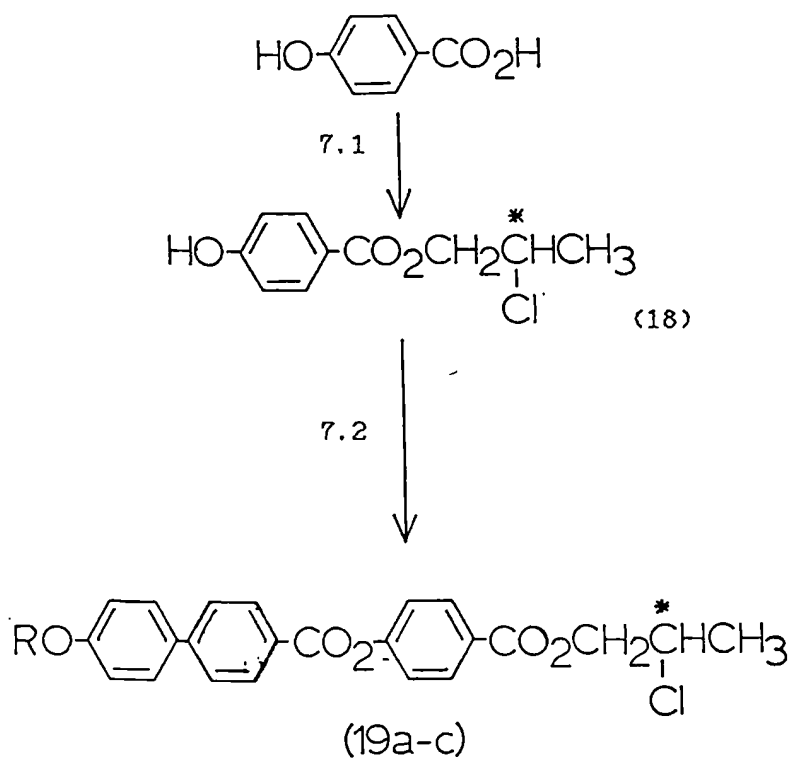
3.3.6.1: ((-)-isopinocampheyl) 4-n-nonyloxybiphenyl-4-carboxylate (17).

A solution of compound (11c) (0.007 mol) in dry dichloromethane (10 ml) was added dropwise to a stirred solution of (-)-isopinocampheyl (1.2g. 0.0077 mol) in dry triethylamine (3 ml) and dry dichloromethane (10 ml) at 0°C. After the addition of the acid chloride was completed, the reaction mixture was stirred at room temperature for 16h.

The reaction mixture was then poured onto ice-cold dilute hydrochloric acid (100 ml) and the product extracted into chloroform (200 ml). The organic layer was washed with water (2 x 200 ml) and dried (MgSO<sub>4</sub>).

The crude product was purified by column chromatography and recrystallisation via a similar method to that outlined for the purification of compounds (8a-d) in Step 2.3, to afford compound (17) as a white crystalline solid, 0.7g (21%); mp. 67.5°C; M/Z 476 (M<sup>+</sup>); purity (hplc) 99.5% (solvent II); ir. 1715, 1605, 1250, 1045, 830 cm<sup>-1</sup>; <sup>1</sup>Hnmr. δ 1.80 - 2.52 (33H, M), 3.95 (2H, T), 5.10 - 5.50 (1H, M), 6.86 - 8.24 (8H, M). The transition temperatures for compound (17) are given in Table VI, Page 61.

SCHEME 7



19a...R=C<sub>8</sub>H<sub>17</sub>-; 19b...R=C<sub>9</sub>H<sub>19</sub>-; 19c...R=C<sub>11</sub>H<sub>23</sub>-.

71: HOCH<sub>2</sub>CH<sup>\*</sup>(Cl)CH<sub>3</sub>, H<sub>2</sub>SO<sub>4</sub>.

72: Compounds (11b,c,e), (C<sub>2</sub>H<sub>5</sub>)<sub>3</sub>N, CH<sub>2</sub>Cl<sub>2</sub>.

For compound (11e), see scheme 10.

### 3.3.7: Scheme 7 - Compounds (19a-c).

#### 3.3.7.1: (R-(-)-2-chloropropyl) 4-hydroxybenzoate (18).

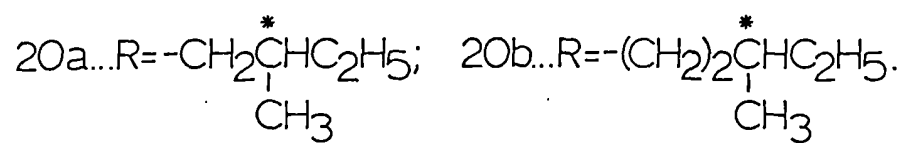
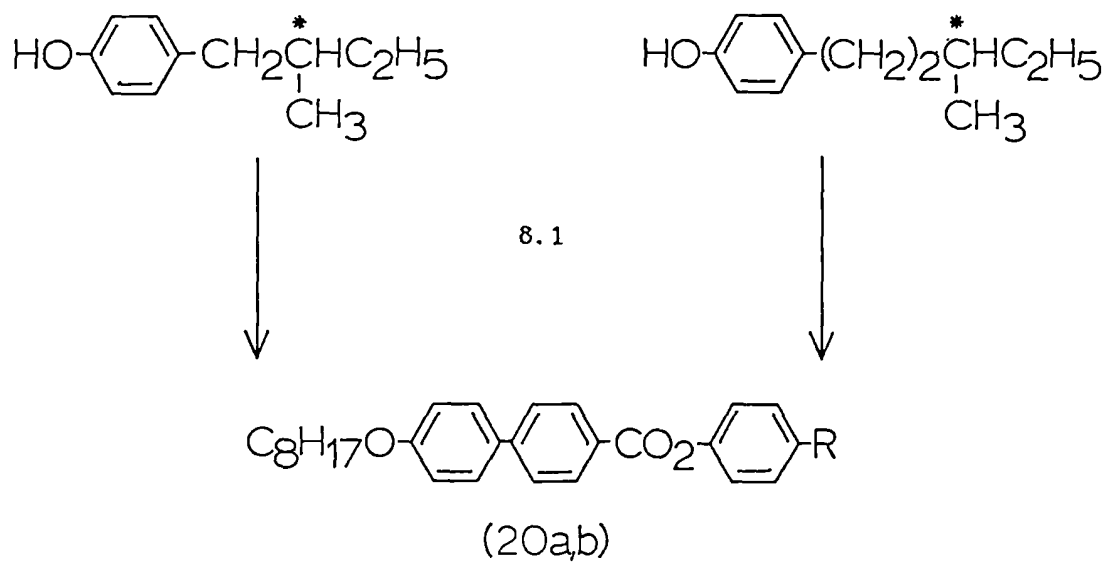
Preparation of compound (18) was carried out using a similar procedure to that described in Step 2.2, using 4-hydroxybenzoic acid (10g 0.072 mol) and S-(-)-2-chloropropanol (18.7g, 0.198 mol) as starting materials. Distillation under reduced pressure produced a yellow oil which solidified on cooling. Recrystallisation from a 2 : 1 mixture of toluene : petroleum fraction (bp. 80° - 100° C) afforded compound (18) as a white crystalline solid, 5.0g (33%); mp. 85.0° C; M/Z 214 (M<sup>+</sup>); ir. 3390, 1690, 1310, 1170, 850 cm<sup>-1</sup>; <sup>1</sup>Hnmr. δ 1.33 - 1.66 (3H, M), 3.61 (1H, D), 4.19 - 4.56 (2H, M), 6.33 (1H, br.S), 6.70 - 8.33 (4H, M).

#### 3.3.7.2: R-(-)-2-chloropropyl 4-(4'-n-alkoxybiphenyl-4-yl) carboxybenzoate (19a-c).

Preparation of compounds (19a - c) was carried out using a similar esterification procedure to that described in Step 2.3, using compounds (11b, c, e) (0.0047 mol) and compound (18) as the starting materials. The diesters were purified by column chromatography on silica gel, using chloroform as eluant. Recrystallisation from petroleum fraction (bp. 60° - 80° C), ethanol, and then ethyl acetate afforded compounds (19a - c) as white crystalline solids. The ir. and <sup>1</sup>Hnmr. data for compounds (19a - c) are exemplified by the data given below for the n - octyloxy homologue (19a). Transition temperatures for these compounds are given in Table VIII, page 65.

- 19a: The yield was 0.42g (17%); mp. 95.0° C; M/Z 522 (M<sup>+</sup>); [α]<sub>D</sub><sup>20</sup> + 0.8°; purity (hplc) 99.0% (solvent II); ir. 1735, 1720, 1250, 1075, 830 cm<sup>-1</sup>; <sup>1</sup>Hnmr. δ 0.67 - 2.13 (18H, M), 3.70 (2H, D), 4.00 (2H, T), 4.42 (1H, M), 6.90 - 8.33 (12H, M).
- 19b: The yield was 0.8g (32%); mp. 88.0° c; M/Z 536 (M<sup>+</sup>); [α]<sub>D</sub><sup>20</sup> + 2.3°; purity (hplc) 99.0% (solvent I).
- 19c: The yield was 0.29g (11%); mp. 92.0° C; M/Z 564 (M<sup>+</sup>); [α]<sub>D</sub><sup>20</sup> -9.2°; purity (hplc); 99.5% (solvent II).

SCHEME 8



81: Compound (11b),  $(\text{C}_2\text{H}_5)_3\text{N}$ ,  $\text{CH}_2\text{Cl}_2$ .

3.3.8: Scheme 8 - Compounds (20a,b).

3.3.8.1: (S)-(-)-4-(2-methylbutylphenyl) and (S)-(-)-4-(3-methylpentylphenyl) 4-n-octyloxybiphenyl-4'-carboxylate (20a, b).

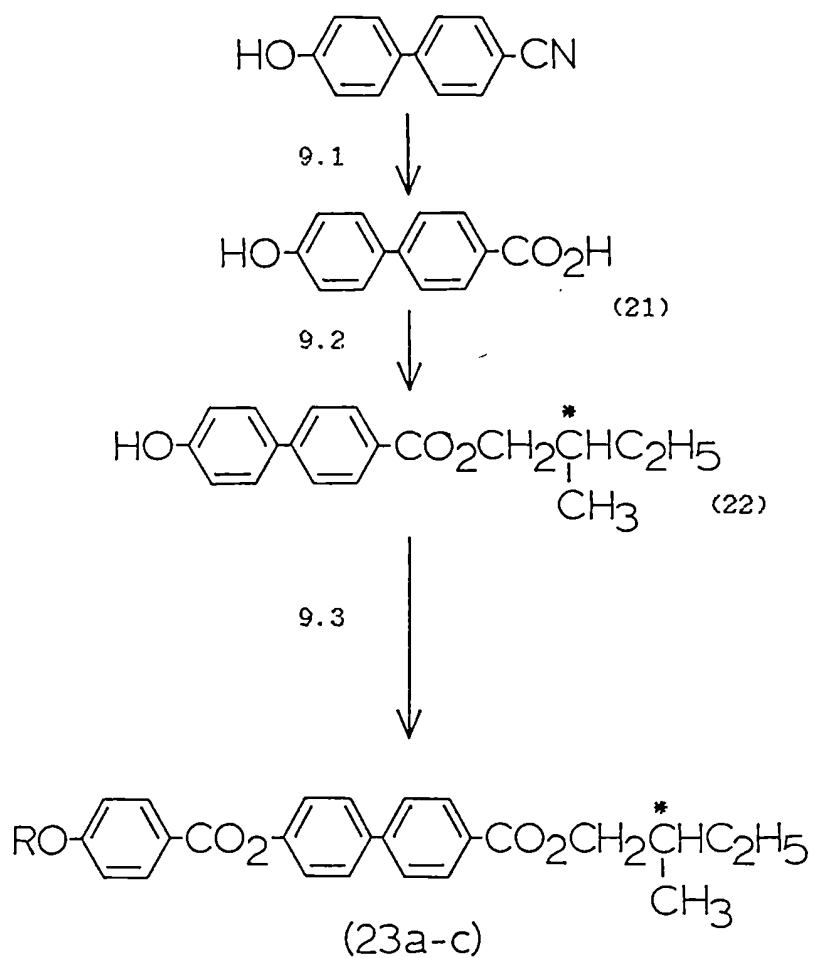
Preparation of compounds (20a, b) was carried out using an esterification procedure similar to that outlined in Step 2.3, using compound (11b) (0.003 mol) with either 4-(S-2-methylbutyl) phenol (0.0033 mol) or 4-(S-3-methylpentyl) phenol (0.0033 mol) as starting materials, to yield compounds (20a, b) as white crystalline solids.

The ir. and <sup>1</sup>Hnmr. data for compounds (20a, b) are exemplified by the data given below for compound (20a). The transition temperatures for these compounds are given in Table IX, page 67.

20a: The yield was 0.45g (32%); mp. 81.0° C; M/Z 472 (M<sup>+</sup>); [α]<sub>D</sub><sup>20</sup> + 5.3°; purity (hplc) >99.9% (solvent I); ir. 1730, 1255, 1070, 830 cm<sup>-1</sup>; <sup>1</sup>Hnmr. δ 0.73 - 1.90 (24H, M), 2.50 (2H, T), 3.95 (2H, T), 6.83 - 8.26 (12H, M).

20b: The yield was 0.58g (40%); mp. 835° C; M/Z 486 (M<sup>+</sup>); [α]<sub>D</sub><sup>20</sup> + 7.0°; purity (hplc) >99.9% (solvent I).

SCHEME 9



23a...R=C<sub>7</sub>H<sub>15</sub>-; 23b...R=C<sub>8</sub>H<sub>17</sub>-; 23c...R=C<sub>9</sub>H<sub>19</sub>-.

91: CH<sub>3</sub>CO<sub>2</sub>H, H<sub>2</sub>SO<sub>4</sub>, H<sub>2</sub>O.

92: HOCH<sub>2</sub>CH<sup>\*</sup>(CH<sub>3</sub>)C<sub>2</sub>H<sub>5</sub>, H<sub>2</sub>SO<sub>4</sub>.

93: Compounds (6b-d), (C<sub>2</sub>H<sub>5</sub>)<sub>3</sub>N, CH<sub>2</sub>Cl<sub>2</sub>.

3.3.9: Scheme 9 - Compounds (23a-c).

3.3.9.1: 4-Hydroxybiphenyl-4'-carboxylic acid (21).

Preparation of compound (21) was carried out using a similar procedure to that outlined in Step 4.1, using 4-hydroxy 4'-cyanobiphenyl (10g, 0.05 mol) as starting material. Recrystallisation from ethyl acetate and then from glacial acetic acid afforded compound (21) as a white crystalline solid, 5.7g (53%), mp. 304.0°C M/Z 214 (M<sup>+</sup>), ir. 3000 (v. broad), 1680, 1195, 930 (broad), 830 cm<sup>-1</sup>, <sup>1</sup>Hnmr. δ 6.00 - 8.17 (10H, M, 2H D<sub>2</sub>O exchanged).

3.3.9.2: (S-(-)-2-methylbutyl) 4-hydroxybiphenyl-4'-carboxylate (22).

Preparation of compound (22) was carried out using a similar procedure to that outlined in Step 2.2, using compound (21) (3g, 0.014 mol) and S-(-)-2-methylbutanol (50 ml) as the starting materials. Recrystallisation from ethyl acetate afforded compound (22) as a white crystalline solid, 2.6g (64%); mp. 113.0°C; M/Z 284 (M<sup>+</sup>); ir. 3400, 1680, 1315, 1190, 835 cm<sup>-1</sup>; <sup>1</sup>Hnmr. δ 0.67 - 2.17 (9H, M), 4.17 (2H, D), 5.33 (1H, S), 6.73 - 8.10 (8H, M).

3.3.9.3: (S-(-)-2-methylbutyl) 4'-(4-n-alkoxyphenyl-1-carboxy) biphenyl-4-carboxylates (23a-c).

Preparation of compounds (23a - c) was carried out using an esterification procedure similar to that outlined in Step 2.3, using compounds (6b - d) (0.0038 mol) and compound (22) (0.0035 mol) as starting materials. The ir and <sup>1</sup>Hnmr data for compounds (23a - c) are exemplified by the data given

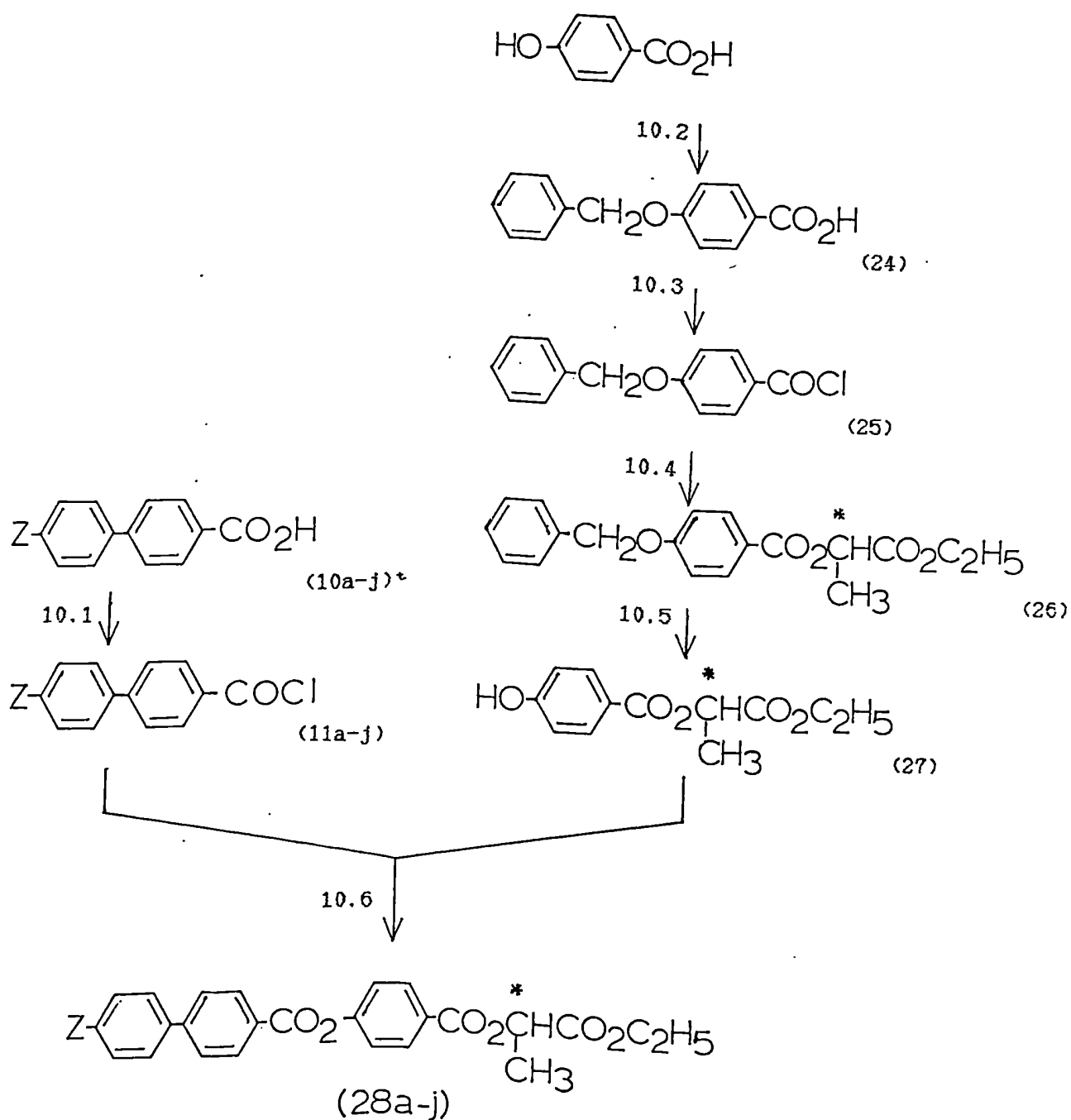
below for the heptyloxy homologue (23a). Transition temperatures for these compounds are given in Table X, page 69.

23a: The yield was 1.52g (84%); mp. 67.5° C; M/Z 502 (M<sup>+</sup>); [α]<sub>D</sub><sup>20</sup> + 3.5°; purity (hplc) >99.9% (solvent I); ir. 1720, 1710, 1260, 1075, 845 cm<sup>-1</sup>; <sup>1</sup>Hnmr. δ 0.50 - 2.26 (22H, M), 4.03 (2H, T), 4.20 (2H, D), 6.10 - 8.33 (12H; M).

23b: The yield was 1.65g (91%); mp. 84.0° C; M/Z 516 (M<sup>+</sup>); [α]<sub>D</sub><sup>20</sup> + 3.6°; purity (hplc) >99.9% (solvent I).

23c: The yield was 1.5g (85%); mp. 83.5° C; M/Z 530 (M<sup>+</sup>); [α]<sub>D</sub><sup>20</sup> + 3.0°; purity (hplc) >99.9% (solvent I).

SCHEME 10



\* - Apart from compounds (10b-d) synthesised earlier, the remaining 4'-alkyl and alkyloxybiphenyl-4-carboxylic acids used here, were supplied by BDH Ltd, Poole, Dorset.

## SCHEME 10

11a,28a... Z = C<sub>7</sub>H<sub>15</sub>O<sup>-</sup>;

11f,28f... Z = C<sub>8</sub>H<sub>17</sub><sup>-</sup>;

11b,28b... Z = C<sub>8</sub>H<sub>17</sub>O<sup>-</sup>;

11g,28g... Z = C<sub>9</sub>H<sub>19</sub><sup>-</sup>;

11c,28c... Z = C<sub>9</sub>H<sub>19</sub>O<sup>-</sup>;

11h,28h... Z = C<sub>10</sub>H<sub>21</sub><sup>-</sup>;

11d,28d... Z = C<sub>10</sub>H<sub>21</sub>O<sup>-</sup>;

11i,28i... Z = C<sub>11</sub>H<sub>23</sub><sup>-</sup>;

11e,28e... Z = C<sub>11</sub>H<sub>23</sub>O<sup>-</sup>;

11j,28j... Z = C<sub>12</sub>H<sub>25</sub><sup>-</sup>.

10·1: (COCl)<sub>2</sub>, DMF, C<sub>6</sub>H<sub>6</sub>.

10·2: (i) PhCH<sub>2</sub>Br, 40% aq NaOH, C<sub>2</sub>H<sub>5</sub>OH; (ii) 10% aq NaOH.

10·3: (COCl)<sub>2</sub>, DMF, C<sub>6</sub>H<sub>6</sub>.

10·4: HOCH(CH<sub>3</sub>)<sup>\*</sup>CO<sub>2</sub>C<sub>2</sub>H<sub>5</sub>, (C<sub>2</sub>H<sub>5</sub>)<sub>3</sub>N, CH<sub>2</sub>Cl<sub>2</sub>.

10·5: Pd/C (5%), C<sub>2</sub>H<sub>5</sub>OH.

10·6: (C<sub>2</sub>H<sub>5</sub>)<sub>3</sub>N, CH<sub>2</sub>Cl<sub>2</sub>.

### 3.3.10: Scheme 10 - Compounds (28a-j).

#### 3.3.10.1: 4-n-alkoxy-, 4-n-alkylbiphenyl-4'-carboxylic acid chloride (11a-j).

Oxalyl chloride (0.01 mol) and dry dimethylformamide (one drop) were added to the appropriate 4-n-alkyl-and-alkoxy-biphenyl-4-yl carboxylic acid (supplied by BDH. Ltd., Poole, Dorset), (0.005 mol) in dry benzene (20 ml), and the resulting reaction mixture was then stirred at room temperature for 3h. The solvent and excess oxalyl chloride were removed by distillation under reduced pressure. The residue was then used immediately, without further purification in Step 10.6.

#### 3.3.10.2: 4-benzyloxybenzoic acid (24).

Benzyl bromide (65g, 0.38 mol) was added dropwise to a stirred solution of 4-hydroxybenzoic acid (50g, 0.36 mol) in 40% w/v aqueous sodium hydroxide solution (70 ml) and 95% ethanol (150 ml) at reflux. The reaction mixture was heated under reflux for 16h. Aqueous sodium hydroxide (10% w/v, 200 ml) was then added to ensure saponification of any ester products formed, and the reaction mixture heated under reflux for a further 2h. The reaction mixture was poured onto crushed ice (200g) before concentrated hydrochloric acid was added dropwise, whilst stirring, until the reaction mixture was acidic to litmus. The reaction mixture was then stirred for 10 mins to ensure complete conversion of the sodium salt to the corresponding carboxylic acid. The product was extracted into ethyl acetate (2 x 200 ml), washed with water (2 x 200 ml) and dried (MgSO<sub>4</sub>). Recrystallisation

from ethanol gave compound (24) as a white crystalline solid, 54g (65%); mp. 193.0° C; M/Z 228 (M<sup>+</sup>); ir. 3000 (v. broad), 1680, 1605, 1255, 850, 740, 695 cm<sup>-1</sup>; <sup>1</sup>Hnmr. δ 5.22 (2H, S), 6.96 - 8.38 (9H, M), 9.80 (1H, br. S, D<sub>2</sub>O exchanged).

### 3.3.10.3: 4-benzyloxybenzoic acid chloride (25).

Preparation of compound (25) was carried out using a similar procedure to that outlined in Step 10.5, with compound (25) (13g, 0.057 mol) as the starting material and the reaction carried out at 40° C. The residue was used in Step 10.3, immediately without further purification.

### 3.3.10.4: (S)-(-)-ethyl 2-(4-benzyloxyphenyl carboxy) propanoate (26).

Compound (25) (0.057 mol) was dissolved in dry dichloromethane (50 ml) and added dropwise to a stirring solution of (S)-(-)-ethyl lactate (8.1g. 0.07 mol) in dry triethylamine (10 ml) and dry dichloromethane (50 ml) at 40° C. After the addition of the acid chloride was completed, the reaction mixture was stirred at 40° C for 5h.

The reaction mixture was then poured onto cold dilute hydrochloric acid (100 ml) and the product extracted into chloroform (100 ml). The combined organic layers were washed with water (2 x 100 ml) and dried (MgSO<sub>4</sub>). Recrystallisation from petroleum fraction (bp. 80° - 100° C) yielded compound (26) as a white crystalline solid, 12g (65%); mp. 78.0° C; M/Z 328 (M<sup>+</sup>); [α]<sub>D</sub><sup>20</sup> + 23.6°; ir. 1755, 1715, 1270, 850, 740, 700 cm<sup>-1</sup>; <sup>1</sup>Hnmr. δ 1.33 (3H, T), 1.70 (3H, D), 4.45 (2H, Q), 5.27 (2H, S), 5.45 (1H, Q), 7.10 - 8.45 (9H, M).

3.3.10.5: (S)-(-)-ethyl 2-(4-hydroxyphenyl carboxy)  
propanoate (27).

A mixture of compound (26) (10g, 0.032 mol) and 5% palladium on carbon (1.4g) in ethanol (750 ml) was stirred under an atmosphere of hydrogen until the correct uptake of hydrogen had been achieved (ca 16 hr.). The palladium on carbon was filtered off and the ethanol was removed from the filtrate by distillation under reduced pressure. The residue was then distilled under reduced pressure to give compound (27) as a yellow oil, 7.4g (97%); bp. 165° C / 0.02 mmHg: M/Z 238 (M<sup>+</sup>);  $[\alpha]_D^{20} + 27.8^\circ$ ; ir. 3400 (broad, 1720, 1690, 1220, 855 cm<sup>-1</sup>; <sup>1</sup>Hnmr.  $\delta$  1.31 (3H, T), 1.76 (3H, D), 4.31 (2H, Q), 5.37 (1H, Q), 6.60 - 8.32 (4H, M), 7.89 [1H, S (D<sub>2</sub>O exchanged).]

3.3.10.6: (S)-(-)-ethyl 2-[4-(4-n-alkoxy-, and -  
alkylbiphenyl-4-ylcarboxy) benzyloxy] propanoate  
(28a-j).

Compounds (11a - j) (0.005 mol) were dissolved in dry dichloromethane (10 ml) and added dropwise to a stirring solution of compound (27) (0.005 mol) in dry triethylamine (1 ml) and dry dichloromethane (10 ml) at 0° C. After the addition of the acid chloride was completed, the reaction mixture was stirred at room temperature for 16h. The reaction mixture was then poured onto ice-cold dilute hydrochloric acid (100 ml) and the product extracted into chloroform (100 ml). The combined organic layers were washed with water (2 x 100 ml) and dried (MgSO<sub>4</sub>). The crude product was purified by flash column chromatography using solvent (B)

as eluant. Recrystallisation alternately from petroleum fraction (bp. 60° - 80° C) and ethanol afforded compounds (28a - j) as white crystalline solids. The ir. and <sup>1</sup>Hnmr. data for compounds where Z = alkoxy (28a-e) and where Z = alkyl (28f-j) are exemplified by the data given below for the heptoxy (28a) and octyl (28f) homologues respectively. The transition temperatures for all the above compounds appear in Table XI, page 75, and the yield, % yield, mp, M/Z value,  $[\alpha]_D^{20}$  value and purity for compounds (28a - j) are tabulated below.

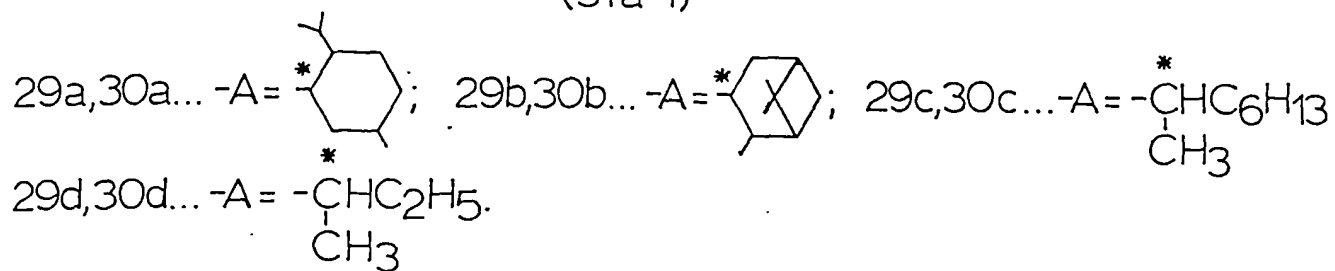
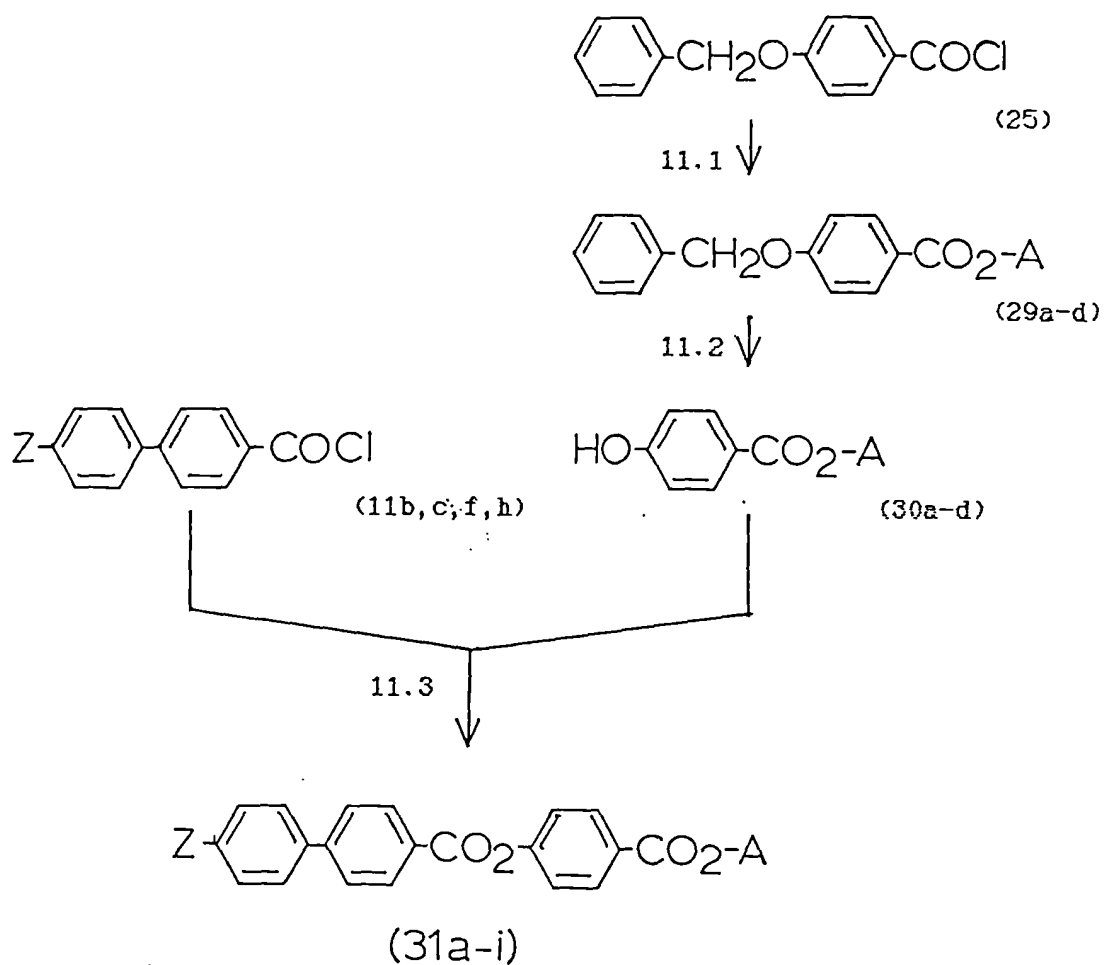
28a: ir. 1765, 1735, 1725, 1275, 830 cm<sup>-1</sup>; <sup>1</sup>Hnmr. δ  
0.64 - 2.04 (19H, M), 3.97 (2H, T), 4.22 (2H,  
Q), 5.30 (1H, Q), 6.84 - 8.38 (12H, M).

28f: ir. 1750, 1735, 1720, 1270, 820 cm<sup>-1</sup>; <sup>1</sup>Hnmr. δ  
0.75 - 2.32 (21H, M), 2.80 (2H, T), 4.38 (2H,  
Q), 5.56 (1H, Q), 7.40 - 8.64 (12H, M).

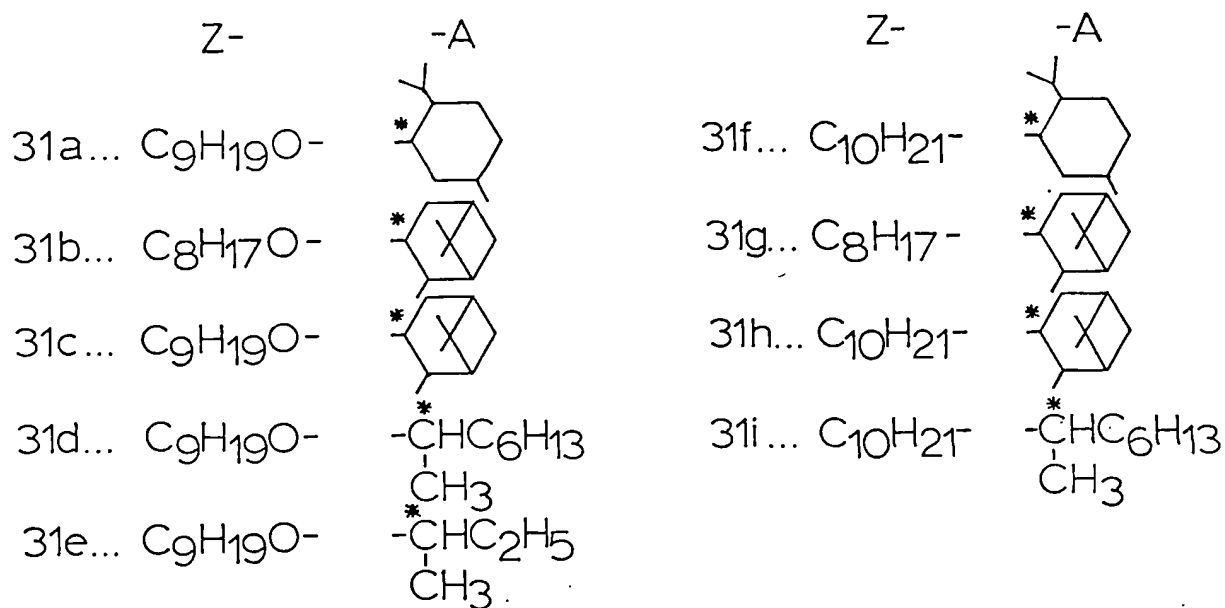
yield /g(%)	mp. /° C	M/Z (M <sup>+</sup> )	[α] <sub>D</sub> <sup>20</sup> /°	purity /% *
28a: 2.0 76	90.0	532	+18.8	>99.9
28b: 1.0 38	75.0	546	+17.5	>99.9
28c: 1.7 61	60.0	560	+15.0	>99.9
28d: 1.8 62	60.5	574	+16.5	>99.9
28e: 1.4 48	65.0	588	+11.5	>99.9
28f: 1.2 45	49.0	530	+18.4	>99.5
28g: 0.6 22	48.5	544	+17.5	>99.9
28h: 1.1 38	57.0	558	+18.5	>99.9
28i: 1.4 48	53.0	572	+14.6	>99.5
28j: 0.7 23	44.0	586	+15.6	>99.9

\* The purity of these compounds was checked by hplc using solvent (I) for compounds (28a-d,f,g and h) and solvent (II) for compounds (28e,i and j).

SCHEME 11



SCHEME 11



11:1: HO-A,  $(C_2H_5)_3N$ ,  $CH_2Cl_2$ .

11:2: Pd/C (5%),  $C_2H_5OH$ .

11:3:  $(C_2H_5)_3N$ ,  $CH_2Cl_2$ .

### 3.3.11: Scheme 11 - Compounds (31a-i).

#### 3.3.11.1: Compounds (29a-d)

Preparation of compounds (29a - d) was carried out using a similar procedure to that outlined in Step 10.3, using compound (25) and the appropriate alcohol as starting materials, in the molar ratio of 1.5 : 1.0 respectively. The reaction was carried out at room temperature.

Compounds (29a - d) were found to be viscous liquids or waxy solids, and were used in Step 11.2 without further purification. The ir. and  $^1\text{Hnmr}$ . data for these materials are exemplified by the following data given below for compound (29a).

29a: The yield was 3.1g (64%); M/Z 366 ( $\text{M}^+$ ) ir. 1710, 1250, 845, 770, 695  $\text{cm}^{-1}$ ;  $^1\text{Hnmr}$ .  $\delta$  0.72 - 2.38 (18H, M), 4.64 - 5.00 (1H, M), 6.86 - 8.12 (9H, M).

29b: The yield was 3.5g (44%); M/Z 364 ( $\text{M}^+$ );  $[\alpha]_{\text{D}}^{20}$  - 29.4°.

29c: The yield was 2.8g (38%); M/Z 340 ( $\text{M}^+$ );  $[\alpha]_{\text{D}}^{20}$  - 33.2°.

29d: The yield was 0.8g (21%); M/Z 284 ( $\text{M}^+$ ).

#### 3.3.11.2: Compounds (30a-d).

Preparation of compounds (30a - d) was carried out using a similar procedure to that outlined in Step 10.4, using compounds (29a - d) (0.007 mol), as starting materials.

Compound (30b) was recrystallised from toluene to give a white crystalline solid. Compounds (30a,c,d) were purified by distillation under reduced pressure to give colourless viscous liquids. The ir. and  $^1\text{Hnmr}$ . data for compounds (30a-d) are exemplified by the following data given below for (30a).

30a: The yield was 1.4g (75%); bp.  $160^\circ\text{C}/0.05\text{mmHg}$ ;  $M/Z$  276 ( $M^+$ );  $[\alpha]_D^{20} - 78.3^\circ$ ; ir. 3350 (broad) 1710, 1165, 850  $\text{cm}^{-1}$ ;  $^1\text{Hnmr}$ .  $\delta$  0.68 - 2.28 (18H, M), 4.56 - 5.12 (1H, M), 6.52 - 8.15 [5H, M, (1H  $\text{D}_2\text{O}$  exchanged)].

30b: The yield was 1.8g (94%); mp.  $136.0^\circ\text{C}$ ;  $M/Z$  274 ( $M^+$ );  $[\alpha]_D^{20} - 40.2^\circ$ .

30c: The yield was 1.7g (97%); bp.  $140^\circ\text{C}/0.05\text{ mmHg}$ ;  $M/Z$  250 ( $M^+$ ).

30d: The yield was 0.4g (84%); bp.  $130^\circ\text{C}/0.05\text{ mmHg}$ ;  $M/Z$  194 ( $M^+$ ).

### 3.3.11.3: Compounds (31a-i).

Preparation of compounds (31a-i) was carried out using an esterification procedure similar to that outlined in Step 10.6 using compounds (11b,c,f,h) 0.0013 mol) and compounds (30a-d) (0.0013 mol) as starting materials. The crude products were purified by flash column chromatography using solvent (A) for compounds (31b,c,d,f); solvent (B) for compounds (31g,h,i); and solvent (C), for compounds (31a,e), as eluant.

Recrystallisation from ethanol [and then from petroleum fraction (bp. 60° - 80° C) for compounds (31a-e,g,h)] afforded compounds (31a-i) as white crystalline solids. The ir. and <sup>1</sup>Hnmr. data for compounds where Z=alkoxy (31a-e) and where Z = alkyl (31f-i) are exemplified by the following data given below for compounds (31a) and (31f) respectively. Transition temperatures for these materials appear in Table XII, page 80, and the yield, % yield, mp, M/Z value, [α]<sub>D</sub><sup>20</sup> value and the purity for compounds (31a-i) are tabulated below.

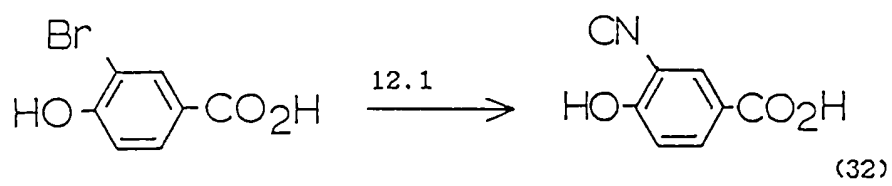
31a: ir. 1735, 1710, 1265, 1255, 825 cm<sup>-1</sup>; <sup>1</sup>Hnmr. δ 0.72 - 2.49 (35H, M), 4.06 (2H, T), 4.88 - 5.23 (1H, M), 6.95 - 8.57 (12H, M).

31f: ir. 1735, 1710, 1265, 820 cm<sup>-1</sup>; <sup>1</sup>Hnmr. δ 0.72 - 2.30 (27H, M), 2.62 (2H, T), 4.60 - 5.11 (1H, M), 7.04 - 8.21 (12H, M).

	yield/g	(%)	mp./° C	M/Z (M <sup>+</sup> )	[α] <sub>D</sub> <sup>20</sup>	purity * (%)
31a	0.50	65	108.0	598	-37.0	>99.9
31b	0.62	81	122.0	582	-21.8	>99.9
31c	0.46	60	108.0	596	-15.5	>99.5
31d	0.60	79	71.0	572	-17.6	>99.5
31e	0.37	55	71.0	516	----	>99.9
31f	0.54	70	91.5	596	-26.4	>99.9
31g	0.55	71	89.0	566	-21.4	>99.9
31h	0.55	71	89.0	594	-17.0	>99.9
31i	0.45	61	61.0	570	-20.5	>99.9

\* The purity of these compounds was checked by hplc using solvent (I) as the eluant.

SCHEME 12



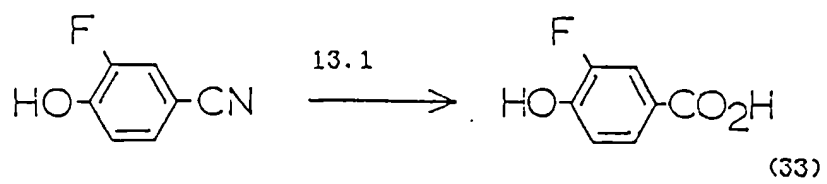
12.1: (i)  $\text{Cu}_2\text{CN}_2 \cdot (\text{H}_2\text{O})$ , NMP; (ii)  $\text{FeSO}_4 \cdot (7\text{H}_2\text{O})$ .

### 3.3.12: Scheme 12 - Compound (32).

#### 3.3.12.1: 3-cyano-4-hydroxybenzoic acid (32).

A mixture of copper (I) cyanide (8.3g, 0.092 mol) and 3-bromo-4-hydroxybenzoic acid (10g, 0.046 mol) in N-methylpyrrolidinone (50 ml) was stirred at 180° C for 3h. The reaction mixture was allowed to cool below 100° C before 1.4M aqueous ferrous sulphate (130ml) was added and the resulting suspension stirred at 100° C for ½h. The mixture was then allowed to cool to room temperature. The insoluble salts were filtered off and washed with acetone until the washings ran clear. The filtrate was basified with 20% w/v aqueous potassium carbonate (150 ml) and washed with ether (2x100ml) to remove the N-methylpyrrolidinone. Concentrated hydrochloric acid was then added to the aqueous solution until the mixture was acidic to litmus. The crude product was extracted into ether (2x200 ml), washed with water (2x200 ml) and dried (MgSO<sub>4</sub>). Purification of compound (32) proved difficult because the product was either too soluble or completely insoluble in all solvents and mixtures of solvents used. However, washing the product in a mixture of 1 : 1 toluene : ethanol and then heating it to reflux in toluene afforded compound (32) as a white powder, 3.8g (51%); mp. 255.0° C; M/Z 163 (M<sup>+</sup>); ir. 3120 (v.broad), 2230, 1685, 1410, 920 (broad), 845, 800 cm<sup>-1</sup>; <sup>1</sup>Hnmr. δ 4.90 (H, br.S), 5.32 - 6.92 (3H, M) 11.84 (H, br.S).

SCHEME 13



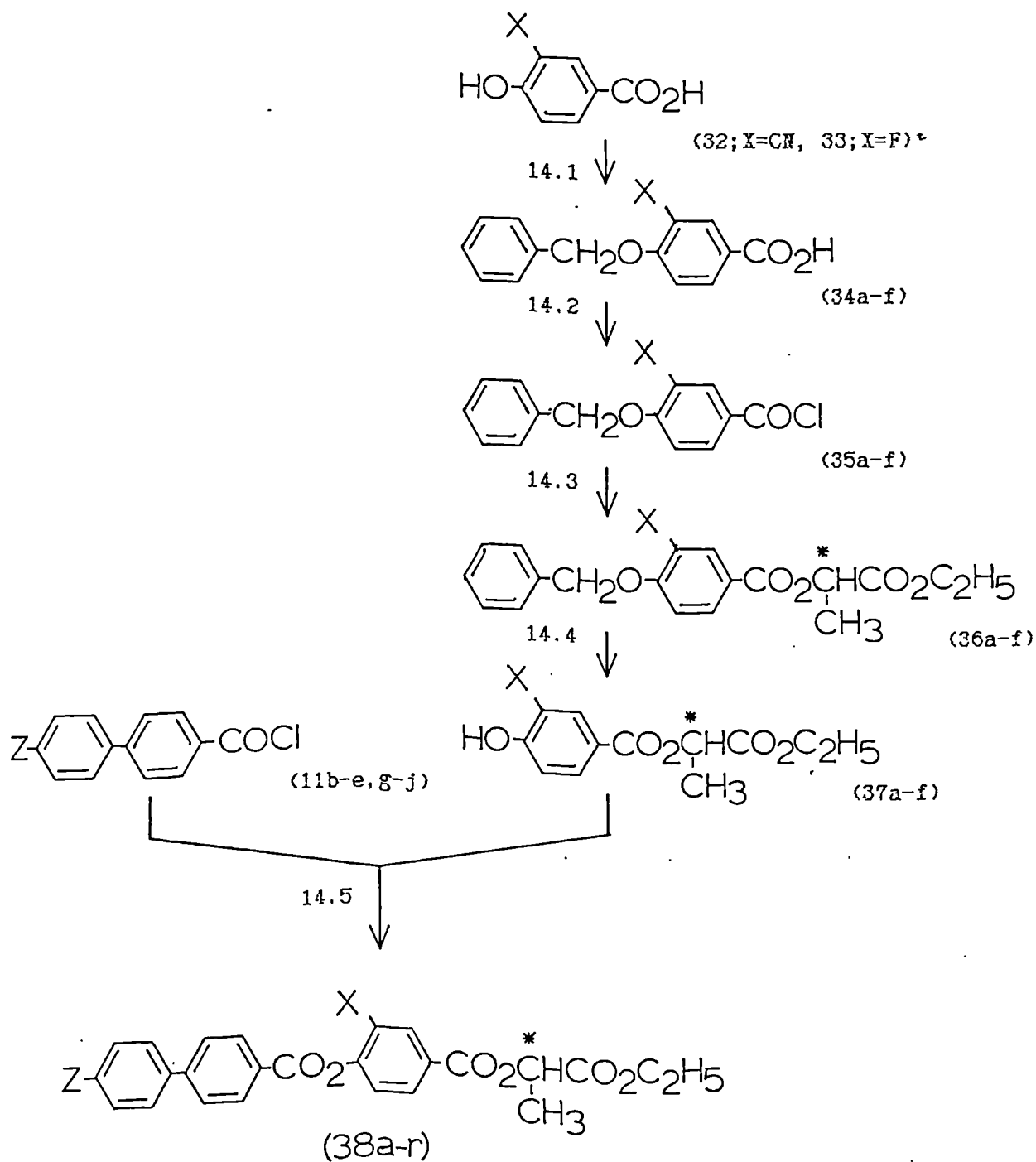
13.1: 10% aq. NaOH.

3.3.13: Scheme 13 - Compound (33).

3.3.13.1: 3-fluoro-4-hydroxybenzoic acid (33).

3-Fluoro-4-hydroxybenzonitrile (5g, 0.0365 mol) was dissolved in 10% w/v aqueous sodium hydroxide (50 ml) and the reaction mixture heated under reflux for 60h. The reaction mixture was allowed to cool, then concentrated hydrochloric acid was added until the mixture became acidic to litmus. The crude product was extracted into ether (2x50 ml) and washed with water (50 ml). Recrystallisation from water afforded 3-fluoro-4-hydroxybenzoic acid as a white crystalline solid, 4.9g (87%); mp. 162.0° C; M/Z 156 (M<sup>+</sup>); ir. 3000 (v.broad), 1680, 1605, 1200, 940, 900, 845 cm<sup>-1</sup>; <sup>1</sup>Hnmr. δ 6.40 - 8.12 [2H, br.M (D<sub>2</sub>O exchanged)], 6.60 - 6.96 (1H, M), 7.20 - 7.58 (2H, M).

SCHEME 14



\* - Also commercially available materials, X=CH<sub>3</sub>, X=OCH<sub>3</sub> and X=Cl.

## SCHEME 14

34a-37a... X=Cl;      34b-37b... X=Me;      34c-37c... X=OMe;  
 34d-37d... X=Br;      34e-37e... X=CN;      34f-37f... X=F.

	Z-	-X		Z-	-X
38a...	C <sub>8</sub> H <sub>17</sub> O-	-Cl	38j...	C <sub>9</sub> H <sub>19</sub> -	-Cl
38b...	C <sub>9</sub> H <sub>19</sub> O-	-Cl	38k...	C <sub>10</sub> H <sub>21</sub> -	-Cl
38c...	C <sub>10</sub> H <sub>21</sub> O-	-Cl	38l...	C <sub>11</sub> H <sub>23</sub> -	-Cl
38d...	C <sub>11</sub> H <sub>23</sub> O-	-Cl	38m...	C <sub>12</sub> H <sub>25</sub> -	-Cl
38e...	C <sub>9</sub> H <sub>19</sub> O-	-Me	38n...	C <sub>10</sub> H <sub>21</sub> -	-Me
38f...	C <sub>9</sub> H <sub>19</sub> O-	-OMe	38o...	C <sub>10</sub> H <sub>21</sub> -	-OMe
38g...	C <sub>9</sub> H <sub>19</sub> O-	-Br	38p...	C <sub>10</sub> H <sub>21</sub> -	-Br
38h...	C <sub>9</sub> H <sub>19</sub> O-	-CN	38q...	C <sub>10</sub> H <sub>21</sub> -	-CN
38i...	C <sub>9</sub> H <sub>19</sub> O-	-F	38r...	C <sub>10</sub> H <sub>21</sub> -	-F

## SCHEME 14

14·1: PhCH<sub>2</sub>-Br, 40% aq. NaOH, C<sub>2</sub>H<sub>5</sub>OH; 10% aq. NaOH.

14·2: (COCl)<sub>2</sub>, DMF, C<sub>6</sub>H<sub>6</sub>.

14·3: HOCH<sup>\*</sup>(CH<sub>3</sub>)CO<sub>2</sub>C<sub>2</sub>H<sub>5</sub>, (C<sub>2</sub>H<sub>5</sub>)<sub>3</sub>N, CH<sub>2</sub>Cl<sub>2</sub>.

14·4: Pd/C (5%), C<sub>2</sub>H<sub>5</sub>OH.

14·5: (C<sub>2</sub>H<sub>5</sub>)<sub>3</sub>N, CH<sub>2</sub>Cl<sub>2</sub>.

### 3.3.14: Scheme 14 - Compounds (38a-r).

#### 3.3.14.1: Compounds (34a-f)

Preparation of compounds (34a-f) was achieved by a similar procedure to that outlined in Step 10.1, using either compound (32), (33) or commercially available, 3-substituted 4-hydroxybenzoic acids (0.021 mol) and benzyl bromide (0.042 mol) as starting materials.

Recrystallisation from toluene afforded compounds (34a-f) as white crystalline solids, and their mps., yields and M/Z values are given below.

34a; The yield was 2.8g (51%); mp. 211.0° C; M/Z 262 (M<sup>+</sup>).

34b; The yield was 2.9g (55%); mp. 183.0° C; M/Z 242 (M<sup>+</sup>).

34c; The yield was 3.1g (58%); mp. 201.0° C; M/Z 258 (M<sup>+</sup>).

34d; The yield was 4.2g (65%); mp. 185.0° C; M/Z 306, 308 (M<sup>+</sup>).

34e; The yield was 2.7g (50%); mp. 195.0° C; M/Z 253(M<sup>+</sup>).

34f; The yield was 3.8g (74%); mp. 189.0° C; M/Z 246(M<sup>+</sup>).

The ir. and <sup>1</sup>Hnmr. data for compounds (34a-f) are exemplified by the following data given for compound (34c) ir. 2900 (v.broad), 1675, 1230, 925 (broad), 875, 820, 760,

695  $\text{cm}^{-1}$ ;  $^1\text{Hnmr.}$   $\delta$  3.95 (2H, S), 5.22 (2H, S), 6.89 - 7.92 (8H, M), 9.50 [H. br.S ( $\text{D}_2\text{O}$  exchanged)].

### 3.3.14.2: Compounds (35a-f).

Preparation of compounds (35a-f) was achieved by a similar procedure to that outlined in Step 10.2, using compounds (34a-f) (0.01 mol) as the starting material. The residue was then used in Step 14.3 immediately, without further purification.

### 3.3.14.3: Compounds (36a-f).

Compounds (36a-f) were prepared by anesterification process similar to that outlined in Step 10.3, using compounds (35a-f) (0.01 mol) and (S)-(-)-ethyl lactate (0.011 mol) as starting materials. The reaction was carried out at room temperature. Compounds (35a-f) all gave yellow viscous oils which were used in Step 14.4 without further purification.

The M/Z values for these compounds are given below. The ir. data given for compound (36d) was typical for the series as a whole.

36d; M/Z = 406, 408 ( $\text{M}^+$ ); ir. 1755, 1725, 1250, 860, 765, 705  $\text{cm}^{-1}$ .

36a M/Z 362 ( $\text{M}^+$ ).

36b M/Z 342 ( $\text{M}^+$ ).

36c M/Z 358 ( $\text{M}^+$ ).

36e M/Z 353 ( $\text{M}^+$ ).

36f M/S 346 ( $\text{M}^+$ ).

#### 3.3.14.4: Compounds (37a-f)

Preparation of compounds (37a-f) was achieved by a similar procedure to that outlined in Step 10.4, using compounds (36a-f) (0.008 mol) and 5% palladium on carbon (0.1g) as starting materials. Distillation under reduced pressure afforded compounds (37a-f) as colourless viscous oils. The bps, yields M/Z values and  $[\alpha]_D^{20}$  values for compounds (37a-f) are given below.

37a: The yield was 1.8g (86%); bp. 125.0° C/0.01 mmHg  
M/Z 272 (M<sup>+</sup>);  $[\alpha]_D^{20} + 28.1^\circ$ .

37b: The yield was 1.67g (83%); bp., 155.0° C/0.01  
mmHg; M/Z 252 (M<sup>+</sup>);  $[\alpha]_D^{20} + 27.9^\circ$ .

37c: The yield was 1.73g (80%); bp. 150.0° C/0.05  
mmHg; M/Z 268 (M<sup>+</sup>);  $[\alpha]_D^{20} + 24.3^\circ$ .

37d: The yield was 2.3g (92%); bp. 150.0° C/0.01 mmHg;  
M/Z 316, 318 (M<sup>+</sup>);  $[\alpha]_D^{20} + 28.7^\circ$ .

37e: The yield was 1.3g (61%); bp. 190.0° C/0.5 mmHg;  
M/Z 263 (M<sup>+</sup>);  $[\alpha]_D^{20} + 31.2^\circ$ .

37f: The yield was 1.7g (82%); bp. 120° C/0.005 mmHg  
M/Z 256 (M<sup>+</sup>);  $[\alpha]_D^{20} + 24.7^\circ$ .

#### 3.3.14.5: Compounds (38a-r).

Preparation of compounds (38a-r) was achieved by an esterification procedure similar to that outlined in Step 10.6, using compounds (11b-e, g-j) (0.0018 mol) and compounds (37a-f) (0.0018 mol) as starting materials. The crude

products were purified by flash column chromatography using solvent (B) for compounds (38a-g, i-p,r) and solvent (A) for compounds (38h, q) as eluant. Recrystallisation from petroleum fraction (bp. 60° - 80° C) and ethanol [followed by refrigeration at 0° C for compounds (38a, j-n, p)] offered compounds (38a-o, q) as white crystalline solids and compound (38p) as a room temperature smectic. The yields, mps, M/Z values,  $[\alpha]_D^{20}$  values and % purity are tabulated below.

The ir. and  $^1\text{Hnmr.}$  data for compounds (38a-i) and (38j-r) are exemplified by the following data given for compounds (38a) and (38j) respectively. Transition temperatures for these materials appear in Tables XIII and XIV, pages 89 & 93.

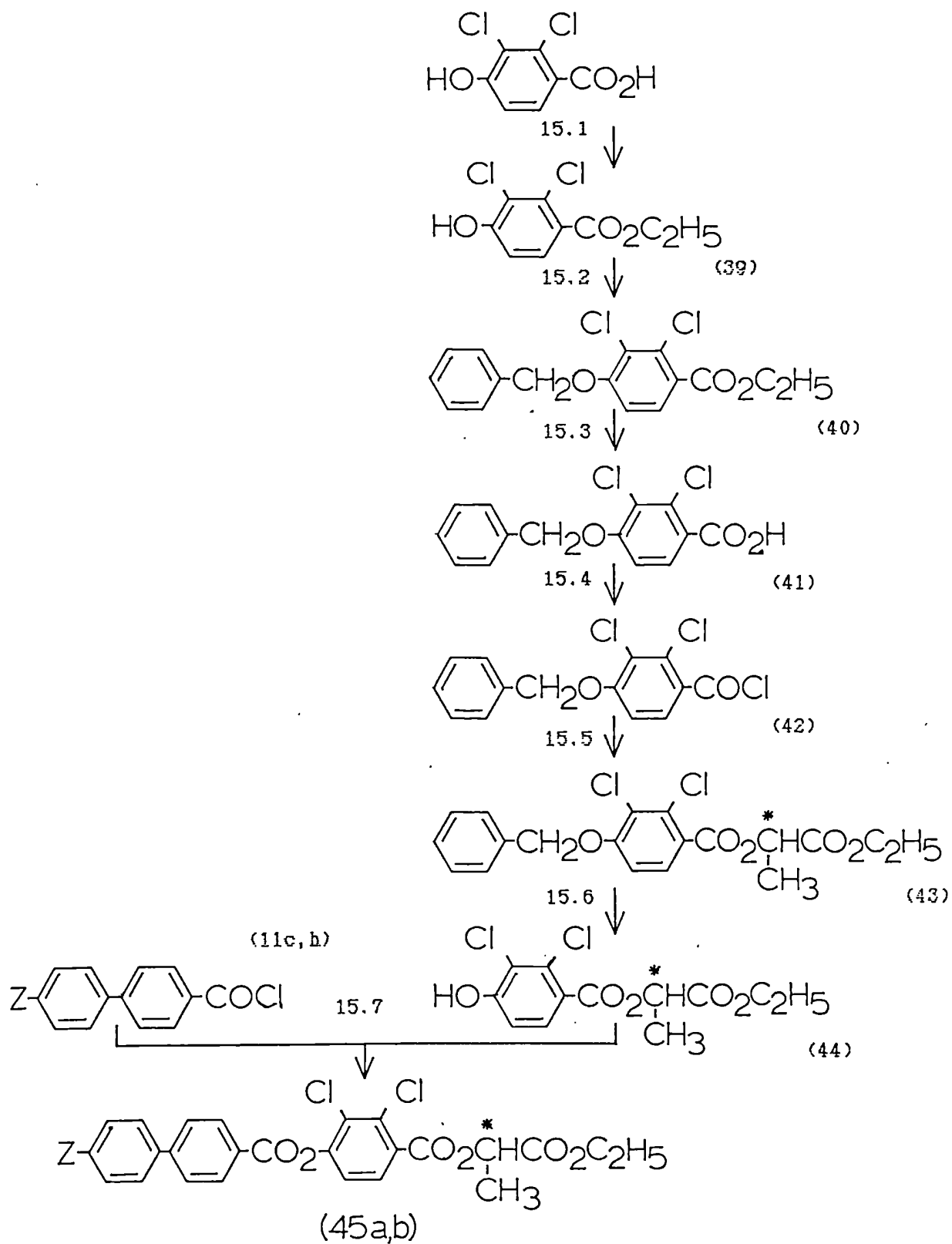
38a: ir. 1740, 1735, 1720, 1250  $\text{cm}^{-1}$ ;  $^1\text{Hnmr.}$   $\delta$  0.64 - 2.11 (21H, M), 4.10 (2H, T), 4.35 (2H, Q), 5.24 (1H, Q), 6.90 - 8.57 (11H, M).

38j: ir. 1750, 1750, 1725,  $\text{cm}^{-1}$ ;  $^1\text{Hnmr.}$   $\delta$  0.68 - 2.20 (23H, M), 2.67 (2H, T), 4.20 (2H, Q), 5.26 (1H, Q), 7.05 - 8.44 (11H, M).

	Yields/g	(%)	mp./° c	M/Z(M <sup>+</sup> )	[α] <sub>D</sub> <sup>20</sup>	Purity * %
38a:	0.65	(63)	60.0	580	+15.9	>99.9
38b:	0.50	(46)	47.5	594	+16.0	>99.9
38c:	0.08	(72)	74.0	608	+15.6	>99.9
38d:	0.95	(83)	79.0	622	+16.0	>99.5
38e:	0.59	(57)	63.0	574	+16.3	>99.9
38f:	0.73	(69)	78.0	590	+14.4	>99.9
38g:	0.64	(55)	63.0	638/640	+17.3	99
38h:	0.55	(52)	73.0	585	+18.8	>99.9
38i:	0.72	(69)	44.4	578	+15.0	>99.9
38j:	0.58	(56)	43.0	578	+17.0	99.5
38k:	0.57	(54)	41.5	592	+14.5	98
38l:	0.73	(67)	28.5	606	+14.1	99.5
38m:	0.53	(48)	37.5	602	+14.2	99.5
38n:	0.69	(67)	47.5	572	+16.3	>99.9
38o:	0.68	(64)	58.0	588	+12.3	>99.9
38p:	0.62	(53)	-30.0	636/638	+18.7	99.5
38q:	0.43	(46)	70.0	583	+17.6	>99.9
38r:	0.59	(57)	49.5	576	+13.3	>99.9

The purity of these compounds was checked by hplc; for compounds (38a-f,h-r) solvent (I) was used and for compound (38g) solvent (II) was used as eluant.

SCHEME 15



## SCHEME 15

45a... Z = C<sub>9</sub>H<sub>19</sub>O<sup>-</sup>;

45b... Z = C<sub>10</sub>H<sub>21</sub><sup>-</sup>.

15.1: C<sub>2</sub>H<sub>5</sub>OH, H<sub>2</sub>SO<sub>4</sub>.

15.2: PhCH<sub>2</sub>-Br, K<sub>2</sub>CO<sub>3</sub>, C<sub>2</sub>H<sub>5</sub>COCH<sub>3</sub>.

15.3: (i) 6M.aq.NaOH, C<sub>2</sub>H<sub>5</sub>OH; (ii) 6M.HCl.

15.4: (COCl)<sub>2</sub>, DMF, C<sub>6</sub>H<sub>6</sub>.

15.5: HOCH(CH<sub>3</sub>)CO<sub>2</sub>C<sub>2</sub>H<sub>5</sub>, (C<sub>2</sub>H<sub>5</sub>)<sub>3</sub>N, CH<sub>2</sub>Cl<sub>2</sub>.

15.6: Pd/C (5%), C<sub>2</sub>H<sub>5</sub>OH.

15.7: (C<sub>2</sub>H<sub>5</sub>)<sub>3</sub>N, CH<sub>2</sub>Cl<sub>2</sub>.

### 3.3.15: Scheme 15 - Compounds (45a,b).

#### 3.3.15.1: ethyl 2,3-dichloro-4-hydroxybenzoate (39).

A solution of 2,3-dichloro-4-hydroxybenzoic acid (2.7g, 0.013 mol) and concentrated sulphuric acid (8 drops) in ethanol (30 ml) was heated under reflux for 16h. The excess ethanol was removed by distillation and the residue dissolved in dichloromethane (50 ml). The organic phase was washed with water (50 ml), saturated aqueous sodium hydrogen carbonate (50 ml), water (50 ml) and finally dried (MgSO<sub>4</sub>).

Recrystallisation from toluene afforded compound (39) as a white crystalline solid, 1.7g (55%); mp. 168° - 170° C; M/Z 234 (M<sup>+</sup>); ir. 3300 (broad, 2995, 1690, 1160, cm<sup>-1</sup>; <sup>1</sup>Hnmr. δ 1.32 (3H, T), 4.26 (2H, Q), 6.80 - 7.71 (2H, M), 10.80 [1H, br.S (D<sub>2</sub>O exchanged)].

#### 3.3.15.2: ethyl 4-benzyloxy-2,3-dichlorobenzoate (40).

Compound (40) was prepared by a similar method to that outlined in Step 1.1, using benzyl bromide (1.2g, 0.0068 mol), compound (39) (1.6g, 0.0068 mol) and potassium carbonate (1g, 0.007 mol) in dry butanone (40 ml). Recrystallisation from petroleum fraction (bp. 60° - 80° C) afforded compound (40) as a white crystalline solid, 2.1g (95%); mp. 84.0° C; M/Z 324 (M<sup>+</sup>); ir. 2995, 1725, 1255, 730, 695 cm<sup>-1</sup>; <sup>1</sup>Hnmr. δ 1.44 (3H, T), 4.43 (2H, Q), 5.27 (2H, S), 6.88 - 7.98 (7H, M).

#### 3.3.15.3: 4-benzyloxy-2,3-dichlorobenzoic acid (41).

A mixture of compound (40) (2g, 0.0062 mol) and ethanol (2 ml) in 6M aqueous sodium hydroxide (40 ml) was heated

under reflux for 16h. The reaction mixture was poured onto crushed ice (100g) and acidified with 6M hydrochloric acid. The product was extracted into ethyl acetate (100 ml), washed with water (2x100 ml) and dried (MgSO<sub>4</sub>). Recrystallisation from toluene, after treatment with a little charcoal, afforded compound (41) as a white crystalline solid, 0.8g (43%); mp. 179.0° C; M/Z 298 (M<sup>+</sup>); ir. cm<sup>-1</sup>; <sup>1</sup>Hnmr. δ 5.17 (2H, S), 6.88 - 8.12 (7H, MØ, 8.73 [1H, br.S (D<sub>2</sub>O exchanged)]).

#### 3.3.15.4: 4-benzyloxy-2,3-dichlorobenzoyl chloride (42).

Compound (42) was prepared by a similar method to that outlined in Step 10.5, using compound (41) (0.7g, 0.0023 mol) as the starting material. Compound (42) was then used immediately in Step 15.5 without further purification.

#### 3.3.15.5: (S)-(-)-ethyl 2-(4-benzyloxy-2,3-dichlorophenyl carboxy) propanoate (43).

Preparation of compound (43) was achieved by an esterification procedure similar to that outlined in Step 10.3, using compound (42) (0.0023 mol) and (S)-(-)-ethyl lactate (0.0025 mol) as the starting materials. The reaction was carried out at room temperature. Compound (43) was obtained as a yellow viscous oil, which was then used without further purification in Step 15.6, 0.9g (98%).

#### 3.3.15.6: (S)-(-)-ethyl 2-(2,3-dichloro-4-hydroxyphenylcarboxy) propanoate (44).

Compound (44) was prepared by a similar method to that outlined in Step 10.4, using compound (43) (0.9g, 0.0022 mol)

and 5% palladium on carbon (0.1g) as starting materials.

Compound (44) was obtained as a yellow viscous oil and was used without further purification in Step 15.7, 0.6g (85%); M/Z ( $M^+$ ); ir. 3400 (broad), 2995, 1730, 1725, 1225  $\text{cm}^{-1}$ .

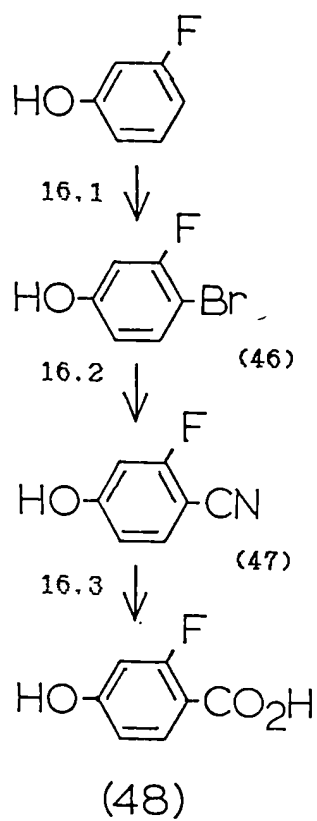
3.3.15.7: (S)-(-)-ethyl 2-[4-(4'-nonoxy- and 4'-decyl-biphenyl-4-ylcarboxyl) 2,3-dichlorobenzo y loxy] propanoate (45a, b).

Preparation of compounds (45a, b) was achieved by an esterification procedure similar to that outlined in Step 10.6, using compounds (11c, h) (0.001 mol) and compound (44) (0.001 mol) as starting materials. The crude products were purified by flash column chromatography, using solvent (A) as eluant. Recrystallisation from ethanol, afforded compounds (45a, b) as white crystalline solids. Transition temperatures for these two materials appear in Table XV, page 100.

45a: the yield was 0.36g (57%); mp. 50.0°C; M/Z 628 ( $M^+$ );  $[\alpha]_D^{20} + 1.4^\circ$  purity (hplc) 99.5% (solvent II); ir. 1755, 1745, 1735, 1250  $\text{cm}^{-1}$ ;  $^1\text{Hnmr. } \delta$  0.67 - 2.13 (23H, M), 4.03 (2H, T), 4.19 (2H, Q), 5.20 (1H, Q), 6.95 - 8.52 (10H, M).

45b: The yield was 0.3g (48%); mp. 35.0°C; M/Z 626 ( $M^+$ ); purity (hplc) 99.5% (solvent II).

## SCHEME 16



16.1: (i) Br<sub>2</sub>, CHCl<sub>3</sub>; (ii) 20% aq. NaOH; (iii) conc. HCl.

16.2: (i) CuCN, NMP; (ii) FeSO<sub>4</sub>·(7 H<sub>2</sub>O).

16.3: (i) 10% aq. NaOH; (ii) conc. HCl.

### 3.3.16: Scheme 16 - Compound (48).

#### 3.3.16.1: 4-bromo-3-fluorophenol (46).

A solution of bromine (40.1g 0.25 mol) in chloroform (112 ml) was added very quickly to a vigorously stirred solution of 3-fluorophenol (27.8g, 0.248 mol) in chloroform (112 ml) at 0°C. After 30 sec., 20% w/v aqueous sodium hydroxide (155 ml) was quickly added to destroy the hydrogen bromide formed and to convert the phenol into the corresponding sodium salt. The aqueous layer was then removed and acidified with concentrated hydrochloric acid. The product was extracted into ether (2x200 ml), washed with water (2x200 ml) and dried (MgSO<sub>4</sub>). Recrystallisation from toluene / petroleum fraction (bp. 40° - 60° C) 1 : 10 afforded compound (46) as a white crystalline solid, 17.5g (37%); mp. 70.0° C (lit., 71.5° C); M/Z 190 (M<sup>+</sup>); ir. 3320 (broad), 1160, 860, 815 cm<sup>-1</sup>; <sup>1</sup>Hnmr. δ 5.12 (1H, S), 6.40 - 7.52 (3H, M).

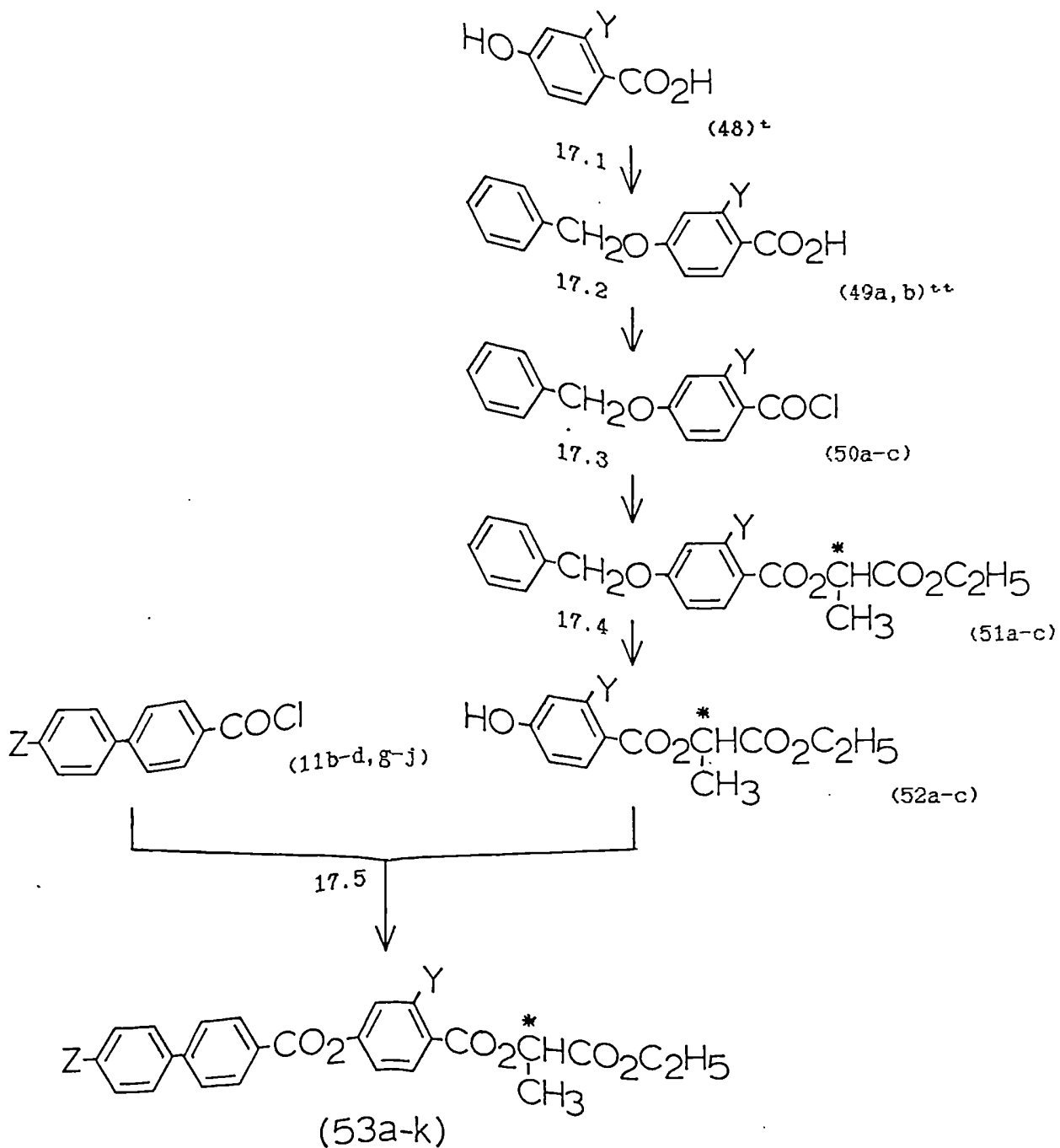
#### 3.3.16.2: 2-fluoro-4-hydroxybenzotrile (47)

Compound (47) was prepared by a similar method to that outlined in Step 12.1, using copper (I) cyanide (15.7g 0.175 mol) and compound (46) (16.7g, 0.0874 mol) as starting materials. Recrystallisation from toluene, after treatment with a little charcoal, afforded compound (47) as a white crystalline solid, 10g (83%); mp. 112.5° C; M/Z 137 (M<sup>+</sup>); ir. 3260 (broad), 2225, 1165, 855, 815 cm<sup>-1</sup>; <sup>1</sup>Hnmr. δ 6.28 - 7.30 (3H, M), 10.14 [1H, br.S (D<sub>2</sub>O exchanged)].

### 3.3.16.3: 2-fluoro-4-hydroxybenzoic acid (48).

Preparation of compound (48) was achieved by a similar procedure to that outlined in Step 13.1, using compound (47) (5g, 0.0365 mol) as the starting material. Recrystallisation from water afforded compound (48) as a white crystalline solid, 5.1g (89%); mp. 205.0° C; M/Z 156 (M<sup>+</sup>); ir. 3400 (broad), 2800 (v.broad), 1680, 1160, 860, 850 cm<sup>-1</sup>; <sup>1</sup>Hnmr. δ 6.61 - 8.48 (3H, M), 9.00 [2H, br.S (D<sub>2</sub>O exchanged)].

SCHEME 17



<sup>†</sup> - compound (48); Y=F, and the commercially available material where Y=CH<sub>3</sub>.  
<sup>††</sup> - compounds (49a, b) and the material; Y=Cl, supplied by David Coates of STC Technology.

## SCHEME 17

49a... Y=F; 49b... Y=Me.

50a-52a... Y=Cl; 50b-52b... Y=Me; 50c-52c... Y=F.

Z-	-Y		Z-	-Y
53a... C <sub>8</sub> H <sub>17</sub> O-	-Cl		53f... C <sub>9</sub> H <sub>19</sub> -	-Cl
53b... C <sub>9</sub> H <sub>19</sub> O-	-Cl		53g... C <sub>10</sub> H <sub>21</sub> -	-Cl
53c... C <sub>10</sub> H <sub>21</sub> O-	-Cl		53h... C <sub>11</sub> H <sub>23</sub> -	-Cl
53d... C <sub>9</sub> H <sub>19</sub> O-	-Me		53i... C <sub>12</sub> H <sub>25</sub> -	-Cl
53e... C <sub>9</sub> H <sub>19</sub> O-	-F		53j... C <sub>10</sub> H <sub>21</sub> -	-Me
			53k... C <sub>10</sub> H <sub>21</sub> -	-F

17.1: (i) PhCH<sub>2</sub>-Br, 40% aq. NaOH, C<sub>2</sub>H<sub>5</sub>OH; (ii) 10% aq. NaOH.

17.2: (COCl)<sub>2</sub>.

17.3: HOCH(CH<sub>3</sub>)\*CO<sub>2</sub>C<sub>2</sub>H<sub>5</sub>, (C<sub>2</sub>H<sub>5</sub>)<sub>3</sub>N, CH<sub>2</sub>Cl<sub>2</sub>.

17.4: Pd/C (5%), C<sub>2</sub>H<sub>5</sub>OH.

17.5: (C<sub>2</sub>H<sub>5</sub>)<sub>3</sub>N, CH<sub>2</sub>Cl<sub>2</sub>.

### 3.3.17: Scheme 17 - Compounds (53a-k).

#### 3.3.17.1: Compounds (49a,b).

Preparation of compounds (49a, b) was achieved by a similar procedure to that outlined in Step 10.1, using either compound (48) or commercially available 2-methyl-4-hydroxybenzoic acid (0.017 mol) and benzyl bromide (0.018 mol) as starting materials. Recrystallisation from toluene afforded compounds (49a, b) as white crystalline solids. The ir. and  $^1\text{Hnmr}$ . data for these materials is exemplified by the data given below for compound (49a).

49a: ir. 2700 (broad), 1690, 1245, 930 (broad), 860, 835, 750, 695  $\text{cm}^{-1}$ ;  $^1\text{Hnmr}$ .  $\delta$  5.24 (2H, S), 6.75 - 8.34 (8H, M), 9.00 [1H, br.S ( $\text{D}_2\text{O}$  exchanged)].

The yields, (% yields), mps and M/Z values for compounds prepared by using the procedure outlined in Step 17.1 are given below.

49a: 3.1g (75%); mp 168.0° C; M/Z 246 ( $\text{M}^+$ ).

49b: 2.0g (48%), mp 130.0° C; M/Z 242 ( $\text{M}^+$ ).

#### 3.3.17.2: Compounds (50a-c).

Compounds (50a - c) were prepared by a similar method to that outlined in Step 10.2, using either compounds (49a, b) or 4-benzyloxy-2-chlorobenzoic acid (0.012 mol) as the starting material. The residue was then used immediately, without further purification in step 17.3.

### 3.3.17.3: Compounds (51a-c).

Preparation of compounds (51a-c) was achieved by a similar procedure to that outlined in Step 10.3, using compounds (50a-c) (0.012 mol) and (S)-(-)-ethyl lactate (0.013 mol) as starting materials. The reaction was carried out at room temperature. Compounds (51a-c) were all obtained as yellow oils which were used in Step 17.4 without further purification. The ir. and  $^1\text{Hnmr.}$  data for these materials are exemplified by the data given below for compound (51b).

51b: ir. 1750, 1715, 1245, 850, 735, 695  $\text{cm}^{-1}$ ;  $^1\text{Hnmr.}$   $\delta$  1.33 (3H, T), 1.69 (3H, D), 2.67 (3H, S), 4.28 (2H, Q), 5.15 (2H, S), 5.35 (1H, Q), 6.72 - 8.30 (8H, M).

The yield (% yield) and M/Z values for compounds prepared by using the procedure outlined in Step 17.3 are given below.

51a: 4.2g (97%) M/Z 362 ( $\text{M}^+$ ).

51b: 4.0g (96%); M/Z 342 ( $\text{M}^+$ ).

51c: 4.1g (98%); M/Z 346 ( $\text{M}^+$ ).

### 3.3.17.4: Compounds (52a-c).

Preparation of compounds (52a-c) was achieved by a similar procedure to that outlined in Step 10.4, using compounds (51a-c) (0.0118 mol) and 5% palladium on carbon (0.2g) as starting materials. Distillation under reduced pressure afforded compounds (52a-c) as colourless viscous oils. The ir. and  $^1\text{Hnmr.}$  data for these materials are

exemplified by the data given below for compound (52a).

52a: ir. 3360 (broad), 2995, 1760, 1690, 1210, 870, 830  $\text{cm}^{-1}$ ;  $^1\text{Hnmr.}$   $\delta$  1.53 (3H, T), 1.86 (3H, D), 4.56 (2H, Q), 4.56 (2H, Q), 4.62 (1H, Q), 6.93 - 8.33 [4H, M (1H  $\text{D}_2\text{O}$  exchanged)].

The yield, (% yield), bps, M/Z values and optical rotation values of compounds prepared by using the procedure outlined in Step 17.4 are given below.

52a: 2.3g (71%); bp. 175°C/0.1 mmHg; M/Z 272 ( $\text{M}^+$ );  
[ $\alpha$ ]  $^20_{\text{D}}$  + 8.9°.

52b: 2.6g (86%); bp. 155.0°C/0.01 mmHg M/Z 252 ( $\text{M}^+$ );  
[ $\alpha$ ]  $^20_{\text{D}}$  + 21.0°.

52c: 2.4g (78%); bp. 185°C/0.5 mmHg; M/Z 256 ( $\text{M}^+$ );  
[ $\alpha$ ]  $^20_{\text{D}}$  + 27.1°.

### 3.3.17.5: Compounds (53a-k).

Preparation of compounds (53a-k) was achieved by an esterification procedure similar to that outlined in Step 10.6, using compounds (11b-d, g-j) (0.0038 mol) and compounds (52a-c) (0.0037 mol) as starting materials.

The crude products were purified by flash column chromatography using solvent (B) as eluant.

Recrystallisation from petroleum fraction (bp. 60° - 80° C) [for compounds (53a-e)] or ethanol [for compounds (53f-k)] afforded compounds (53a, c-e, i,k) as white crystalline solids and compounds (53b, f-h, j) as room temperature smectics.

The ir. and  $^1\text{Hnmr.}$  data for compounds (53a-e) and (53f-k) are exemplified by compounds (53a) and (53f) respectively and appear below. Transition temperatures for these compounds appear in Tables XVI<sup>and XVII</sup>, pages 102 and 107 ~~103~~.

53a: ir. 1735 (broad), 1715, 1245  $\text{cm}^{-1}$ ;  $^1\text{Hnmr.}$   $\delta$  0.64 - 2.00 (21H, M), 4.00 (2H, T), 4.23 (2H, Q), 5.33 (1H, Q), 6.87 - 8.35 (1, M).

53f: ir. 1755, 1740, 1725,  $\text{cm}^{-1}$ ;  $^1\text{Hnmr.}$   $\delta$  0.55 - 1.92 (23H, M), 2.74 (2H, T), 4.36 (2H, Q), 5.50 (1H, Q), 7.32 - 8.63 (11H, M).

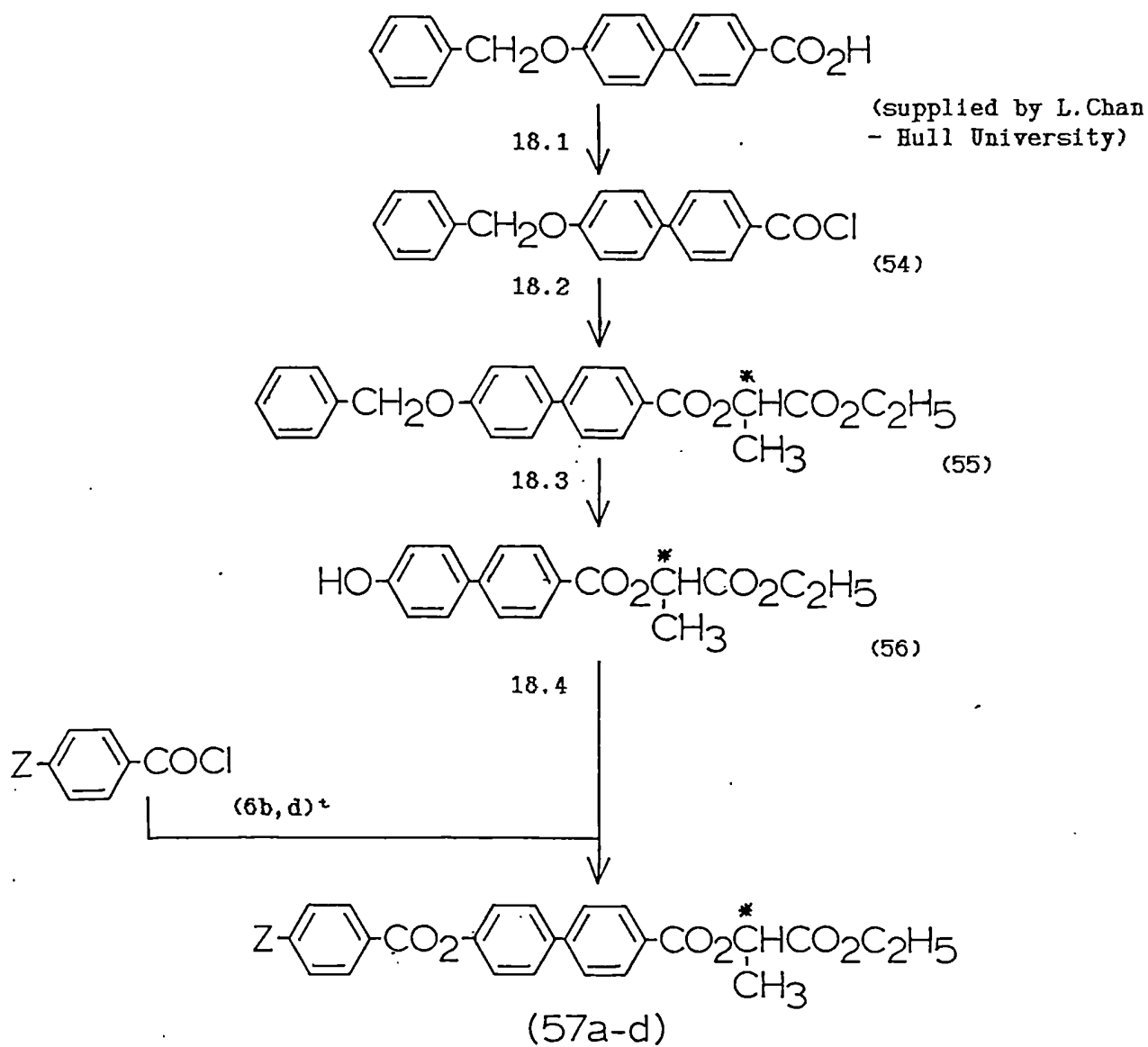
The yield (% yield), mps, M/Z values, optical rotation values and purity for compounds prepared by using the procedure outlined in Step 17.5 are tabulated below.

	Yields/g	(%)	mp./° C	M/Z(M <sup>+</sup> ),	$[\alpha]_{\text{D}}^{20}$	Purity/%,*
53a:	0.51	(24)	44.0	580	+4.6	>99.9
53b:	0.84	(38)	19.0	594	+8.5	>99.9
53c:	0.51	(23)	33.0	608	+4.8	98.0
53d:	1.07	(50)	33.0	574	+10.7	>99.9
53e:	1.47	(69)	55.0	578	+14.4	>99.9
53f:	1.60	(75)	-33.0 <sup>†</sup>	578	+5.5	>99.9
53g:	0.84	(38)	2.0	592	+6.1	98.0
53h:	1.50	(67)	28.5	606	+4.9	>99.9
53i:	1.50	(63)	30.0	620	+5.3	>99.9
53j:	1.20	(57)	26.0	572	+11.2	>99.9
53k:	1.55	(69)	31.5	576	+13.6	99.5

\* The purity of these compounds was checked by hplc using solvent (I), for compounds (53a-c, e, i-k) and solvent (II), for compounds (53d, f-h).

† Obtained by DSC.

SCHEME 18



<sup>†</sup> - The acid chlorides of n-octyl and n-decyl benzoic acid were supplied by BDH Ltd, Poole, Dorset.

## SCHEME 18

6b,57a... Z = C<sub>7</sub>H<sub>15</sub>O-; 6d,57b... Z = C<sub>9</sub>H<sub>19</sub>O-; 57c... Z = C<sub>8</sub>H<sub>17</sub>-;  
57d... Z = C<sub>10</sub>H<sub>21</sub>-.

18:1: (COCl)<sub>2</sub>.

18:2: HOCH(CH<sub>3</sub>)<sup>\*</sup>CO<sub>2</sub>C<sub>2</sub>H<sub>5</sub>, (C<sub>2</sub>H<sub>5</sub>)<sub>3</sub>N, CH<sub>2</sub>Cl<sub>2</sub>.

18:3: Pd/C (5%), THF.

18:4: (C<sub>2</sub>H<sub>5</sub>)<sub>3</sub>N, CH<sub>2</sub>Cl<sub>2</sub>.

3.3.18: Scheme 18 - Compounds (57a-d).

3.3.18.1: 4'-benzyloxybiphenyl carboxylic acid chloride  
(54).

Compound (54) was prepared by a similar method to that outlined in Step 17.1, using 4'-benzyloxybiphenyl carboxylic acid (10g, 0.0329 mol) as the starting material. The residue was then used in Step 18.2 immediately without further purification.

3.3.18.2: (S)-(-)-ethyl 2-(4-benzyloxybiphenyl carboxy)  
propanoate (55).

Preparation of compound (55) was achieved by a similar procedure to that outlined in Step 17.3 using compound (54) (0.0329 mol) and (S)-(-)-ethyl lactate (0.0345 mol) as starting materials. The reaction was carried out at room temperature. Compound (55) was obtained as a viscous yellow oil which was used immediately in Step 18.3 without further purification.

3.3.18.3: (S)-(-)-ethyl 2-(4-hydroxybiphenyl) propanoate  
(56).

Compound (56) was prepared by a similar method to that outlined in Step 17.4, using compound (55) (0.0329 mol) and 5% palladium on carbon (1g) in T.H.F. (150 ml) as starting materials. Distillation under reduced pressure produced a small amount of impurity which sublimed at 140° C/0.1 mmHg. Further distillation at reduced pressure (160° C/0.1 mmHg) afforded compound (56) as a yellow oil which crystallised on cooling. Recrystallisation from toluene: petroleum fraction

(bp. 60 - 80°C) 1 : 1, afforded compound (56) as a white crystalline solid, 2.5g (25%);, mp. 152.0°C; M/Z 314 (M<sup>+</sup>); ir. 3470 (broad), 1745, 1715, 1195, 835 cm<sup>-1</sup>; <sup>1</sup>Hnmr. δ 1.28 (3H, T), 1.63 (3H, D), 4.24 (2H, Q), 5.22 [1H, br.S (D<sub>2</sub>O exchanged)], 5.32 (1H, Q), 6.75 8.20 (8H, M).

#### 3.3.18.4: Compounds (57a-d).

Preparation of compounds (57a-d) was achieved by a similar procedure to that described in step 10.6, using compounds (6b,d), n-octyl and n-decylbenzoyl chloride (0.002 mol) and compound (56) (0.00197 mol) as starting materials. The crude products were purified by flash column chromatography using solvent (B), as eluant. Recrystallisation from ethanol afforded compounds (57a-d) as white crystalline solids.

The ir. and <sup>1</sup>Hnmr. data for the alkyloxy and alkyl materials are exemplified by the respective nonyloxy and decyl homologues, compounds (57b,d). Transition temperatures for these compounds appear in Table XVII, page 108.<sup>112</sup>

57b; 0.65g (59%); mp. 72.0°C; M/Z 560 (M<sup>+</sup>); [α]<sub>D</sub><sup>20</sup> + 23.4, purity (hplc) 99.5% (solvent I); ir. 1755, 1745, 1730, 1610, 1265, 850 cm<sup>-1</sup>, <sup>1</sup>Hnmr. δ 0.68 - 2.00 (23H, M), 4.02 (2H, E), 4.20 (2H, Q), 5.31 (1H, Q), 6.80 - 8.33 (12H, M).

57d; 0.6g (55%), mp. 53.0°C, M/Z 558 (M<sup>+</sup>), [α]<sub>D</sub><sup>20</sup> + 24.4°, purity (h.p.l.c.) 99.5% (solvent I); ir. 1765, 1740, 1725, 1615, 860 cm<sup>-1</sup>; <sup>1</sup>Hnmr. δ 0.67 - 1.78 (25H, M), 2.63 (2H, T), 4.14 (2H, Q), 5.23 (1H, Q), 7.01 - 8.12 (12H, M).

57a: 0.6g (57%), mp. 82.0°C, M/Z 532 (M<sup>+</sup>), [α]<sub>D</sub><sup>20</sup> + 25.8°, purity (hplc) >99.9% (solvent II).

57c: 0.4g (38%), mp. 41.0°C, M/Z 530 (M<sup>+</sup>), [α]<sub>D</sub><sup>20</sup> + 24.5°, purity (hplc) 99.3% (solvent I).

4. APPENDICES.

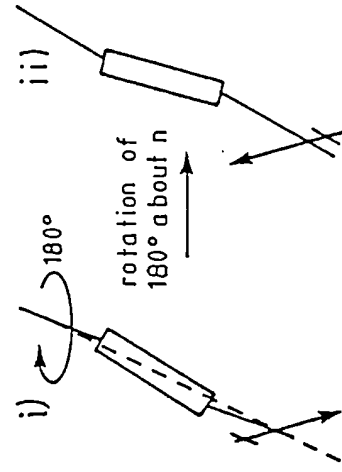
#### 4.1: Origin of Ferroelectricity in the $S_C^*$ phase

The occurrence of ferroelectricity in the  $S_C^*$  phase has been explained in terms of symmetry arguments, which relate its monoclinic molecular environment to that of crystalline ferroelectrics. Other similar arguments have also been given, but these generally offer a mathematical representation of how a spontaneous polarisation arises, and often a clear physical interpretation is difficult to perceive. Recently Walba has proposed a more pictorial representation of the origin of ferroelectricity in the  $S_C^*$  phase, explaining the phenomenon by way of unsymmetrical binding sites which tend to force the chiral molecules into a preferred tilt orientation.

Both Goodby and Walba have inextricably linked the direction of  $P_S$  with a particular tilt orientation, corresponding to a time-averaged, all-trans (anti), lowest energy conformer. This idea has already been used earlier in the thesis as the basis of a model to illustrate the symmetry arguments outlined by Meyer (Fig. a).

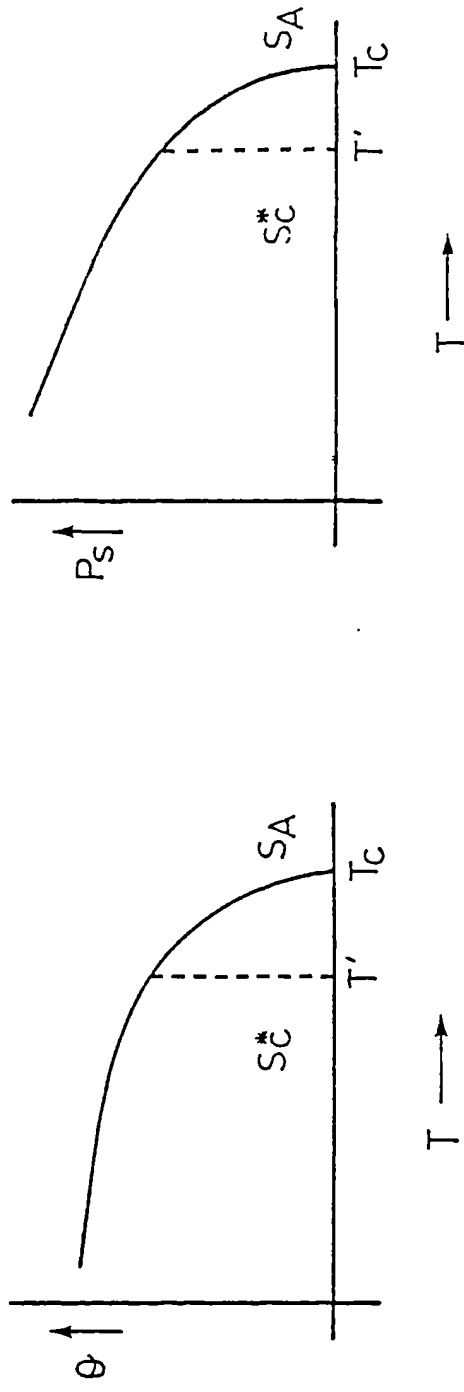
A common observation on cooling from the  $S_A$  to the  $S_C^*$  phase is that both  $\theta$  and  $P_S$  tend to follow a similar curve with decreasing temperature. From a zero value at the transition temperature ( $T_C$ ), both initially increase quite rapidly as the temperature falls to a value  $T^1$  (commonly between  $3^\circ$  to  $15^\circ$  C below  $T_C$ ). Beyond  $T^1$ ,  $\theta$  and  $P_S$  increase less steeply and approximately linearly as the temperature decreases further, with  $\theta$  tending to level off at a saturation value (Fig. b).

Fig.(a): Direction of  $P_S$  vs tilt orientation.



Polarisation ( $\oplus \rightarrow$ ) rigidly coupled to a particular orientation, conformation  $i$ ) is arbitrarily designated tilt orientation of lowest energy.

Fig.(b): Commonly observed curves for  $\theta$  and  $P_S$  vs.  $T$ .



Cooling from  $T_c \rightarrow T'$ ; both  $\theta$  and  $P_S$  rise steeply whereas below  $T'$ ,  $\theta$  and  $P_S$  increase approximately linearly with increasing temperature.

However, it has already been mentioned that in the  $S_A$  phase the layer spacing is often less than the extended molecular length for many materials. This is due to the molecules already being tilted, but in a random fashion which leads to an overall perpendicular orientation of the director ( $\bar{n}$ ), with respect to the layer plane. A second point worth noting is that D.S.C. measurements show the  $S_A$  to  $S_C^*$  phase transition to have a very low enthalpy, indicating only a small physical change at  $T_C$  and not a sudden jump in the value of the tilt angle from zero to a finite value.

By combining these observations with the model described above, a simple pictorial explanation is offered as to the occurrence of ferroelectricity in the  $S_C^*$  phase and its variation with temperature.

It is first of all suggested that the random tilt orientations in the  $S_A$  phase result in an overall polarisation reduced to zero, (Fig. c).

At  $T_C$  two things may occur, initially the tilt angle can increase as some function of falling temperature, but more importantly there will be a tendency for the previously random molecular tilt orientations to begin aligning with a preferred direction. It is this latter operation which then results in the sudden appearance of a non-zero value of  $P_S$  at  $T_C$  (Fig. d).

On cooling further below  $T_C$  the tendency for tilt orientations to align with the preferred direction increases, leading to a rapid increase in both  $P_S$  and the

Fig.(c): Random tilt orientation and polarisation direction in the SA phase  
 (circles represent plan view).

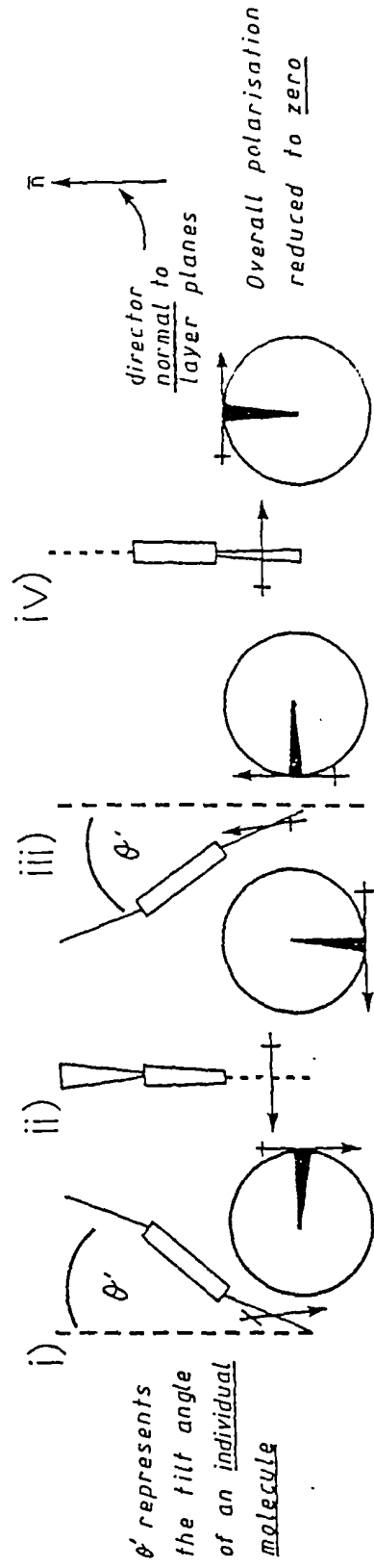
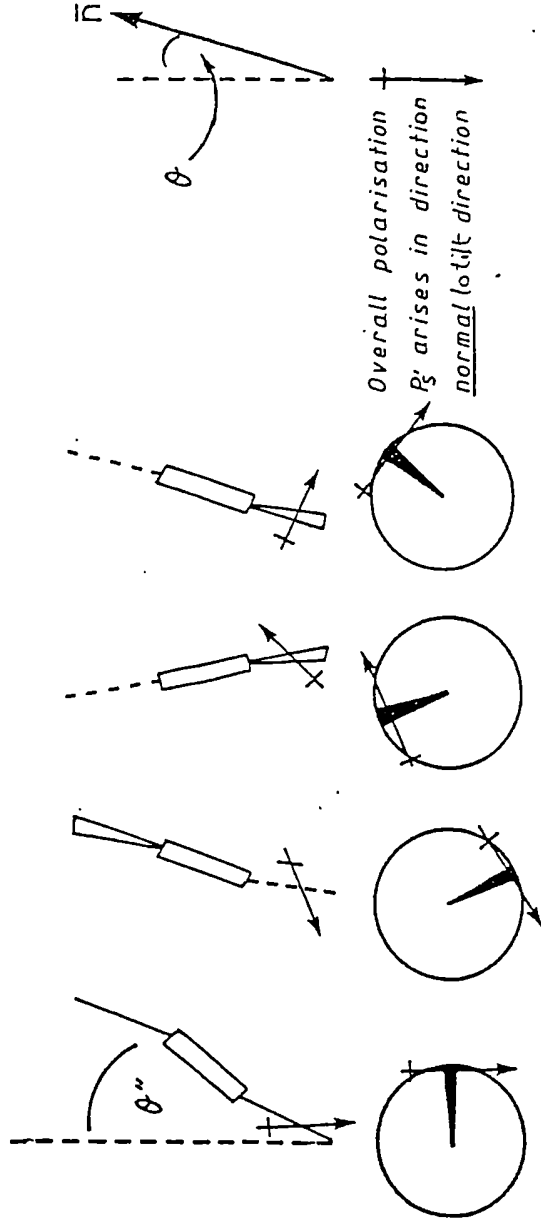


Fig. (d): Tilt orientations begin to align in particular direction at  $T_c$ .



$\theta$  represents the observed small optical tilt angle measured just below  $T_c$ , so that  $\theta < \theta''$  and  $\theta''$  is slightly larger than  $\theta'$ , due to decrease in temperature.

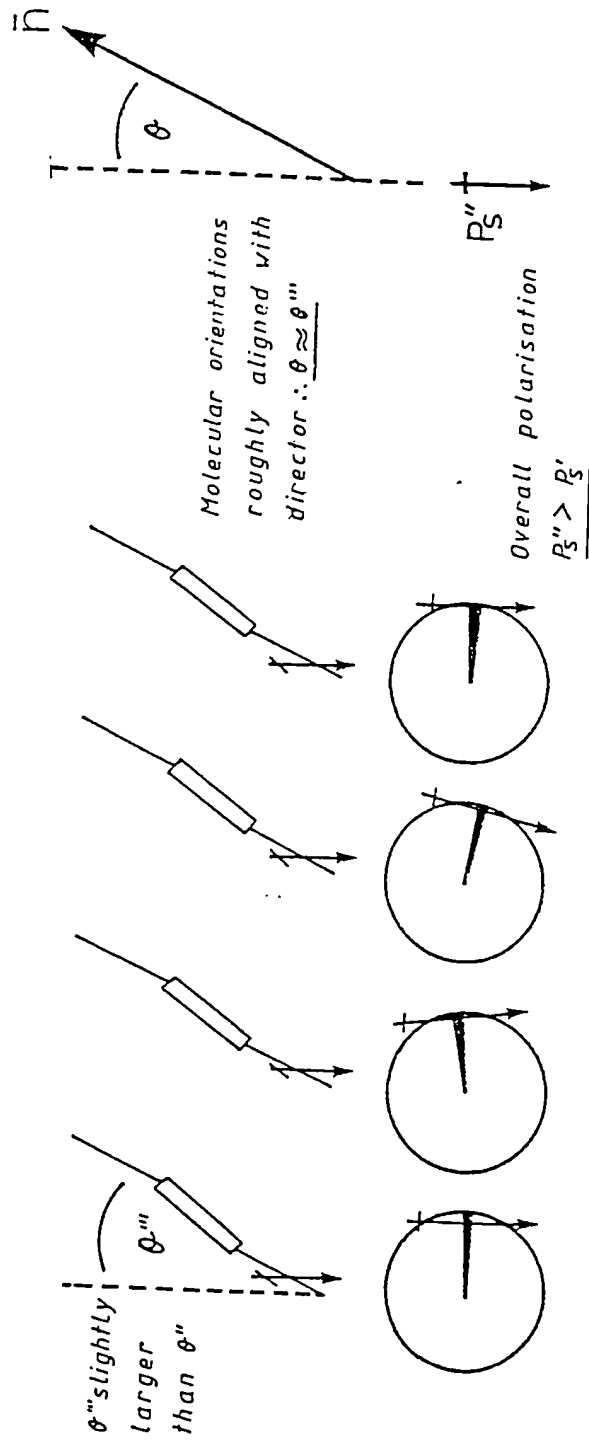
optical tilt angle, until at  $T^1$ , the vast majority of the molecules have their tilt orientations roughly aligned with the director (Fig. e).

Below  $T^1$ , the approximately linear increase of  $P_g$  with decreasing temperature may simply result from an increasing tendency of the molecules to adopt the all-trans, lowest energy conformation more frequently, thereby increasing its time-averaged life span.

A most obvious deficiency in the above hypothesis, is that the behaviour of  $\theta$  described above could only be observed by an optical technique. X-ray studies of such a transition would be expected to show an approximately linear increase in tilt angle as temperature falls, whereas in actual fact these measurements also tend to show  $\theta$  varying as in figure b. To counter this observation it may be argued that X-ray data very close to the  $S_A$  to  $S_C^*$  phase transition can be difficult to determine with any great accuracy and particularly so for the type of transition outlined above, where there is little immediate change in layer spacing. However, a more plausible overall explanation may be that at the  $S_A$  to  $S_C^*$  phase transition a significant increase in  $\theta$  begins to take place, although the molecules initially maintain a similarly random orientation to that in the preceding  $S_A$  phase. As the temperature falls below  $T_C$  the tilt angle can increase rapidly, before beginning to level off at what will now be referred to as  $T^\theta$ .

Simultaneously, as  $\theta$  is increasing, there will be a separate tendency for the molecular orientations to become

Fig.(e): Tilt orientations at  $T'$



aligned with a preferred direction, so that a sudden appearance of  $P_S$  also occurs at  $T_C$ , and as before, increases quickly until  $T^1$  is reached. From the above it is obvious that  $T^\theta$  and  $T^1$  do not necessarily coincide with each other and may occur in any order below  $T_C$  (Fig. f).

Values of  $T^1$  and  $T^\theta$  have not been determined for materials in this thesis, which in any case would be of a fairly arbitrary nature. Nonetheless, superimposed  $P_S$  vs  $T$  and  $\theta$  vs  $T$  curves resembling those of figure f are observed for some of the materials prepared in this work, two of the best examples arising from compounds (38a) and (53d) respectively (Fig. g).

One consequence of the proposal outlined above, is the implication that the value of  $P_S$  is not dependent on the magnitude of  $\theta$  in the  $S_C^*$  phase. This is contrary to Meyers' original hypothesis, which suggests that the relative value of  $P_S$  is actually a function of  $\theta$ . Although difficult to prove either way, there is at least some evidence to support the independent nature of  $P_S$  with respect to  $\theta$ .

In section 5, figure 42 illustrates how extending the alkyloxy chain length in the homologous series of compounds (28 a-e), has a fairly uniform effect on increasing the value of  $\theta$  at  $10^\circ C$  below the  $S_A$  to  $S_C^*$  phase transition. Conversely, although there is no change in the environment of the asymmetric centre in these materials, the actual magnitude of  $P_S$  tends to fall with increasing alkyloxy chain length.

Fig.(f): Two possible combinations of  $R_S$  v  $T$  and  $\theta$  v  $T$  curves for a material  
 with:~ i)  $T' > T^\theta$ , ii)  $T' < T^\theta$ .

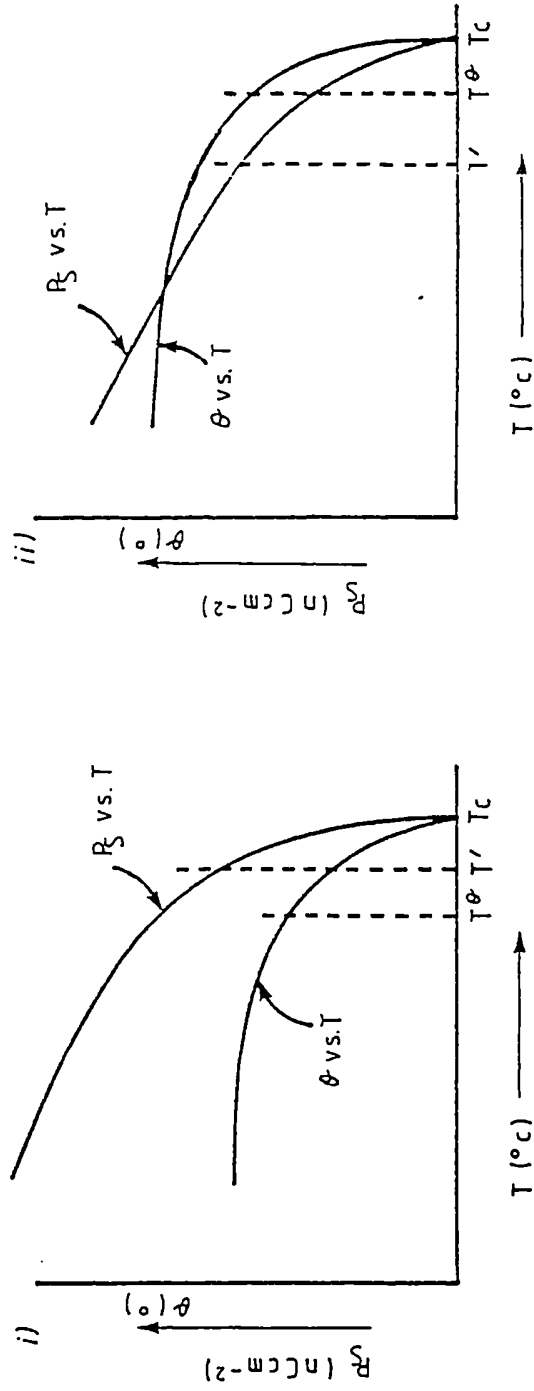
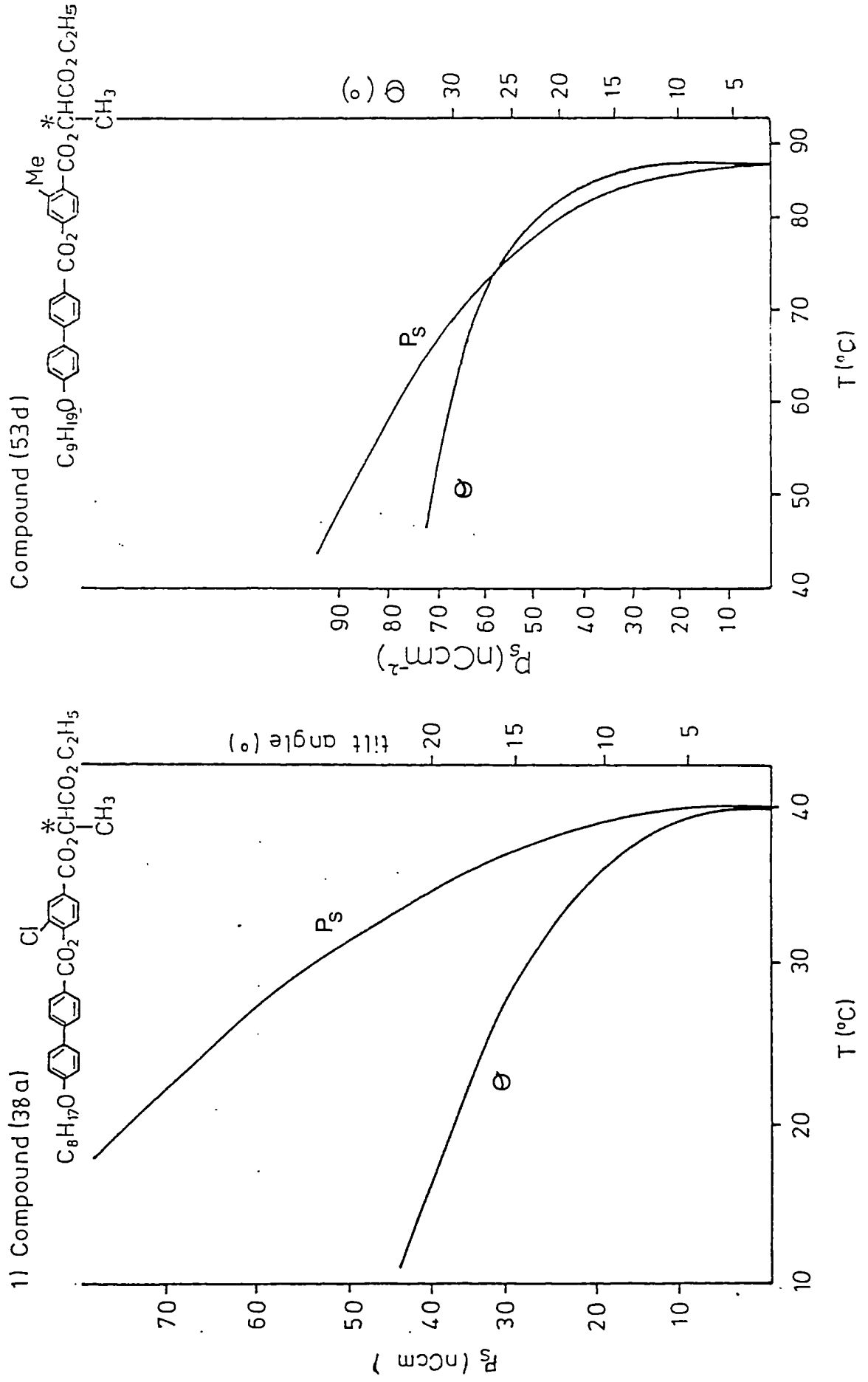


Fig.(g): Superimposed  $P_S$  and  $\theta$  vs T curves for compounds <sup>i)</sup>(38 a), <sup>iii)</sup>(54 d).

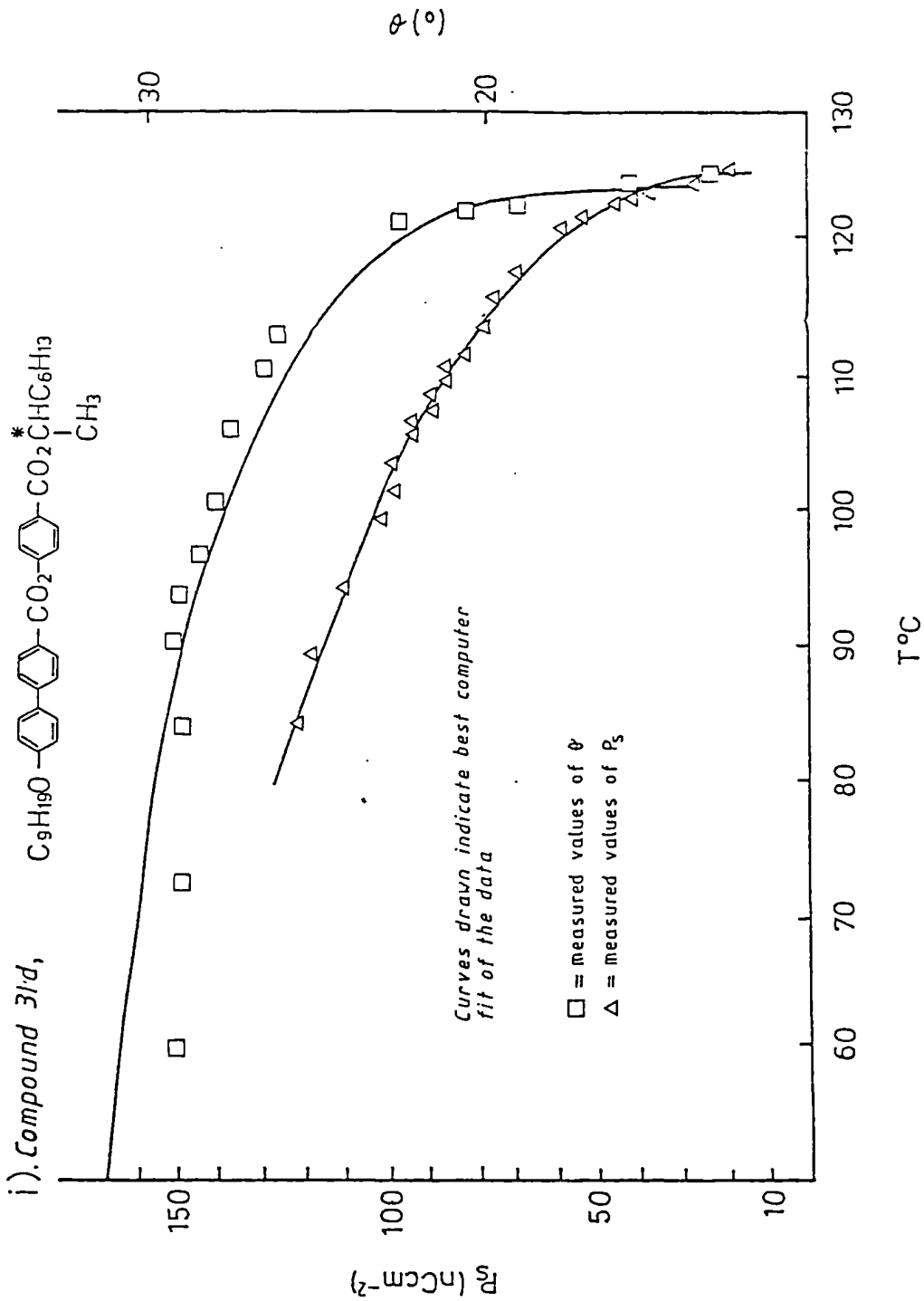


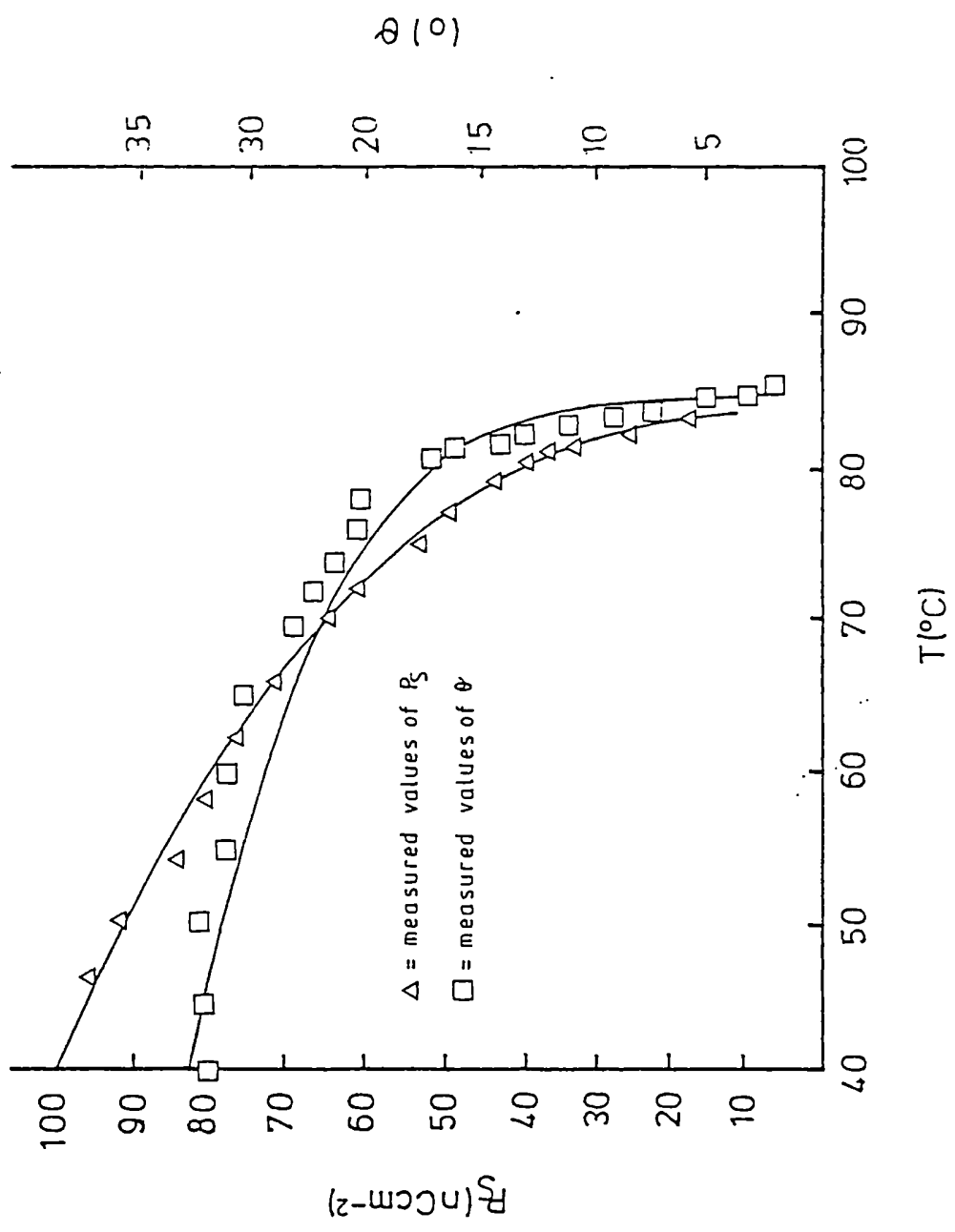
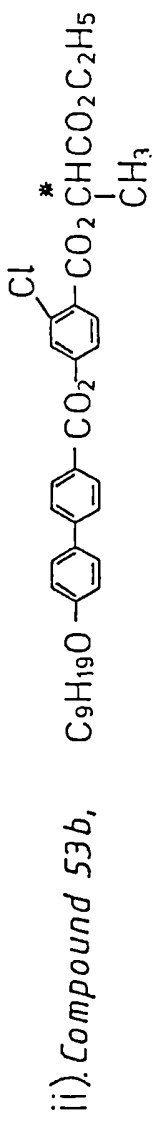
A more convincing case is perhaps made by considering how both  $P_g$  and  $\theta$  vary with decreasing temperature, beyond  $T^1$  and  $T^\theta$ . Much of the relevant data taken from the materials in this work, indicates that beyond  $T^\theta$  the tilt angle generally tends to level off and eventually becomes fairly constant. However as the value of  $\theta$  saturates, the magnitude of  $P_g$  often continues to rise in a fairly linear fashion, implying that it may simply be a function of temperature, and therefore not necessarily dependent on  $\theta$ . The extent of this relative increase in  $P_g$  may vary considerably for different materials, but on average there is an approximately 20-25% rise in the magnitude of  $P_g$ , while the tilt angle remains fairly constant. Some of the clearest examples of this behaviour are exhibited by compounds (31d) and (53b,d), shown in figure h.

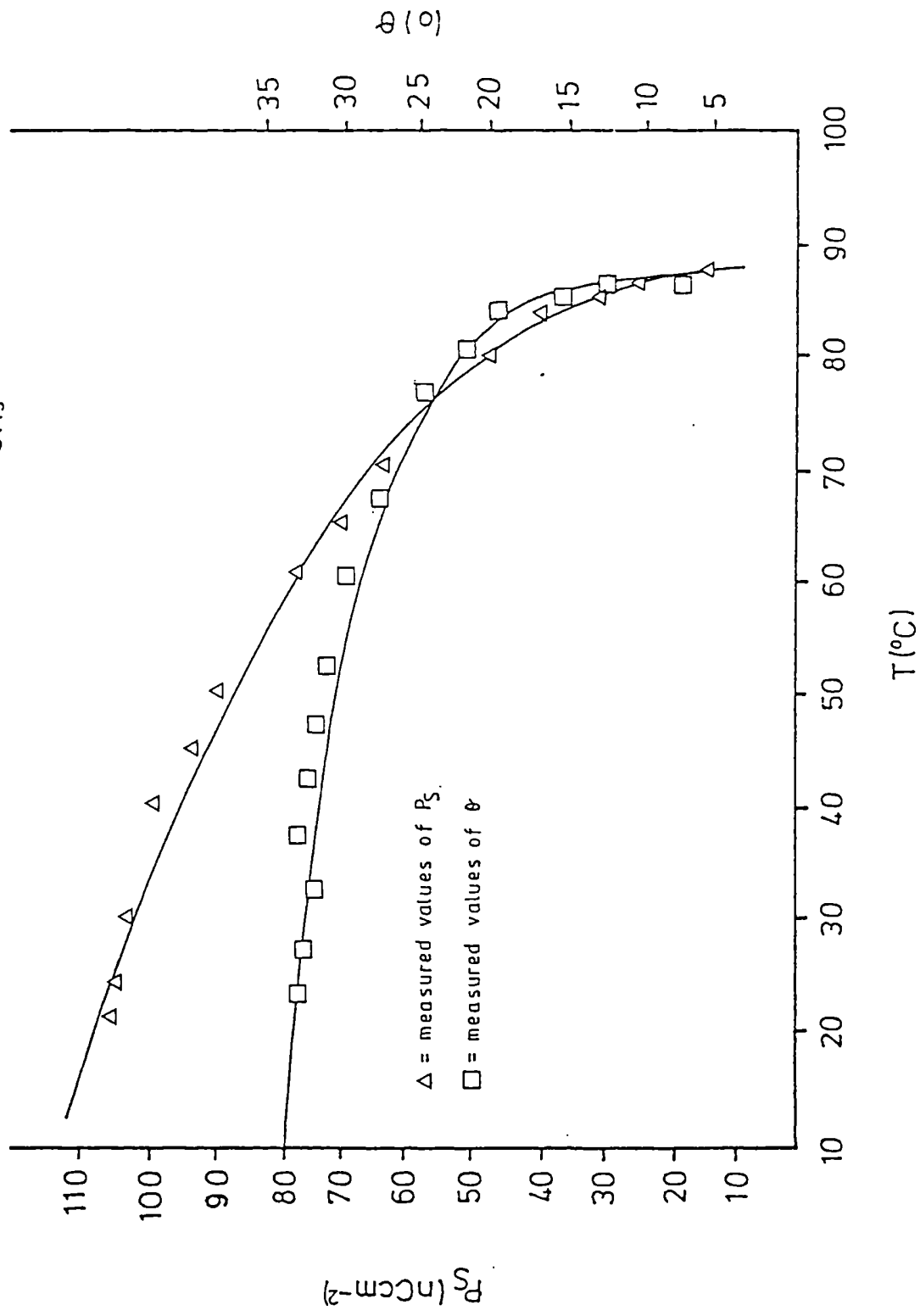
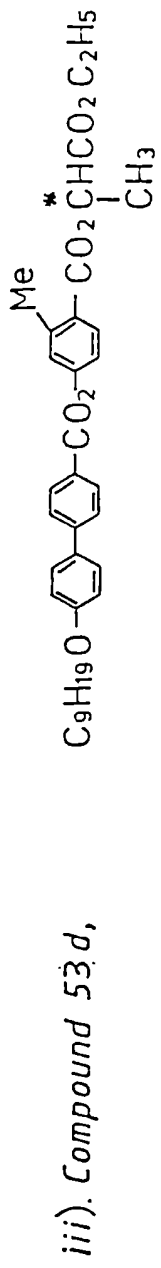
For compound (31d), the measured value of  $\theta$  remains constant on cooling between 93° and 60° C, whereas between 93° and 80° C, the magnitude of  $P_g$  has already risen by over 12%. A continuation of this increase at the same rate would lead to an overall rise in  $P_g$  of 30% between 93° and 60° C. Although there has been a small (9%) increase in the measured value of  $\theta$  between 40° and 60° C for compound (53b), the magnitude of  $P_g$  over the same temperature range has risen by almost 30%. Similarly for compound (53d), between 23.5° and 48° C there has been a rise in the value of  $P_g$  by over 30%, but only a 9% increase in the measured value of  $\theta$ .

Finally the above arguments do not of course give any explanation as to the origin of the tilt mechanism in the  $S_C^*$  phase. However, they may account for the sudden appearance of a spontaneous polarisation at  $T_C$ , and the nature of its variation with temperature, in a more simply understood manner.

i). Compound 31d,  $C_9H_{19}O$  CCCCCCCCCOc1ccc(cc1)C(=O)c2ccc(cc2)C(=O)C(C)C and fairly constant  $\theta$  vs. Temperature for compounds (31d) and (53b,d).







#### 4.2: The Pseudo-Homeotropic Texture of the $S_C^*$ phase.

Although a general discussion concerning the optical textures of various phases has not been undertaken in this work, special mention must be made of the unique, pseudo-homeotropic texture of the  $S_C^*$  phase. This texture is obtained by cooling into the  $S_C^*$  phase from the homeotropic texture of the preceding  $S_A$  phase.

In some cases a colour change will occur at the transition temperature, from the black homeotropic texture of the  $S_A$  phase to a red, green or blue pseudo-homeotropic texture, often having a 'petal' like appearance. More frequently no change in the homeotropic texture is observed at the  $S_A$  to  $S_C^*$  transition and 'colouring' occurs at lower temperatures.

This phenomenon arises from changes in the pitch-length ( $P$ ) of the  $S_C^*$  helix. As the temperature decreases,  $\theta$  increases causing  $P$  to fall into the wavelength range of visible light. When this occurs, the homeotropically aligned texture begins to give selective reflection of red light. As  $P$  continues to decrease, light of shorter wavelengths is reflected. Beyond a given value of  $P$ , the reflected wavelength is no longer in the visible spectrum, and the homeotropically aligned texture again appears black.

Plates 1 - 8 (page 177) show a particularly interesting example of this texture obtained from a homeotropically aligned sample of compound (31c). At the  $S_A$  to  $S_C^*$  transition temperature, the texture remains black. As the temperature

falls the pseudo-homeotropic texture takes on a red tinge and then becomes more highly coloured. Further reductions in temperature cause the pseudo-homeotropic texture to appear in various shades of red, green and blue, before finally becoming black again.

The pseudo-homeotropic texture of compound (31c).

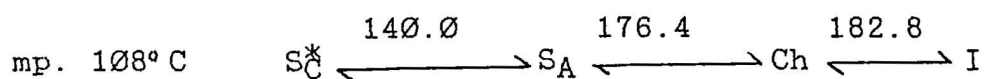


Plate 1: 137° C.

Slight reddish 'petal' texture begins to emerge from the black pseudo-homeotropic texture.

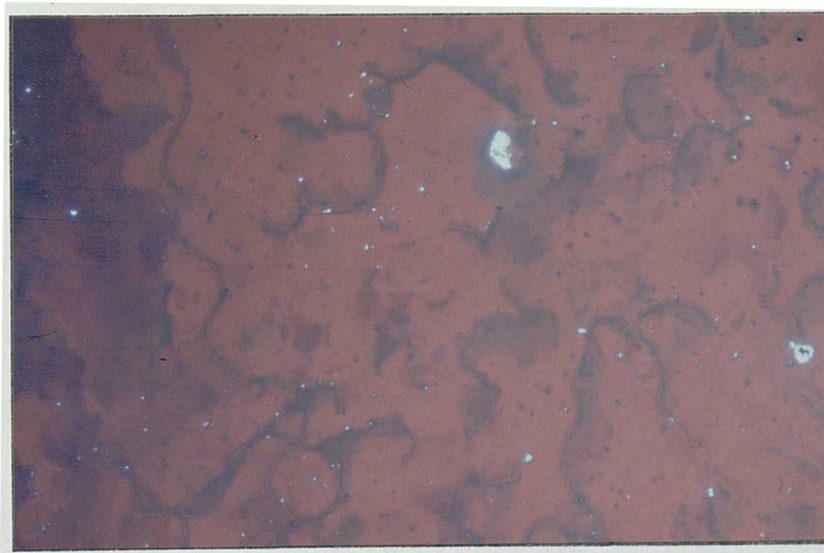


Plate 2: 135° C.

Red 'petal' texture is now evident.



Plate 3: 133° C. As pitch-length decreases, the texture begins to reflect green light.

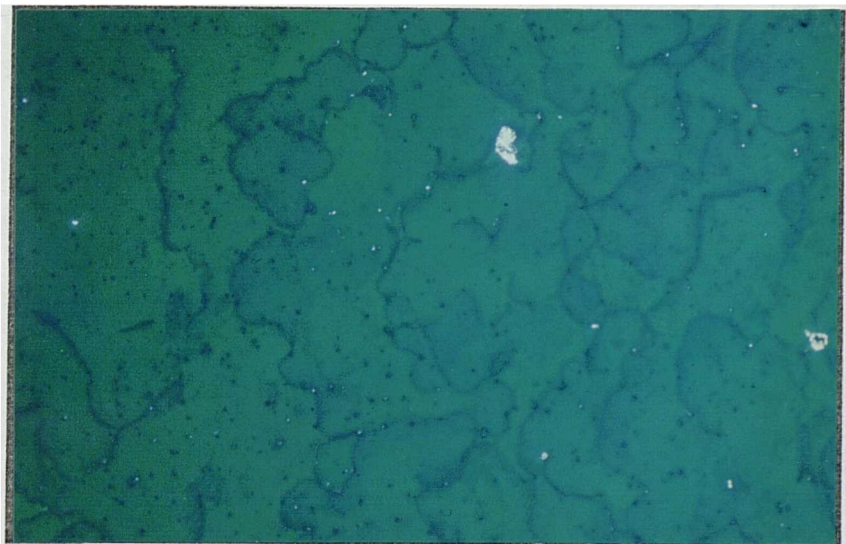


Plate 4: 131° C. The 'petal' texture takes on a vivid green appearance.



Plate 5: 129° C. Blue light begins to emerge.



Plate 6: 127° C. A deep blue appearance is now evident.



Plate 7: 125° C. As the temperature continues to fall, the blue 'petal' texture begins to fade.



Plate 8: 123° C. Further cooling causes the petal texture to disappear, the sample returns to the 'black' pseudo-homeotropic texture.

## 5. REFERENCES .

## REFERENCES

1. Schadt, M., Helfrich, W. *Appl. Phys. Lett.*, 18 (4), 127 (1971).
2. Clark, N.A., Lagerwall, S.T. *Recent Developments in Condensed Matter Physics.*, 4, 309 (1981).
3. Meyer, R.B., Liebert, L., Strzelecki, L., Keller, P. *J. Phys. (Paris) Lett.*, 36, L-69 (1975).
4. Nicastro, A.J. *American Laboratory*. December, 12 (1982).
5. Frank, F.C. *Discuss Faraday Soc.*, 25, 19 (1958).
6. Hori, K. *Mol. Cryst. Liq. Cryst.*, 100, 75 (1983).
7. Gray, G.W., McDonnell, D.G. *Mol. Cryst. Liq. Cryst. Lett.*, 34, 211 (1977).
8. DeVries, A. *Mol. Cryst. Liq. Cryst. Lett.*, 41, 27 (1977).
9. Gray, G.W., Brynmor Jones., Marson, F. *J. Chem. Soc.*, 393 (1957).
10. Goodby, J.W., Gray, G.W. *Smectic Liquid Crystals (Leonard Hill)*, pp. 72-73. (1984).
11. Etherington, G., Leadbetter, A.J., Wang, X.J., Gray, G.W., Tajbakhsh, A. *Liquid Crystals.*, 1 (3), 209 (1986).
12. Bryan, R.F., Leadbetter, A.J., Mehta, A.I., Tucker, P.A. *Mol. Cryst. Liq. Cryst.*, 104, 257 (1984).
13. Kostromin, S.G., Sinitzyn, V.V., Talroze, R.V., Shibaev, V.P., Platé, N.A. *Makromol. Chem., Rapid Commun.*, 3, 809 (1982).
14. McMillan, W.L. *Phys. Rev.*, A8 (4), 1921 (1973).
15. Wulf, A. *Phys. Rev.*, A11 (1), 365 (1975).
16. Goodby, J.W. *PhD. Thesis, University of Hull.* (1977).
17. Van der Meer, B.W., Vertogen, G. *J. Phys (Paris).*, 40, 222 (1979).

18. Goodby, J.W., Leslie, T.M. *Mol. Cryst. Liq. Cryst.*, 110, 175 (1984).
19. Goodby, J.W., Gray, G.W. *Smectic Liquid Crystals (Leonard Hill)*, p.98 (1984).
20. Gane, P.A.C., Leadbetter, A.J., Wrighton, P.G., Goodby, J.W., Gray, G.W., Tajbakhsh, A.R. *Mol. Cryst. Liq. Cryst.*, 100, 67 (1983).
21. Goodby, J.W., Gray, G.W., *Mol. Cryst. Liq. Cryst.*, 48, 127 (1978).
22. Bone, M.F. 'Ferroelectric Liquid Crystal Materials and Devices', S.I.D. Branch Meeting, 17th September (1985).
23. Brand, H.R., Cladis, P.E. *J. Phys Lett.*, 45 (5), 217 (1984).
24. Valasek, J. *Phys. Rev.*, 15 (6), 537 (1920). *Phys. Rev.*, 17 (4), 475 (1921).
25. Zaky, A.A., Hawley, R. *Dielectric Solids (Routledge and Kegan Paul, Ltd.)*, p.66 (1970).
26. Herbert, J.M. *Chemistry in Britain*, September, 728 (1983).
27. Goodby, J.W., Chin, E., Leslie, T.M., Geary, J.M., Patel, J.S. *J. Am. Chem. Soc.*, 108, 4724 (1986).
28. Walba, D.M., Slater, S.C., Thurmes, W.N., Clark, N.A., Handschy, M.A., Supon, F. *J. Am. Chem. Soc.*, 108, 5210 (1986).
29. Meyer, R.B. *Mol. Cryst. Liq. Cryst.*, 40, 33 (1977).
30. Martinot-Lagarde, P.H., Duke, R., Durand, G. *Mol. Cryst. Liq. Cryst.*, 75 249 (1981).
31. Pieranski, P., Guyon, E., Keller, P. *J. Phys. (Paris)*. 36, 1005 (1975).
32. Pieranski, P., Guyon, E., Keller, P., Liebert, L., Kuczyński, W., Pieranski, Piotr. *Mol. Cryst. Liq. Cryst.*, 38, 275 (1977).

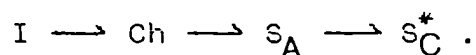
33. Parmar, D.S., Raina, K.K., Shankar, J. *Mol. Cryst. Liq. Cryst.*, 103, 77 (1983).
34. Clarke, N.A., Lagerwall, S.T., *Appl. Phys. Lett.*, 36, 11 (1980).
35. Clarke, N.A., Handschy, M.A., Lagerwall, S.T., *Mol. Cryst. Liq. Cryst.*, 94, 213 (1983).
36. Lagerwall, S.T., Wahl, J., Clarke, N.A. 'Ferroelectric Liquid Crystals for Displays', *International Display Research Conference*, 213 (1985).
37. Martinot-Lagarde, Ph. *J. Phys. (Paris)*, 37, C3-129 (1976).
38. Skarp, K., Flatischler, K., Kondo, K., Sato, Y., Miyasato, K., Takezoe, H., Kuze, E. *Jpn. J. Appl. Phys.*, 20 (4), 566 (1983).
39. Bone, M.F., Coates, D., Davey, A.B. *Mol. Cryst. Liq. Cryst. Lett.*, 102, 231 (1984).
40. Inukai, T. Chisso Corporation, Yokohama, Japan 236, Private Communication.
41. Osipov, M.A., Pikin, S.A., *Mol. Cryst. Liq. Cryst.*, 103, 57 (1983).
42. Pavel, J., Glogarovã, M., Demus, D., Mädicke, A., Pelzl, G. *Crystal Res. & Technol.*, 18 (7), 915 (1983).
43. Cladis, P.E., Brand, H.R., Finn, P.L. *Phys. Rev.*, A28 (1), 512 (1983).
44. Rutherford Appleton Laboratory. Report to 5th Alvey Technical Working Party meeting, 19th May (1986).
45. Wood, E.A. *Crystals and Light* (Dover Publications Inc.), 94 (1977).
46. Goodby, J.W., Chin, E. *J. Am. Chem. Soc.*, 108, 4736 (1986).
47. Martinot-Lagarde, Ph. *J. Phys. (Paris) Lett.*, 38, L-17 (1977).

48. Diamont, H., Drenck, K., Pepinsky, R. *Rev. Sci. Instr.*, 28 (1), 30 (1957).
49. Hoffman, J., Kuczynski, W., Malecki, J. *Mol. Cryst. Liq. Cryst.*, 44, 287 (1978).
50. Yoshino, K., Ozaki, M., Sakurai, T., Sakamoto, K., Honma, M. *Jpn. J. Appl. Phys.*, 23 (3), L175 (1984).
51. Martinot-Lagarde, Ph. *Mol. Cryst. Liq. Cryst.*, 66, 61 (1981).
52. Beresnev, L.A., Baikalov, V.A., Blinov, L.M. *Sov. Phys. Tech. Phys.*, 27 (10), 1296 (1982).
53. Skarp, K., Dahl, I., Lagerwall, S.T., Stebler, B. *Mol. Cryst. Liq. Cryst.*, 114, 283 (1984).
54. Bone, M.F., Bradshaw, M.J. Private Communication.
55. Bone, M.F., Coates, D., Gunn, P., Ross, P.W., Report to 5th Alvey Technical Working Party meeting, 19th May (1986).
56. Escher, C. *Kontakte (Darmstadt)*., 2, 3 (1986).
57. Bone, M.F., Private Communication.

6. CONCLUDING REMARKS.

## 6. Concluding Remarks.

The principal aims of this work have all been achieved. A large number of compounds that exhibit wide temperature range  $S_C^*$  phases, occurring around room temperature have been synthesised. Many of these materials give desirable values of  $P_s$  and  $\theta$ , in conjunction with the desired phase sequence;



These materials are particularly useful as additives in ferroelectric mixtures, as all four combinations of  $P_s$  (+/-) with helical twist sense (D/L) have now been synthesised.

It is also worth noting that the majority of these compounds follow the rules developed by Goodby, which relate absolute configuration, distance of the chiral centre from the molecular core and the twist sense of the  $S_C^*$  helix, to the inductive nature of substituents at the chiral centre.

A close study of the above materials has helped to elucidate the effect of molecular structure on mesomorphic properties, and more importantly on the magnitude of  $P_s$ .

At the outset of this work, the magnitude of  $P_s$  was thought to depend critically on the proximity of the chiral centre to polarisable  $\pi$  electrons in the molecule, and/or a significant dipole. While these criteria remain valid, the importance of 'damping' of intramolecular rotations at the chiral centre and steric hindrance have also been demonstrated.

A long terminal alkyl chain beyond the chiral centre has a great effect in diminishing rotation about the chiral centre. This 'damping' effect is emphasised by the 6-fold increase in  $P_s$  which occurs when the 1-methylpropyl end group of a molecule is replaced with 1-methylheptyl.

The effect of steric hindrance at the chiral centre is demonstrated by compounds having terpenyl end groups. Despite the relatively small dipoles operating at the chiral centre, the hindrance to rotation about the chiral centre caused by the bulky menthyl and isopinocampheyl end groups results in relatively large values of  $P_s$  being displayed.

Further evidence for the importance of steric effects on  $P_s$  is found when the relative size of laterally substituted groups close to the chiral centre is considered. If these groups face toward the chiral centre,  $P_s$  is shown to increase approximately with the size of the substituted group.

Finally, taking into account the observations made in this thesis, a simplified theory has been developed in order to explain the ferroelectric effect in the  $S_C^*$  phase.